STRUCTURE, METAMORPHISM AND TECTONIC SETTING OF METASEDIMENTARY ROCKS AND MAFIC-ULTRAMAFIC INCLUSIONS IN THE DASHWOODS SUBZONE OF THE DUNNAGE ZONE, SOUTHWESTERN NEWFOUNDLAND

DON FOX, B.Sc.(Honours)

NOTICE

The quality of this microform is heavily dependent upon the quality of the original thesis submitted for microfilming. Every effort has been made to ensure the highest quality of reproduction possible.

If pages are missing, contact the university which granted the degree.

Some pages may have indistinct print especially if the original pages were typed with a poor typewriter ribbon or if the university sent us an inferior photocopy.

Reproduction in full or in part of this microform is governed by the Canadian Copyright Act, R.S.C. 1970, c. C-30, and subsequent amendments.

AVIS

La qualité de cette microforme dépend grandement de la qualité de la thèse soumise au microfilmage. Nous avons tout fait pour assurer une qualité supérieure de reproduction.

S'il manque des pages, veuillez communiquer avec l'université qui a conféré le grade.

La qualité d'impression de certaines pages peut laisser à désirer, surtout si les pages originales ont été dactylographiées à l'aide d'un ruban usé ou si l'université nous a fait parvenir une photocopie de qualité inférieure.

La reproduction, même partielle, de cette microforme est soumise à la Loi canadienne sur le droit d'auteur, SRC 1970, c. C-30, et ses amendements subséquents.

Canada

STRUCTURE, METAMORPHISM AND TECTONIC SETTING OF METASEDIMENTARY ROCKS AND MAFIC-ULTRAMAFIC INCLUSIONS IN THE DASHWOODS SUBZONE OF THE DUNNAGE ZONE, SOUTHWESTERN NEWFOUNDLAND

BY

© DON FOX, B.Sc.(Honours)

A thesis submitted to the school of Graduate
Studies in partial fulfillment of the
requirements for the degree of
Master of Science

Department of Earth Science
Memorial University of Newfoundland

June 1992

St. John's Newfoundland

ISBN 0-315-78129-7

Abstract

The Dashwoods subzone of the Dunnage zone in southwestern Newfoundland is characterized by high grade metasedimentary schists and gneisses and disrupted ophiolite complexes (Annieopsquotch Complex and Long Range Mafic-Ultramafic Complex) all intruded by hornblende-biotite granodiorite to tonalite. A previously reported age of the granitoid rocks is 456 ± 3Ma. This study focuses on an area east of the Long Range Fault, on the western side of the Dashwoods subzone and contains all the major lithostratigraphic units characteristic of the Dashwoods subzone.

Metasedimentary rocks are separated into two main units: metapsammites to the west and metapelites to the east. Mafic-ultramafic inclusions lie within shear zones in the metapelites and are interpreted to represent parts of a disrupted ophiolite suite. All rocks within the shear zones (both metapelite and mafic-ultramafic) are extensively retrogressed to greenschist facies mineral assemblages but evidence of a higher grade, amphibolite facies metamorphism is evident in rocks that have not been completely retrogressed. The mafic-ultramafic rocks are interpreted to have undergone the full range of metamorphism and deformation that has affected the metasedimentary rocks. Geothermobarometry calculations suggest that the higher grade metamorphic event may have reached temperatures in the order of 800°C with pressures in the order of 5 to 7 kbars.

The metasedimentary rocks are correlated with the Fleur de Lys metasediments found in northeastern Newfoundland on the basis of similar stratigraphic position along the eastern edge of the miogeocline of eastern North America. An upper age of deposition of the metasediments is approximately middle Ordovician as constrained by the age of the granitoid rocks. Silurian mafic bodies in the Dashwoods subzone have not been affected by high grade metamorphism or high degree of deformation and the Dashwoods subzone had probably stabilized by late Ordovician to Silurian time.

TABLE OF CONTENTS

CHAPTER 3 GEOLOGY OF THE STUDY AREA

CHAPTER 4 ORIGIN OF THE MAFIC-ULTRAMAFIC ROCKS

CHAPTER 5 STRUCTURAL ANALYSIS

CHAPTER 6 METAMORPHISM

List of Figures

List of Tables

ACKNOWLEDGEMENTS

I would like to thank the Smith family (Peter, Bonnie, Debbie and Todd) for providing an opportunity to complete this project. Thanks also to Gerry & Cyril Webber for continual encouragement and support.

I also thank the Geological Survey of Canada for summer employment and the opportunity to work in southwestern Newfoundland. Tim van Nostrand provided excellent guidance and discussions throughout the field season "despite the weather". This project also benefitted from discussions with J.T. van Berkel and Mark Piasecki.

Finally I would like to thank my supervisor, Toby Rivers for guidance throughout this study. Hats off to the many fine friends made along the way who made it all worthwhile.

CHAPTER 1

INTRODUCTION

1.1 PURPOSE AND SCOPE

This study was initiated as a contribution to a regional mapping project in southwestern Newfoundland funded by the Geological Survey of Canada and directed by Dr. J. T. van Berkel. Prior to the inception of this study, reconnaissance mapping by van Berkel within the present map area had outlined several bodies of mafic-ultramafic rocks associated with metasedimentary and granitoid rocks (Fig. 1-1). This study was undertaken in order to determine the origin and subsequent structural and metamorphic history of these rocks and to ascertain their position in the Paleozoic evolution of western Newfoundland. In this context a detailed study of the area was initiated by the author when employed as a field assistant with the GSC.

Specifically, the purpose of this study was to provide detailed mapping of the mafic-ultramafic, metasedimentary and granitoid rocks and to determine the origin of the mafic-ultramafic rocks. However, before possible origins can be ascertained it is necessary to outline the regional metamorphic history of the mafic-ultramafic and adjacent metasedimentary rocks. Their metamorphism is discussed in terms of mineralogy, mineral chemistry, phase relationships and thermobarometry in order to determine as complete a metamorphic history as possible.

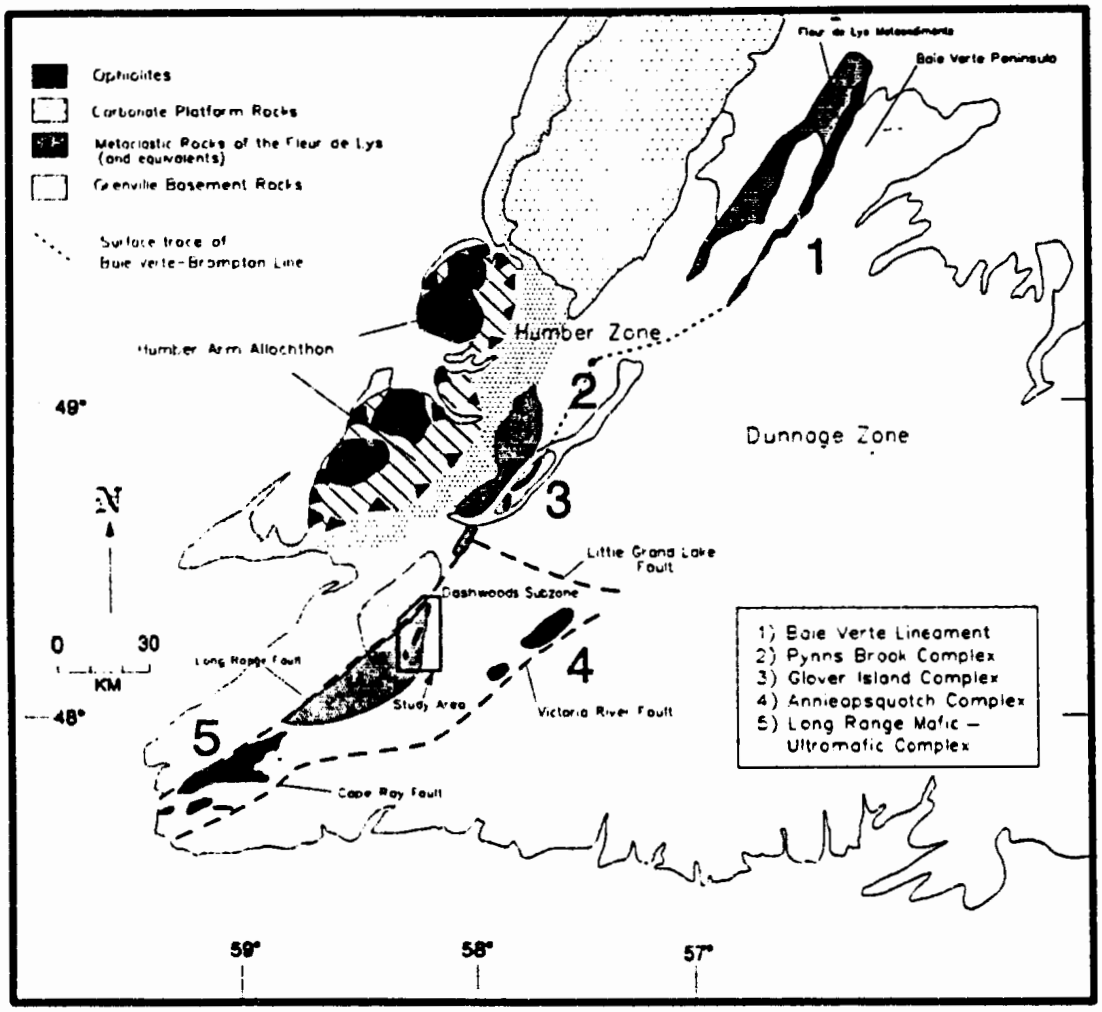

Fig. 1-1 Generalized geological map of western Newfoundland showing the location of the Baie Verte-Brompton Line which is considered to separate the Humber and Dunnage Zones, the location of the major ophiolite bodies and the miogeoclinal rocks of the Fleur de Lys Supergroup and its inferred equivalents to the south. The study area lies in the Dashwoods subzone of the Dunnage Zone according to recent interpretations of Piasecki et al. (1990). See text for discussion.

Prior to the inception of this project, the area had not been studied in detail. However, it was included within the 1:250,000 scale Stephenville map sheet of Riley (1962), where the map area of this study was included in the "Long Range Igneous and Metamorphic Complex".

1.2 LOCATION AND ACCESS

The study area is located in the southern Long Range Mountains of Newfoundland, is bounded by longitudes 58°10' - 58°20' and latitudes 48°10' - 48°20' and lies immediately east of the Long Range Fault (Fig. 1-1). The area is not accessible by road and field work was accomplished by traversing from helicopter supported fly camps. Outcrop is abundant in high ground which comprises over 50% of some parts of the map area. Two major valleys occupied by Flat Bay Brook and Fischells Brook transect the map area in an east-west direction. The Trans-Canada highway lies approximately 15 km to the west and the Burgeo Road (route 480) lies 10 km to the north of the map area.

1.3 REGIONAL GEOLOGY AND AGE RELATIONSHIPS OF WESTERN NEWFOUNDLAND

The Canadian Appalachians have been subdivided into "tectonic zones" or "suspect terranes" of contrasting stratigraphic and structural style several times in the past 20 years (eg. Williams et al., 1972; Williams, 1979; Williams and Hatcher, 1983). The most widely utilized subdivision is a 5-fold zonation, based upon contrasts between middle Ordovician and

older rocks, that separates the orogen into the Humber, Dunnage, Gander, Avalon and Meguma Zones from west to east respectively (Williams, 1979). Of these five zones, only the Meguma Zone is not represented in Newfoundland. This study is concerned with relationships in an area near the common boundary between the Humber and Dunnage Zones in southwest Newfoundland.

The Humber Zone represents the ancient continental margin of eastern North America (i.e. the miogeocline) and consists of Precambrian basement rocks overlain by clastic metasediments of the Fleur de Lys Supergroup which are themselves conformably overlain by rocks of the carbonate platform. Figure 1-1 shows the extent of the carbonate platform as well as the Fleur de Lys Supergroup and correlatives as interpreted by Hibbard (1983). The age of the Fleur de Lys Supergroup is not precisely established, but is believed to be between Late Upper Proterozoic and Early Ordovician (Hibbard, 1983).

The Dunnage Zone occurs to the east of the Humber Zone and consists mainly of ophiolitic and volcanic arc sequences that have been widely interpreted to represent remnants of the ancient Lower Paleozoic Iapetus Ocean. These rocks and their sedimentary cover were obducted onto the eastern margin of North America (the miogeocline) during the middle Ordovician Taconian orogeny. A well-preserved example of the obducted ophiolitic rocks and associated transported sedimentary rocks in western Newfoundland is the Humber Arm Allochthon (Fig. 1-1).

The traditional location of the boundary between the Humber and Dunnage Zones is marked by the Baie Verte-Brompton Line (Williams and St. Julien, 1982). This steeply-dipping structural sequence of altered mafic-ultramafic rocks is considered to be the surface trace of the tectonic boundary between the North American continental margin and ancient oceanic crust. The most continuous exposure of the Baie Verte-Brompton Line in Newfoundland is on the Baie Verte Peninsula where it is known as the Baie Verte Lineament. From there, it has been extended to the southwest through the Pynns Brook Complex (O'Laughlin, 1982) and further south through the Glover Island Complex (Knapp, 1980). All of these complexes have been interpreted as ophiolitic fragments (Fig. 1-1).

Where ophiolite fragments mark the Baie Verte-Brompton Line it is relatively easy to trace. However, south of the Little Grand Lake Fault (van Berkel & Currie, 1988) the trace of the Line and the division between Humber and Dunnage Zones is not straightforward. As originally defined, the Line bends eastward, along the Little Grand Lake Fault to include the Annieopsquotch Complex (Dunning, 1984) and was inferred to continue to the southwest along the Cape Ray Fault (Fig. 1-1). The placement of the Line in this area was a result of the interpretation that the Cape Ray Fault was a suture zone between two Precambrian continental margins from opposite sides of the early Paleozoic Iapetus Ocean (Brown, 1976). In this context, the area between the Long Range Fault and the Cape Ray Fault was considered to be part of the Humber Zone (see map of the Appalachian Orogen by Williams, 1978).

However, more recent mapping in the southern Long Range Mountains has led to a re-interpretation of the geology in this part of Newfoundland. The area south of the Little Grand Lake Fault and between the Cape Ray and Long Range Faults is now included in the Dashwoods subzone of the Dunnage Zone (Piasecki et al., 1990). The lithotectonic character of the Dashwoods subzone is discussed in the following chapter.

CHAPTER 2

REGIONAL GEOLOGY AND AGE RELATIONSHIPS OF THE DASHWOODS SUBZONE

2.1 INTRODUCTION

The Dashwoods subzone is composed mainly of a suite of undifferentiated granitoid rocks, and metasedimentary and mafic-ultramafic rocks (Fig. 2-1). The relationships between these lithologies in this part of Newfoundland have an important bearing on tectonostratigraphic interpretations of the Humber and Dunnage zones in Newfoundland and are central to the present study since all three lithologies are located within the present map area.

Although the present map area had not been studied in detail prior to this project, various aspects of the main lithologies had been previously studied in other localities throughout the Dashwoods subzone. This chapter summarizes the regional geology and age relationships of the three main lithologies in the Dashwoods subzone (granitoid suite, metasediments and mafic-ultramafic rocks) on the basis of this previous work.

2.2 LOCATION OF PREVIOUS WORK

The geology of the southwestern part of the Dashwoods subzone (1:50,000 map sheets 110/11, 110/14 and 110/15, Fig. 2-1) was compiled by Chorlton (1984) as part of her Ph.D. thesis. Her compilation was based

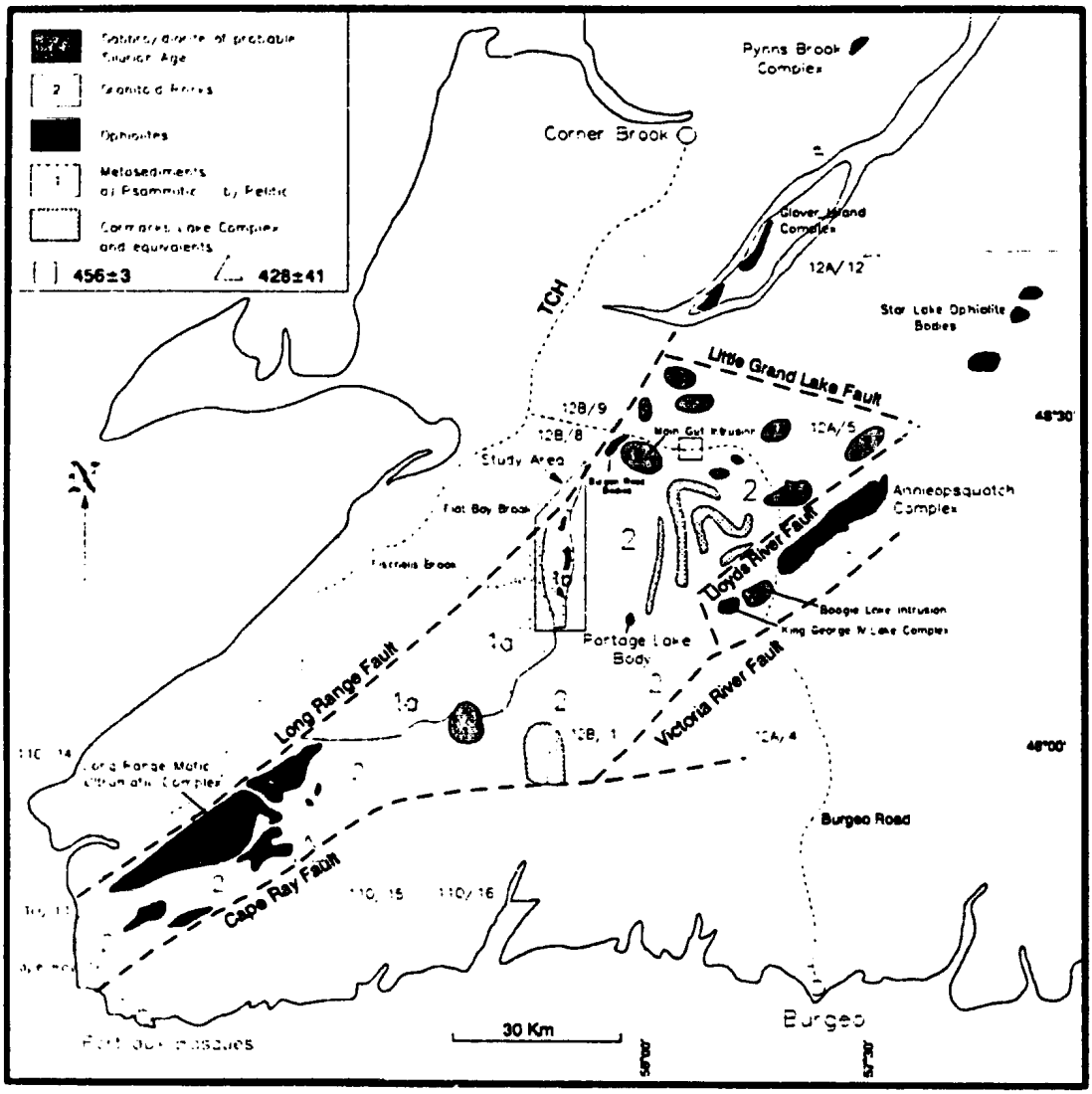

Fig. 2-1. Generalized geological map of the Dashwoods subzone showing the location of ophiolite bodies, metasedimentary rocks, granitoid suite and Silurian gabbro-diorite bodies. The boundaries of 1:50,000 map sheets referred to in the text are shown.

mainly on her own mapping, but utilized in part the work of Brown (1975; 1977) and Knight & Brown (1977).

Wilton (1984) also mapped part of the southwestern Dashwoods subzone as part of his Ph.D. thesis which concentrated mainly on a metallogenic study within the Cape Ray Fault Zone, but also included a regional study of surrounding granitoid rocks (Wilton, 1985).

In the northeastern part of the Dashwoods subzone, the Puddle Pond map sheet (12A/5) was initially mapped at 1:50,000 scale by Herd (1978) and Herd & Dunning (1979). Subsequently, Dunning mapped the Annieopsquotch Complex and surrounding areas, including the Star Lake ophiolite bodies (Fig. 2-1) as part of his Ph.D. thesis and several publications stem from his work (Dunning & Herd, 1980; Dunning, 1981; Dunning et al., 1982; Dunning & Chorlton, 1985).

In 1985 a regional mapping project was initiated by van Berkel in the northeastern part of the Dashwoods subzone (1:50,000 map sheets 12B/1, 12B/8, 12B/9, 12A/12, 12A/5 and 12A/4, Fig. 2-1) and is the subject of several publications (van Berkel et al., 1986; van Berkel, 1987a, 1987b, 1987c; van Berkel & Currie, 1986, 1988).

2.3 UNDIFFERENTIATED GRANITOID SUITE

The granitoid rocks were initially mapped as Precambrian tonalitic gneisses in the Port aux Basques region by Brown (1975, 1977) who called

the unit the Long Range Gneiss. The gneiss was described as a variably deformed rock consisting of plagioclase, hornblende and quartz and containing inclusions of earlier amphibolite and quartz-biotite-garnet paragneiss. The amphibolite and paragneiss inclusions were interpreted to contain a previously developed fabric, but a contact relationship between the two units was not found. Brown also mapped part of the Long Range Mafic-Ultramafic Complex (see below) and interpreted the complex to be part of an ophiolite suite exposed in several separate thrust sheets that were thrust onto the Precambrian tonalitic gneiss complex.

Subsequent mapping (Chorlton & Knight, 1983; Chorlton, 1984) of 1:50,000 sheet 110/15 revealed that the "tonalitic gneiss complex" of Brown intrudes the Long Range Mafic-Ultramafic Complex. For this reason, Chorlton suggested that use of the term "Long Range Gneiss" be dropped, and the tonalite complex was referred to as a synkinematic and synmetamorphic granitoid suite. Chorlton described the granitoids as variable in composition from biotite tonalite, granodiorite to granite, and noted that they are gneissic in part and locally garnetiferous. These rocks were considered to be of Ordovician-Silurian (?) age based on surrounding field relationships.

Wilton (1984) also mapped granitoid rocks in the vicinity of the Cape Ray Fault Zone, which he referred to as the "Cape Ray Granite". He separated the unit into two phases, an extensive tonalite to granodiorite phase that lies along the northwestern edge of the Cape Ray Fault extending inland from the coast for over 40 km, and a less aerially

extensive phase of megacrystic granite located near Cape Ray. The tonalite to granodiorite was described as coarse-grained and equigranular containing mainly quartz, feldspar and biotite and is typically retrogressed to sericite, chlorite and epidote. Wilton also noted that amphibolite xenoliths are ubiquitous throughout the unit and increase in abundance and size towards the Long Range Mafic-Ultramafic Complex, so that rocks near the contact are transitional between tonalite and gabbro. He noted that in other places throughout the unit the xenoliths are so abundant that the unit is best described as an agmatite. Wilton (1983) concluded the rocks do not have a gneissic aspect, in contradiction to the descriptions of Brown (1977). The interpretation by Wilton, based on both field and geochemical evidence is that the granitoids were produced by partial melting of the ophiolites.

Part of the granitoid suite around the Annieopsquotch Complex in the Puddle Pond map sheet (12A/5) was mapped by Dunning (1984), who referred to it as the "Southwest Brook Complex". In this area the granitoids are also retrogressed to greenschist facies assemblages and agmatite zones consisting of inclusions of mafic rocks in the granitoids are well developed. Metasedimentary inclusions are also common. A sample of undeformed tonalite of the Southwest Brook Complex from the Burgeo Road has yielded a U/Pb zircon age of 456 ±3 Ma (Fig. 2-1, Dunning et al., 1989). They also report a U/Pb zircon age of 428 ±41 Ma for the Cape Ray Granite (Fig. 2-1) but in the later case the zircon analyses do not define a co-linear array and the age is therefore rather imprecise.

2.4 METASEDIMENTARY ROCKS

Metamorphosed quartzofeldspathic to pelitic rocks interpreted to be sedimentary in origin are widespread throughout the Dashwoods subzone. In the northeastern part of the subzone, the "Cormacks Lake Complex" consists of conformable layers of foliated granite, paragneiss and amphibolite (Herd & Dunning, 1979). The paragneisses consist of quartz, feldspar, biotite, cordierite, sillimanite, gedrite, hornblende and actinolite and have been affected by at least three phases of folding. Herd & Dunning (1979) correlated these lithologies to Grenvillian gneisses known elsewhere in Newfoundland, but admitted that it was impossible to be sure of any rock ages in this area. A K/Ar (hornblende) age of 360 ± 25 Ma from amphibolite within this unit, reported by Stevens et al. (1982), was interpreted to date the latest metamorphic event undergone by the Complex.

The southern extension of the Cormacks Lake Complex, mapped by Chorlton (1980) in 1:50,000 map sheet 110/16 (Fig. 2-1), was called the "Keepings Gneiss". She described it as being composed of felsic paragneiss and interbanded amphibolite and interpreted the unit to be Ordovician in age.

Chorlton (1983) also reported the occurrence of metasedimentary rocks throughout 1:50,000 map sheet 110/15 (Figs. 2-1 and 2-2). In her "western high strain zone" (Fig. 2-2, inset) she described semipelitic paragneisses and marble, whereas a wider variety of metasedimentary

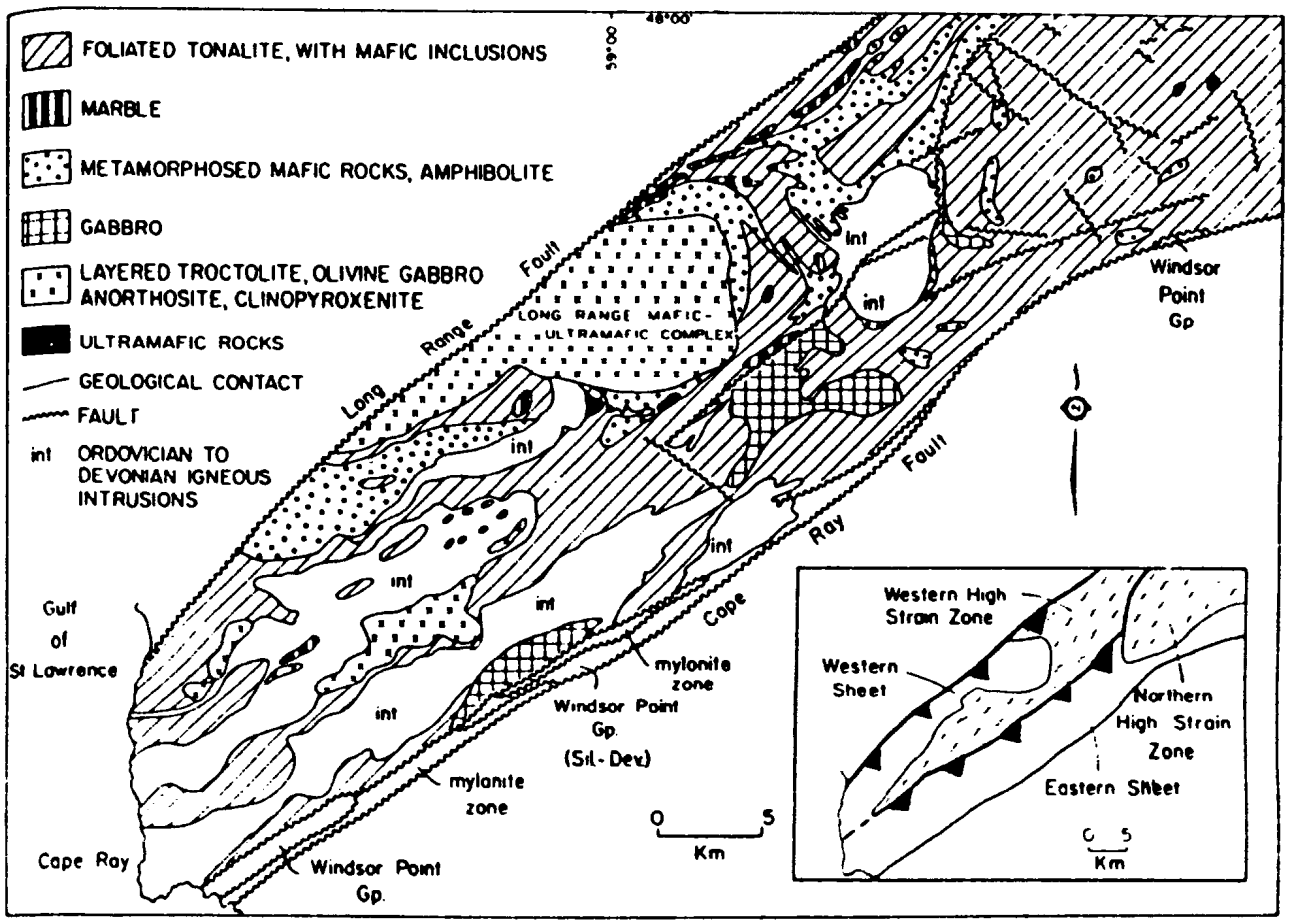

Fig. 2-2 General geological map of Long Range Mafic-Ultramafic Complex, showing associated high strain zones in inset map. (after Dunning & Chorlton, 1985).

inclusions was reported from the "northern high strain zone". Detailed descriptions of these rocks are presented by Chorlton (1984) in her Ph.D. thesis. Her interpretation of the metasedimentary rocks in this area is that they formed an overlying conformable sequence on the ophiolitic rocks of the Long Range Mafic-Ultramafic Complex (see below) and were initially deposited in an oceanic environment. Subsequently they were thrust into their present position together with the ophiolitic rocks.

More recent mapping in the northeast part of the Dashwoods subzone, has outlined rather extensive belts of metasedimentary rocks with only minor occurrences of mafic-ultramafic rocks (van Berkel et al., 1986; van Berkel, 1987; Piasecki, 1988). In this area of the Dashwoods subzone, the metasedimentary rocks are divided into two belts, a western belt composed principally of metapsammites and a less extensive eastern belt containing predominantly metapelitic rocks. The map area of this study is located mainly within the eastern belt of metapelitic rocks (Fig. 2-1).

The relationship of the two metasedimentary belts in the northeastern part of the Dashwoods subzone (described by van Berkel) to the metasedimentary rocks in the southwestern part of the Dashwoods subzone (described by Chorlton) is difficult to interpret. In the southwestern Dashwoods subzone, the metasediments typically occur as inclusions in the granitoid rocks and have not been mapped as separate units. Because of this, the two metasedimentary belts in the northeastern part of the Dashwoods subzone cannot be extended precisely to the southwest. However the similarity of lithologies between the two areas suggests the

metasediments once formed a continuous belt from the Port aux Basques region to at least the Little Grand Lake Fault.

The relationship between the metasedimentary rocks of the Cormacks Lake Complex and those to the west (i.e. those studied in this project) is not precisely established. However, van Berkel (1987) tentatively proposed that lithologies in the Cormacks Lake Complex represent a continental rift facies sequence whereas the metasedimentary rocks to the west were interpreted to represent part of the continental miogeocline of eastern North America and were therefore correlated with the Fleur de Lys Supergroup of northern Newfoundland (Fig. 1-1).

2.5 MAFIC-ULTRAMAFIC ROCKS

Mafic-ultramafic rocks are common throughout the Dashwoods subzone. Some of these have been studied in detail, some only on a reconnaissance basis and some remain unstudied. On the basis of previous work the mafic-ultramafic occurrences can be divided into two groups: 1) remnants of ophiolite complexes; and 2) gabbro/diorite intrusions with minor ultramafic differentiates.

Two major partial ophiolite complexes are the Annieopsquotch Complex (Dunning, 1984) and the Long Range Mafic-Ultramafic Complex (Brown, 1976; Chorlton, 1984). Non-ophiolitic gabbro/diorite intrusions are widely distributed but, to date are recognized mainly in the northeastern part of the Dashwoods subzone (Fig. 2-1).

2.5.1 Long Range Mafic-Ultramafic Complex

Brown (1976) introduced the name "Long Range Mafic-Ultramafic Complex" for the mafic-ultramafic rocks in the southwestern part of the Dashwoods subzone, and proposed that the rocks represent part of an ophiolite suite. He interpreted the ophiolite to be exposed in two major thrust sheets that were obducted onto metasedimentary rocks of the ancient continental margin of eastern North America.

Brown described the lower, westernmost sheet as consisting of tectonized harzburgite, lherzolite and wehrlite pods within serpentinized dunite. Locally the lower thrust contact is marked by a serpentinite mélange with blocks of serpentinite set in a carbonate matrix. The eastern and uppermost sheet is less tectonized than the lower sheet and consists of feldspathic dunite at the base, a layered sequence of troctolite, olivine gabbro, norite and anorthosite, and massive gabbro at the top. Brown's descriptions and interpretations were based on mapping of the Complex in 1:50,000 scale map sheets 110/11 and 110/14 (Fig. 2-1).

Chorlton (1984) also mapped part of the Long Range Mafic-Ultramafic Complex in 1:50,000 map sheet 110/15 (Fig. 2-1) and concurred with Brown's interpretation that the ophiolite complex was exposed as several thrust sheets. Subsequently, Dunning & Chorlton (1985) compiled a general geological map of the entire Long Range Mafic-Ultramafic Complex (presented here as Fig. 2-2). The westernmost and structurally lowest thrust sheet was described by these authors as consisting of layered

metaperidotite at the base, through interlayered olivine metagabbro, troctolite, feldspathic dunite and anorthosite, to banded as well as massive clinopyroxene metagabbro at the top. The layered metagabbros locally contain a granulite facies fabric. The eastern thrust sheet is a mega-agmatite zone composed of layered cumulate metagabbro in the southwest through massive (high level) metagabbro in the northeast, all engulfed by tonalite (Fig. 2-2). Although these descriptions differ in part from those of Brown (1976), both authors agree the ophiolitic rocks are exposed as several thrust sheets, and the differences may result from the emphasis of detailed mapping in different parts of the complex.

Several regional amphibolite facies high strain zones affect the Long Range Mafic-Ultramafic Complex and surrounding rocks (Chorlton, 1984; Dunning & Chorlton, 1985). The Western High Strain Zone (Fig. 2-2 inset) overprints the ophiolitic rocks as well as marble and associated metasedimentary rocks in the western thrust sheet. The Northern High Strain Zone affects the tonalite, ophiolitic rocks and metasedimentary rocks in the northeastern part of the eastern thrust sheet (Fig. 2-2 inset). The amphibolite facies metamorphism in the high strain zones is locally overprinted by greenschist facies assemblages.

2.5.2 Annieopsquotch Complex

The Annieopsquotch Complex was the subject of a Ph.D thesis by Dunning (1984). The Complex consists of the ophiolitic rocks in the Annieopsquotch Mountains, but the "Annieopsquotch Ophiolite Belt" (Fig. 2-

3) consists of at least five massifs that include the Star Lake ophiolite bodies and the King George IV Lake ophiolite body (Dunning, 1981). The "Annieopsquotch Ophiolite Belt" was further extended to include all ophiolitic rocks of the Long Range Mafic-Ultramafic Complex by Dunning & Chorlton, 1985.

The Annieopsquotch Complex exposes an ophiolite stratigraphy from layered cumulate gabbro (critical zone) through high-level gabbro, sheeted dikes, pillow lava and chert. Locally gabbros near the base of the gabbro zone have been metamorphosed to hornblende-plagioclase amphibolites especially where associated with shear zones. In other places near the base of the gabbro zone, two-pyroxene mafic granulites grade into massive gabbro.

The Star Lake bodies are mainly gabbro but have some layered troctolite, olivine gabbro, anorthosite and clinopyroxenite. The King George IV Lake body is composed predominantly of sheeted dikes and pillow lava.

2.5.3 Portage Lake Body

The Portage Lake body (Fig. 2-1) was described by van Berkel (1987) and interpreted as part of an ophiolite sequence. The body consists of metagabbro, pyroxenite, harzburgite and dunite and occurs within gneissic granite. The metagabbro encloses dunite with minor harzburgite in the east which passes into pyroxenite veined by harzburgite in the west. The metagabbro is moderately to highly strained and the ultramafic rocks are

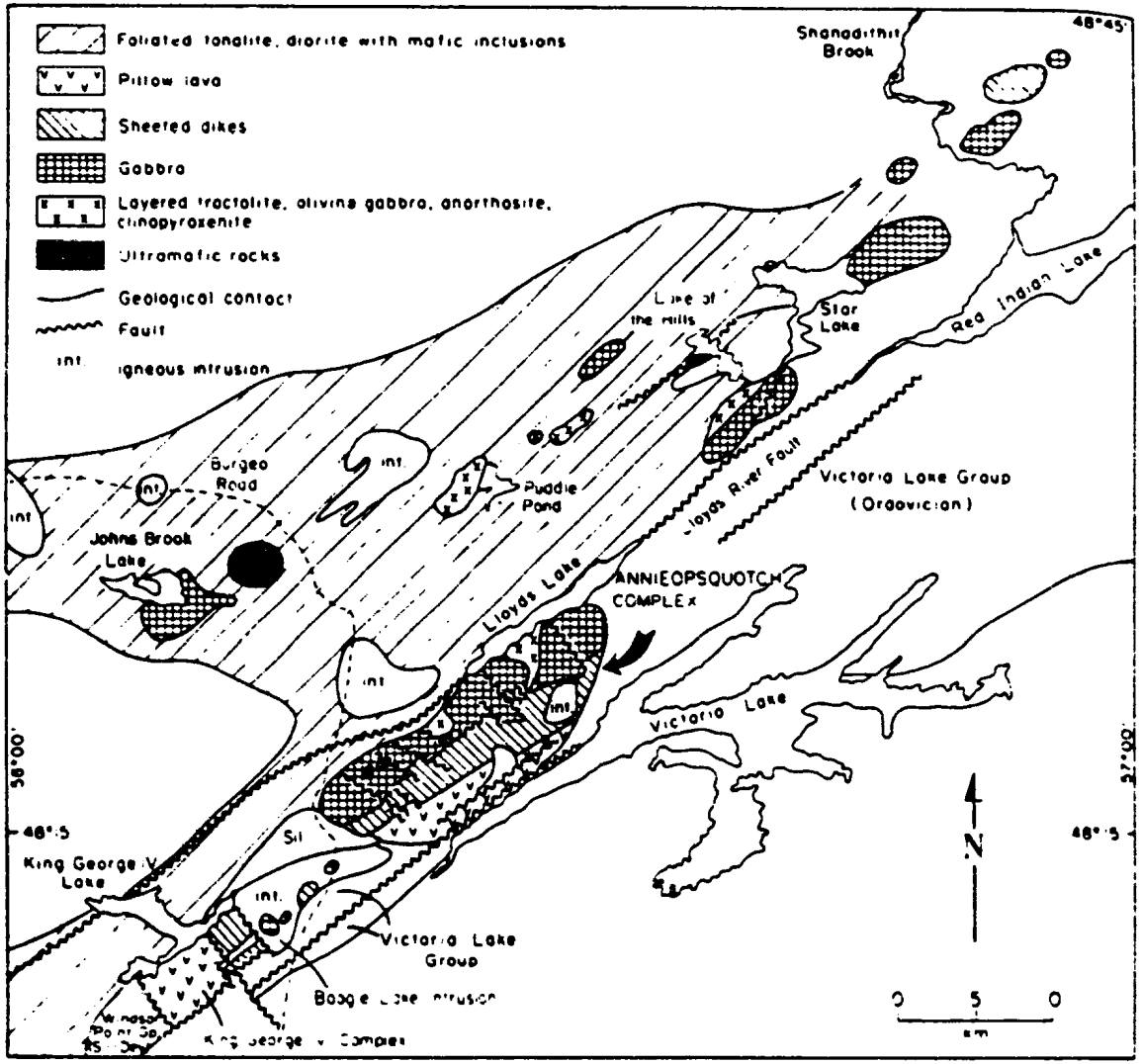

Fig. 2-3 Geological map of the Annieopsquotch Complex (after Dunning & Chorlton, 1985)

variably serpentinized.

2.5.4 Significance of Structure, Metamorphism and Age of the Ophiolites

An important aspect of the ophiolitic rocks in the Dashwoods subzone is the relationship of ophiolite formation and obduction to metamorphism and deformation and other later processes that occurred after emplacement. Although the Annieopsquotch and Long Range Mafic-Ultramafic Complexes show differing degrees of both metamorphism and deformation, together they show affects of the entire spectrum of ophiolite formation, obduction and later orogenic processes.

Dunning & Chorlton (1985) have proposed that the granulite facies metamorphism developed locally in both the Annieopsquotch and Long Range Mafic-Ultramafic complexes was the result of ocean-floor processes related to ophiolite formation. Amphibolite facies metamorphism and related deformation developed in the high strain zones associated with the Long Range Mafic-Ultramafic Complex were interpreted to result from obduction and closure of the ancient Iapetus Ocean. Greenschist facies overprinting assemblages developed along shear zones in the Long Range Mafic-Ultramafic Complex were believed to result from later orogenic processes on the basis that they also affect surrounding Carboniferous rocks.

U/Pb zircon ages of 477.5 +1.3/-1.0 and 481.4 +4.0/-1.9 Ma have been reported for the Annieopsquotch Complex (Dunning & Krogh, 1985). Additional age dates of ophiolites from various places in Newfoundland (e.g.

Bay of Islands, Betts Cove, Pipestone Pond and Coy Pond) reveal a time span of only 17 Ma for ophiolite formation (Dunning & Krogh, 1985). It is widely accepted that emplacement of the ophiolites began soon after their formation and the emplacement process had at least started during the Ordovician Taconian Orogeny.

2.5.5 Gabbro/Diorite Intrusions

Figure 2-1 shows the location of gabbro/diorite intrusions in the northeastern Dashwoods subzone that are interpreted to be Silurian in age. Several of these bodies (e.g. Boogie Lake Intrusion) were recognized by Dunning (1984) near the Annieopsquotch Complex (Figs. 2-1 and 2-3). The Boogie Lake Intrusion consists of gabbro and differentiates of hornblende diorite and biotite monzonite and is not penetratively deformed. A U/Pb zircon age of 435 +6/-3 Ma (i.e. Silurian) was reported for the intrusion by Dunning et al., (1990).

The Main Gut Intrusion (Fig. 2-1) consists of a body of tholeiitic gabbro/diorite containing leucogabbro in various forms (e.g. pods, sheets, dikes etc.) and later cross-cutting diabase dikes (Carew, 1979). A less extensive noritic body with well-developed cumulate layering occurs to the east, and disrupted ultramafic occurrences lie to the west. Figure 2-4 shows a simplified geological map of this area. The ultramafic bodies to the west of the main gabbroic body consist of serpentinite and metapyroxenite and their host rock was initially mapped as granite (Carew, 1979). Subsequent mapping by van Berkel (1986) resulted in revision to the

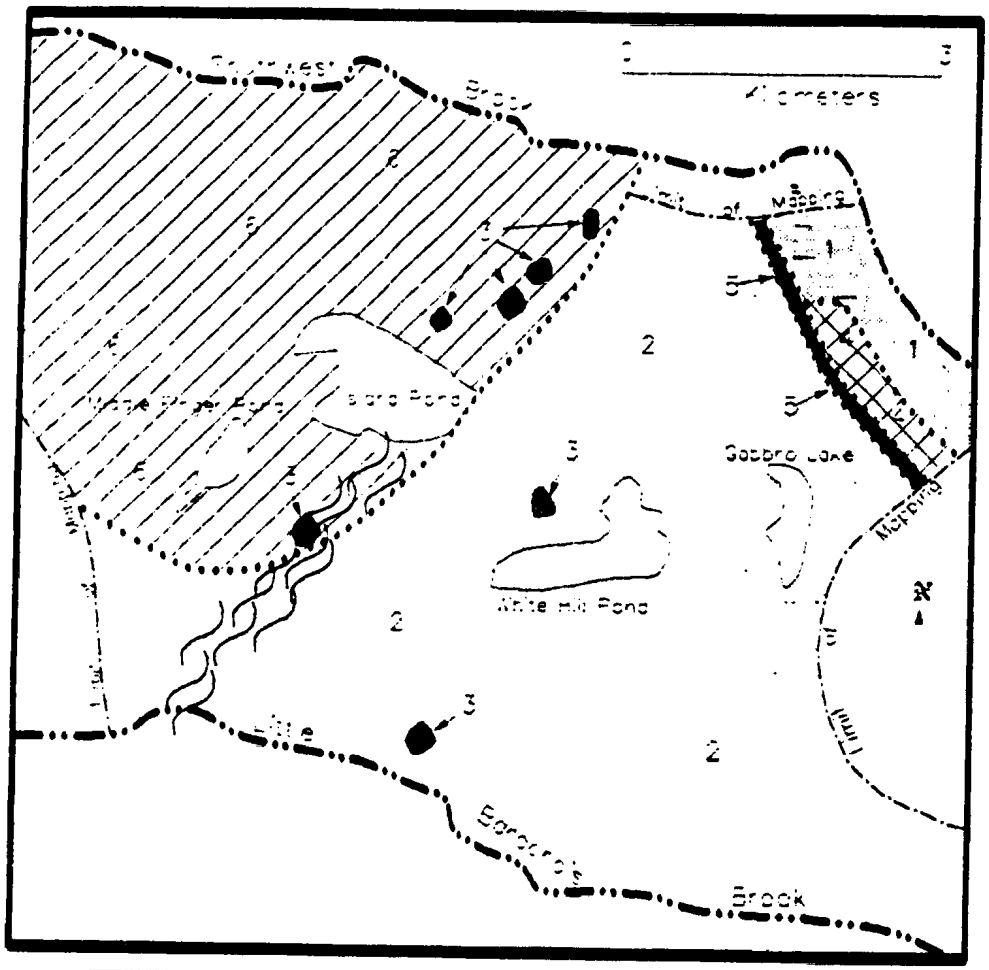

Fig. 2-4. Simplified geological map of the Main Gut Intrusion (modified from Carew, 1979 and van Berkel, 1985).

geology in this area and the granite was remapped as metasediments. In this context, these bodies are probably an extension of the mafic-ultramafic rocks and metasedimentary belt examined in this study.

The relationship between the three bodies of mafic-ultramafic rocks in this area is not clear, and Carew was unable to determine if there was a genetic link between them. However several aspects about this area are important to the present study and should be noted here. Metagabbro and amphibolite occur side by side with the ultramafic occurrences in the metasedimentary rocks. The main gabbro/diorite body is deformed at least locally, as Carew noted the layering (foliation?) in this body is steepened, hornblendes are bent and kinked and localized shear zones are common especially near the Long Range Fault. Greenschist facies assemblages of actinolite, chlorite and epidote are locally developed. A U/Pb zircon age of 431 ± 2 Ma was reported for the Main Gut Intrusion (Dunning et al., 1990).

Currie & van Berkel (1989) suggested that several other mafic plutonic bodies belong to this Silurian suite of intrusives (Fig. 2-1) and described all of them as gabbro/diabase bodies which exhibit "within-plate" to "island-arc" geochemical affinities. There are however, conflicting opinions as to which bodies are ophiolite fragments and which ones are later non-ophiolitic intrusions. For example, the mafic-ultramafic rocks near John's Brook Lake (Fig. 2-3) was initially described by Dunning & Herd (1980) and interpreted as an ophiolite fragment on the basis of the similarity of lithologies to other ophiolites. This body contains a sequence of harzburgite, dunite and gabbro. The harzburgite and dunite is variably

serpentinized and chloritized, and contains a weak cleavage (van Berkel & Currie, 1988).

However, this same body is described by Currie & van Berkel (1989) as fresh except for minor alteration and shows no sign of a penetrative foliation. It was therefore correlated with the other Silurian intrusions. Clearly there are conflicting opinions and interpretations among authors. One thing that is clear however, is that there are Silurian mafic intrusions as well as Ordovician ophiolitic rocks within the Dashwoods subzone. Further work is required to assign individual bodies into these categories.

CHAPTER 3

GEOLOGY OF THE STUDY AREA

3.1 INTRODUCTION

The study area (Fig. 3-1), includes clastic metasedimentary rocks, mafic-ultramafic rocks and a suite of granitoid rocks that characterize the Dashwoods subzone of the Dunnage zone elsewhere. The metasedimentary rocks, comprising metapsammites and metapelites, contain thin discontinuous belts of metamorphosed mafic-ultramafic rocks and are intruded to the east by the granitoid suite that includes tonalite, hornblende-biotite granodiorite and minor granite that extends at least the entire length of the Dashwoods subzone. The distribution of the different types of granitoid rocks in the complex is not well known and they are not separated in Figure 3-1. The pelitic metasediments lie to the east of the metapsammites in apparent conformity although both units are metamorphosed in the amphibolite facies and original contact relations are obscured. The contact is apparently gradational over several hundred metres.

This chapter describes the lithologies within the map area with emphasis on the pelitic metasedimentary rocks and the metamorphosed mafic-ultramafic rocks contained within them. General descriptions of the psammitic rocks and the granitoid suite are also included, for comparison with the units elsewhere in the Dashwoods subzone.

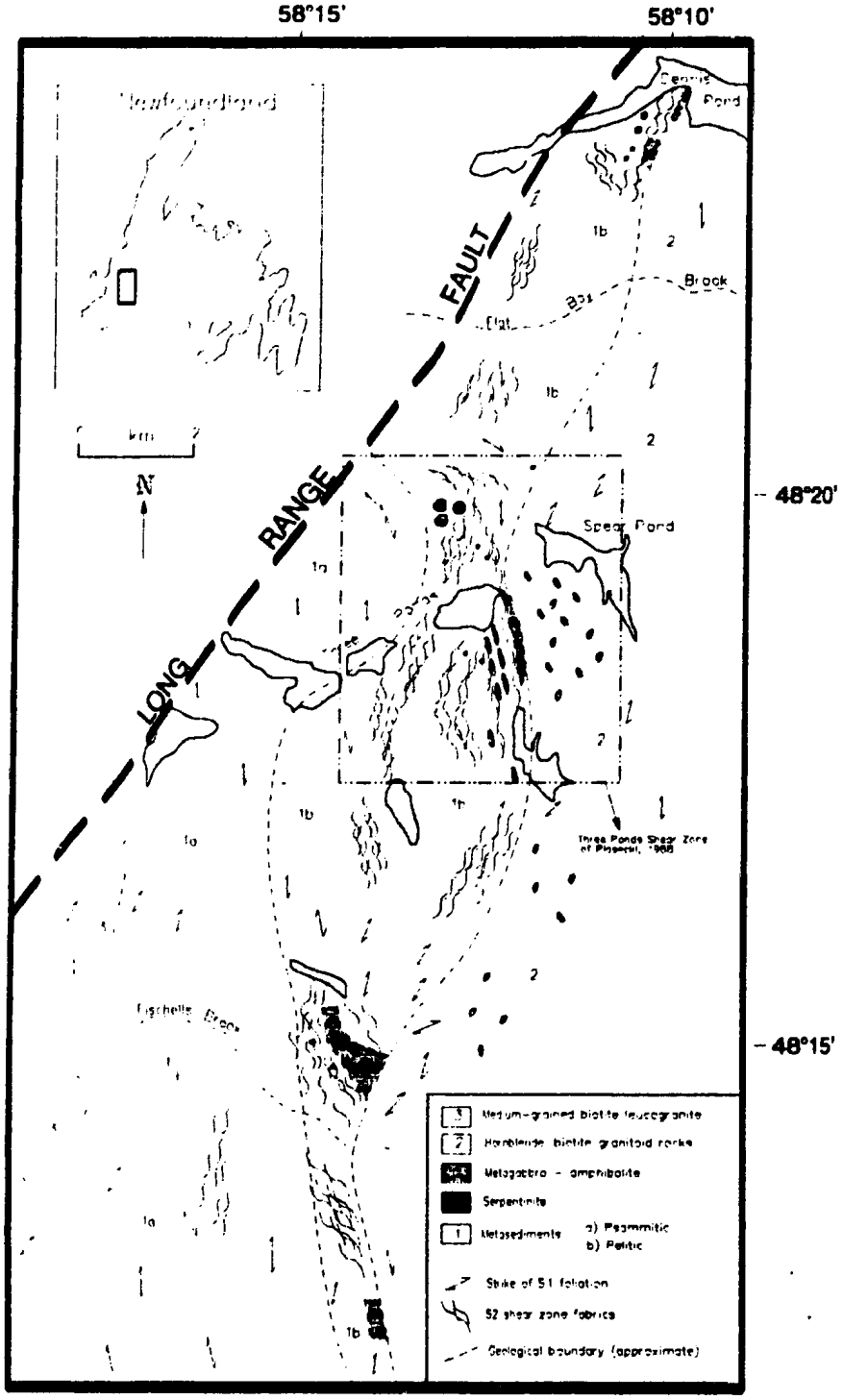

Fig. 3-1. Simplified geological map of the study area.

3.2 METASEDIMENTARY ROCKS

The metasedimentary rocks are separated into two main units, a predominantly psammitic unit to the west and southwest (Fig. 3-1) and a less aerially extensive pelitic unit to the east. The units are correlated with clastic metasedimentary rocks of the Fleur de Lys Supergroup in northern Newfoundland on the basis of similar stratigraphic position along the eastern edge of the North American miogeocline. On this basis the age of the metasedimentary rocks of this study would be between Late Upper Proterozoic and Early Ordovician (i.e. similar to the Fleur de Lys Supergroup). The lower limit is not precisely established but the upper limit is constrained by intrusion of the granodiorite which is dated at 456 ±3 Ma as noted in Chapter 2.

3.2.1 Psammitic Metasedimentary Rocks

Samples of the psammitic metasedimentary rocks near the contact with the pelitic rocks were examined as part of this study. The psammites are biotite + quartz + plagioclase feldspar ± garnet ± K-feldspar gneisses with variable amounts of retrograde chlorite and muscovite. The well-developed stromatic gneissosity is defined by biotite-rich layers alternating with quartz + plagioclase feldspar-rich layers (Fig. 3-2). Layering is variable in thickness but generally on a cm scale. A schistosity defined by the preferred orientation of biotite is developed in the biotite-rich layers but the quartz + plagioclase feldspar-rich leucosomes have no preferred orientation of their constituent minerals.

Fig. 3-2. Two samples of the metapsammitic rocks showing well-developed stromatic layering defined by alternating quartz + plagioclase (± K-feldspar) + minor biotite leucosomes and biotite (± garnet) + quartz + minor plagioclase melanosomes. Secondary muscovite and chlorite are common.

Farther to the southwest of the area shown in Figure 3-1, the unit has been mapped only on a reconnaissance basis, but the stromatic layering appears to be a characteristic feature. The pervasive and dense network of leucosomes suggests that at least some may have formed by partial melting of the psammite, an interpretation reinforced by the discontinuous nature of some of them. However an injection origin for some of the leucosomes cannot be ruled out and is indeed likely on account of their tonalitic composition.

The psammitic gneiss unit has been penetratively deformed at least two times. Figure 3-3 shows original sedimentary layering that is subparallel to metamorphic (gneissic) layering, implying the existence of large scale isoclinal folding. The leucosomes were subsequently irregularly refolded about more open fold axes.

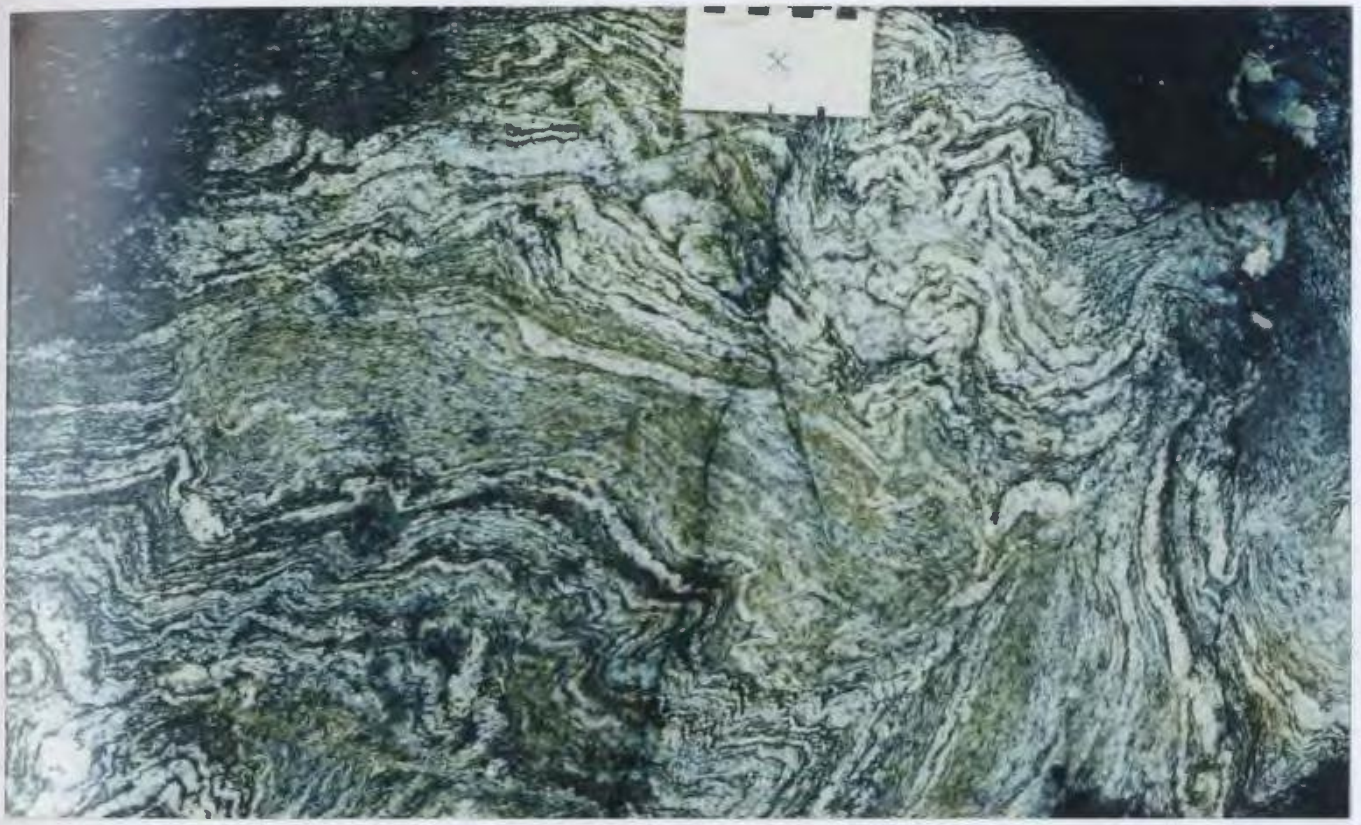

Fig. 3-3. Complexly folded stromatic layering in semi-pelitic gneiss south of Fischells Brook. Gneissic layering is subparallel to original sedimentary layering that can be seen as compositional banding. Scale is 9 cm across.

Figure 3-4 shows deformed, stretched and pulled apart leucosomes and Figure 3-5 shows a porphyroclastic augen texture, both features that developed in high strain zones.

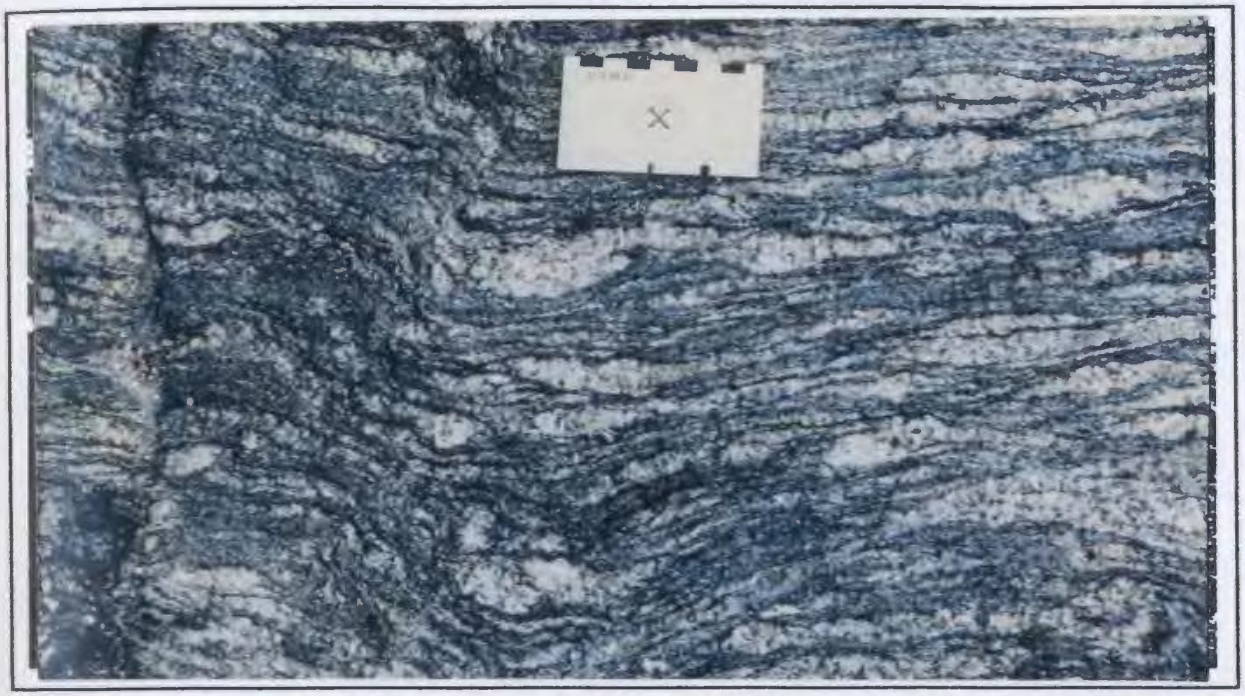

Fig. 3-4. Psammitic gneiss with deformed and sheared leucosomes composed predominantly of quartz-feldspar in a biotite-rich matrix. Scale is 9 cm across.

Fig. 3-5. Psammitic gneiss similar to that in Figure 3-4, although more highly sheared. Quartz-feldspar aggregates and feldspar porphyroclasts are substantially smaller and show augen texture in biotite-rich matrix. Scale is 9 cm across.

Chorlton (1983) describes large scale, high strain domains associated with the metasediments in the southwestern part of the Dashwoods subzone (Fig. 2-2) and the psammitic gneisses in the study area are thus probably part of a much larger scale high strain zone developed throughout much of the Dashwoods subzone.

Metapelitic layers occur locally within the psammitic gneiss unit but their abundance and distribution are not well known. One example observed in this study contains abundant sillimanite (fibrolite), garnet, quartz, plagioclase feldspar and biotite along with secondary muscovite. Metamorphic interpretations of this sample are discussed further in Chapters 5 & 6.

3.2.2 Pelitic Metasediments

The rocks in the pelitic metasedimentary unit are variable in grain size, texture and overall rock fabric. The variability is interpreted to result in part from "in situ" partial melting (see Chapter 6) and in part from differing degrees of deformation (see Chapter 5). In general, the rocks within this unit can be separated into unsheared and sheared varieties.

Figure 3-6 shows four samples of unsheared pelitic rocks. Leucosomes are quartz + plagioclase feldspar-rich but cordierite has been recognized locally. Melanosomes consist mainly of sillimanite + biotite + garnet + Fe-Ti oxides. Locally a thin, irregular gneissic banding is

developed that is parallel to compositional layering, a relationship that is interpreted to have formed as a result of regional isoclinal folding.

Fig. 3-6. Four samples of unsheared leucosome-poor pelitic metasediments showing that generally the leucosomes are not as well-developed as those in the metapsammites (Fig. 3-2). Leucosomes are quartz + plagioclase + minor biotite + cordierite (in places) and melanosomes are biotite + sillimanite-rich in addition to garnet in places.

Although the pelitic metasedimentary rocks do contain a gneissosity, it is not as well-developed nor as consistent in orientation as that in the psammitic metasedimentary rocks. A schistosity defined by the preferred orientation of biotite is well-developed in the melanosomes.

Locally the unsheared pelitic metasediments have been engulfed by tonalite (Fig. 3-7). In these examples, the rocks are composed predominantly of coarse-grained quartz + plagioclase feldspar with irregularly shaped pelitic enclaves of cordierite + garnet with retrograde sillimanite, biotite, staurolite, kyanite and chlorite. These retrograde minerals do not have a preferred orientation and any preexisting fabric that may have been developed in these rocks is completely obliterated.

Fig. 3-7. Two samples of metapelite engulfed by tonalite. Note no layering or foliation is developed. Dark patches are composed of pinitized cordierite, garnet, sillimanite and biotite with retrograde chlorite, staurolite and kyanite.

The majority of the rocks in the pelitic unit contain a protomylonitic to mylonitic fabric (Fig. 3-8) commonly with associated layer-parallel quartz plates (Fig. 3-9) both of which imply the existence of high strain. The quartz plates are interpreted to be a syn-shear zone product (Piasecki,

Fig. 3-8. Mylonitic fabric developed in shear zone rocks in the metapelite unit.

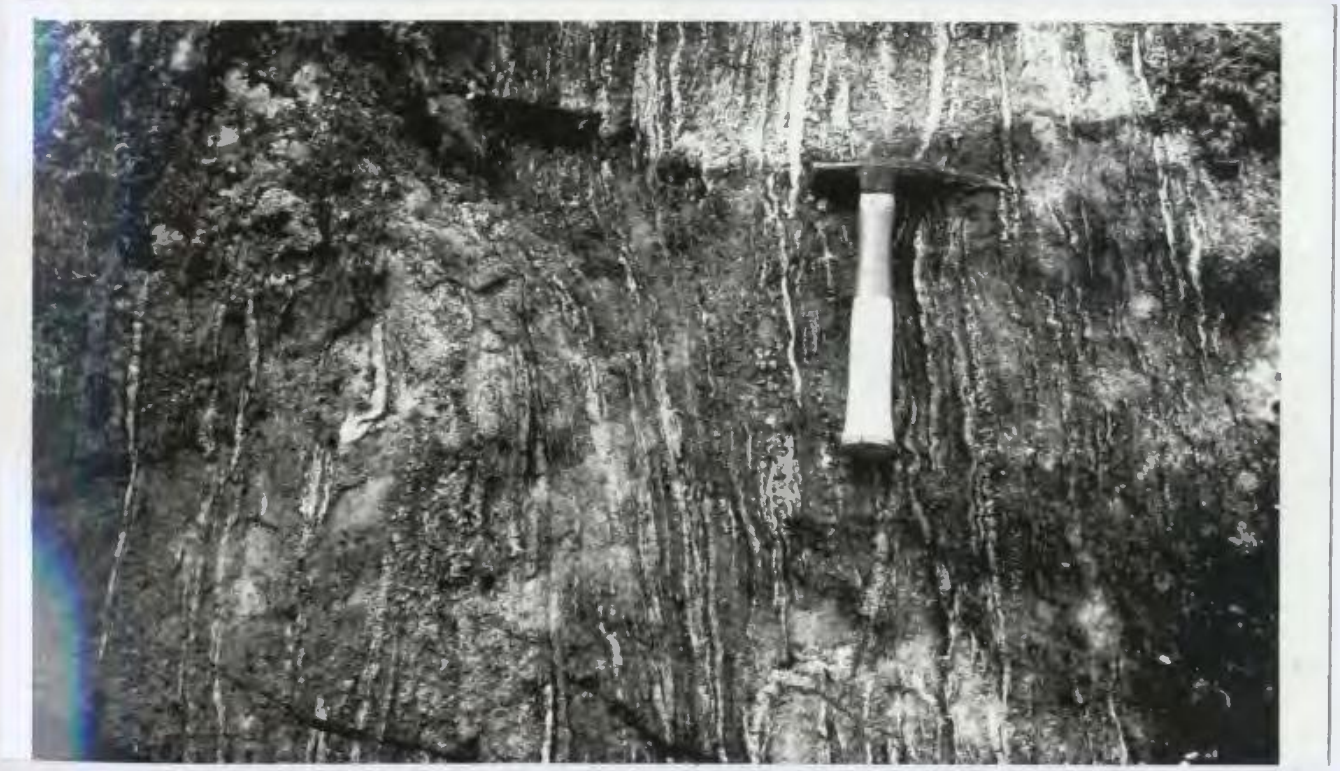

Fig. 3-9. Layer parallel quartz plates interpreted to develope at the time of shearing in the pelitic metasediments. The quartz plates are parallel to the mylonitic fabric in the host rocks. Photo taken in the Three Ponds area. Hammer for scale.

1988). The shear zone fabric overprints the high grade gneissic fabric and there is a complete gradation between the two. The sheared rocks are partially to completely retrogressed to a greenschist facies assemblage consisting of quartz, sericite, chlorite, epidote and Fe-Ti oxides. Further microstructural evidence of mylonite fabrics and shear zones is presented in Chapter 5 and more details of the metamorphism are presented in Chapters 6 & 7.

The contact relationship of the pelitic metasedimentary rocks with the psammitic rocks to the west and southwest is gradational and a precise boundary between the two units is difficult to map in the field. However the boundary is quite distinct on an aeromagnetic map (Fig. 3-10). The psammitic rocks have a much lower magnetic signature than the pelitic rocks that are characterized by both higher values and more magnetic relief. This presumably reflects the abundance of Fe-Ti oxide minerals in the pelitic rocks and the lack of these minerals in the psammitic rocks.

The contact with the granitoid rocks to the east of the pelitic metasediments is intrusive and occurs over several hundred metres. Numerous, small scale, concentric magnetic highs are the typical pattern of the granitoid suite on the aeromagnetic anomaly map.

3.3 AMPHIBOLITE BODIES IN THE PSAMMITIC METASEDIMENTARY ROCKS

Amphibolite inclusions are common in the psammitic unit, but have been mapped only on a reconnaissance basis. They are pre-kinematic with

Fig. 3-10. Aeromagnetic map of the study area (part of GSC map 7050G, 1968). Scale 1:253,440.

respect to the fabric developed in the metasediments as seen in Figure 3-11 where the fabric in the metasedimentary gneisses can be seen to wrap around a small amphibolite inclusion.

Fig. 3-11. Gneissic layering wrapping around an amphibolite inclusion in psammitic metasediments. Scale is 9 cm across.

Figure 3-12 shows an amphibolite inclusion extensively veined by undeformed tonalite, a feature common to all lithologies in the unit. The inclusions continue to the southwest and increase in abundance towards the Long Range Mafic-Ultramafic Complex.

3.4 MAFIC-ULTRAMAFIC ROCKS IN THE PELITIC METASEDIMENTS

In the pelitic metasedimentary unit, mafic-ultramafic rocks outcrop along several north-south trending belts that extend from Dennis Pond to

Fig. 3-12. Amphibolite inclusion veined by undeformed tonalite in the psammitic metasedimentary rocks . Scale is 9 cm across.

south of Fischells Brook (Fig. 3-1). They occur as isolated bodies that range in size from centimetres to several metres across (Figs. 3-13 & 3-14) up to larger linear ridges that have been traced for over a kilometre. The larger bodies are typically intruded by granitoid rocks that results in the formation of agmatite zones (Fig. 3-15).

Three lithologically distinct types of metamorphosed mafic-ultramafic rocks have been recognized within the metapelites. These are: 1) serpentinite (metadunite); 2) Ca amphibole-rich rocks (metapyroxenite); and 3) metagabbro-amphibolite. Both mafic and ultramafic rocks are interlayered locally, but more commonly bands of one lithology predominate. In the larger linear ridges where the granitoid rocks intrude, the mafic and

Fig. 3-13. Talc inclusion in pelitic metsedimentary rocks north of Fischells Brook. Shear fabric in the metasediments wraps around the inclusion indicating the mafic-ultramafic rocks are pre- to syn- kinematic. Scale is 9 cm across.

Fig. 3-14. Serpentinite inclusion in metasedimentary rocks north of Three Ponds. The inclusion is several metres across. Hammer for scale.

Fig. 3-15. Agmatite formed by the intrusion of granitoids into metagabbro. North of Fischells Brook. Scale is 9 cm across.

ultramafic lithologies have been observed in close proximity to each other. The three different rock types are described below.

3.4.1 Metadunite

The metadunites are variable in color depending on the degree of hydration. Olivine-rich samples weather a rusty yellow to brown color, whereas serpentine-rich samples commonly weather white but are dark grey on fresh surfaces. Reddish brown zones enriched in carbonate (magnesite) and bluish white zones enriched in talc are developed locally.

The majority of the metadunites are composed of combinations of serpentine minerals (lizardite, chrysotile and antigorite) ± olivine. Accessory minerals include layered and disseminated chromite, magnetite, chlorite, talc, and carbonate. Cross-cutting veins of chrysotile and chlorite are common. Microprobe analyses of olivine, serpentine, chromite, and carbonate are presented in Appendix A and discussed in Chapters 4 and 6.

Layering in the serpentinites is developed locally, and varies from a centimetre to half a metre in scale. The layering is of two types: 1) an igneous layering defined by accumulations of chromite (probably cumulate in origin, Fig. 3-16); and 2) a layering (fabric) composed mainly of different proportions and types of serpentine ± olivine (Figs. 3-17 & 3-18).

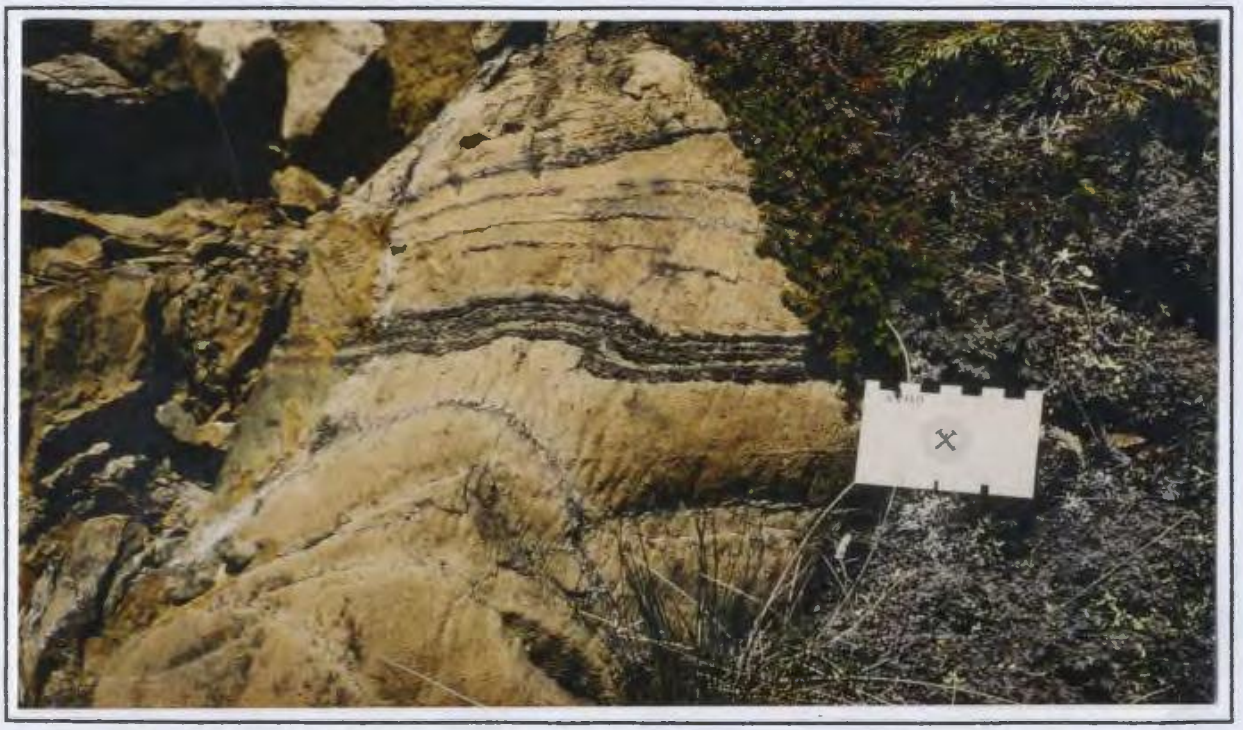

Fig. 3-16. Relatively little deformed chromite layers in serpentinite near Dennis Pond. Scale is 9 cm across.

Fig. 3-17. Tectonic layering in ultramafic rocks near Dennis Pond. Layering is defined by different proportions and types of serpentine (± olivine) and is interpreted to be the result of shearing. Scale is 9 cm across.

Fig. 3-18. Tectonic layering in serpentinite defined by various proportions and types of serpentine (± olivine). This layering is interpreted to result from shearing. The "fold-like" structure at the bottom right may be an isoclinal fold or a boudinaged layer, but in either case is the result of high strain. At (A) in the photograph, thin, low-angle cross-cutting fibers of serpentine (chrysotile) are also a result of shearing. Located near Three Ponds. Scale is 9 cm across.

In these examples, the fabric is interpreted to be the result of shearing. The "fold-like" feature in the bottom right of Figure 3-18 may be an isoclinal fold or a boudinage structure. In either case it is indicative of high strain.

In some areas mafic rocks are interlayered with those of ultramafic composition. Figure 3-19 shows an example of interlayering of metagabbro/amphibolite and serpentinite/metapyroxenite north of Fischells Brook. The straight layering in this example is defined by compositional bands comprising serpentinite, metapyroxenite, and layers of gabbroic composition.

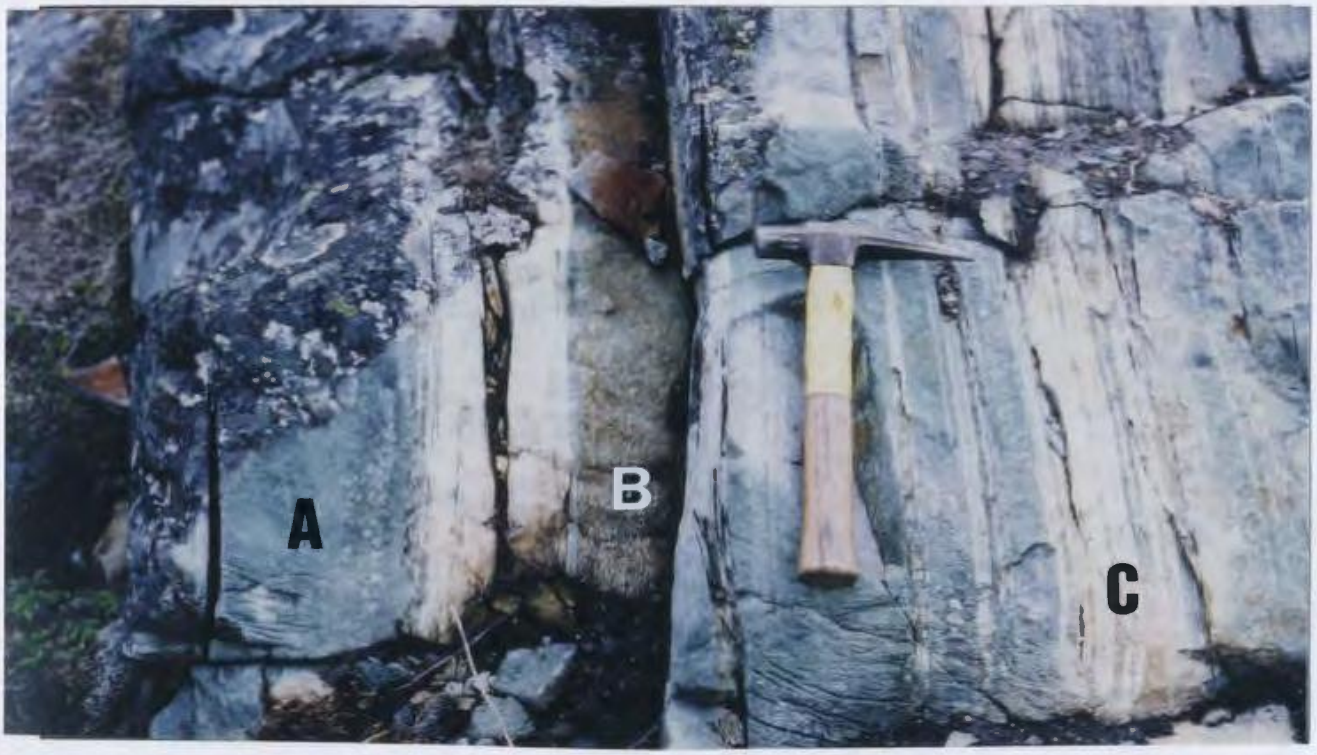

Fig. 3-19. Layered mafic-ultramafic rocks. A) Metapyroxenite layer. B) Metagabbro layer. C) Serpentinite layers. This layering is interpreted to be the result of high strain and is located along strike from quartz plates developed in metagabbro (see Figure 3-20). Located north of Fischells Brook. Hammer for scale.

Straight fabrics such as these are of tectonic origin, an interpretation reinforced by the presence of shear zone fabrics with quartz plates in metagabbro (Fig. 3-20) several metres along strike from this outcrop. Therefore, the layering shown in Figure 3-19 is interpreted to be a high-strain mylonitic fabric.

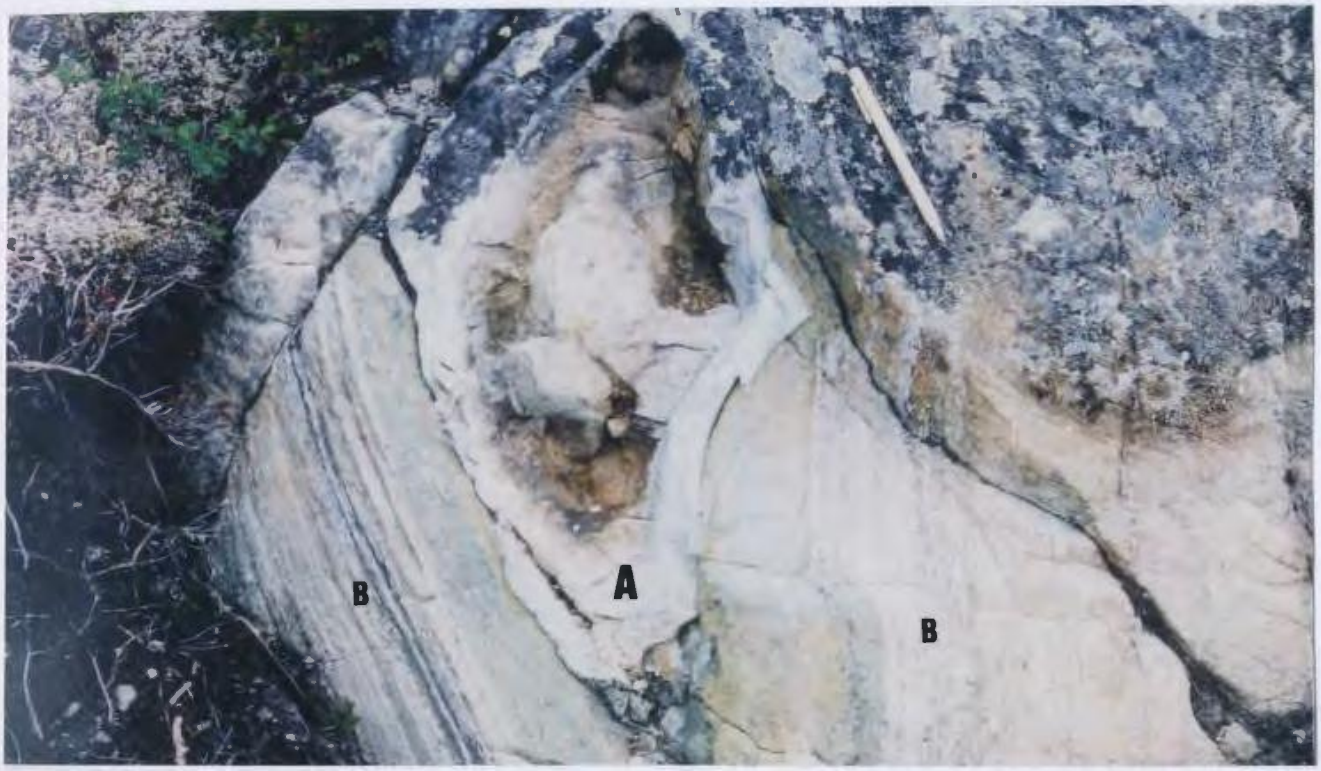

Fig. 3-20. Serpentinite inclusion in greenschist facies mafic rocks near Fischells Brook. A) Rim of talc around inclusion. B) Quartz plates developed in mafic host rocks. Pencil for scale.

In several places throughout the map area, the serpentinites display a concentric mineralogical zonation that can be attributed to reaction between the inclusion and the host rock. Almost monomineralic concentric rims of talc, tremolite and chlorite from the center to the rims respectively have been observed. Inclusion cores may still have serpentine preserved, or reaction may have proceeded to such a stage that the core is entirely replaced by talc rimmed by tremolite. Figure 3-20 shows a small inclusion

of serpentinite with a single monomineralic rim of talc.

3.4.2 Metapyroxenite

These rocks are typically dark green in color and composed of medium to coarse-grained randomly orientated tremolite and/or actinolite with up to 20% chlorite. Microprobe analyses of several amphiboles from these rocks are presented in Appendix A and discussed in Chapter 6. Plagioclase is notably absent in these rocks, distinguishing them from metagabbro. Figure 3-21 shows an example of the tremolite-rich rocks where subsequent granitoid intrusion has formed an agmatite.

Fig. 3-21. Mafic agmatite of tremolite-rich metapyroxenite intruded by granitoids. North of Fischells Brook. Scale is 9 cm across.

In places, the inclusions in the granitoid have the appearance of pillow breccias but on closer observation, layering can be found in some of the better preserved examples. The rounded nature of some of these inclusions is probably due to partial assimilation by the granitoid.

The protolith of these rocks is uncertain. Locally they are interlayered with serpentinite and metagabbro, but they are chemically and mineralogically distinct from both these lithologies (Appendix D). Considering the present mineralogy, the original ultramafic protolith was most likely a clinopyroxenite.

3.4.3 Metagabbro/Amphibolite

The mafic rocks vary substantially in grain size from fine-grained to pegmatitic. Most rocks contain greenschist facies assemblages of chlorite, tremolite-actinolite, clinozoisite-epidote, ± quartz, ± biotite, ± muscovite, ± Fe-Ti oxides. However, some samples contain hornblende-plagioclase assemblages suggesting that they were previously metamorphosed in the amphibolite facies prior to greenschist facies retrogression. In many cases the greenschist facies retrogression is not pervasive and various combinations of amphibolite and greenschist facies mineralogy are preserved.

Because of the metamorphism, disrupted nature and co-mingling of the rocks, a proper igneous classification of the major lithologies is difficult. A possible range of igneous compositions is diorite, leucogabbro,

gabbro and anorthositic gabbro based on grain size and present mineralogy. However many of the mafic rocks appear similar to that shown in Figure 3-22 which is a homogeneous gabbro that still preserves relict igneous textures. No fine-grained extrusive rocks such as basaltic flows or pillow lavas have been identified in the map area.

Fig. 3-22. Metagabbro inclusions in granitoid rocks near Fischells Brook. The metagabbro still has igneous gabbroic texture preserved. Hammer for scale.

In addition to the massive type of metagabbro, a layered variety has also been recognized (Fig. 3-23). The centimetre scale layering is defined by green amphibole (tremolite - actinolite) alternating with clinozoisite - epidote-rich layers. The origin of the layering is ambiguous. One possibility is that the original gabbro contained cumulate phase layering composed of variable proportions of plagioclase and clinopyroxene. However in light of the pervasive deformation throughout the map area (see Chapter 5), the

layering could also be the result of metamorphic differentiation during shearing.

Fig. 3-23. Layered metagabbro. Layering may be original phase layering of plagioclase and clinopyroxene or may be the result of shearing in massive metagabbro shown in Figure 3-22. North of Fischells Brook. Scale is 9 cm across.

Such an origin is difficult to prove because the rock has subsequently been retrogressed to a greenschist facies assemblage, and the original microstructure has been obliterated. Although no stretched porphyroblasts have been noted in these rocks, recrystallization may have obliterated such features, and it is feasible that these rocks could have developed from the massive metagabbro shown in Figure 3-22.

3.5 UNDIFFERENTIATED GRANITOID SUITE

Although detailed mapping of the granitoid suite was not part of this

thesis, some examples were examined near the boundary with the pelitic metasediments. The granitoid rocks are fine to medium-grained and moderately foliated to massive (Fig. 3-24). The unit outcrops extensively to the east of the pelitic metasedimentary rocks and consists mainly of hornblende-biotite granodiorite, but also includes subordinate tonalite and granite. Amphibolite inclusions are common in the granitoid suite in the areas examined; they are similar to those in the metapsammites and metapelites and are probably related to them.

Fig. 3-24. Unfoliated granodiorite from the granitoid suite. Mafic minerals are hornblende and biotite.

3.6 FORMATION OF AGMATITE ZONES

Several of the examples from the previous discussions show well-developed agmatite zones consisting of mafic-ultramafic rocks engulfed by granitoid rocks. It is important to discuss here the timing of formation of these zones. In several places throughout the map area, it is obvious the mafic-ultramafic rocks have been intruded by the granitoid suite that lies to the east of the metasedimentary rocks. This is especially true along their contact. However in other areas, the mafic-ultramafic rocks are intruded by tonalitic rocks that are not obviously linked to the granitoid suite to the east. This is true especially where the compositions of the granitoid rocks are apparently different (compare Figures 3-22 and 3-24). The tonalites in Figure 3-22 do not contain hornblende whereas the granitoid suite to the east typically contains hornblende as the mafic phase (Fig. 3-24). In light of this, it is possible that at least some of the agmatite zones formed as a result of unrelated? granitoid intrusions. Thus it is also possible that some of the agmatite zones formed prior to their emplacement into their present stratigraphic position. This would require additional work to prove.

3.7 MINOR LITHOLOGIES IN THE MAP AREA

Additional lithologies found in minor amounts throughout the map area include undeformed two mica granite, large biotite bearing pegmatites and large massive quartz veins several metres in thickness. The granite outcrops most extensively in the Dennis Pond area and intrudes all

previously discussed rock units. It occurs as thin veins or sheets, but is not large enough to be mapped as a separate unit. The pegmatites and quartz veins are found throughout the map area. The quartz veins are up to two metres in width and undeformed, cross-cutting all other lithologies. They are younger than the swarms of quartz plates that occur in shear zones in the pelitic metasedimentary unit (see Chapter 5).

CHAPTER 4

ORIGIN OF THE MAFIC-ULTRAMAFIC ROCKS

4.1 INTRODUCTION

One of the objectives of this study was to determine the origin of the mafic-ultramafic rocks. Genetic classification schemes for mafic-ultramafic rocks have been the focus of much debate in the geological literature and are constantly revised as new data becomes available. Of relevance to this study is the subdivision of mafic-ultramafic rocks into two main categories: 1) ophiolites (either an entire sequence or parts of it, or ophiolitic fragments in mélange zones); or 2) mafic-ultramafic differentiates of plutons intruded into continental crust. Since it is well established that ophiolites represent parts of oceanic crust and upper mantle material and imply the previous existence of an ocean, the distinction between these two mafic-ultramafic categories is essential to the understanding of the tectonic processes involved in the formation of any orogen.

The recognition of ophiolites however, especially in deformed and metamorphosed sequences is not always straightforward. Misra & Keller (1978) suggested that ophiolitic mafic-ultramafic bodies have certain characteristics that set them aside as a group from stratiform layered mafic-ultramafic complexes and concentrically zones plutons. These include: 1) irregular to lensoid form; 2) absence of chilled margins and contact

metamorphic effects; 3) high magnesian compositions of the constituent olivine, pyroxene and chrome spinel; 4) presence of a tectonic fabric; and 5) the presence of podiform chromite. In this context, it may be possible to use these and other criteria to distinguish ophiolitic bodies from other types of mafic-ultramafic intrusions. However, all these characteristics may be obliterated to a greater or lesser degree by metamorphism and deformation resulting from emplacement and/or subsequent orogenic processes.

Due to polymetamorphism in the field area (described in detail in Chapter 6), the use of detailed geochemical analysis based on trace element abundances to determine igneous petrogenesis would probably produce equivocal results, and has therefore not been attempted except for general descriptions presented in Appendix D. In the absence of convincing chemical correlations, the best approach to this problem is to compare the stratigraphy and tectonic setting of the mafic-ultramafic bodies of this study to surrounding rocks of known origin. An additional method of determining the igneous origin is to use mineral compositions (such as chrome spinels and olivine) as petrogenetic indicators. These two approaches are presented below.

4.2 COMPARISON OF THE MAFIC-ULTRAMAFIC ROCKS TO OPHIOLITES

Figure 4-1 shows schematic cross sections of the mafic-ultramafic bodies in the Dashwoods subzone that are interpreted to be ophiolitic fragments. These bodies are compared to a complete ophiolite stratigraphy

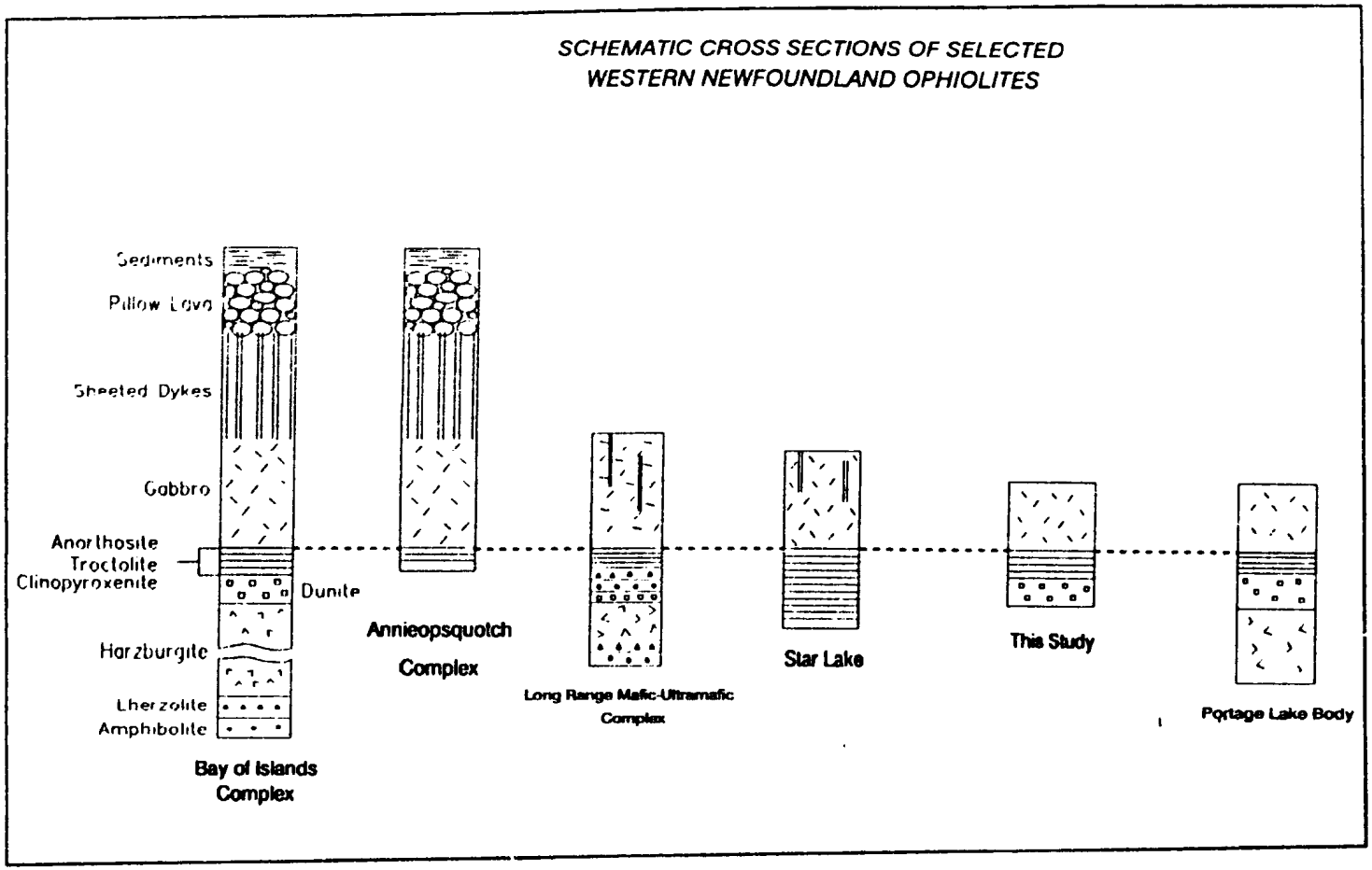

Fig. 4-1 Schematic cross-sections of selected western Newfoundland ophiolites

from the Bay of Islands Complex in western Newfoundland. It is evident that mantle rocks are relatively rare in the Dashwoods subzone ophiolites. Most bodies are composed of high level gabbro, interlayered rocks of the critical zone and dunite. Harzburgite occurs only in the Long Range Matic Ultramafic Complex and the Portage Lake body. The post tectonic Silurian intrusive rocks described in Chapter 2 consist mainly of hornblende gabbro/diorite. Segregations of pyroxenite and monzonitic to syenitic dikes are locally developed (Currie & van Berkel, 1989).

On the basis of lithology, it is apparent the mafic-ultramafic rocks of this study are not distinct and cannot be proven to be of ophiolitic origin. It is also apparent that the rocks of this study have some similar characteristics to the Silurian intrusions as described in Chapter 2 (see also Appendix D). One aspect that has been used to distinguish between the two types of mafic-ultramafic rocks in the Dashwoods subzone is the presence or absence of tectonic fabrics (Currie & van Berkel, 1988). However it is difficult to use the absence of deformation as a distinguishing characteristic because the mafic-ultramafic rocks may show (as in the rocks of this study) an entire spectrum from undeformed to highly deformed within the same body. However, on the basis of regional setting as presented in Chapter 2, the mafic-ultramafic rocks of this study are apparently part of the Long Range Mafic-Ultramafic Complex, although the sequence is disrupted throughout most of the Dashwoods subzone. In this context the rocks of this study are most likely of ophiolitic origin. If the rocks of this study are fragments of an ophiolite suite, then only a small central portion of the suite is present, i.e. the section from dunite,

through the transitional zone pyroxenites to gabbro. Interlayering of these lithologies occurs in the rocks of this study and is common at this stratigraphic location within ophiolite suites.

It is also apparent that if the mafic-ultramafic rocks of this study are ophiolitic in origin, then the Burgeo Road bodies (Fig. 2-1) are likely to be of the same origin. In view of their close proximity to the Main Gut Intrusion however, this interpretation is tentative and would require additional work to be conclusive.

4.3 CHROME SPINEL

4.3.1 Introduction

Spinels have the general composition $[X][Y]_2O_4$ where X and Y represent the tetrahedral and octahedral ions respectively. Spinels can be divided into two major groups: normal (aluminochrome) spinels and inverse (magnetite) spinels. The Ti-bearing ulvospinel group is not included here because the Ti content of chrome spinels in this study is less than 0.3 wt.% (Appendix A). In normal spinels, X ions are divalent (Fe^{2+} and Mg^{2+}) and Y ions are trivalent (Al^{3+} and Cr^{3+}). Inverse (magnetite) spinels have the Y site divided between divalent and trivalent ions and the X site contains Fe^{3+}.

The most common oxides in chrome spinel are MgO, FeO, Cr_2O_3, Al_2O_3, and Fe_2O_3 and typically comprise over 98% of components (Irvine, 1965).

From these five common oxides, six end-member spinel-group minerals predominate. These are:

Inverse Spinels

Magnetite $Fe^{3+}(Fe^{2+},Fe^{3+})_2O_4$

Magnesioferrite $Fe^{3+}(Mg^{2+},Fe^{3+})_2O_4$

Normal Al Spinels

Spinel $Mg^{2+}(Al^{3+})_2O_4$

Hercynite $Fe^{2+}(Al^{3+})_2O_4$

Normal Cr Spinels

Picrochromite $Mg^{2+}(Cr^{3+})_2O_4$

Chromite $Fe^{2+}(Cr^{3+})_2O_4$

The chemistry of these common chrome spinel group minerals is commonly portrayed in a prism with the upper apical edge representing the inverse spinels (Fig. 4-2). Three sides are used to plot the mineral chemistry two-dimensionally (A, B and C of Fig. 4-2); the triangular section representing the trivalent ions (Fe^{3+}, Cr^{3+} and Al^{3+}) and the horizontal axis representing the divalent ions Fe^{2+} and Mg^{2+}.

4.3.2 Composition of chrome spinels from this study

In this study chrome spinel occurs throughout the metadunites in the form of individual euhedral grains which comprise less than 1% of the rock and in veins. Microprobe analyses from six samples are presented in

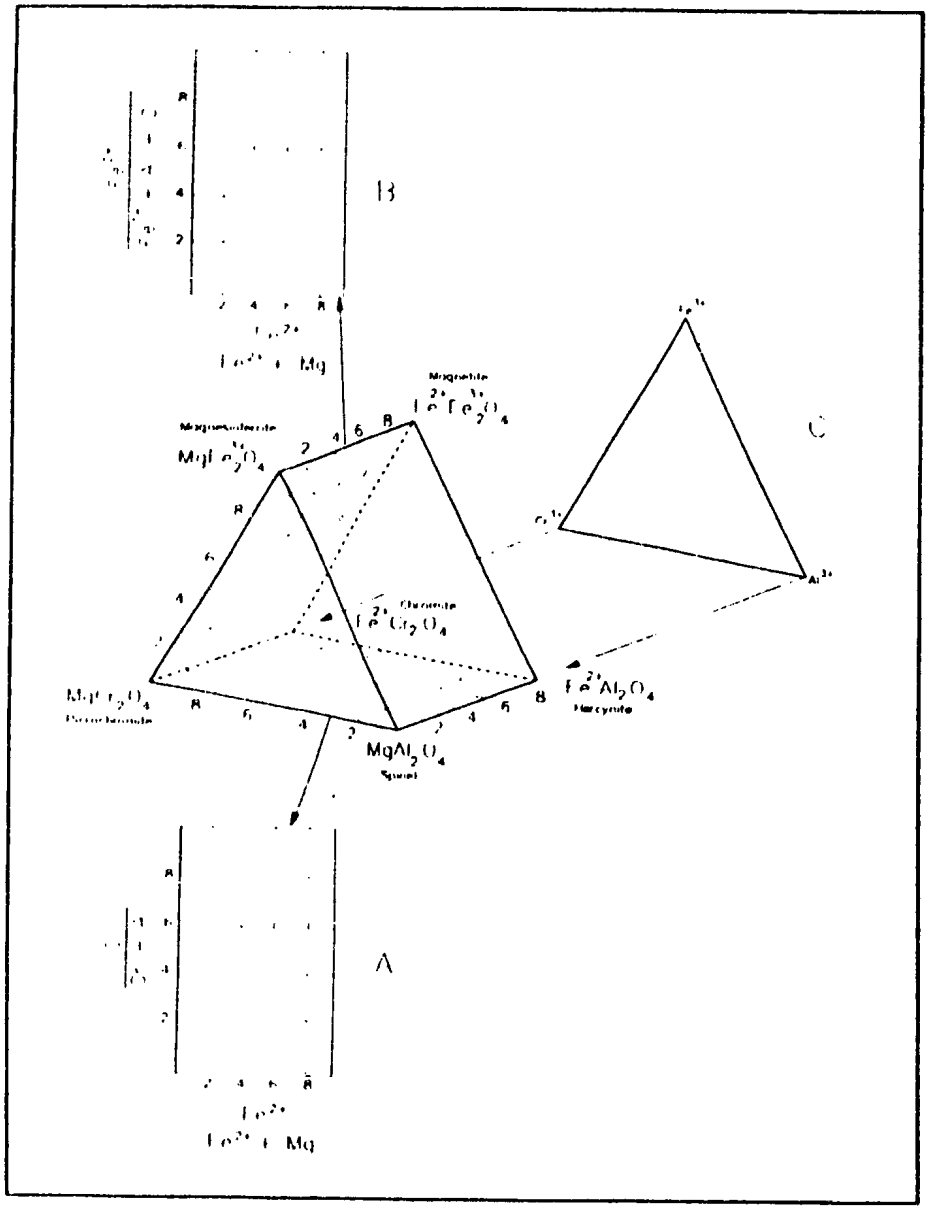

Fig. 4-2 The spinel prism showing the six principal end-members of chrome spinel. The three faces of the prism most often used to plot chrome spinel compositions are shown. The lengths of the rectangular faces are twice as long as the width and permit X^{2+} and X^{3+} variations to be compared graphically (Irvine, 1965).

Appendix A. The metadunite samples range from olivine-rich with no antigorite to antigorite-rich with no olivine. The grains in the antigorite-rich samples typically have discrete rims; either one rim of relatively light reflectance with a core of medium reflectance; or two rims, the inner rim of medium reflectance, the outer rim of light reflectance and the core is much darker than either rim (Fig. 4-3). The occurrence of one or two rims, and the size of rims is variable both within and between samples.

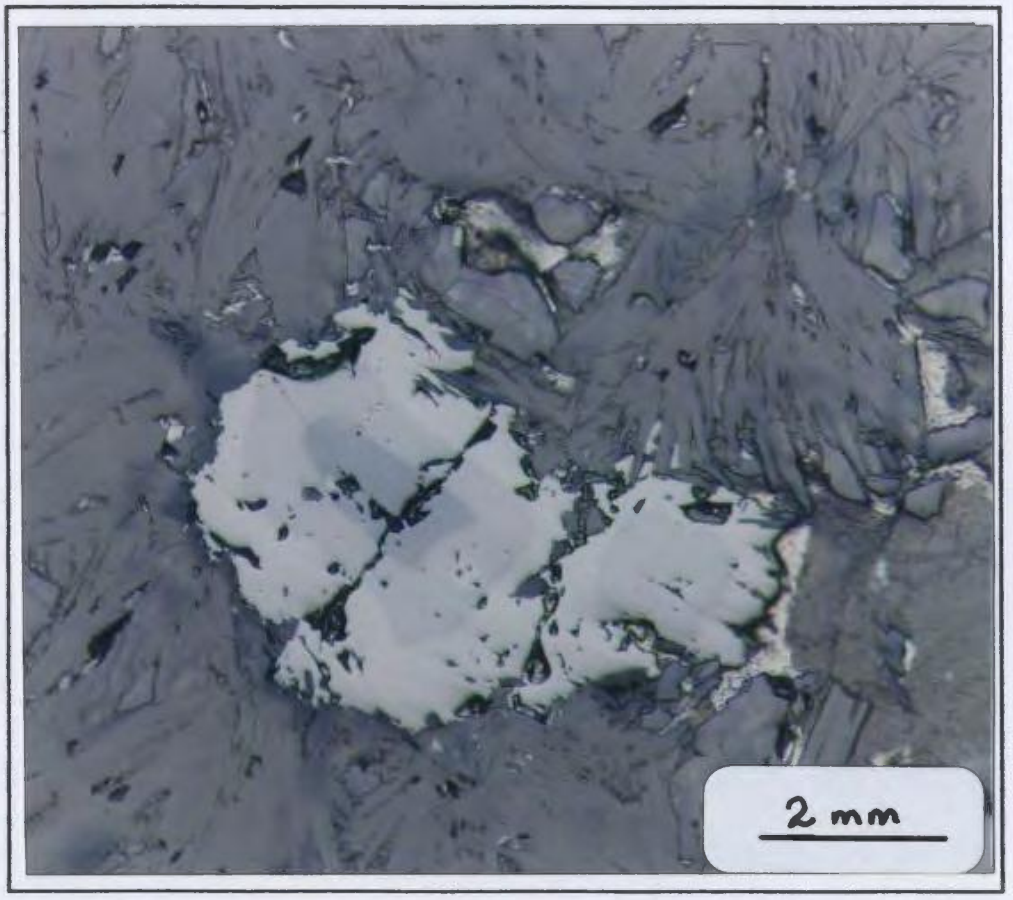

Fig. 4-3. Photomicrograph of zoning in spinel grains. The larger grain in the center of the photo has two rims and the smaller grain to the lower right of the photo has only one rim. (Reflected light).

Several microprobe traverses from the center to rim of grains with one rim were completed and the results of a typical traverse are shown in Figure 4-4. The rims have a substantial decrease in Al and Mg cations and a minor decrease in Cr. Fe^{2+} and Fe^{3+} increase at the rims.

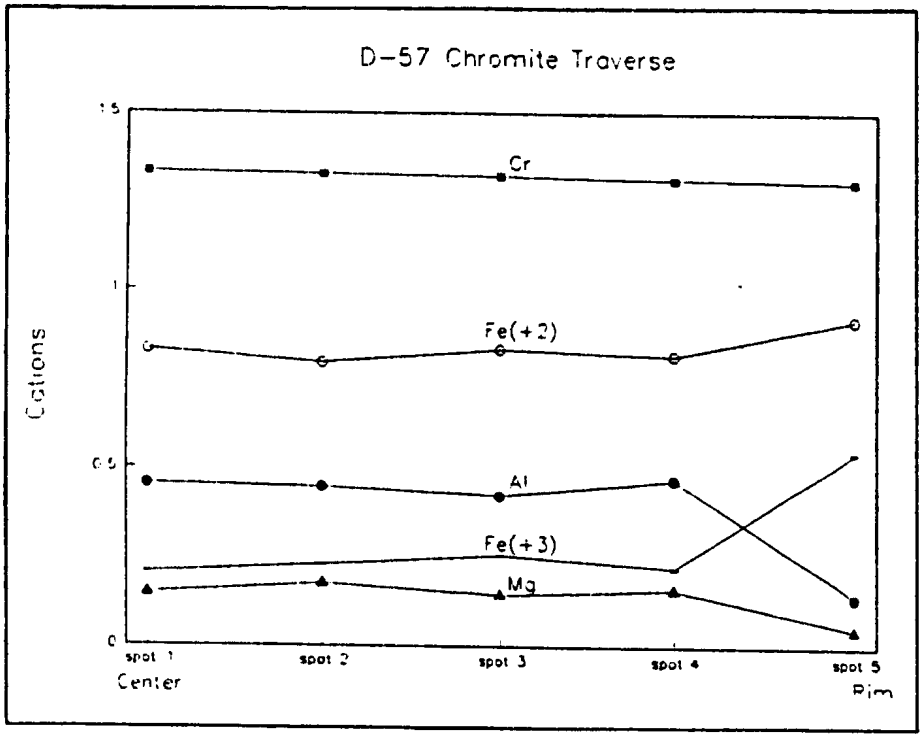

Fig. 4-4. Plot of Cr, Al, Fe^{2+}, Fe^{3+}, and Mg cations in the mineral formula from a microprobe traverse from the center to the rim of a chrome spinel grain. The rim is ferritchromite and contains less Al, Mg and Cr (minor decrease) and has an increase in Fe^{2+} and Fe^{3+}.

Figure 4-6 shows a plot of all chrome spinels analyzed in this study (both cores and rims) on the three principal faces of the spinel prism. Fe^{+3} was estimated by charge balance using ideal spinel stoichiometry (an example

Fig. 4-5. Plot of Cr# vs Fe^{3+}# for chrome spinels probed during this study.

Closed squares = chrome spinel from olivine-rich metadunite with mesh textured lizardite and less than 5% antigorite.

solid circles = chrome spinel from antigorite rock with minor lizardite but no olivine.

solid triangles = chrome spinel from layered antigorite-rich and olivine-rich sample.

open triangles = chrome spinels from massive antigorite samples. Arrows point from core to rim of the same grain.

All other analyses are cores of grains. The rims of chrome spinel grains generally have lower Al, Mg, and Cr and higher Fe^{2+} and Fe^{3+}. Also note the same variation of centers of grains between samples and within the same sample. This trend is interpreted to result from variable interaction with a fluid-phase. See text for further discussion.

Diagram and fields for ophiolites and stratiform intrusions from Irvine (1967).

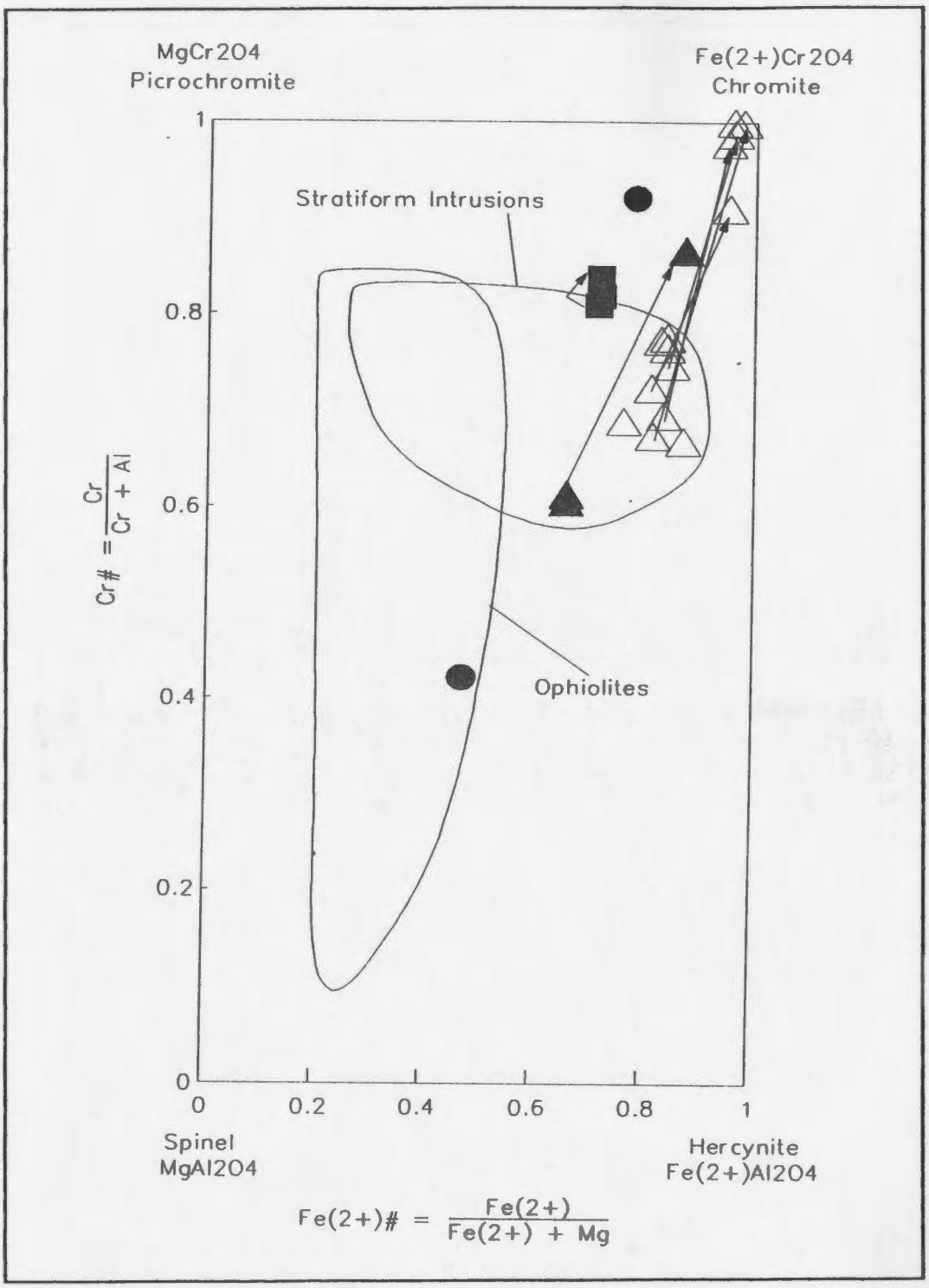
MgCr2O4
Picrochromite
Fe(2+)Cr2O4
Chromite
Stratiform Intrusions
Ophiolites
Cr# = Cr / (Cr + Al)
1
0.8
0.6
0.4
0.2
0
0
0.2
0.4
0.6
0.8
1
Spinel
MgAl2O4
Hercynite
Fe(2+)Al2O4
Fe(2+)# = Fe(2+) / (Fe(2+) + Mg)

Fig. 4-5 (Continued). Plot of Fe^{3+}# against Fe^{2+}# for chrome spinels from this study. The arrows point from cores to rims and show that rims have an increase in Fe^{3+} which also coincides with a decrease in Al and Mg. All other analyses are cores of grains. Note the variation of chemistry in the cores both between samples and in the same sample. The compositions of cores are interpreted to be modified by the interaction of the chrome spinels with a fluid phase. See text for further discussion.

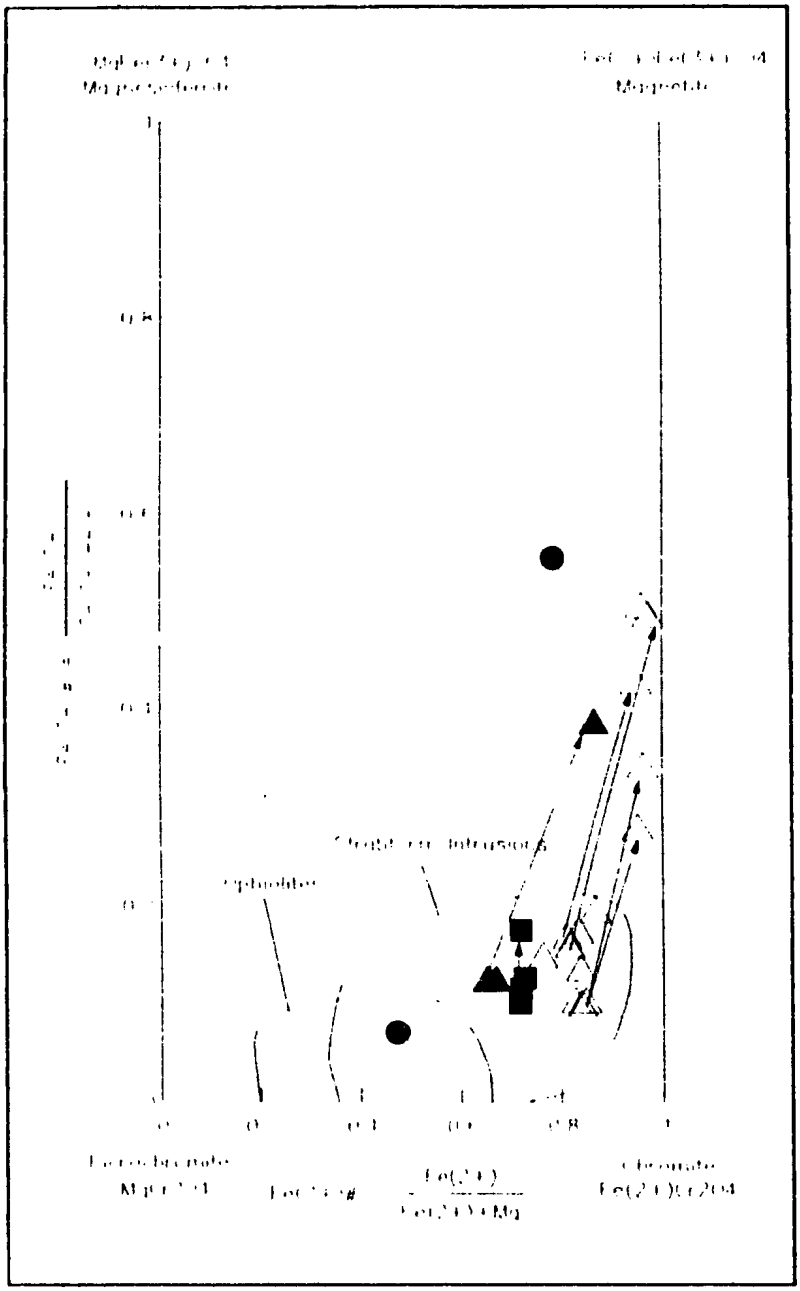

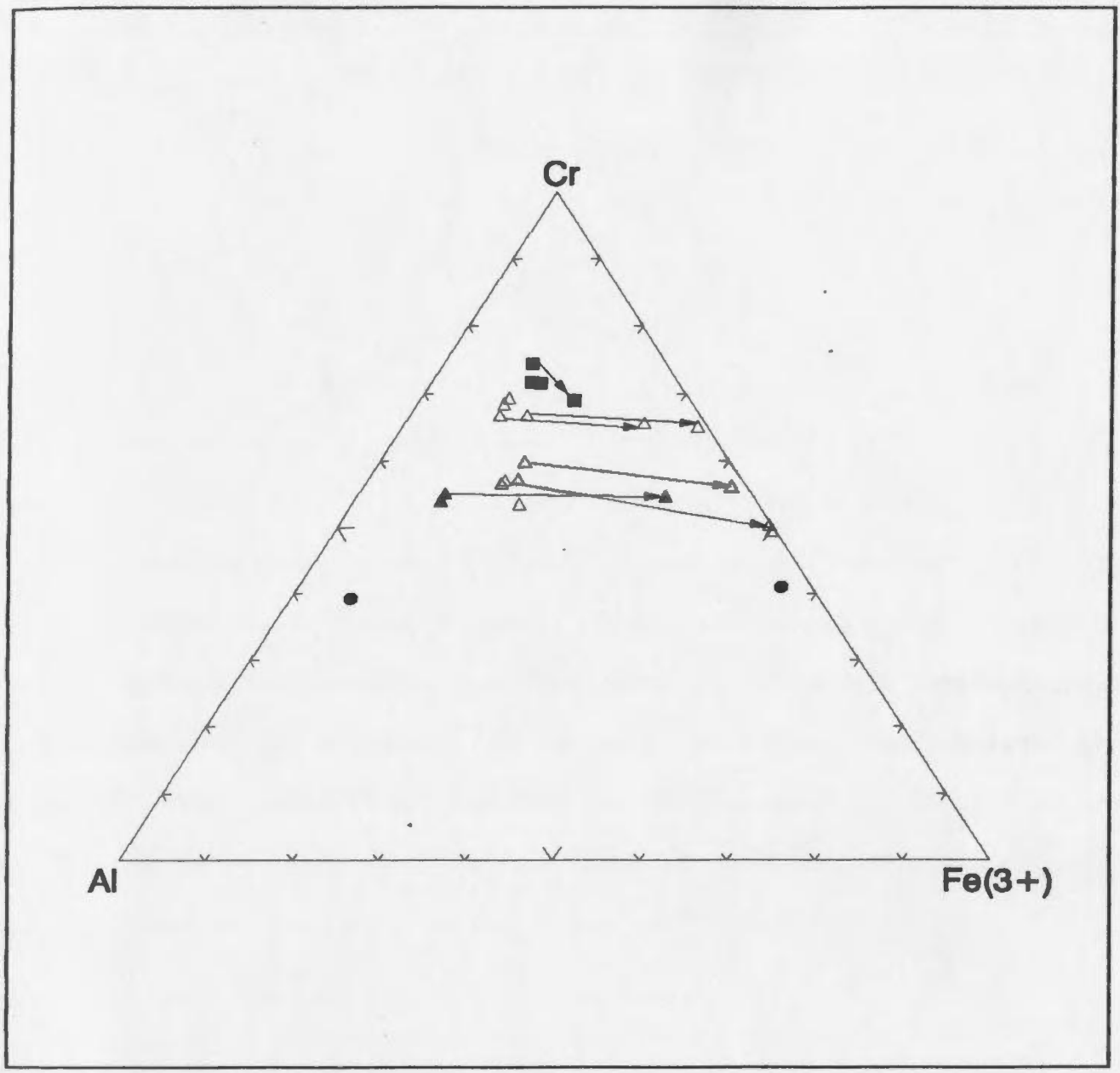

Fig. 4-5 (Continued).

Triangular diagram showing plot of Al, Cr and Fe^{3+} cations for chrome spinel cores and rims.

of this procedure is presented in Appendix B). In general, the chromites are characterized by medium to low Mg-Al and high Cr-Fe^{+2} contents. Rims trend towards the chromite corner and have a higher Fe^{+3} content than cores. It is also evident that the composition of cores is variable within and between samples.

Similar rims of chrome spinels have been described previously (Onyeagocha, 1974; Ulmer, 1974; Bliss & Maclean, 1975; Hoffman & Walker, 1978; Lipin, 1984) and are referred to as ferritchromite. The term ferritchromite was first used by Spangenberg (1943) to describe highly reflecting rims around chromite grains (Bliss & Maclean, 1975), it is not a mineral of specific composition but describes an alteration product whose main features are a depletion in Al and Mg. The intermediate rims developed in some cases have a composition between that of the core and outer rim. In several studies, it has been shown that the outer rim is essentially magnetite and the inner rim is ferritchromite.

The origin of the ferritchromite has been debated in the geological literature and various proposals have been outlined for its formation. Some authors suggest it forms prior to serpentinization; some suggest it forms subsequent to serpentinization and some have suggested it results from magmatic alteration (Bliss & MacLean, 1975 and references therein). However the most common interpretation is that the ferritchromite alteration is in some way formed either during or after serpentinization and is related to the serpentinization process.

In a study of chromites from central Manitoba, Bliss & MacLean (1975) interpreted the magnetite rims to have formed around chromite grains during serpentinization, and that during subsequent metamorphism to (at least) epidote amphibolite facies, Mg, Al and Cr diffused outward from the chromite core. They proposed that subsequently, the magnetite rim reacted with the chromite core to produce Al and Mg deficient ferritchromite rims. Therefore their main interpretation is that ferritchromite forms during metamorphism after serpentinization and that it is a later reaction product between magnetite and chromite.

However Hoffman & Walker (1978) preferred an interpretation whereby ferritchromite is an intermediate chemical step between the overall reaction of chromite to magnetite during serpentinization and thus it need not form subsequent to the magnetite. This interpretation is favoured for the metadunites in this study mainly because they are not interpreted to have been subsequently metamorphosed after serpentinization (see Chapter 7).

4.3.3 Chromite As a Petrogenetic Indicator

Irvine (1967) found that chromites from ophiolites vs. stratiform intrusions such as Bushveld, Stillwater and Muskox generally plot in separate fields (with a small overlapping area) with respect to their Mg, Al, Cr and Fe^{+2} contents (Fig. 4-6). As presented previously, Figure 4-5 shows plots of chrome spinels from this study on the Cr/Cr+Al vs $Mg/Mg+Fe^{+2}$ and $Fe^{+3}/Cr+Al+Fe^{+3}$ vs $Mg/Mg+Fe^{+2}$ diagrams showing Irvine's compositional fields for ophiolites and stratiform intrusions. The chromites

of this study are characterized by low Mg-Al and high Cr-Fe^{+2} contents; rims of grains generally trend towards the chromite corner; cores of spinel grains are variable within the same sample and between different samples; and rims have a higher Fe^{+3} content than cores.

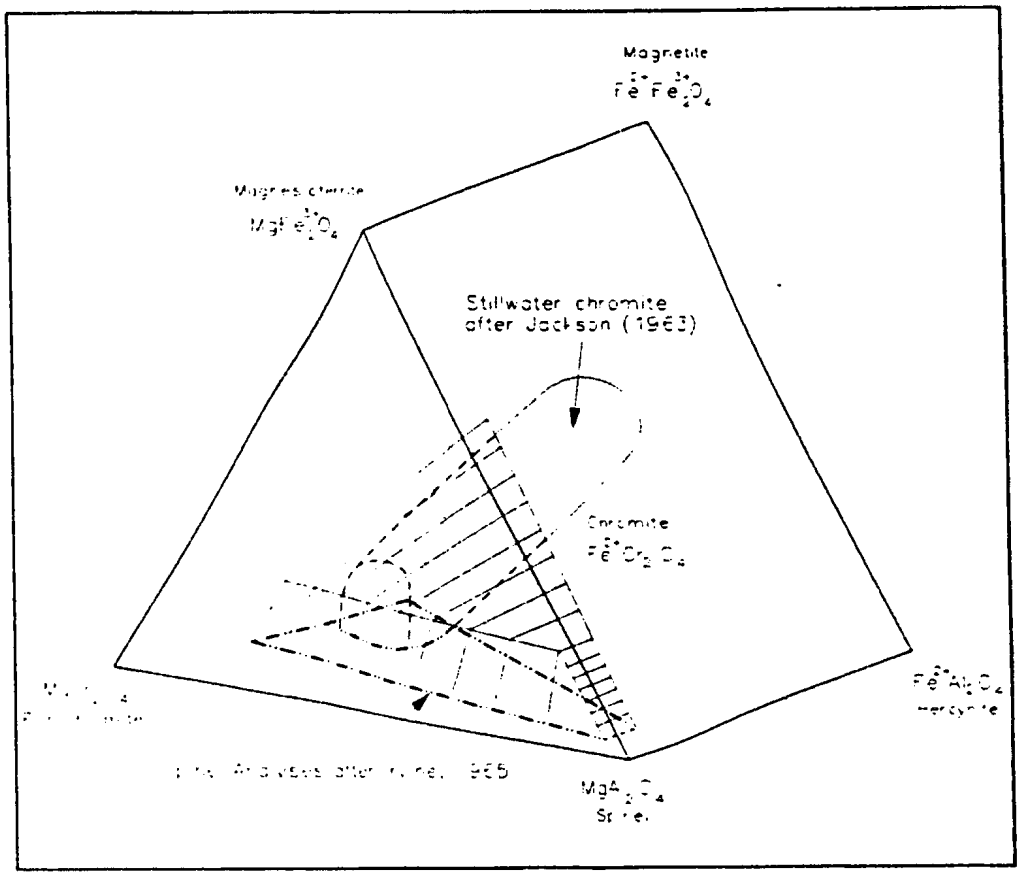

Fig. 4-6. Plot of chrome spinels from ophiolites and stratiform intrusions showing separate fields with small overlapping area with respect to their Mg, Al, Cr and Fe^{+2} contents (after Irvine, 1967).

It is evident the chromites of this study generally plot within the stratiform field, however a core of one grain does plot within the ophiolitic

field. It is important to recall here that in general the chromites of this study are highly altered to ferritchromite and therefore in most cases cannot be used reliably as a petrogenetic indicator unless the original core is still preserved. Similar trends for chromites from the Pipestone Pond and Great Bend ophiolites of central Newfoundland and for ophiolite complexes from the Burlington Peninsula of northern Newfoundland have been attributed to metamorphism (Malpas & Strong, 1975).

4.4 OLIVINE

Olivine was found in only three samples collected. It is everywhere fractured and veined by lizardite and forms a mesh texture which separates smaller olivine grains that are optically continuous, indicating the former presence of larger grains. These larger grains appear to have been less than 2mm in diameter, and to have formed a mosaic texture with 120° triple point junctions (Fig. 4-7). In several places kink bands are developed (Fig. 4-8). Microprobe analyses (presented in Appendix A) of olivines from each of the three samples have a very restricted compositional range of $Fo_{92} \pm 0.7$. The only other minor constituents are NiO (0.19 to 0.38 wt.%) and MnO (0.12 to 0.15 wt.%).

Some authors believe that olivine composition can be used to distinguish igneous from metamorphic origin. For example, Carpenter & Phyfer (1976) showed that olivines from geographically separated ultramafic rocks in the southern Appalachians have a consistent chemistry of Fo_{92} (average) within and between bodies and that no compositional zoning is

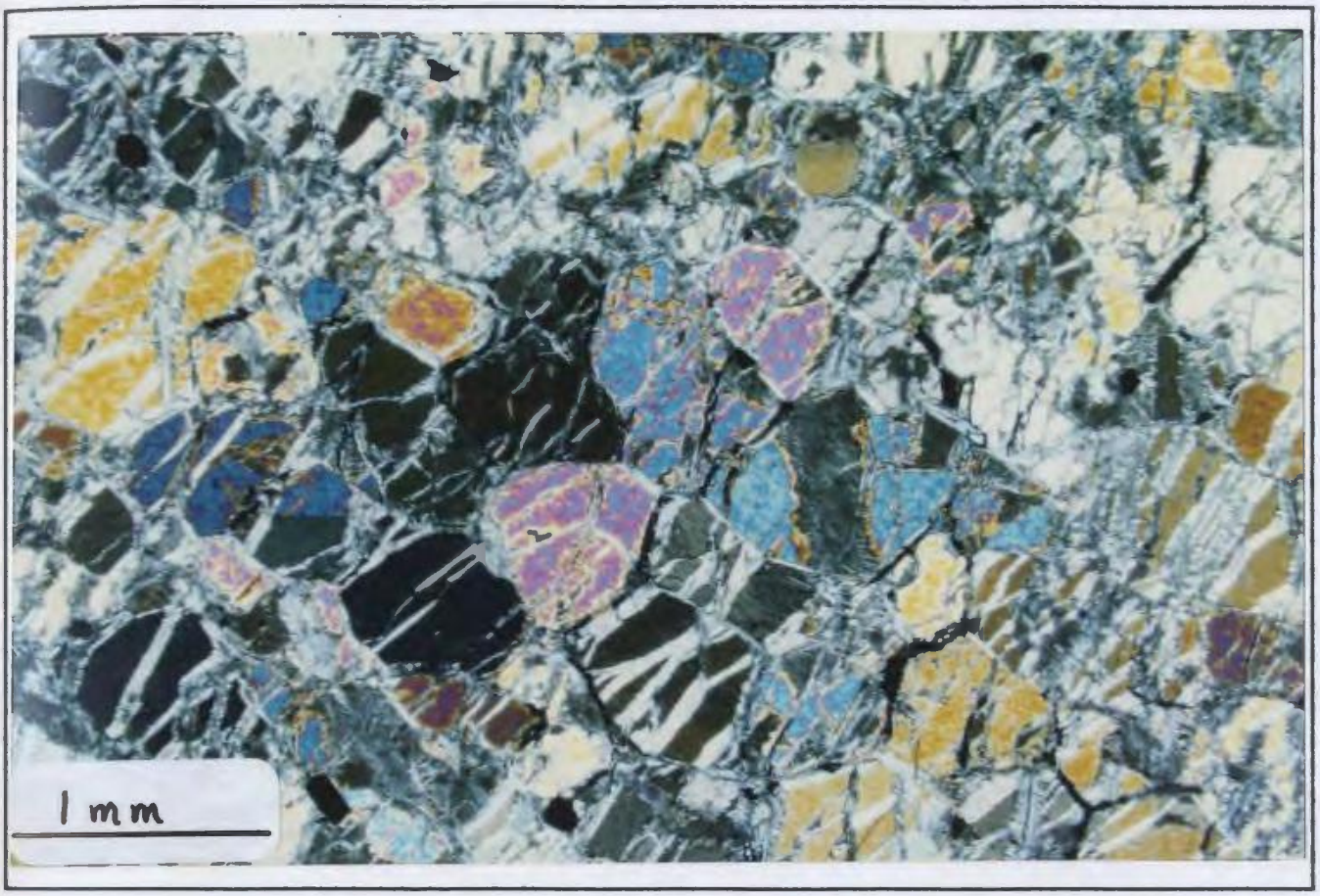

Fig. 4-7. Photomicrograph of olivine with 120° triple-point junctions and pseudomorphic serpentine (lizardite) forming mesh texture. (X-polarized light).

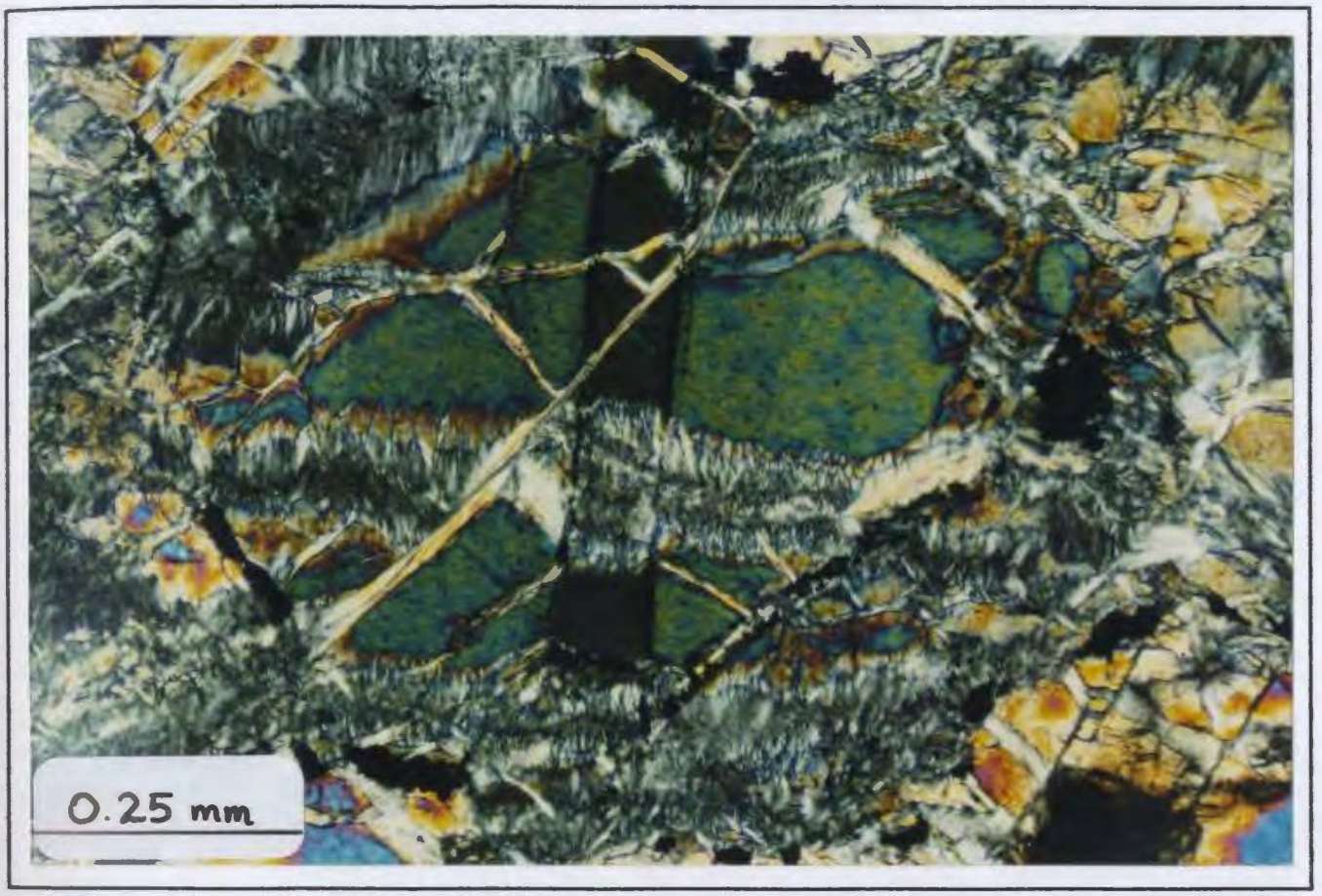

Fig. 4-8. Photomicrograph of kink-band in olivine grain. (X-polarized light).

present in the olivine grains. They argued that during serpentinization, iron is released from olivine and during subsequent prograde metamorphism and recrystallization of serpentine back to olivine, the iron was not re-incorporated into the olivine structure. Therefore metamorphic olivine is expected to be more forsteritic than its igneous percursor, and they interpreted most of the olivine to be of metamorphic origin in this case.

Evans (1977) reported that olivine compositions of Fo_{95} are not uncommon for rocks that were formerly serpentinized. However, he also stated that despite a possible range of metamorphic temperatures from approximately 400°C to over 1000°C, he could find no systematic chemical changes in olivine composition with metamorphic grade. He found that the majority of metamorphic olivines fall within the compositional range of olivines from layered intrusions and ophiolites, and subsequently their compositional variation is largely a result of the Fe/Mg ratio of the original rock, oxygen fugacity, and the nature and amounts of coexisting phases.

The olivines from this study fall within the range of those in igneous dunites (Fo_{88} to Fo_{92}) from ophiolite complexes (Malpas & Stevens, 1979; Savelyev and Savelyeva, 1979). However it should be noted that the forsterite component of olivine from dunites within ophiolite complexes is variable and may be as low as Fo_{88}. Serpentinization and recrystallization could have increased this value to Fo_{92}. It is therefore clear that the forsterite components of igneous and metamorphic olivines may overlap in some cases, and is not a useful indicator of mode of origin unless both types are found together and their chemical compositions can be directly

compared (e.g. Hoffman & Walker, 1978).

In the absence of definitive chemical evidence, another possible way to interpret the origin of olivine is by using textural relationships. Igneous adcumulate textures may show similar 120° microstructural relationships as the rocks of this study. However the olivine crystal boundaries are so well-developed and straight in the rocks of this study, they may well have formed by microstructural equilibration that resulted from metamorphic recrystallization during amphibolite facies metamorphism. In light of this it is not possible to come to a definite conclusion as to the origin of olivine from this study.

4.5 SUMMARY

One of the objectives of this study was to determine the origin of the mafic-ultramafic rocks. Petrogenetic interpretations are usually done using whole rock geochemical characteristics, however due to polymetamorphism of the rocks of this study the results would probably be equivocal. Alternatively, the rocks are compared to other mafic-ultramafic rocks in southwestern Newfoundland. Lithologically they are not distinct from either ophiolitic fragments or from Silurian gabbro/diorite intrusions. However, the rocks of this study are apparently part of the Long Range Mafic-Ultramafic Complex that forms a discontinuous belt throughout much of the Dashwoods subzone. In this context they are probably of ophiolitic origin.

Mineral chemistry cannot be used reliably as petrogenetic indicators because the minerals are affected by fluids. However, one core of a chrome spinel grain plots in the ophiolitic field of Irvine (1967). Although the evidence may be considered weak, it is concluded the mafic-ultramafic rocks of this study are most likely of ophiolitic origin. Chapter 5 outlines the structural aspects of the study area followed by an account of the metamorphism in Chapters 6 and 7.

CHAPTER 5

STRUCTURAL ANALYSIS

5.1 INTRODUCTION

In this chapter an interpretation of the structural elements of the rocks within the map area is presented. Firstly the regional high grade planar fabrics in the metapsammites, metapelites, and granitoid rocks are described, followed by an account of the superimposed shear zones in the metapelites. The shear zones are not easily recognized because the rocks have been extensively recrystallized. Because of this, a review of common shear zone features and of mylonite fabrics is presented, followed by a description of the shear zones of this study and the criteria used to recognize them.

The structural elements of the mafic-ultramafic rocks are then reviewed. The mafic-ultramafic rocks occur as disrupted and isolated bodies within the metasedimentary rocks, a relationship that may be described in terms of a mélange zone. Therefore the final aspect of this chapter reviews mélange zone terminology and how the present study area fits into currently accepted concepts concerning mélange zones.

5.2 HIGH GRADE PLANAR FABRICS IN THE METASEDIMENTARY ROCKS

The psammitic metasedimentary rocks display a well-developed

stromatic gneissosity whereas the fabric in the metapelites is better described as foliated to gneissic. Both fabrics are the first tectonic fabrics recognized in the units, and are referred to as S_1. The high grade gneissosity is subparallel to relict lithological layering (S_0) that is still recognizable in places. This relationship is interpreted to result from isoclinal folding, however any F_1 fold axes or L_1 mineral lineations that may have developed as part of the deformational phase (D_1) have not been recognized.

The S_1 fabric in the metasedimentary rocks has been affected by a second period of isoclinal folding and therefore the original orientation of S_1 has been transposed. Figure 5-1 shows plots of poles to S_1 foliations in the metapsammites and metapelites which show that the fabrics in both units generally trend north-northeast and are steeply northwest-southeast dipping to vertical. Figure 5-2 shows an example of a second generation isoclinal fold. This was the only such example recognized throughout the map area and it appears this event is not penetrative.

5.3 FABRIC IN THE GRANITOID SUITE

The granitoid rocks contain a weak to well-developed foliation defined by the preferred orientation of biotite. Figure 5-3 is a plot of poles to foliations and shows their orientation is similar to those in the metasedimentary rocks, although they are more widely dispersed than the other units. No folds have been recognized in the granitoid rocks.

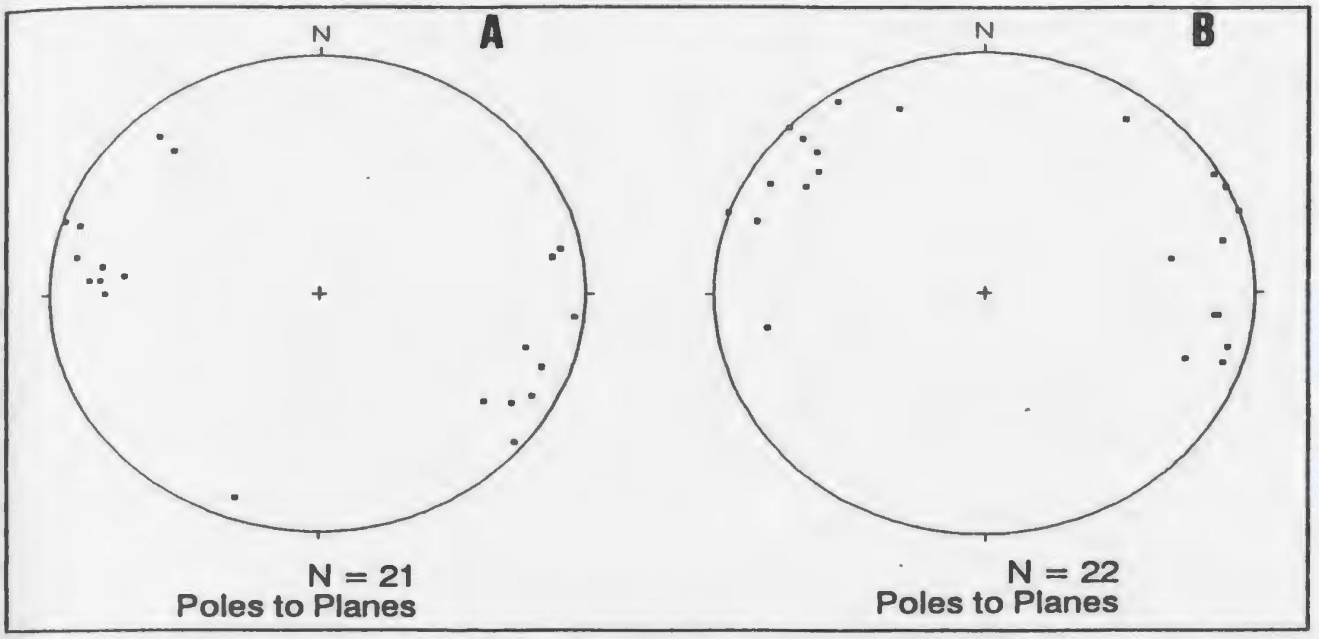

Fig. 5-1. Lower hemisphere, equal-area stereonet plot of poles to foliations in psammitic (A) and pelitic (B) metasediments. Foliations strike predominantly northeast and dip steeply to the northwest or southeast or are vertical.

Fig. 5-2. Second generation isoclinal fold in pelitic metasedimentary unit. Fold axis dips moderately to the north. Hammer in center of fold for scale.

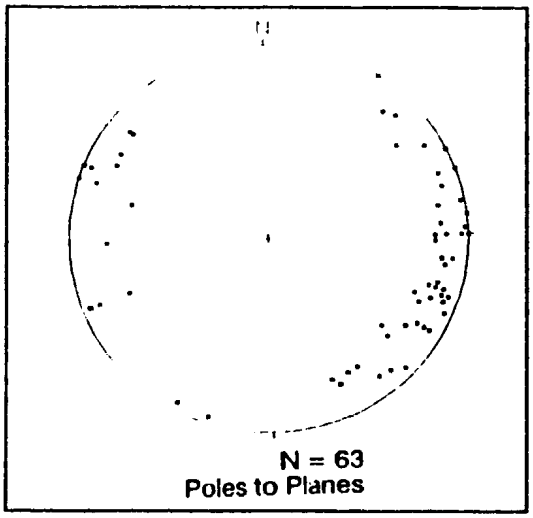

Fig. 5-3. Lower hemisphere, equal area stereonet plot of poles to foliations in the granitoid rocks. Orientation is similar to that in the psammitic and pelitic metasediments although more widely dispersed.

5.4 SHEAR ZONES IN THE PELITIC METASEDIMENTARY ROCKS

Shear zones in the pelitic metasedimentary rocks are commonly developed but they are not easily recognized in the field on account of extensive recrystallization throughout this unit. This leads to difficulty in determining the sequence of folding events and other such features when high grade rocks cannot be readily distinguished from shear zone rocks in the field. Therefore the emphasis of structural interpretation in this chapter is placed on a review of common shear zone features followed by an account of the shear zone fabric developed in the rocks of this study.

5.4.1 Review of Common Criteria Used to Recognize Shear Zones

Shear zones are most easily recognized where they cut a pre-existing foliation, dike or other marker which is offset or deflected across the zone. However, such features are most useful only in relatively narrow shear zones where the relationship between the deflected marker and the shear zone boundary is observable. However, since some shear zones tens of kilometres wide are known (White et al., 1980), and since in many cases the shear zone boundaries are not abrupt but occur as zones of variable strain partitioned into anastomosing fabrics, other criteria are also necessary.

An alternative way to identify shear zones is by recognition of common shear zone products. One such product in ductile shear zones is "mylonite", a term originally proposed for rocks that were thought to develop from brittle processes (cataclasis), but is now well established to be the product of principally ductile processes such as crystalline plastic flow. Formation of mylonites is generally considered to have involved a significant component of grain-size reduction that results in subgrain formation from strained grains and in some cases their subsequent recovery during recrystallization. Mylonitic rocks form an entire spectrum from protomylonites which are weakly sheared rocks with a small component of grain size reduction through mylonites to ultramylonites which are strongly sheared rocks with a considerable component of grain size reduction (Sibson, 1977). The term "blastomylonite" is used for mylonitic rocks that show evidence of recovery (grain growth after deformation) and the term "phyllonite" is used for mylonites and ultramylonites that have

been extensively hydrated to a mica-rich rock with a phyllitic appearance.

In the past few years, numerous studies of mylonites in shear zones have been performed which have facilitated recognition of not only the apparent sense of shear movement, but also in the definition of the characteristic features of the shear zone itself. It follows that if a rock can be recognized as a mylonite, then the zone in which it occurs can be interpreted as a shear zone. Some of the more common and useful kinematic indicators in mylonites are S-C fabrics (Berthé et al., 1979) which are so widespread in shear zones that the terms S-C mylonites and S-C tectonites have been used in the recent geological literature (Lister & Snoke, 1984). Other indicators such as asymmetric porphyroclastic augen (e.g. mica, feldspar, garnet), asymmetric folds, asymmetric pressure shadows or broken and displaced grains have been used extensively to recognize mylonites and to determine the apparent sense of shear (Simpson and Schmid, 1983).

Where mylonites are well-developed and several of the above criteria can be recognized, ductile shear zones are relatively straightforward to recognize. However, in older reworked shear zones that have been extensively recrystallized or those that have been altered and retrogressed to phyllonites, mylonites and the mylonitic fabric are not as easily recognized.

Several such shear zones have been studied by Piasecki (1988), who has shown that quartz plates (oblate quartz veins) or ribbons (elongated in the direction of shear zone extension lineation) are typically developed

in these zones and are usually subparallel to the mylonitic fabric developed in the host rocks. This conclusion is based on recognition of quartz plates along with more common shear zone features such as S-C fabrics, augened porphyroclasts etc., as well as other strain induced syn-shear zone products such as micas, feldspars and shear zone pegmatites. The quartz plates and ribbons are interpreted to be strain-induced shear zone products. Their formation is not well established but may result from local segregation and/or larger scale mobility of SiO_2 and H_2O during shearing. An important aspect of the quartz plates is they may form at various time intervals during the shear zone history. Therefore depending on their timing of formation, they may show various aspects of typical shear zones from initial elongate quartz grains with relatively little strain through grains that have recovered dynamically to form subgrains to aggregates of grains that have been extensively recrystallized.

The usefulness of recognizing quartz plates as a product of shear zones becomes obvious in older reworked zones where quartz plates may be the only relic left of the previous mylonitic fabric. The shear zones of the present study area fit into this category and their mylonitic fabrics are not obvious in the field. However, Piasecki (1988) examined some of the metapelitic rocks in part of the study area and interpreted they represent up to a 4 km wide anastomosing ductile shear zone (Three Ponds shear zone in Fig. 3-1). This interpretation was based mainly on a study of quartz plates.

5.4.2 Shear Zones in the Study Area

The shear zones in the present study area are recognized in the field mainly on the basis of quartz plates. Figure 3-9 shows an example of quartz plates in the field and Figures 5-4 & 5-5 shows their appearance in thin section. The quartz displays various stages of undulose extinction and subgrain formation and is variably recrystallized so that some grains are markedly elongate, whereas others approach polygonal (minimum surface area) shapes.

In addition to the development of quartz plates, a mylonitic fabric is also recognizable in thin section. Elongate feldspars are preserved between quartz plates (Figs. 5-6 & 5-7). These grains may be dynamically recrystallized into fine-grained aggregates under conditions of continuing strain. There are also rare examples of augen garnet porphyroblasts "wrapped" by the shear zone fabric (Fig. 5-8) and garnets elongated in the plane of shear (Fig. 5-9). Elongate aggregates of relic sillimanite are also preserved (Figs. 5-10 & 5-11) and Fe-Ti oxide minerals are highly elongated (Fig. 5-12). In most examples, the mineralogy between the quartz plates has been completely retrogressed to fine-grained sericite to produce phyllonites (Figs. 5-4 & 5-5). In places, mica is aligned at an angle to the quartz plates producing an S-C fabric (Fig. 5-13). These examples indicate unequivocally that the quartz plates are associated with shear zones in the present study area.

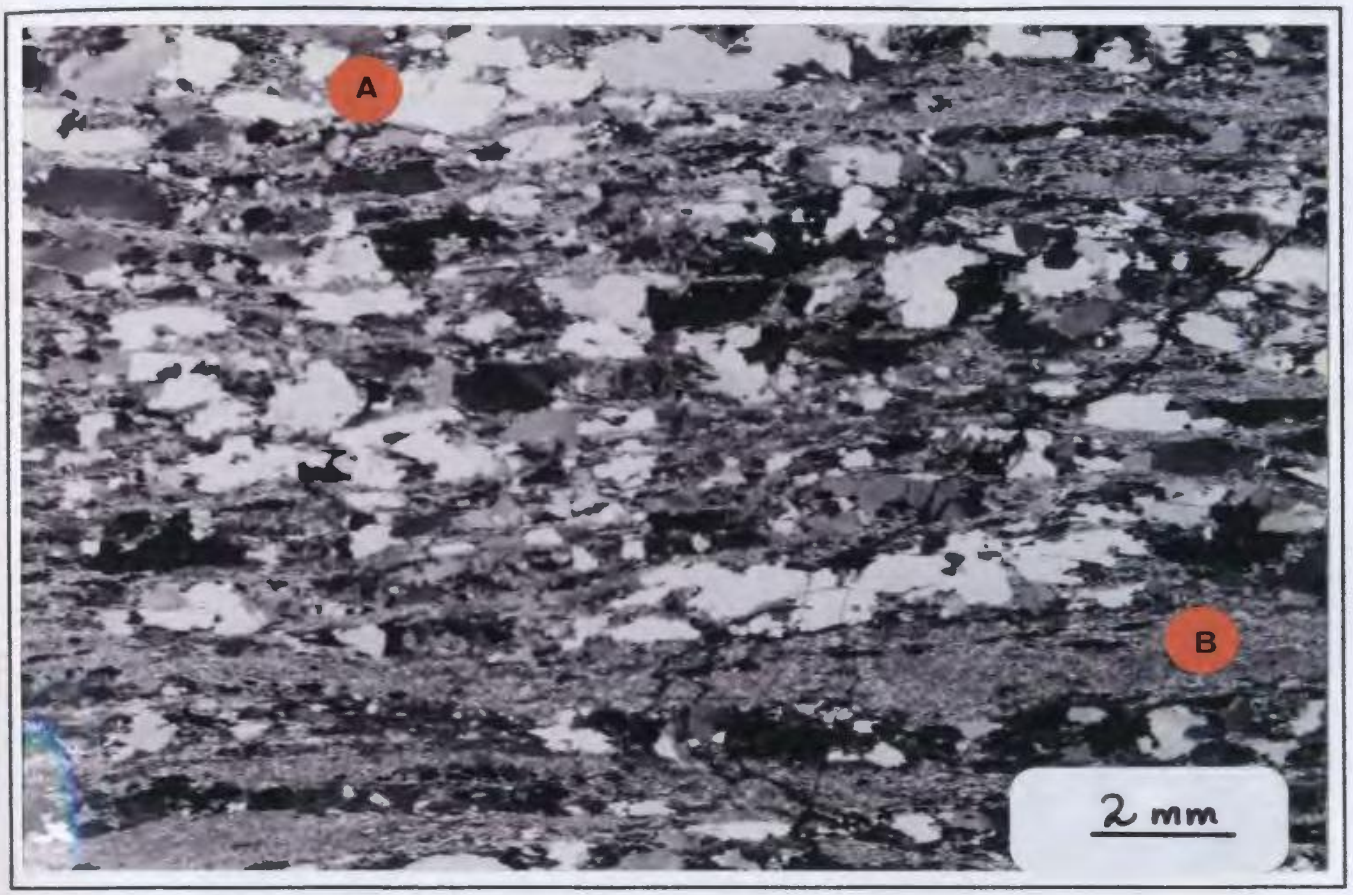

Fig. 5-4. Photomicrograph of quartz plates in the pelitic metasediments. A) quartz plates and B) fine-grained sericite and chlorite.

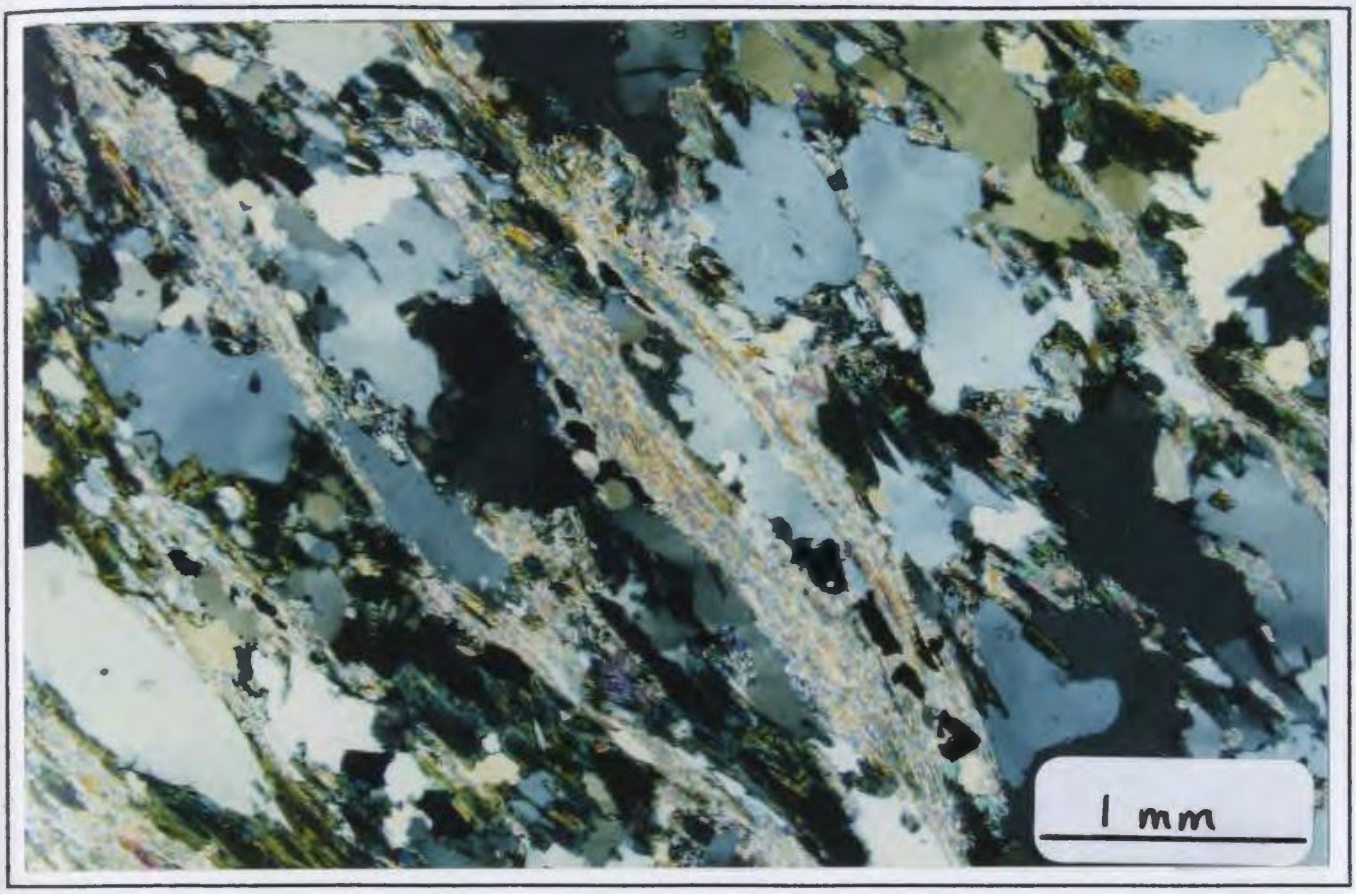

Fig. 5-5. Photomicrograph of quartz plates showing formation of subgrains and various stages of recrystallization between grains. Several quartz plates in the center of the photograph show the pinch and swell feature that is typical of ribbon quartz grains developed in mylonites. (X-polarized light).

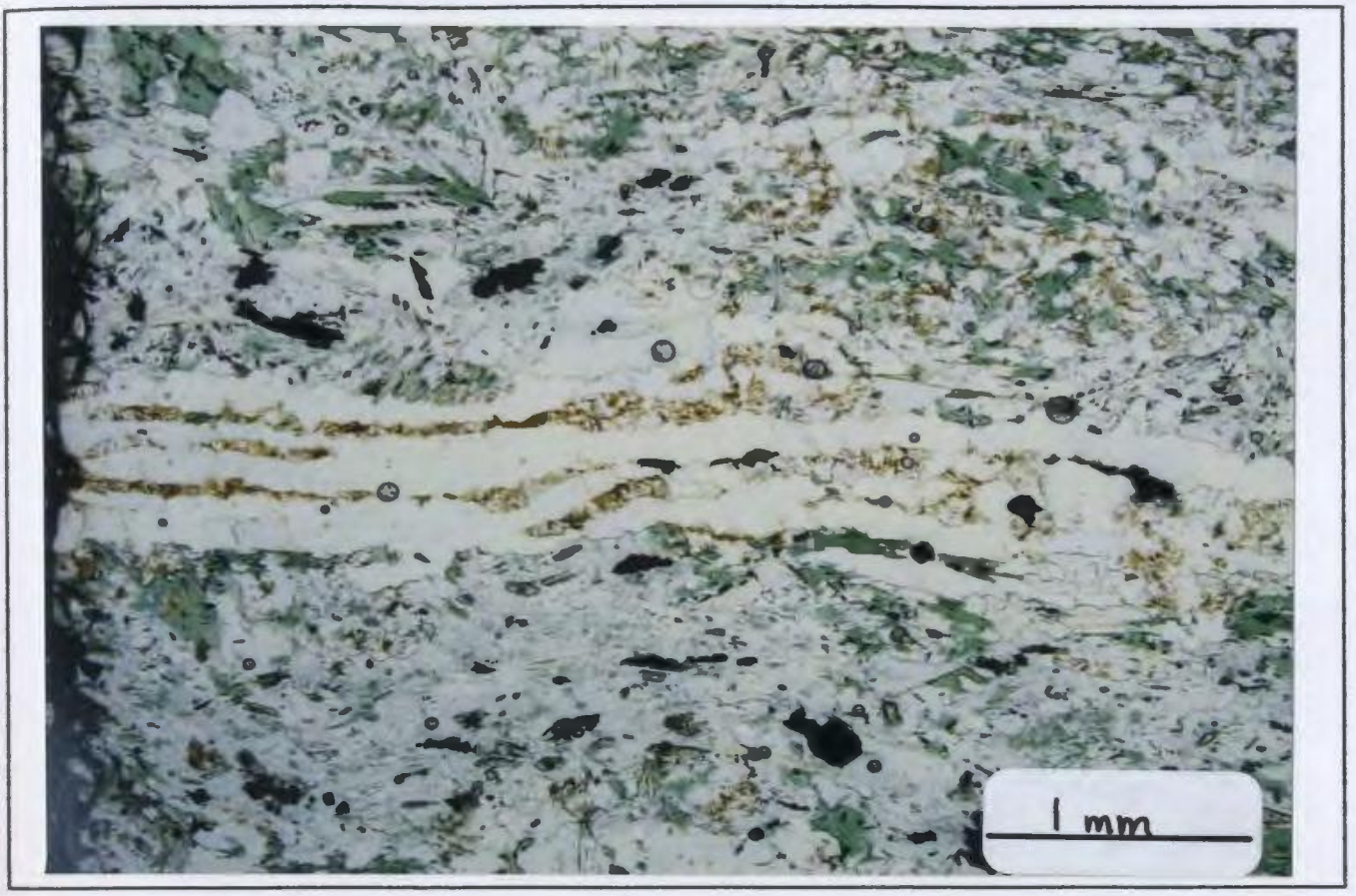

Fig. 5-6. Thin bands of plagioclase feldspar between quartz plates in shear zone. Green mineral is chlorite (Plane polarized light).

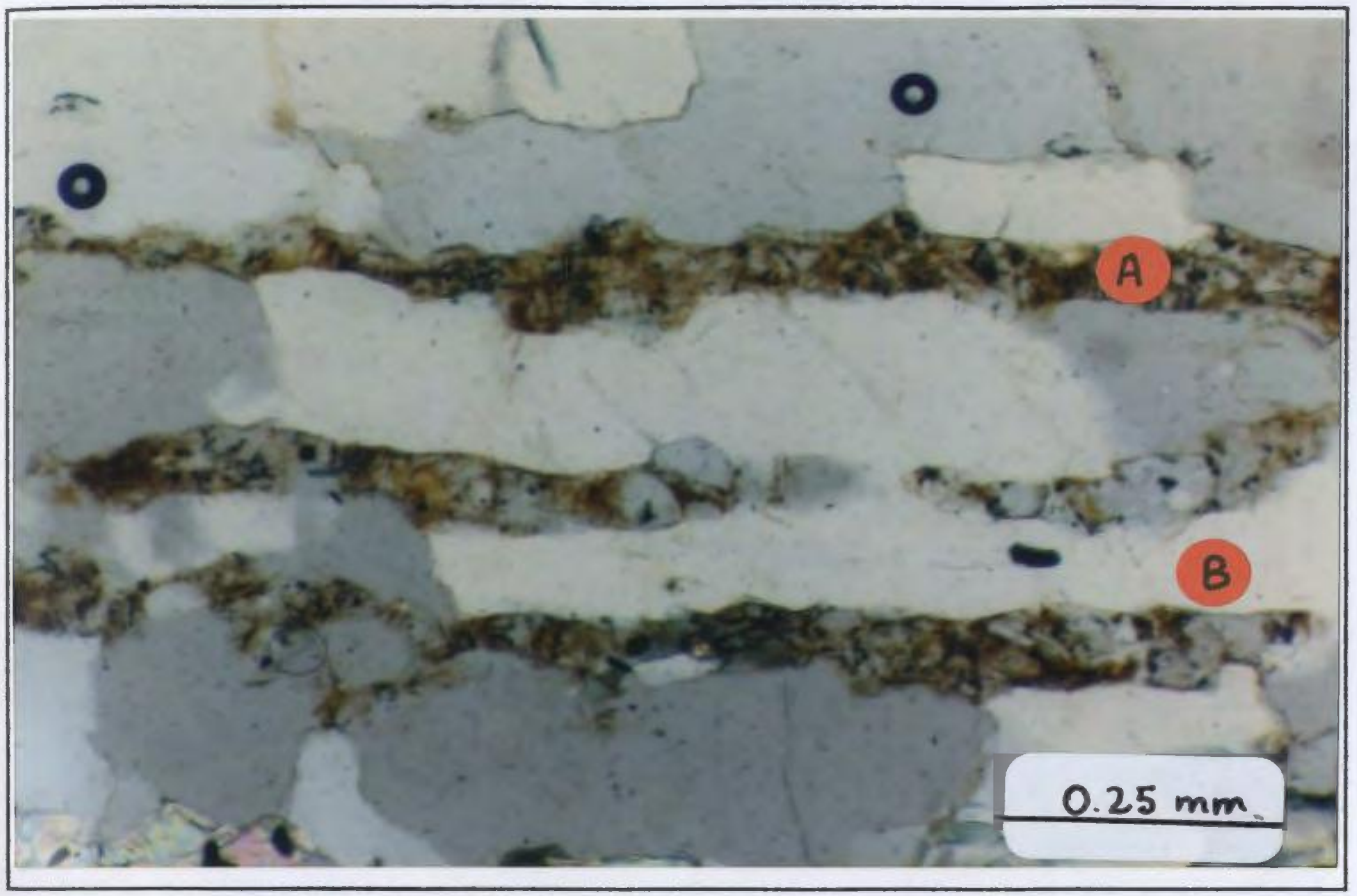

Fig. 5-7. Close-up of Figure 5-6 showing thin bands of plagioclase feldspar (A) between ribbon quartz grains (B). Shear zone in pelitic metasediments. (Plane polarized light).

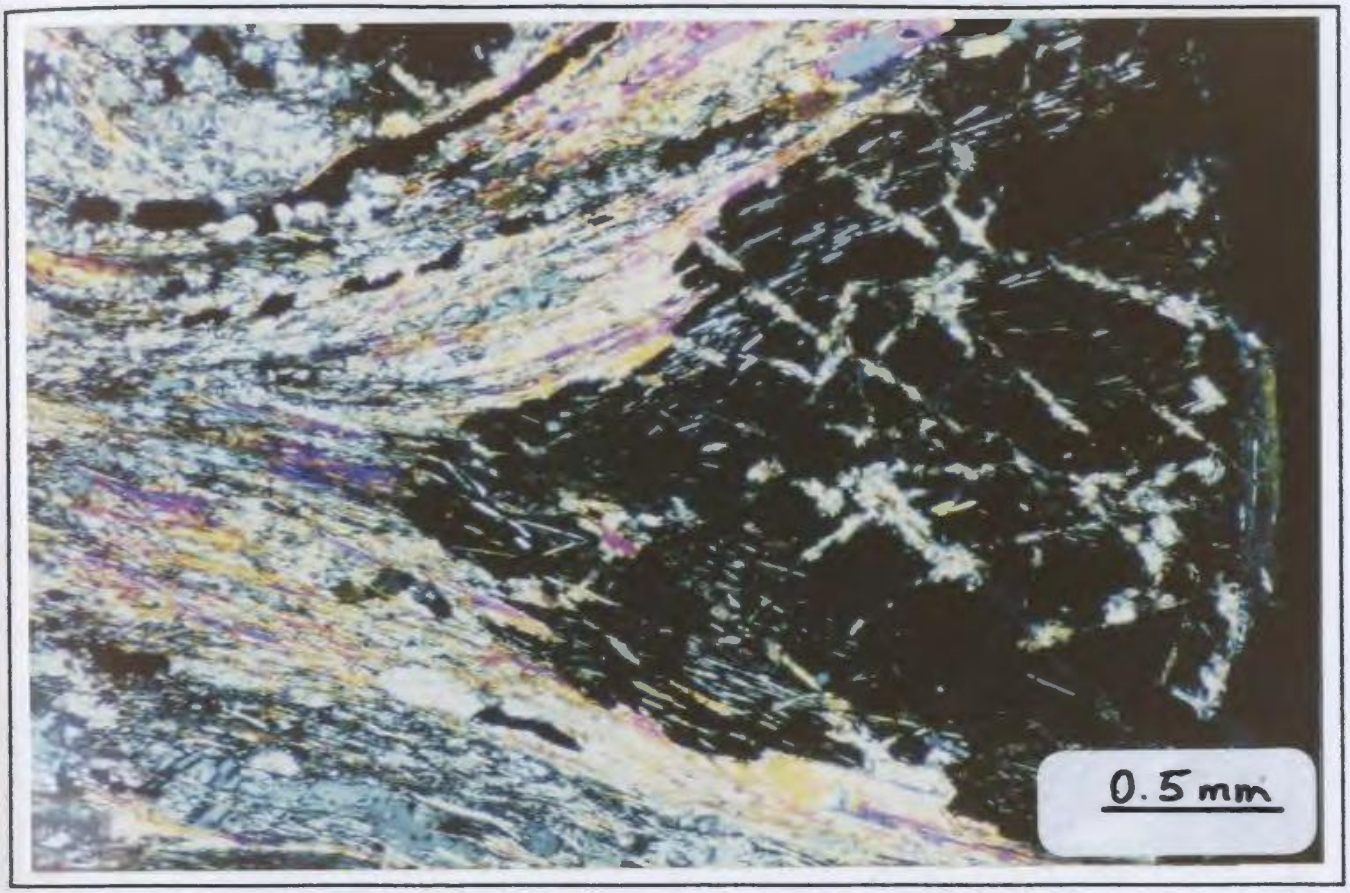

Fig. 5-8. Augen garnet porphyroblast wrapped by shear zone fabric in pelitic metasediments. Matrix consists of fine-grained sillimanite (fibrolite), sericite, and Fe-Ti oxides. (X-polarized light).

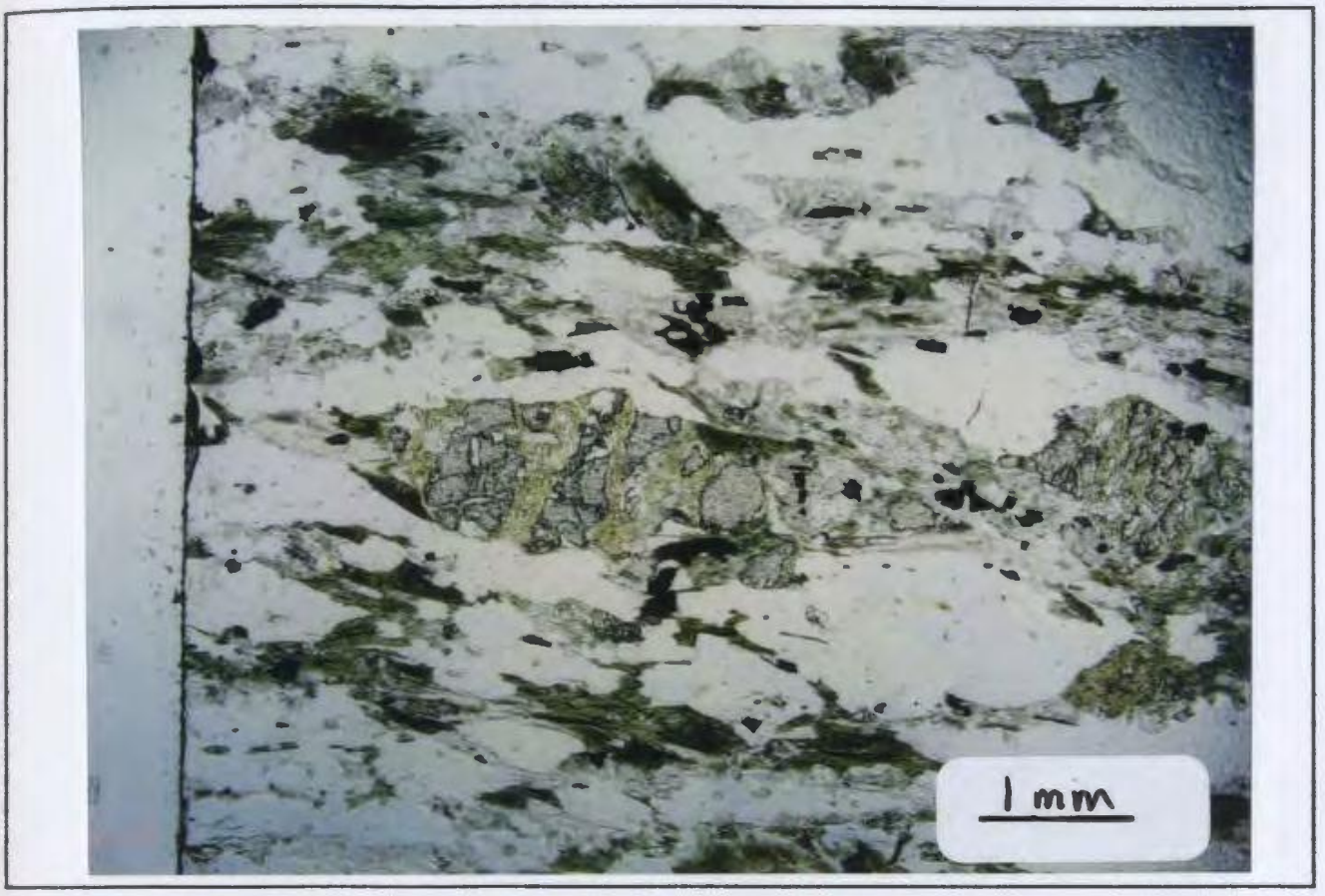

Fig. 5-9. Boudinaged garnet in shear zone. Fractures now filled with chlorite and sericite. (Plane polarized light).

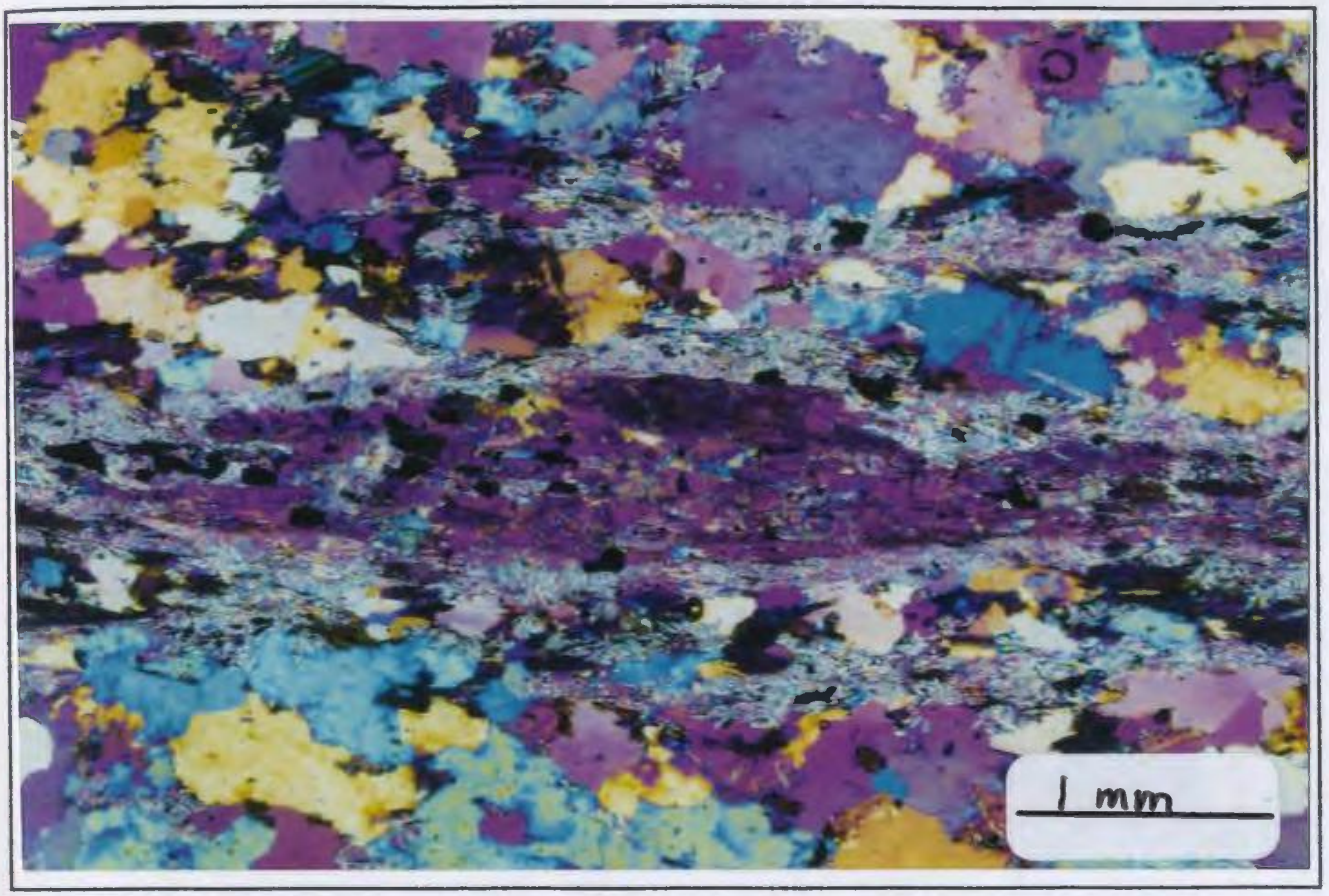

Fig. 5-10. Elongate and lozenged-shaped aggregate of sillimanite (purple) in shear zone. Such features are unrecognizable without use of the quartz plate. (X polarized light with quartz plate inserted).

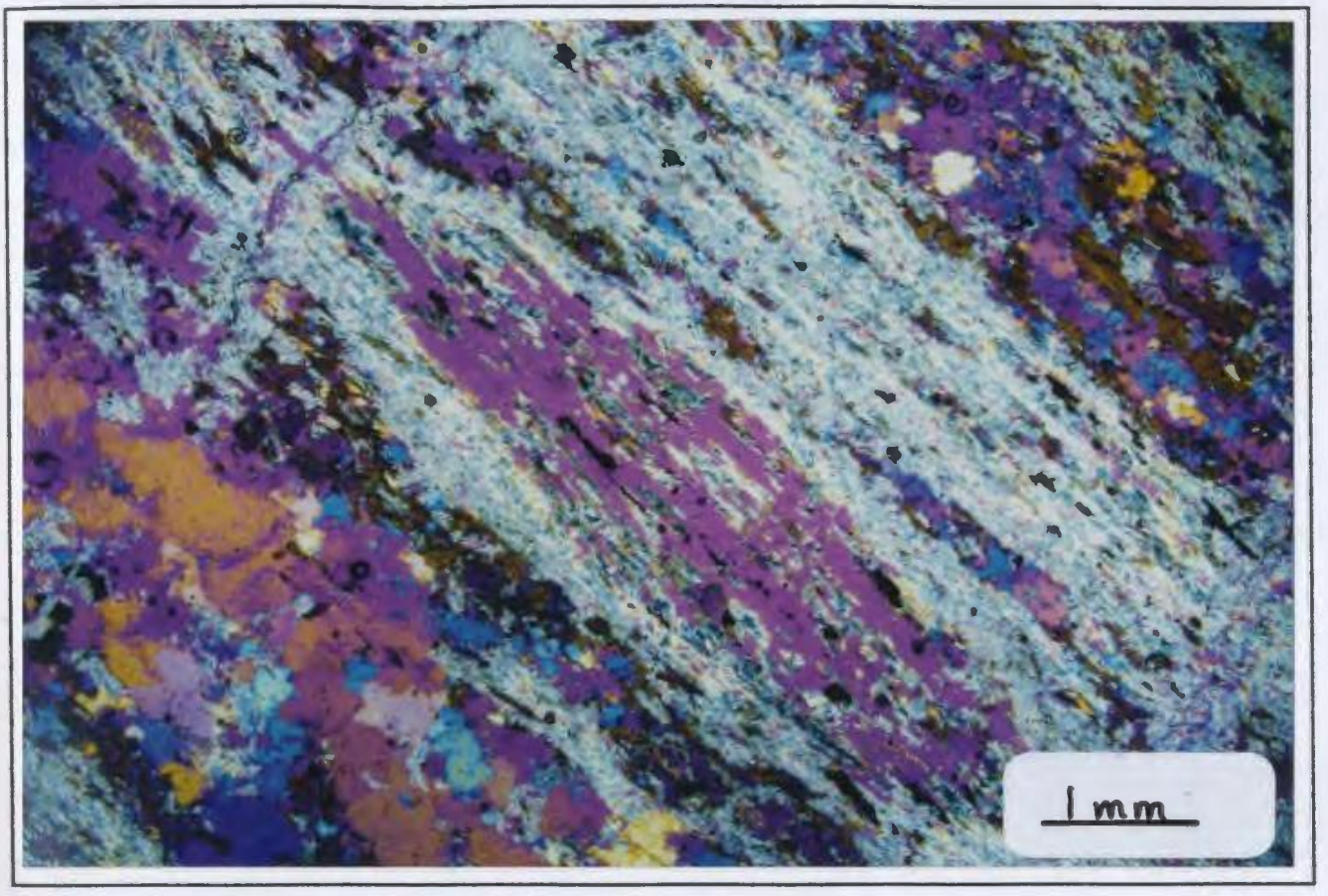

Fig. 5-11. Elongate aggregate of sillimanite (purple) in shear zone. (X-polarized light with quartz plate inserted).

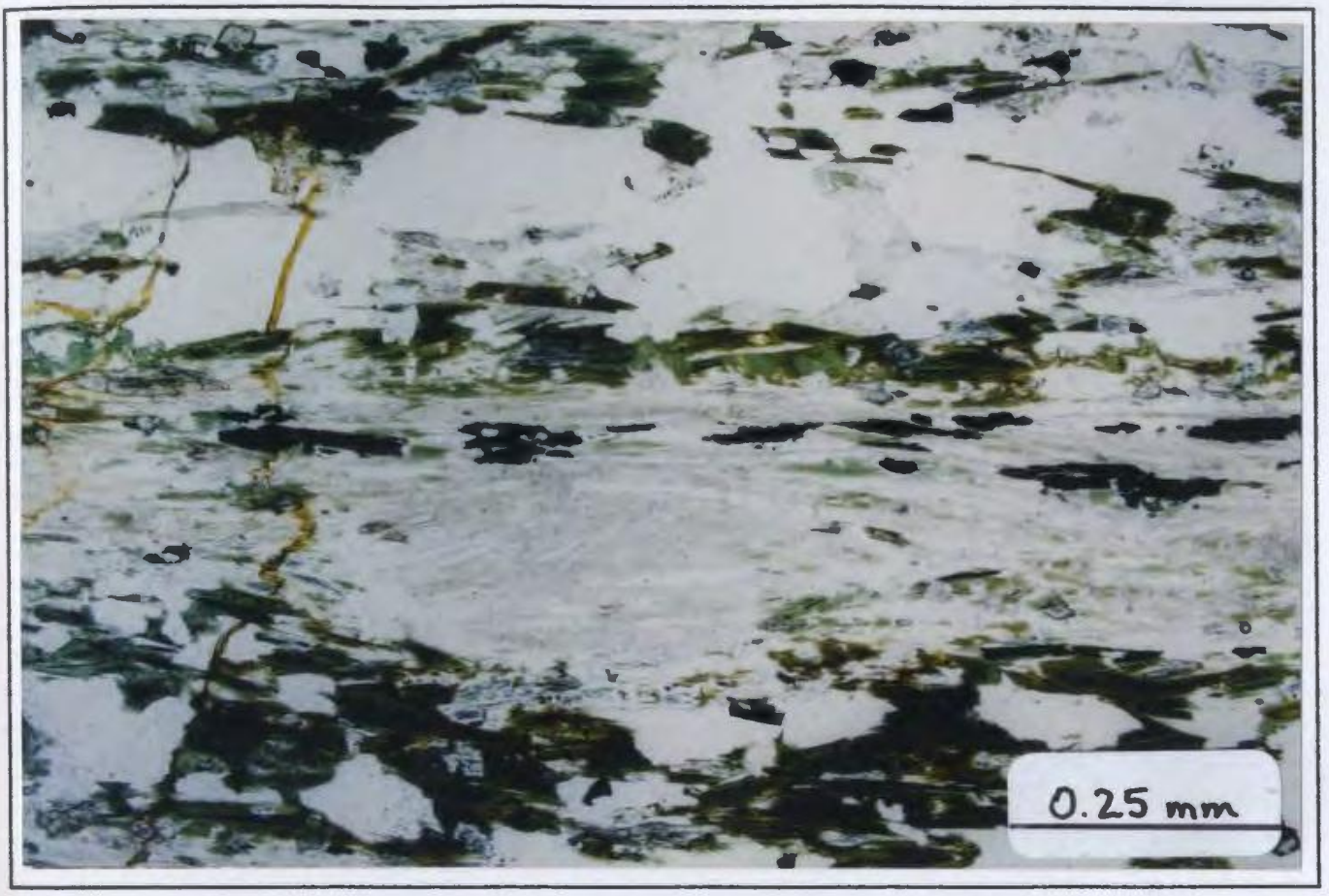

Fig. 5-12. Elongate Fe-Ti oxides in sericite layer in shear zone. (Plane polarized light). Sericite pseudomorphs sillimanite.

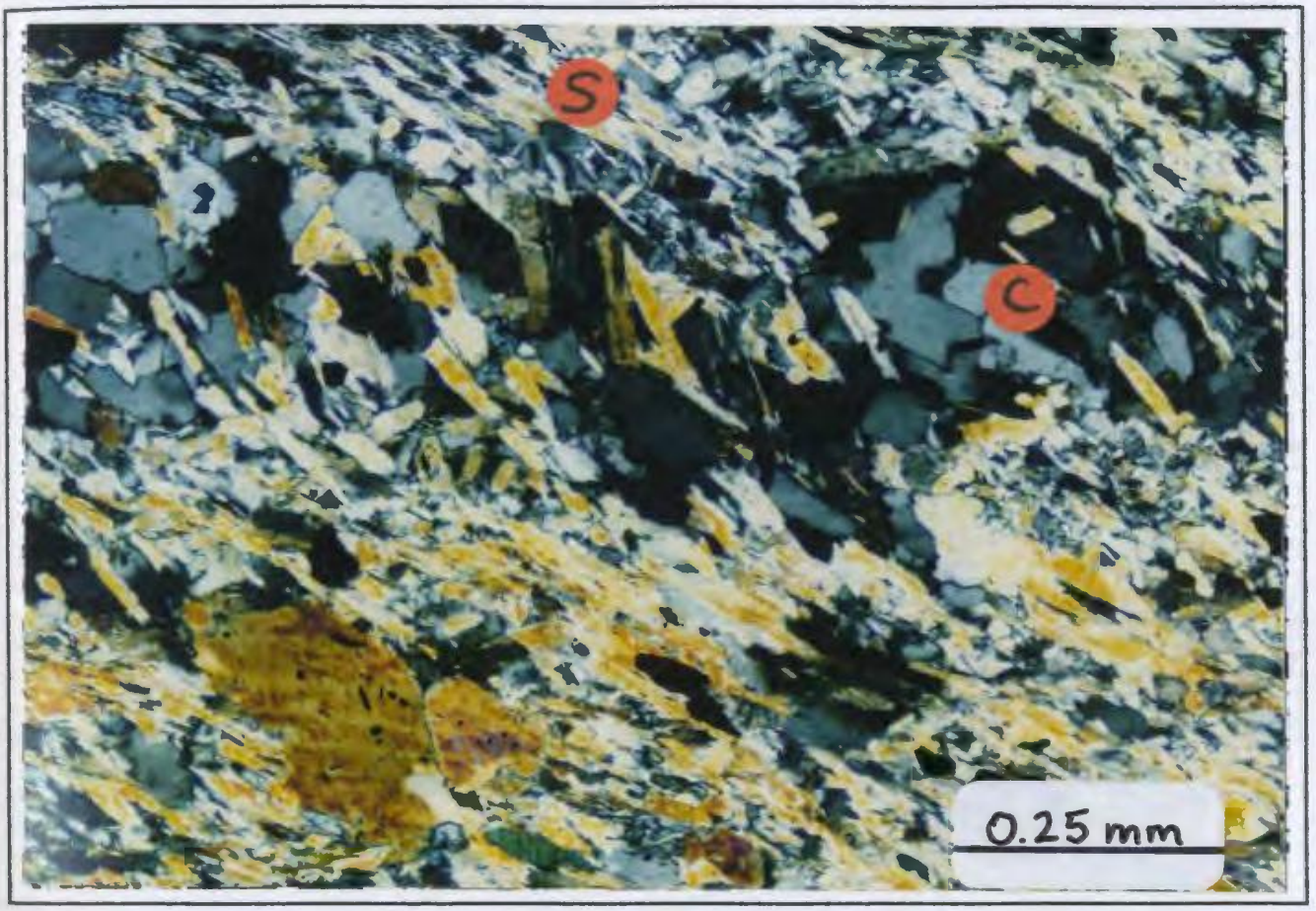

Fig. 5-13. Photomicrograph of S-C shear zone fabric in the pelitic metasediments showing fine-grained sericite (S) aligned at an angle to quartz plates (C). South of Dennis Pond. (X-polarized light).

From the above examples it is clear that the shear zone fabric has overprinted the high grade fabric in the pelitic metasediments. Figure 5-14 is a stereonet plot of poles to shear zone fabrics and quartz plates and shows their orientations are similar to those of the high grade schistose to gneissic fabric in the surrounding lithologies. The shear zones anastomose on a regional scale as shown in Figure 3-1 and including the Three Ponds shear zone, the belt is at least 15 km in length and up to 4 km wide in places.

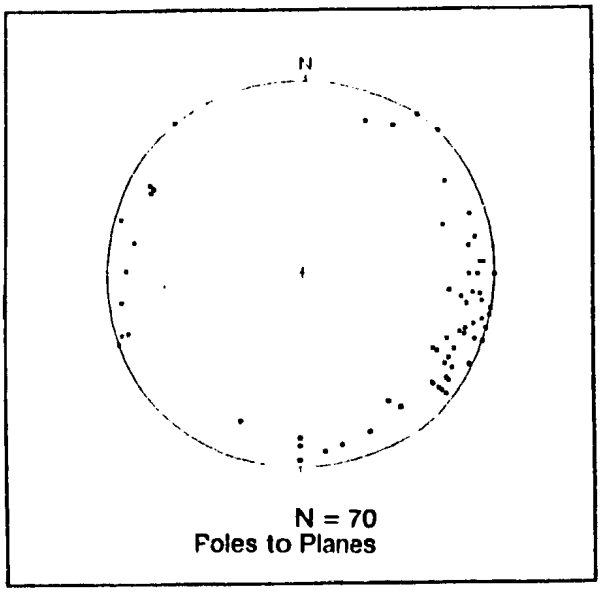

Fig. 5-14. Lower hemisphere, equal area stereonet plot of poles to shear zone fabrics (quartz plates) in the pelitic metasediments. Shear zone fabrics have similar orientations to the high grade fabric and lithological layering in the pelitic metasediments and to the fabric in surrounding lithologies.

5.5 FOLDING AND LINEATIONS

Figure 5-15 shows a stereonet plot of all fold axes measured in this study. They are moderately to steeply plunging to the north and south and cluster around the vertical. The fold axes however, have not been assigned to F_1, F_2 or syn-shearing folds on account of a lack of overprinting criteria as well as difficulty in distinguishing sheared from unsheared rocks in the field.

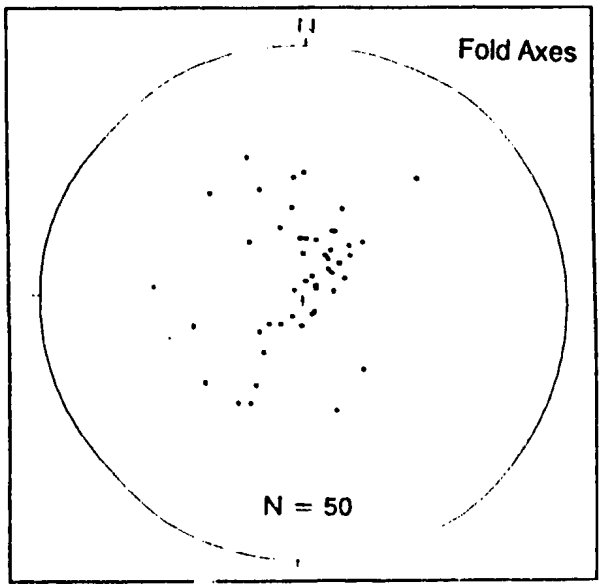

Fig. 5-15. Lower hemisphere, equal area stereonet plot of poles to fold axes in the pelitic metasediments. Plunge varies from moderate to steep to either the north or south.

A stereonet plot of the orientation of quartz rods and mineral elongation lineations in shear zones measured as part of this study is shown in Figure 5-16. They are subparallel to the orientations of fold axes. Piasecki

(1988) determined that asymmetric syn-shearing folds are common in the Three Ponds shear zone (Fig. 3-1) and their hinges are subparallel to stretching lineations developed as a result of shearing. He found that stretching lineations, defined by ribbons of quartz and aggregates of granulated feldspar have a northerly trend and gentle to moderate plunge. He also interpreted an apparent sense of overthrusting towards the north. This is in conflict to the orientation of lineations measured in this study which cluster around the vertical.

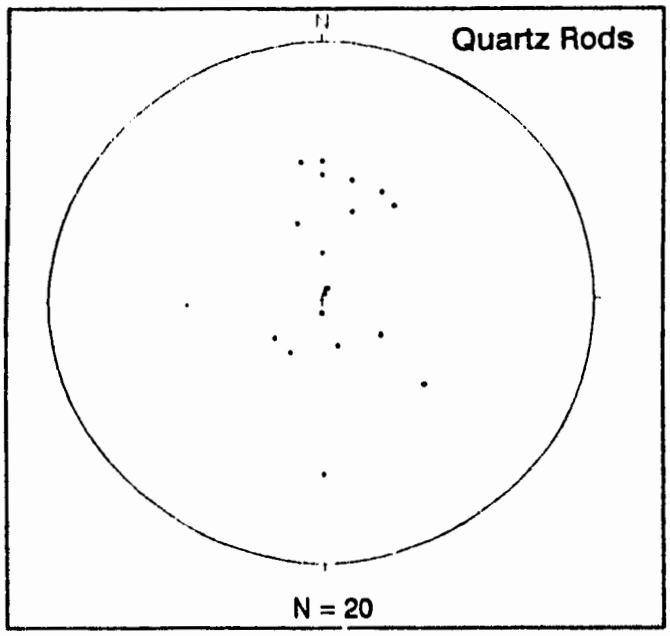

Fig. 5-16. Lower hemisphere equal area stereonet plot of poles to mineral lineations (quartz rods and elongated quartz-feldspar segregations). These lineations are generally parallel to fold axes.

5.6 FABRICS IN THE MAFIC-ULTRAMAFIC ROCKS

An important aspect of the tectonic development of the map area is

the timing of emplacement of the mafic-ultramafic rocks in relation to the shearing in the metasedimentary rocks. Figures 3-11 and 3-13 show that shear zone fabrics in the metasedimentary rocks wrap around mafic-ultramafic inclusions. This relationship suggests the inclusions are pre- to syn-kinematic and that the shearing has affected both the metasedimentary and mafic-ultramafic rocks. The preservation of tectonic inclusions is a common feature of mylonite zones.

Field evidence of high strain in the mafic-ultramafic rocks has already been discussed in Chapter 3. Microstructural evidence that the mafic-ultramafic rocks have been sheared is found in several examples. In metadunites, spinels are elongate (Fig. 5-17) to sigmoidal in shape (Fig. 5-18). Ductile deformation of spinels is known to be a high temperature phenomenon, and has been widely recorded in the mantle tectonites of ophiolite suites. As can be seen from Figures 5-17 and 5-18 the primary silicate minerals are entirely replaced by serpentine group minerals, so other indications of high temperature deformation have been erased. The serpentine group minerals do not define a penetrative foliation.

In the examples presented above it is clear that the mafic-ultramafic rocks have been highly sheared. However the timing of development of the shear fabric is not clear. Figure 5-19 shows a plot of poles to layering (fabric) in the mafic-ultramafic rocks. The attitude of the layering changes substantially from one exposure to the next and is not always parallel to the shear zone fabrics in the adjacent metasediments. This suggests that the layering (fabric) in the mafic-ultramafic rocks was developed prior to

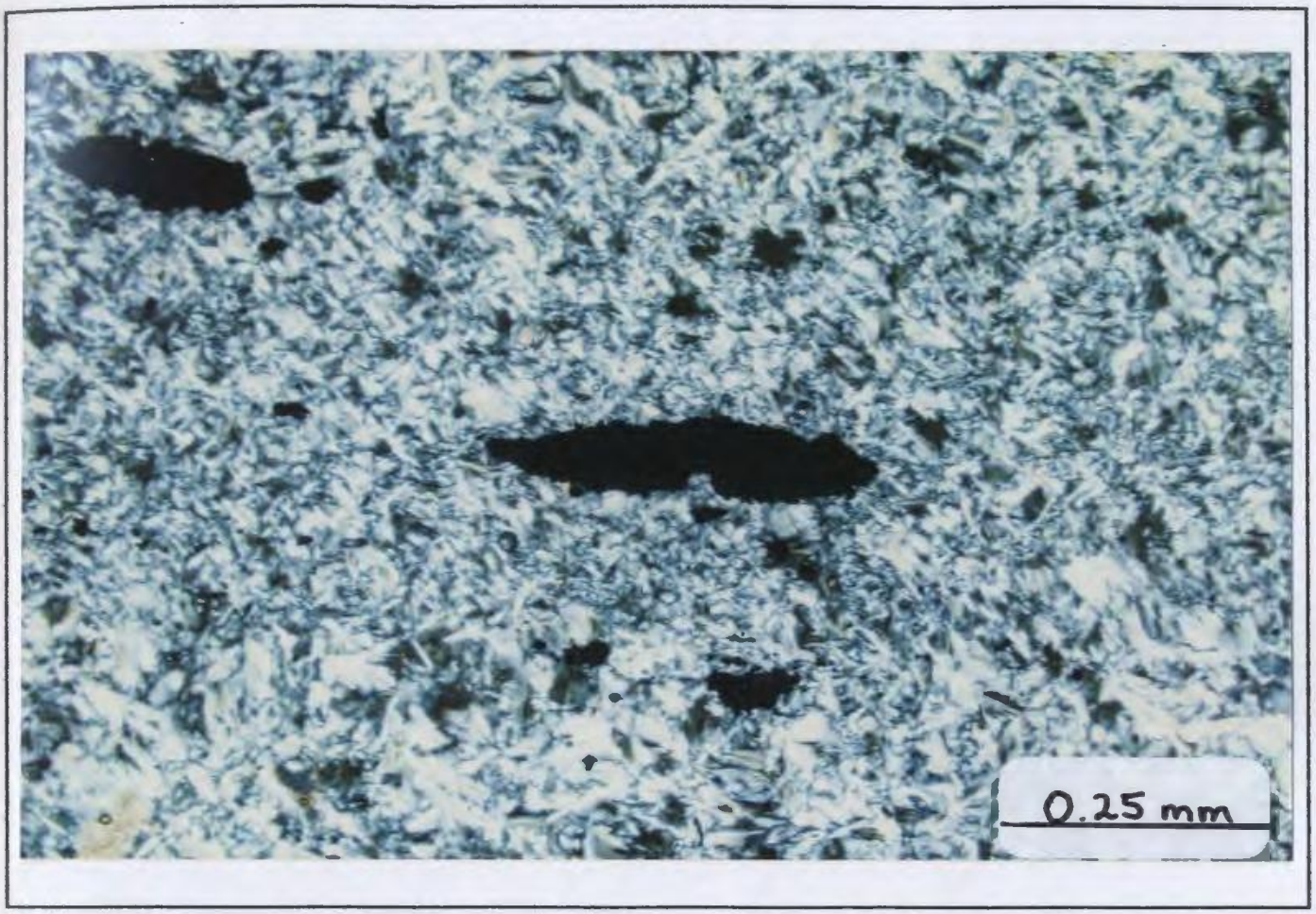

Fig. 5-17. Elongate spinel in antigorite-rich metadunite sample. (X-polarized light).

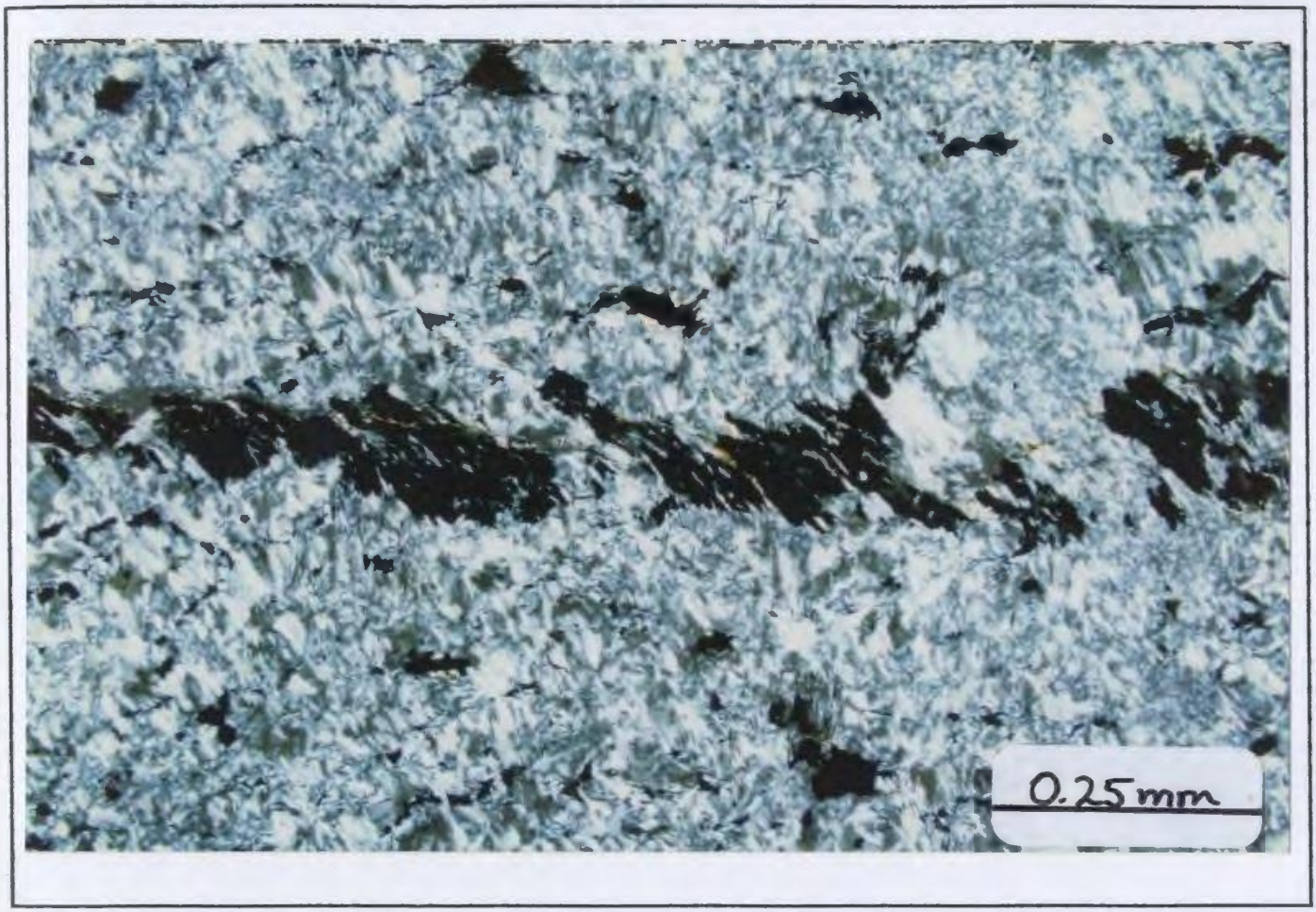

Fig. 5-18. Deformed spinel in antigorite-rich metadunite sample. Spinel in almost S-shaped. (X-polarized light).

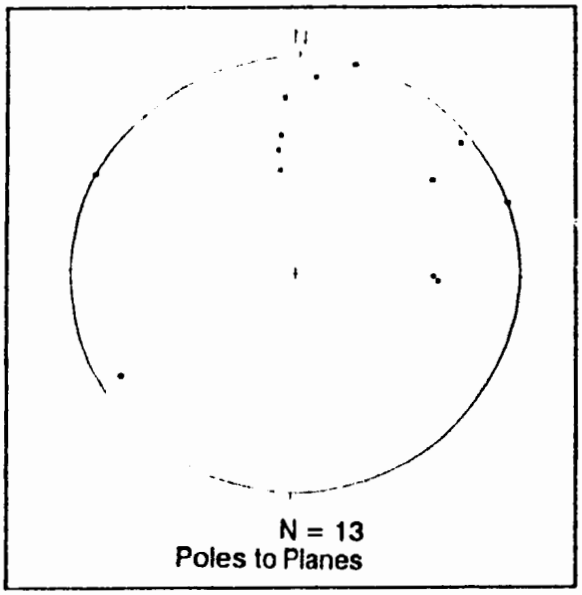

Fig. 5.19. Lower hemisphere, equal area stereonet plot of poles to layering in the ultramafic rocks. Layering is generally not parallel to shear zone fabrics in the pelitic metasediments.

the development of shear zone fabrics in the metasedimentary rocks. This relationship can be explained if the layering (fabric) is related to an earlier high temperature event such as formation of a mantle tectonite fabric, which is commonly defined by elongate spinels.

5.7 MELANGE ZONES

An obvious feature of the mafic-ultramafic rocks in this study is the disrupted nature of the bodies. This feature may be described in terms of a melange zone. However mélange zone terminology is varied and controversial and the origin of mélanges is in most cases equivocal. With this in mind, the following sections present a review of recent concepts concerning mélange zones, followed by a discussion of the situation in the

present map area.

5.7.1 Review of Mélange Zones

The term "mélange" was first used by Greenly (1919) for a rock unit in the Precambrian Mona Complex of Anglesey Island, Wales. Greenly used the term for a tectonic mixture of rocks and the term "autoclastic" was used as a descriptive term (i.e. autoclastic mélange). Since that time the term has been the focus of much debate in the geological literature. It has subsequently been recognized that mélanges may be developed by sedimentary as well as tectonic processes or even by a combination of both. Thus use of the term requires a decision as to the mode of origin. Clearly the two end-members are important with regard to large scale processes such as subduction, obduction and converging plate margins.

Hsu (1968) noted that although there is a complete gradation between the two end-member processes (tectonic and sedimentary), there is also a need to distinguish between the two where possible. He therefore proposed the term mélange for a mappable unit formed purely by tectonic processes and the term "olistostrome" for a unit formed purely by sedimentary processes. Hsu also recognized that in many instances, later deformation and/or metamorphism may obliterate any recognizable indicators and proposed that some other term such as "wildflysch" be used as a non-genetic term where the pure end-member processes cannot be determined.

Since then, the term mélange has been redefined by Berkland et al.

(1972), and has been the subject of a Penrose Conference (Silver & Beutner, 1980) where it was proposed to be a non-genetic term used to describe a mappable rock unit that is internally fragmented, containing a variety of blocks, and commonly has a deformed matrix. The processes involved in mélange formation are typically sedimentary sliding, tectonic movements or a combination of both, but no one process is excluded. It also has become common practice by many authors to use a genetic word to describe mélanges where the processes of formation can be recognized. Hence terms such as tectonic mélange, sedimentary mélange, olistostromal mélange etc. are common in the geological literature.

It is a common observation that many mélange zones throughout the world have mafic-ultramafic rocks within them, either as the matrix or as exotic blocks (or both). This observation is not surprising since many mélange zones are known to occur in zones of plate convergence usually involving oceanic lithosphere. Since the general term "mélange" does not refer to specific lithologies, Gansser (1974) proposed the term "ophiolitic mélange" for mélange zones that contain rocks of the ophiolite complex. An ophiolitic mélange was thought to result from a combination of both sedimentary and tectonic processes. The matrix of these mélange zones could be ophiolitic (typically tectonically sheared serpentinites) or sedimentary in origin. Gansser believed that the formation of ophiolitic mélanges could not be purely tectonic because that could not explain the mixture of exotic blocks of very varied composition. He also proposed that the main process of ophiolite mélange formation is "obduction" since many are exposed today. If subduction was the main process of formation, they

would be consumed during the subduction process. He did however, note that some ophiolitic mélanges contain blueschist facies assemblages and were related to subduction and subsequent uplift, but noted that this was not the most common origin.

Cowan (1985) presented a review of mélange zones from the Mesozoic and Cenozoic rocks in the western Cordillera of North America. He recognized four types of mélange zones (designated types I to IV) on the basis of mesoscopic fabric and lithologic composition. Of particular interest here is that mélange zones have also been classified on the bases of lithology. Cowan's type III mélange is of relevance to this study, being composed of inclusions of various sizes, shapes and compositions in a pelitic matrix (also analogous to ophiolitic mélange zones in which serpentinite matrix predominates). Cowan admits that the ultimate source of the inclusions in this type of mélange is obscure, but they are considered to be foreign to the presently adjacent rock units. He therefore proposes that the origin of type III mélange is due to final emplacement as olistostromes (muddy debris-flow deposits) or possibly mud diapirs.

In the Appalachian Mountain chain, a zone of matic-ultramatic rocks occurs along the eastern edge of the miogeocline. These bodies were viewed as olistoliths structurally mingled with their host rocks to form an olistostromal rock unit by Williams and Hatcher (1983). In this context, the entire eastern edge of the miogeocline may be interpreted as a large scale mélange zone. On a larger scale, the eastern edge of the miogeocline also contains individual units that have been mapped as mélange zones. For

example, in the Baie Verte Peninsula of northern Newfoundland, the Birchy Complex, a unit composed principally of mafic rocks in the greenschist facies, lies to the east of, and is interpreted to be conformable with the Fleur de Lys Supergroup (Williams, 1977). The Birchy Complex includes several units, one of which is the Coachman's Mélange that contains exotic ophiolitic and sedimentary blocks of varied character. Williams considered the Coachman's Mélange to be an olistostrome with a black shale matrix formed during emplacement of the ophiolite. Numerous other olistostromal mélange zones have been described in Newfoundland and all of them contain a black shale matrix (Williams & Piasecki, 1990).

Horton et al. (1986) described what they interpreted to be a metamorphosed mélange zone in the eastern Piedmont Terrane of North Carolina, U.S. Appalachians. The Falls Lake mélange is composed of mafic and ultramafic blocks and pods that have no apparent stratigraphic continuity and are diverse in shape and size. The matrix is pelitic schist and biotite-muscovite-plagioclase-quartz gneiss. The area is important to the present study in that it is one of the few described mélange zones in the literature (and in the Appalachian Orogen) that has high grade metamorphic rocks as the matrix. They concluded that the zone was formed by a combination of sedimentary and tectonic processes, possibly in the accretionary wedge of a convergent plate margin. The criterion used to infer "sedimentary processes" is that some of the small blocks have rounded to angular shapes and embayed margins. However clearly the original shapes of the blocks may have been modified during subsequent regional metamorphism, so this criterion is not readily applicable in areas

of high strain.

5.7.2 The Map Area As Part Of A Mélange Zone

Some areas of the present study clearly show the "block in matrix" pattern typical of many mélange zones described in the geological literature. Figure 3-14 shows an "isolated" inclusion of ultramafic rocks sitting within metasedimentary rocks (matrix). Such features are widespread in the metasedimentary units, and are not restricted to the map-scale bodies shown in Figure 3-1. The problem then is whether the "block in matrix" relationship resulted by progressive deformation as a result of shearing of a sequence of metasediments and mafic-ultramafic plutonic rocks, or is the result of sedimentary processes associated with obduction of an ophiolite, or a combination of both.

As discussed in previous sections, the high strain and high grade metamorphism and subsequent partial retrogression in shear zones has rendered any sedimentary relationships difficult to interpret. Although some angular shaped blocks with embayed margins occur within the map area, they have only been observed within granitoid agmatite zones (Fig. 3-21) and their angular nature is interpreted to be a result of the injection of the granitoid. Therefore sedimentary processes (and an origin as an olistostrome) cannot be unequivocally proved for the present study area.

In conclusion, there is a mixture of mafic-ultramafic and

metasedimentary rocks in the map area, but its origin, whether tectonic or sedimentary (or both), is not readily apparent on account of the high metamorphic grade and strain. Nevertheless, there is widespread evidence of shearing in the study area, suggesting that the origin of the mélange is at least in part tectonic in origin. Thus, although new information concerning the mafic-ultramafic and surrounding rocks of this study is presented in this thesis, the origin of the mélange cannot be unambiguously answered. Therefore, the area should not be described as mélange or olistostrome using the terms as proposed by Hsu (1968), but certainly constitutes a mélange zone in the sense of a non-genetic term as defined at the Penrose Conference. Use of the term "type III mélange" (Cowan, 1985) should also be avoided because of its genetic implications. The term "ophiolitic mélange" (Gansser, 1974) may be used for the study area provided the mafic-ultramafic rocks are proven to be of ophiolitic origin. However, it should be noted that the rocks in this study area are not typical of the many other ophiolitic and/or olistostromal mélanges found throughout Newfoundland. The grade of metamorphism is much higher in the study area and the typical black shale matrix of other Newfoundland mélanges is not present.

5.8 SUMMARY

At least three main phases of deformation have affected the pelitic metasedimentary rocks. An initial phase of isoclinal folding (D1) with associated layer-parallel fabric (S1) was followed by the development of high strain zones with associated mylonitic fabrics. The mylonitic fabrics

anastomose on a regional scale and the unit is envisaged as one large scale shear belt. A second generation of isoclinal folding is also recognized but the timing of development has not been determined (i.e. before, during or after shearing). A lower limit on the age of deformation events D1 and D2 is not well constrained. However an upper limit is the age of the granodiorite (456 ±3 Ma) that intrudes the metasediments since no isoclinal folding or major shear zones have been recognized in the granodiorite.

The matic-ultramafic rocks were emplaced into the metasedimentary rocks prior to or during the deformational event related to shearing (D2) and are highly deformed themselves. The field relationships that resulted from incorporation of the matic-ultramafic rocks into the sedimentary rocks are consistent with a typical mélange zone and the present evidence suggests shearing is the major mechanism of disruption of these rocks. Evidence for sedimentary processes involved in the mélange formation cannot be proven.

Chapter 6

METAMORPHISM

6.1 INTRODUCTION

In a mélange zone it is possible that the host rocks and their inclusions could possess different metamorphic signatures, and so in this case it is necessary to compare the metamorphic histories of both the metasedimentary rocks and their mafic-ultramafic inclusions. This chapter therefore presents a summary of the metamorphic features of the rocks in terms of lithology and is presented in two parts. Firstly the regional metamorphism in the metasedimentary rocks (psammitic and pelitic units) is presented, followed by an account of the metamorphism of the mafic-ultramafic rocks (metadunite, metapyroxenite and metagabbro).

All rocks within the map area are interpreted to have been metamorphosed to at least the upper amphibolite facies, but some have subsequently been variably retrogressed to greenschist facies assemblages. The greenschist facies metamorphism appears to have resulted from the migration of hydrous fluids through the shear zones described in the previous chapter, but has locally affected adjacent, non-sheared rocks, so that there is a complete gradation from rocks that contain mainly high grade assemblages through rocks that are completely retrogressed to greenschist facies assemblages.

6.2 METASEDIMENTARY ROCKS

The metasedimentary rocks are discussed in terms of the two units psammitic and pelitic as presented in Figure 3-1. Although the psammitic unit consists predominantly of psammitic rocks, minor layers of pelitic composition occur. In addition, the predominantly pelitic unit contains minor layers of psammitic composition. The pelitic unit is catagorized further in terms of unsheared rocks and sheared rocks. The majority of the rocks in this unit are highly sheared and have been retrogressed in the greenschist facies. However, evidence of a pre-existing high grade metamorphic event can be found in a few unsheared samples. Shear zones have been observed in the psammitic metasedimentary unit, but they have not been mapped in detail as part of this study.

Representative mineral assemblages from the metasedimentary rocks are presented in Table 6-1. K-feldspar was checked for by the K-cobaltinitrate staining method in all lithologies but was found in only one sample from the psammitic unit (sample T-76).

6.2.1 Psammitic Metasedimentary Unit

The psammitic metasedimentary rocks are migmatitic and typically display a well-developed stromatic layering described in Chapter 3. The samples examined in detail as part of this study are from along the contact with the pelitic metasediments. Mineral assemblages are presented in Table 6-1. Leucosomes are coarse-grained and typically contain plagioclase +

TABLE 6-1

REPRESENTATIVE MINERAL ASSEMBLAGES

Psammitic Metasedimentary Unit

	Melanosomes	Leucosomes
T-33	bio+gnt+pla+qtz+(chl)+(mus)	qtz+pla+bio
T-69	bio+gnt+pla+qtz+(chl)+(mus)	qtz+pla+bio
T-73	bio+gnt+pla+qtz+(chl)+(mus)	qtz+pla+bio
T-76	bio+gnt+pla+qtz +(mus)	qtz+pla+K-spar+bio
T-193	bio+ +pla+qtz +(mus)	qtz+pla+bio

T-13 (pelitic schist) sil(fibrolite)+gnt+bio+pla+qtz+(mus)+(chl)

Pelitic Metasedimentary Unit

Unsheared Pelitic Rocks

T-3	herc+sil+bio	+gnt+pla+qtz+mt+ilm+(mus)	
T-24	sil+bio	+gnt+pla+qtz+mt+ilm+(mus)	
T-26	sil+bio	+gnt+pla+qtz+mt+ilm+(mus)	
T-32	sil+bio	+gnt+pla+qtz+mt+ilm+(mus)+(chl)	
T-44	sil+bio+crd	+pla+qtz+mt+ilm+(mus)+(chl)+(kya)+(sta)	
T-19	sil+bio+crd	+gnt+pla+qtz+mt+ilm+(mus)+(chl)+(kya)+(sta)	
T-39	bio+crd	+gnt+pla+qtz+mt+ilm+(mus)+(chl)+(kya)+(sta)	
T-40	sil +crd	+pla+qtz+mt+ilm+(mus)+(chl)+(kya)+(sta)	
T-42	sil +crd	+gnt+pla+qtz+mt+ilm +(chl)+(kya)+(sta)	
T-67	sil +crd	+gnt+pla+qtz+mt+ilm+(mus)+(chl)+(and)	

T-15 qtz+pla+bio+mt+ilm+(mus)+(chl)+(epi)
T-48 qtz+pla+bio+mt+ilm+(mus)+(chl)+(epi)
T-58 qtz+pla+bio+mt+ilm+(mus)
D-208 qtz+pla+bio+mt+ilm+(mus)+(chl)

Note samples contain minor leucosomes of qtz+pla

Sheared retrograde rocks

T-59 qtz+pla+chl+ser+mus+epi+mt+ilm
T-61 qtz+pla+chl+ser+mus+epi+mt+ilm +[gnt]
T-77 qtz+pla+chl+ser+mus+epi+mt+ilm+[bio]
T-142 qtz+pla+chl+ser +mt+ilm+[bio]+[sil]+[gnt]
T-150 qtz +chl+ser+mus+epi+mt+ilm
T-154 qtz +chl+ser +epi+mt+ilm+[bio] +[gnt]

[ ] represents relic phases
( ) represents retrograde phase
Underlined samples used for thermometry and barometry.

quartz + minor biotite; however up to 20% coarse-grained K-feldspar occurs with this assemblage in sample T-76. Melanosome portions are finer-grained, containing mainly biotite (± garnet) with lesser amounts of quartz + plagioclase. In the melanosomes the biotite has a preferred orientation that defines a planar fabric. In all samples, minor retrograde coarse-grained chlorite and muscovite have developed along the edges of biotite and locally plagioclase is altered to sericite. Typically the psammitic metasedimentary rocks lack the aluminous (sillimanite/kyanite) and Fe-Ti oxide phases that are characteristic of the pelitic metasedimentary unit (see below).

One sample from a lens of pelitic schist within the metapsammite unit contains the assemblage sillimanite + biotite + garnet + quartz + plagioclase. The sillimanite is fibrolite and distinctly different from the prismatic sillimanite characteristic of the rocks in the pelitic metasedimentary unit (see below). The sillimanite and biotite define a well-developed schistosity that wraps around the garnets. Up to 20% coarse-grained muscovite occurs, but is interpreted to be a later retrograde phase because the crystals cross-cut the main fabric. Leucosome layers of quartz + plagioclase also occur parallel to the schistosity.

The common mineral assemblage of biotite (± garnet) + plagioclase (± K-feldspar) + quartz in the metapsammites is stable over a wide range of metamorphic grade. However, the sub-assemblage of sillimanite + garnet + biotite in the pelitic schist lens within this unit implies conditions above the stability of staurolite + muscovite + quartz, which break down

according to the reaction:

(A) staurolite + muscovite + quartz = sillimanite + biotite + garnet + H_2O

In this case all staurolite and primary muscovite have been consumed so microstructural evidence for the reaction is not available. The origin of the leucosome layers of quartz + plagioclase is not firmly established, but their tonalitic composition suggests that they may be of injection (rather than partial melting) origin. There is no evidence of melting reactions such as

(B) biotite + sillimanite + albite + quartz + H_2O = cordierite + liquid

(C) biotite + sillimanite + albite + quartz + H_2O = K-feldspar + cordierite (± garnet) + liquid

which might be expected in rocks of this composition.

6.2.2 Pelitic Metasedimentary Unit

Mineral assemblages of rocks within the pelitic metasedimentary unit are presented in Table 6-1. The assemblages are variable and reflect different bulk rock compositions as well as prograde and retrograde metamorphic reactions. All samples contain the common assemblage of plagioclase + quartz + Fe-Ti oxides. No primary muscovite was observed and K-feldspar was not formed. For descriptive purposes, the rocks within this unit are divided into unsheared rocks and sheared rocks.

6.2.2.1 Unsheared rocks

The stable AFM sub-assemblage in four samples (T-3, T-24, T-26, T-32) is garnet + biotite + sillimanite implying conditions above the stability of staurolite (reaction A). Biotite typically displays an equilibrium decussate texture of interlocking grains and sillimanite occurs as coarse prismatic crystals. Garnets range from tiny (less than 0.25 mm) inclusion free grains to relatively large grains (up to 3 mm) that contain abundant inclusions of sillimanite + biotite + quartz + Fe-Ti oxides (see Chapter 7 for further discussion on garnets).

One sample (T-44) contains cordierite that is associated with leucosome (quartz + plagioclase) layers (Fig. 6-1). This sample also contains melanosome layers consisting of abundant biotite + sillimanite and no garnet has been observed. This texture suggests that the rocks may have partially melted according to reaction B during their prograde metamorphism. Although no garnet was found in this particular sample, there is evidence in other samples (T-19, T-39, T-42 and T-67) that garnet + cordierite did occur together. This may indicate partial melting according to the reaction:

(D) biotite + sillimanite + quartz + H_2O = cordierite + garnet + liquid

Evidence of a higher temperature assemblage has been observed in sample T-3 where spinel (hercynite) was observed enclosed in garnet and in coarse prismatic sillimanite (Fig. 6-2). Quartz occurs adjacent to garnet

Fig. 6-1. Photomicrograph of cordierite grains associated with leucosome (quartz + feldspar). Melanosome consists of biotite + sillimanite + Fe-Ti oxides. (Plane polarized light).

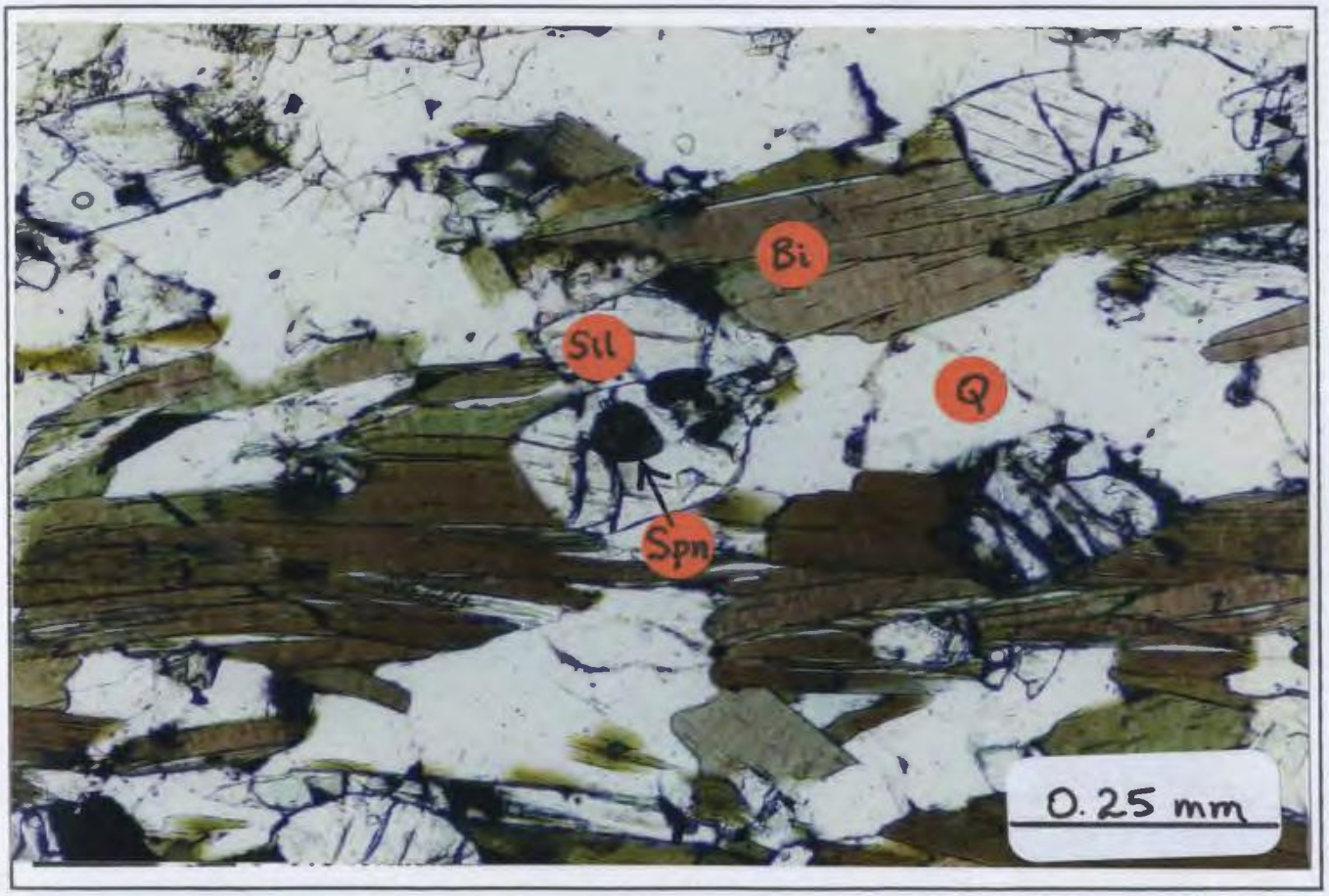

Fig. 6-2. Photomicrograph of spinel (hercynite) in prismatic sillimanite grain. (Plane polarized light).

and sillimanite, but is isolated from hercynite. This texture suggests that the garnet and prismatic sillimanite formed by the reaction:

(E) spinel + quartz = garnet + Al_2SiO_5

The former existence of the stable assemblage spinel + quartz, in addition to the possible partial melting reactions as outlined above implies the attainment of relatively high temperature conditions early in the metamorphic event. The existance of the stable assemblage sillimanite + biotite + garnet, the coexistance of cordierite + garnet and the occurrence of cordierite in leucosome layers suggests the variations in stable, high grade mineral assemblages through this unit may be a result of sampling through different layers of a partially melted migmatite complex. It should be noted here that no K-feldspar has been observed in these rocks and therefore a reaction such as A cannot be proven.

Subsequent lower grade metamorphism has overprinted all the high grade mineral assemblages outlined above. Figures 6-3 and 6-4 are photomicrographs of sample T-19 showing evidence of the breakdown of garnet and cordierite. In Figure 6-3, garnet is rimmed by prismatic sillimanite and in Figure 6-4 a former cordierite grain has been replaced by sillimanite + biotite (some of the biotite has subsequently been replaced by chlorite). These textures suggest the reaction:

(F) cordierite + garnet + H_2O = sillimanite + biotite

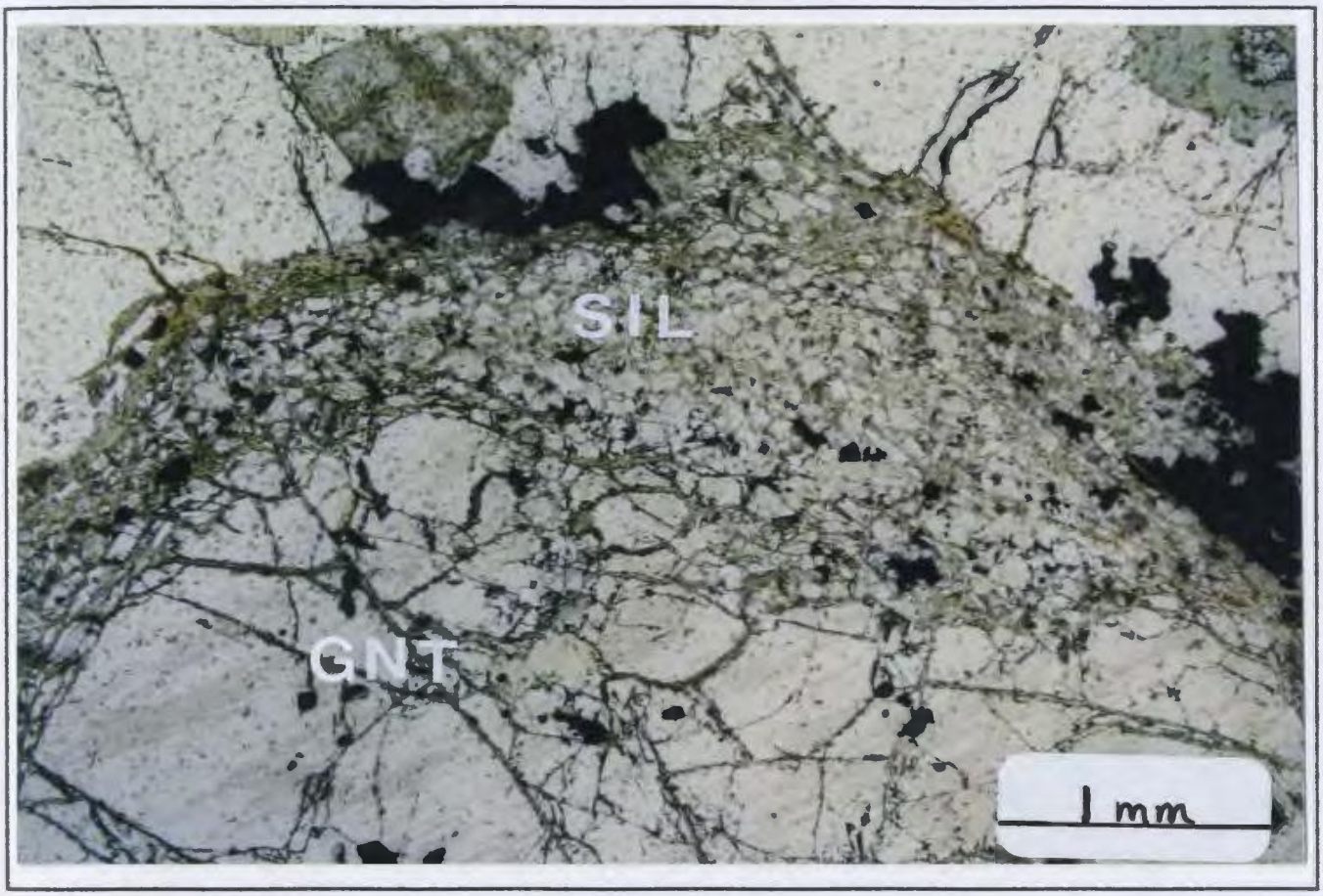

Fig. 6-3. Photomicrograph of garnet rimmed by prismatic sillimanite. Small grain of pinnitized cordierite near top of photograph. Retrograde reaction discussed in text. (Plane polarized light).

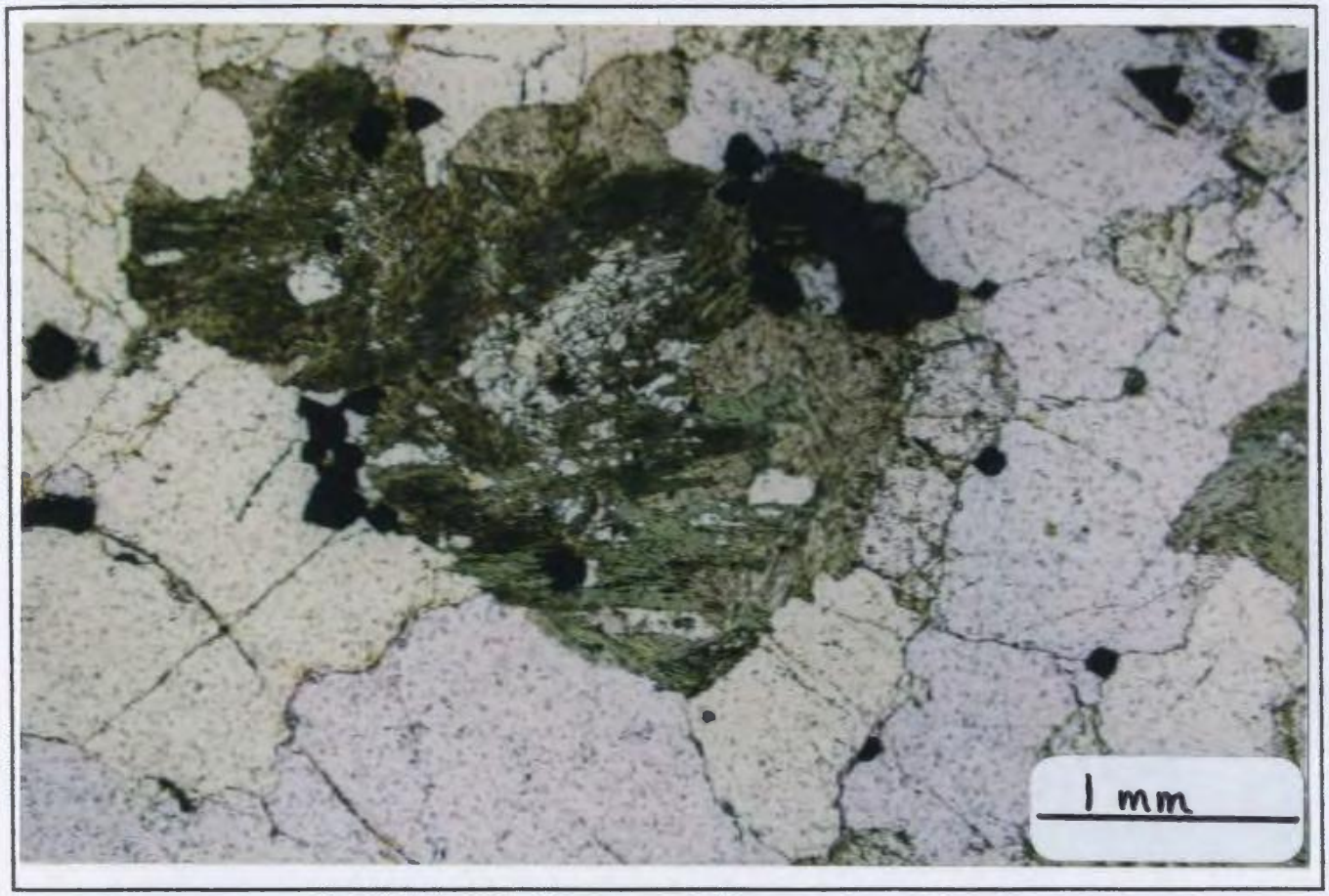

Fig. 6-4. Photomicrograph of highly pinnitized cordierite replaced by an assemblage of biotite + sillimanite which is subsequently altered to chlorite. Same sample as Figure 6-3. (Plane polarized light).

Figure 6-5 shows evidence of a lower grade reaction whereby sillimanite + biotite have reacted to form staurolite + chlorite + quartz by the reaction:

(G) sillimanite + biotite + H_2O = staurolite + chlorite + quartz

Figure 6-6 shows cordierite breaking down to chlorite + kyanite + quartz by the reaction:

(H) cordierite + H_2O = chlorite + kyanite + quartz

In contrast to the early high temperature phases, kyanite and staurolite are always associated with chlorite and do not exhibit a preferred orientation. This textural evidence suggests that the kyanite and staurolite are retrograde phases. Although the typical retrograde Al_2SiO_5 phase is kyanite, sample T-67 contains andalusite as the Al_2SiO_5 retrograde phase. Since most samples show evidence of crossing the sillimanite/kyanite boundary and at least one sample shows evidence of crossing the sillimanite/andalusite boundary, the overall path of retrograde metamorphism likely spaned the Al_2SiO_5 triple point junction.

In addition to the above retrograde reactions cordierite shows variable affects of pinnitization from unaltered to completely pinnitized and garnet is replaced by chlorite ± muscovite ± quartz. Large poikiloblasts of secondary muscovite are also common and contain inclusions of sillimanite in places (Fig. 6-7).

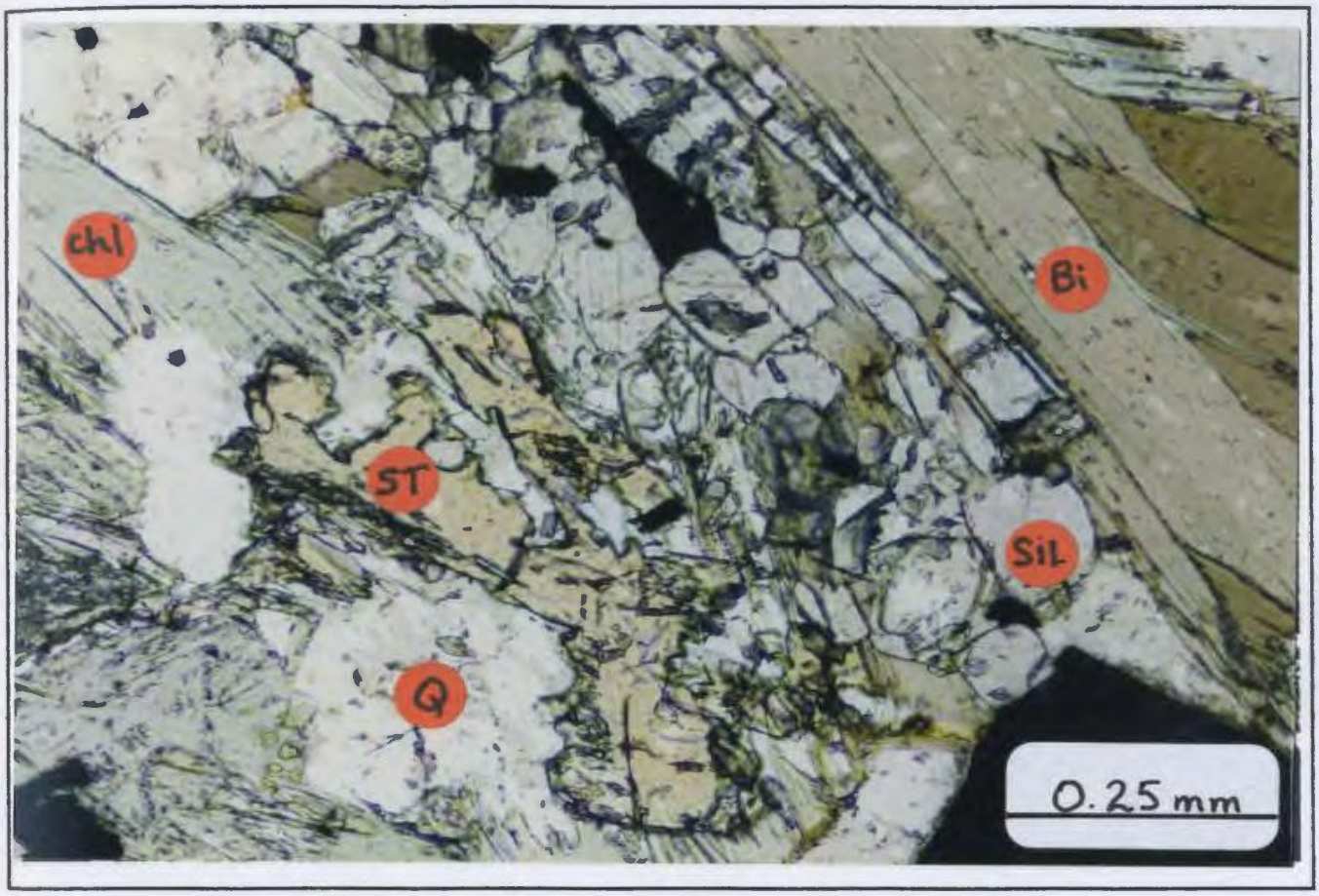

Fig. 6-5. Photomicrograph of retrograde reaction sillimanite + biotite = staurolite + chlorite + quartz. (Plane polarized light).

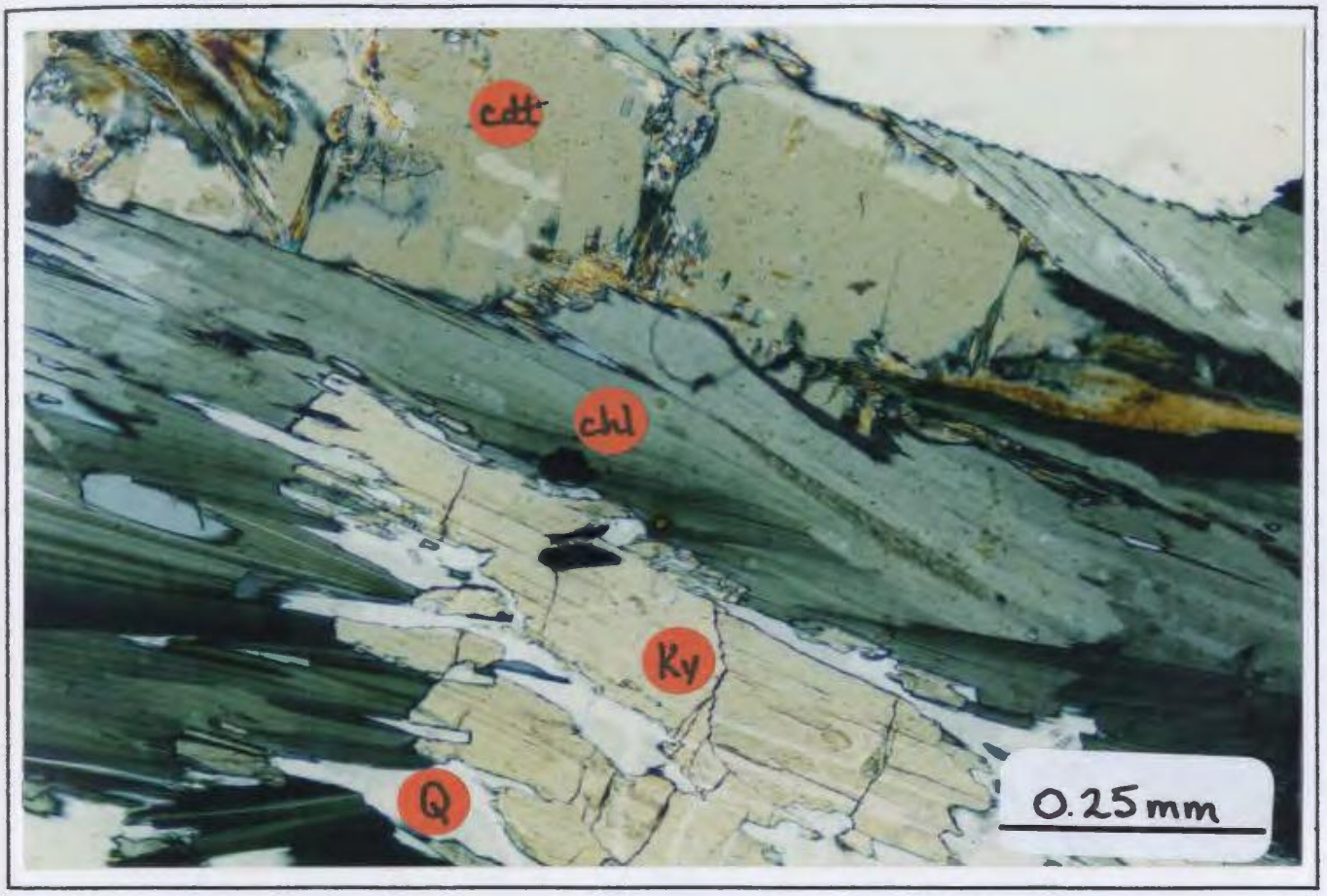

Fig. 6-6. Photomicrograph of retrograde reaction cordierite + H_2O = kyanite + chlorite + quartz. (X-polarized light).

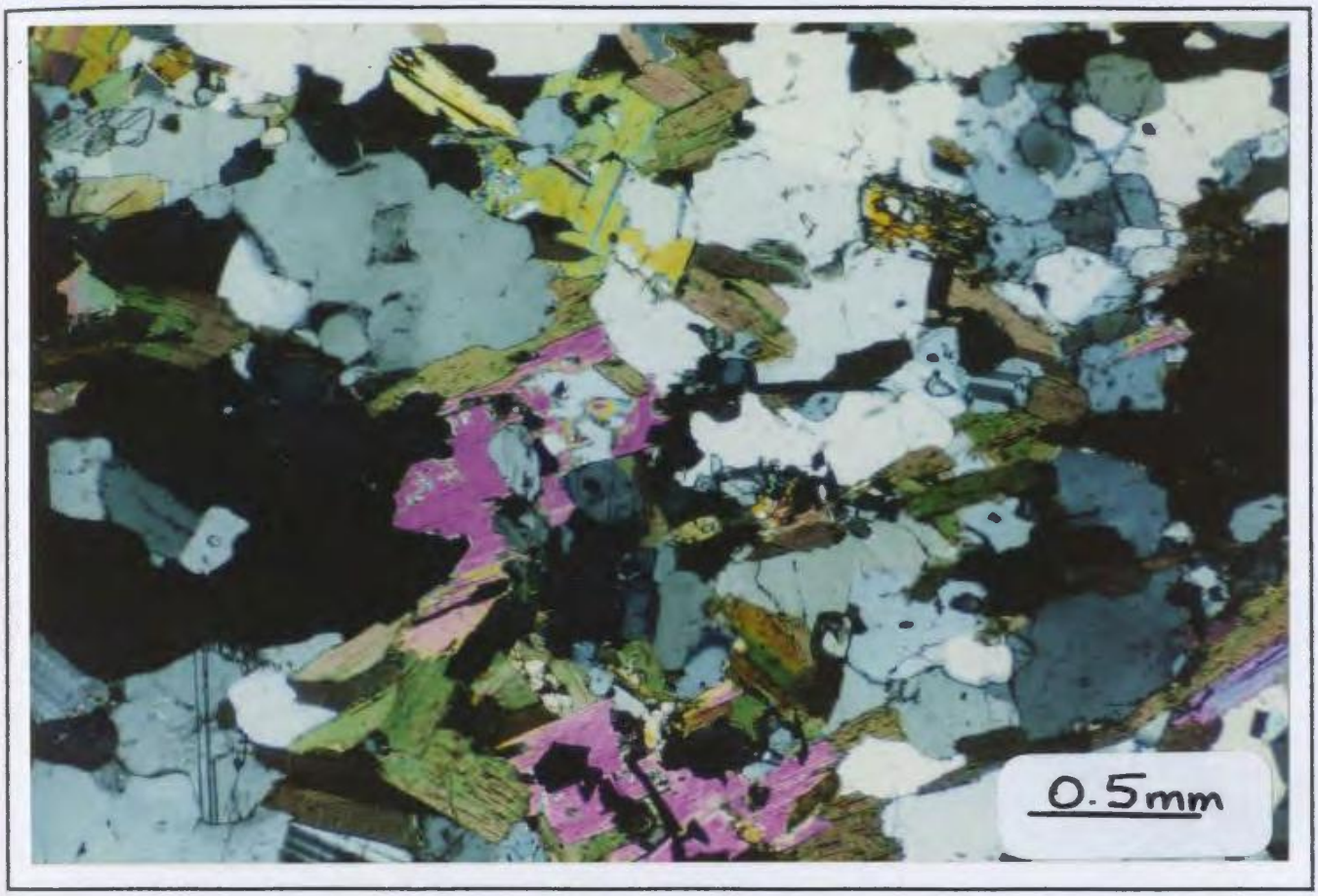

Fig. 6-7. Photomicrograph of sample T-26 showing late secondary muscovite poikiloblasts that overgrow the high grade fabric. The muscovite in the center of the photograph contains inclusions of sillimanite and quartz. (X-polarized light).

Minor layers of psammitic rocks that contain the assemblage quartz + plagioclase + biotite + Fe-Ti oxides also occur within the pelitic metasedimentary unit. Retrograde epidote occurs in several samples and muscovite and chlorite are developed on the edges of biotite grains. The stable assemblage in these psammitic rocks does not indicate a precise metamorphic grade but can occur over a range from greenschist to amphibolite facies.

6.2.2.2 Sheared rocks

Most of the highly sheared rocks within the pelitic metasedimentary unit contain greenschist facies mineral assemblages consisting of chlorite + muscovite + quartz + Fe-Ti oxides. However remnant garnet, sillimanite and biotite were observed in several samples. The garnet and sillimanite both occur as augen in a highly sheared matrix of sericite and chlorite (see Chapter 5). Where garnet is still preserved in the highly retrogressed samples, it is typically fractured and partially retrogressed to chlorite ± muscovite ± quartz. Although the matrix of highly sheared samples is typically very fine-grained sericite, large (overprinting) muscovite poikiloblasts are common. These grains are commonly kinked and typically grow across the shear fabric suggesting they formed after the main shearing event, but before the end of deformation.

6.3 THE PETROGENETIC GRID

Figure 6-8 is a pressure-temperature diagram with approximate

Fig. 6-8. Petrogenetic grid with reactions for metapelites.

Reaction 1 Bohlen et al., 1986
Reaction 2 Grant, 1985
Reaction 3 Thompson, 1976
Reaction 4 Hsu, 1968
Reaction 5 Hess, 1969
Reaction A Hoffer, 1978

Reactions 1-5 are retrograde reactions and reaction A is a possible prograde reaction as discussed in text.

Al_2SiO_5 triple-point junction after Holdaway, 1971.

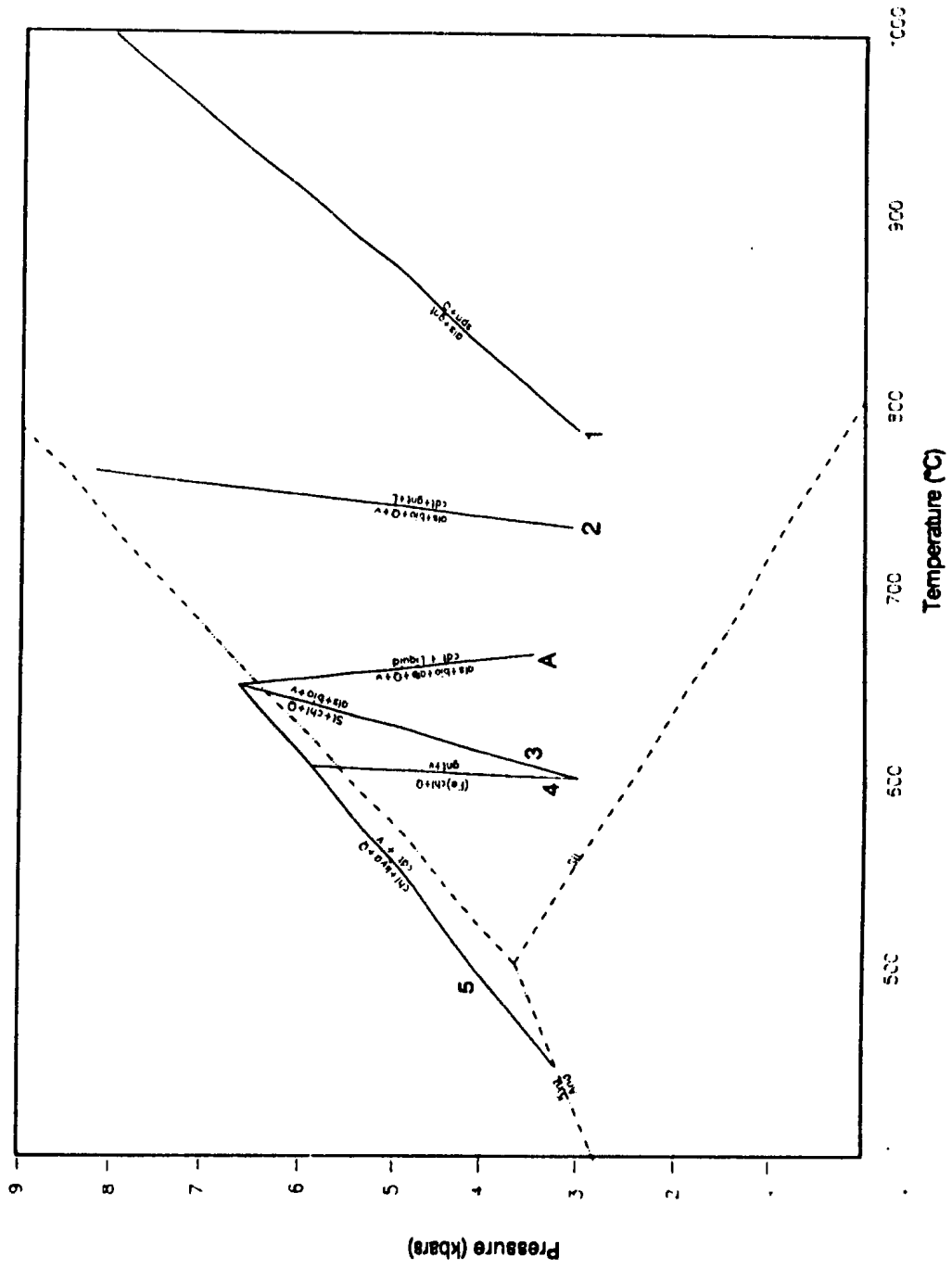
Pressure (kbars)
Temperature (°C)
1
2
3
4
5
A
H2O

locations of the reactions discussed above. The majority of the reactions are retrograde from the high temperature stable assemblage of spinel + quartz through to low grade greenschist facies assemblages. On the basis of the observed mineral assemblages, pressures are not well constrained with the exception that kyanite is the typical retrograde phase but andalusite was noted in sample T-67. Therefore a minimum pressure is interpreted to be near the Al_2SiO_5 triple point junction.

It should be noted here that if the rocks containing cordierite partially melted by a biotite + sillimanite breakdown reaction as suggested above, then K_2O would be expected, at least as a component in the melt if not as a separate phase in K-feldspar. However no K-feldspar has been observed in these rocks. Ashworth (1985) has outlined several reasons why this is possible and noted that a scarcity of K-feldspar also has been described from various other migmatitic terranes around the world (e.g. Brown, 1983). One possible explanation for a lack of K-feldspar is that that fraction of the melt has escaped and is now somewhere else.

6.4 MAFIC-ULTRAMAFIC ROCKS

Mafic-ultramafic rocks occur as inclusions in the metasedimentary rocks and granitoid suite. They contain a diverse sequence of metamorphic assemblages recording the metamorphic history of the belt. The mafic-ultramafic rocks described below are mainly from the metapelite unit and are typically associated with the shear zones in that unit. The rocks are classified as metadunite, metapyroxenite or metagabbro. These will be described in detail below to assess their metamorphic history. This will then be compared to the metamorphic history of the metasedimentary rocks described in previous sections.

The inclusions in the surrounding metapsammite unit and granitoid suite were observed only on a reconaissance basis and were mapped as "amphibolites" in the field. A detailed analysis of their composition was not undertaken as part of this study and therefore a classification of rock types is not possible.

6.4.1 Metadunite

The metadunites are partially to totally hydrated and/or carbonatized to serpentine and talc-carbonate assemblages. As discussed in Chapter 4, olivine was found in only three samples and is interpreted to be recrystallized, metamorphic olivine. If this is indeed the correct interpretation, the original igneous rock must still have been a dunite. Therefore the original igneous assemblage was probably olivine + chrome

spinel. No orthopyroxene, clinopyroxene or plagioclase have been observed in the metadunites.

In most samples, the early assemblage is pervasively replaced by one of the following metamorphic assemblages:

(1) antigorite (± brucite ?) + magnetite + ferritchromite + chlorite
(2) talc + magnesite + chlorite
(3) lizardite (± brucite ?) + magnetite + minor ferritchromite

In order to understand the metamorphic history of the metadunites it is essential to determine the type of serpentine present since it is commonly accepted that lizardite is the low temperature mineral and antigorite is the high temperature mineral. This can only be done with confidence using a combination of petrographic observations of serpentine textures, XRD analyses and serpentine chemistry. These aspects are presented in detail below.

6.4.2 Serpentine Textures in Metadunites

A brief literature review of serpentine textures is given in Appendix E. The metadunites examined in this study show a wide range of serpentine textures which are described below with the serpentine type being classified according to optical properties. XRD and microprobe analyses (see below) show that the pseudomorphic serpentine is generally lizardite whereas the non-pseudomorphic serpentine is antigorite. However a detailed

interpretation of serpentine types (lizardite, chrysotile or antigorite) in all the textures described below is not possible without microbeam X-ray camera analyses (e.g. Wicks & Whittaker, 1977).

6.4.2.1 Pseudomorphic textures

Where olivine is still preserved, it contains serpentine in fractures that displays the typical mesh texture. The serpentine is aligned with its apparent fiber axis at right angles to the central parting and is always α serpentine (Fig. 6-9). In this example, hydration is not complete and olivine remains in the mesh center.

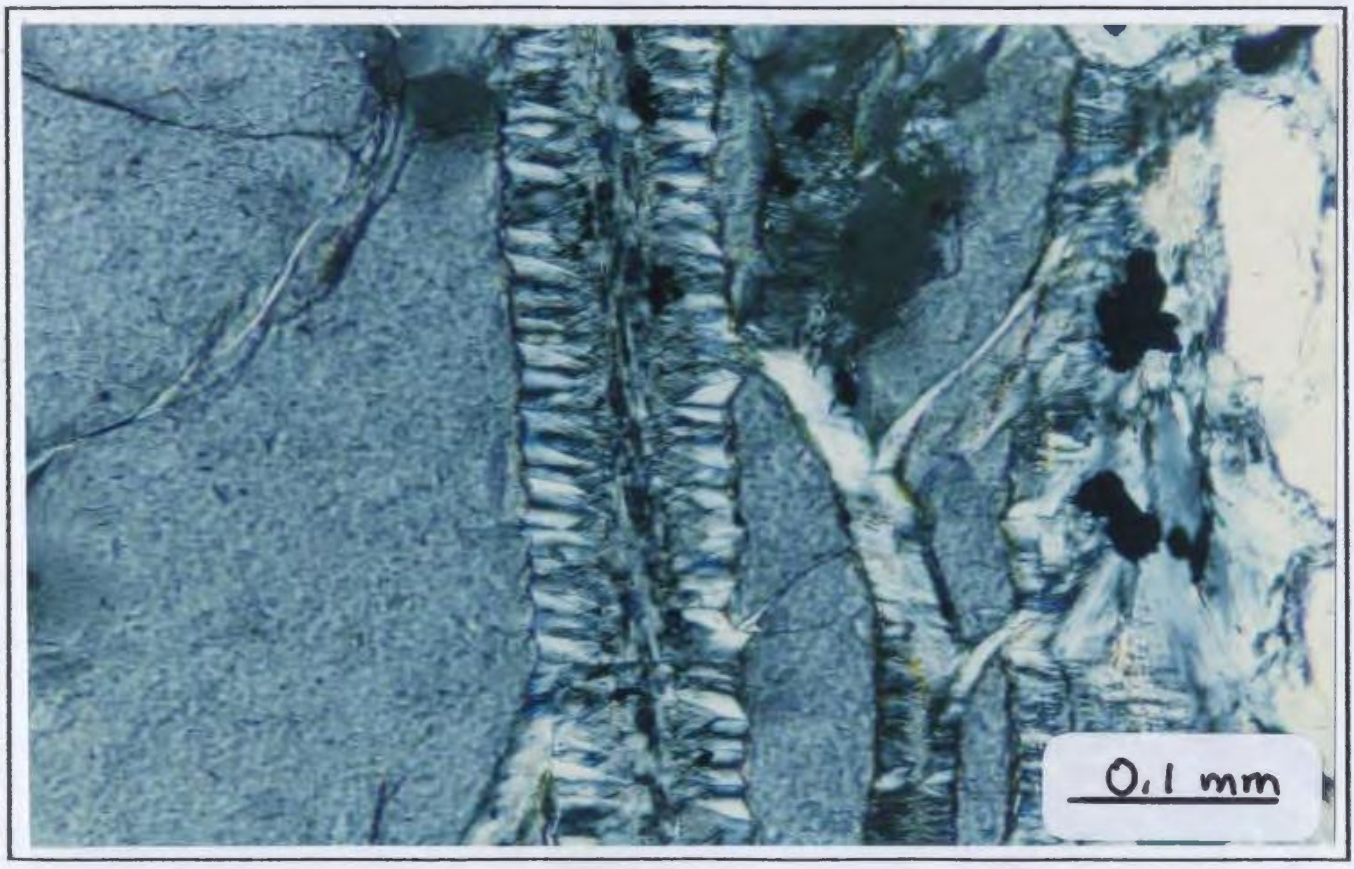

Fig. 6-9 Photomicrograph of lizardite vein in olivine. The lizardite is aligned with its apparent fibre axis at right angles to the vein boundary. (X-polarixed light).

Mesh textures have also been observed where hydration reactions have consumed all the olivine in the mesh centers and only serpentine remains (Fig. 6-10). In this example, mesh rims and centers are composed of α serpentine and the centers have apparent fibers that are optically continuous with those in the mesh rims. The serpentine in the mesh centers is yellowish in color and may be intergrown with a fine-grained phase tentatively identified as brucite. Several central partings are filled with magnetite whereas others contain serpentine. The dark outlines around mesh centers and in mesh rims may be magnetite or weathered serpentine.

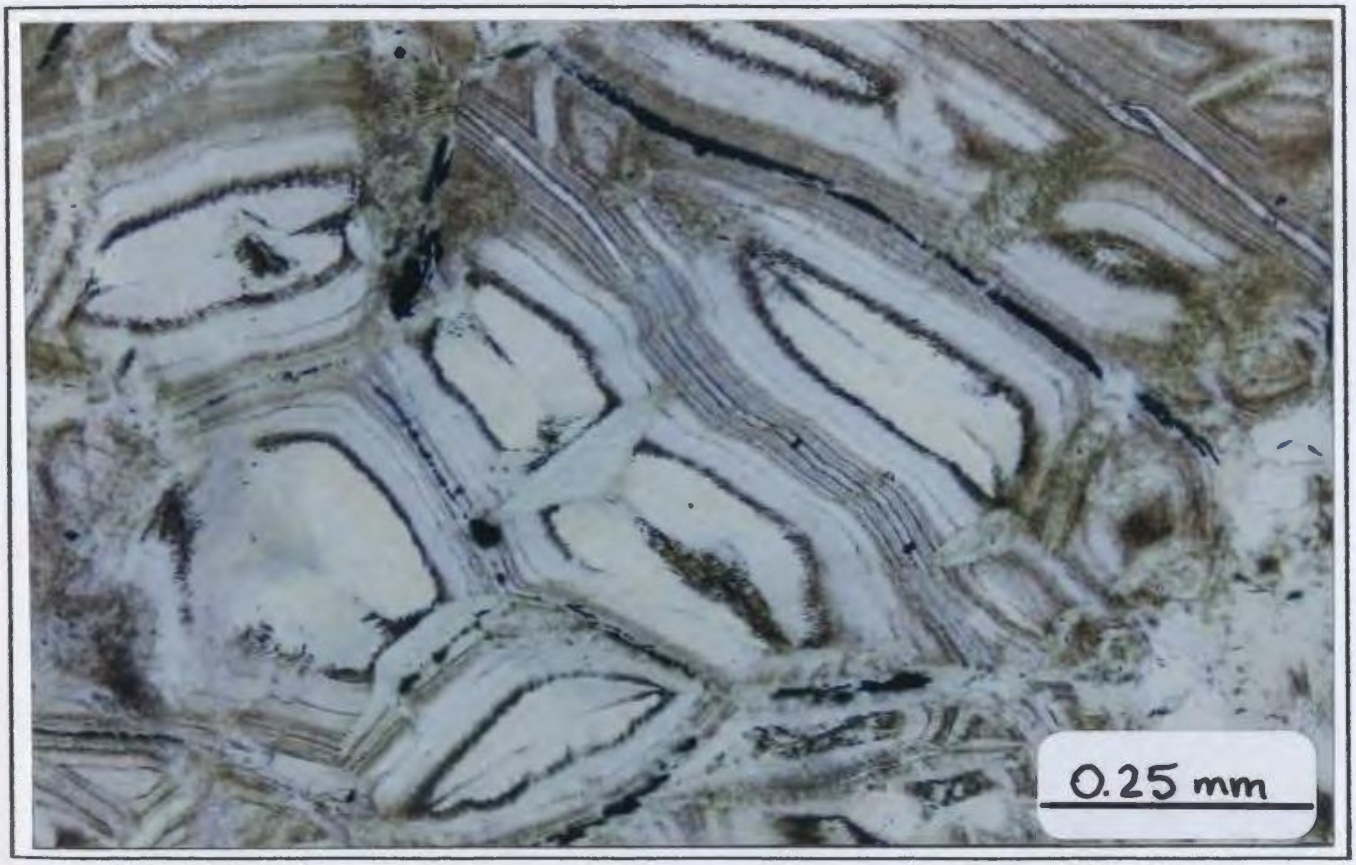

Fig. 6-10. Photomicrograph of pseudomorphic serpentine (lizardite) forming mesh texture after olivine but no olivine remains in the sample (i.e. total hydration). Note that some central partings are filled with magnetite and others are filled with serpentine. (Plane polarized light).

The mesh texture forms asymmetrical mesh cells developed by the bifurcation of central partings which probably follow initial fractures in the olivine grains. Some areas also contain three central partings which form tripartite veins and corresponding compound mesh rims (Fig. 6-11).

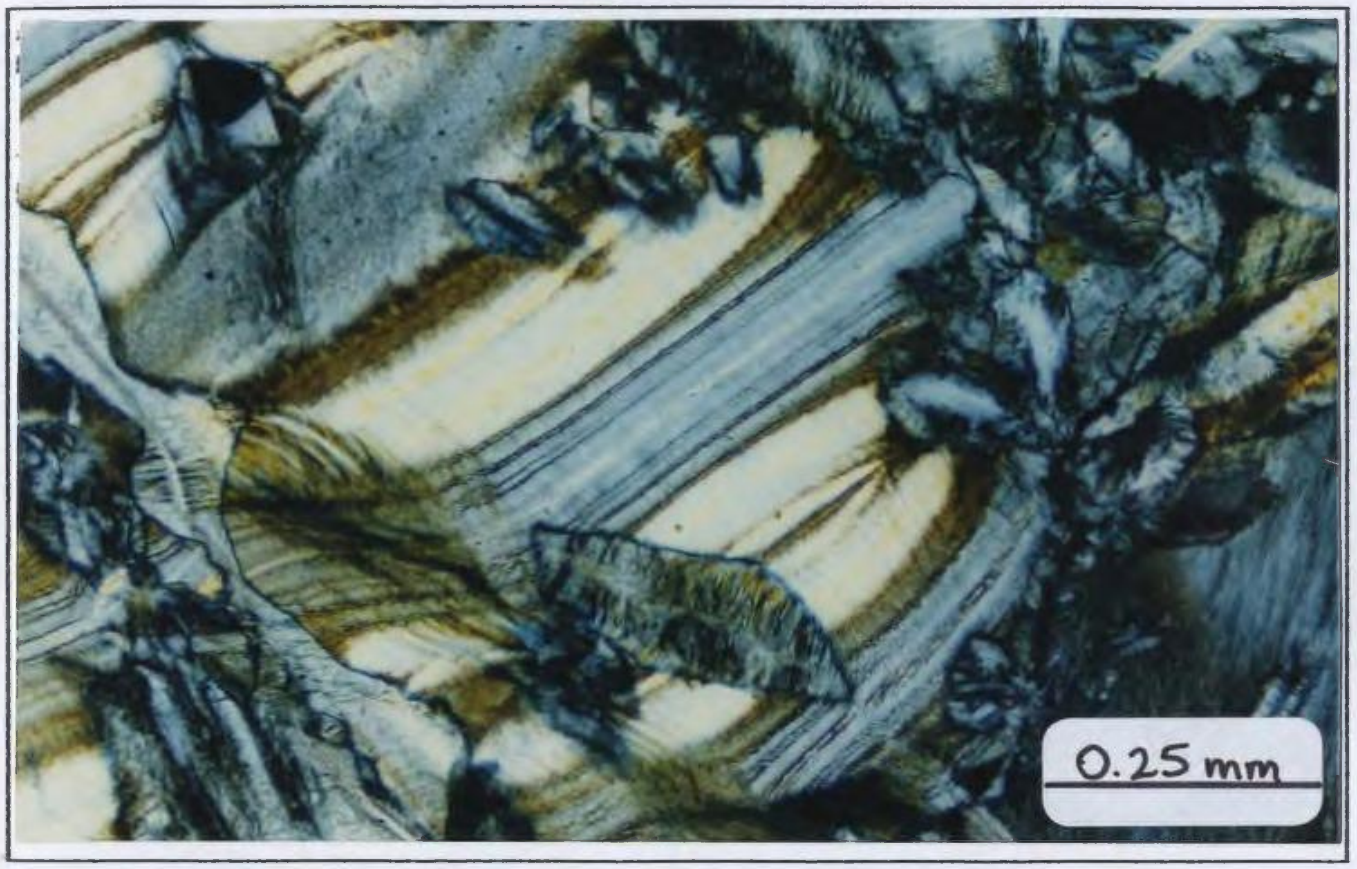

Fig. 6-11. Photomicrograph of tripartite lizardite veining. (X-polarized light).

Hourglass textures occur locally and where developed, no olivine remains in the rock (Fig. 6-12). In this example, the pseudomorphic serpentine in the hourglass texture is γ serpentine (type unknown) and is distinctly different from the α serpentine (lizardite) in the mesh textures described previously. Surrounding the hourglass texture is non-pseudomorphic serpentine (see below) with an interlocking texture which is γ serpentine (antigorite).

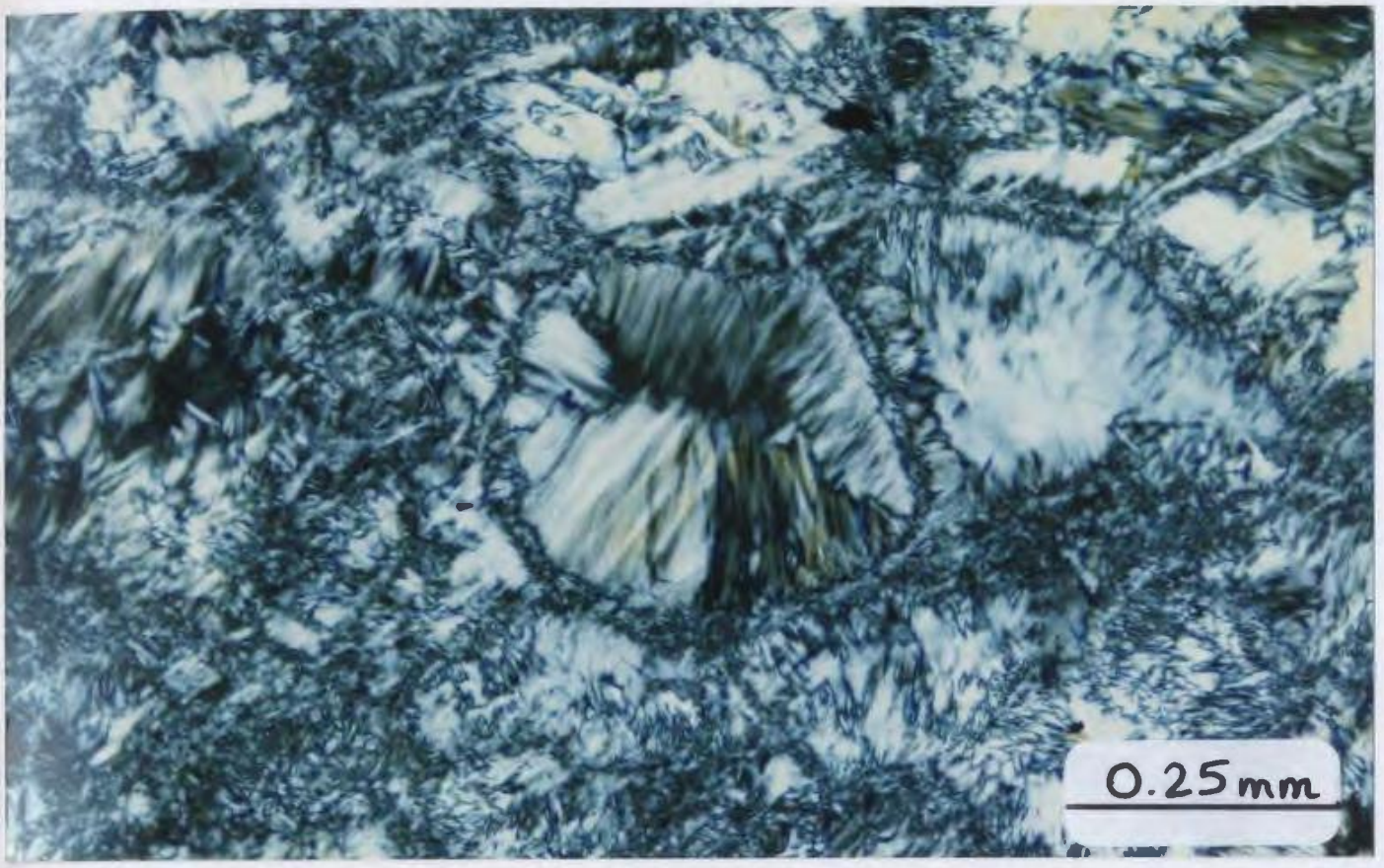

Fig. 6-12. Photomicrograph of pseudomorphic serpentine (type unknown) hourglass texture. (X-polarized light).

Another example of pseudomorphic serpentine is shown in Fig. 6-13. This example shows yellowish serpentine pseudomorphs (possibly tremolite bastites?) surrounded by non-pseudomorphic antigorite. The tiny flakes of serpentine with an interlocking texture that appear to have nucleated on the serpentine pseudomorphs are possibly antigorite.

6.4.2.2 Non-pseudomorphic textures

The most common type of serpentine developed in the rocks of this study occurs in non-pseudomorphic textures. Radiating blades with an

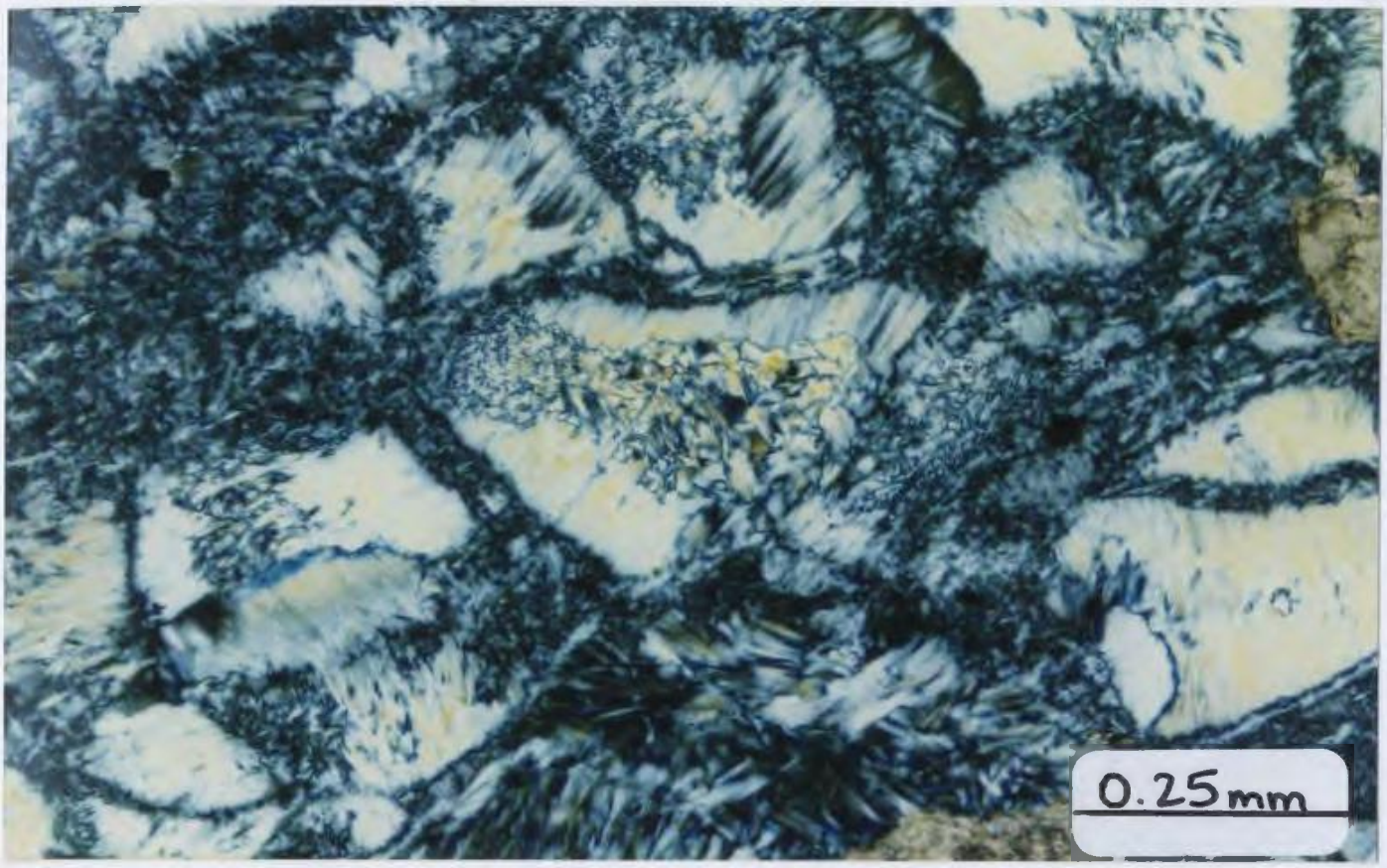

Fig. 6-13. Photomicrograph of pseudomorphic serpentine (type unknown). (X-polarized light).

interpenetrating texture (Fig. 6-14) are widespread and in all cases are composed of γ serpentine (antigorite). In many areas only massive γ serpentine (antigorite) with interlocking and/or interpenetrating textures remain (Fig 6-15).

It is interesting to note here that in many rocks of this study, recognition of pseudomorphic serpentine (lizardite) is difficult on account of the amount of massive serpentine (antigorite) developed. Small patches of lizardite can easily be overlooked in thin section because in most cases all serpentine is of similar color and relief. An easy way to overcome this

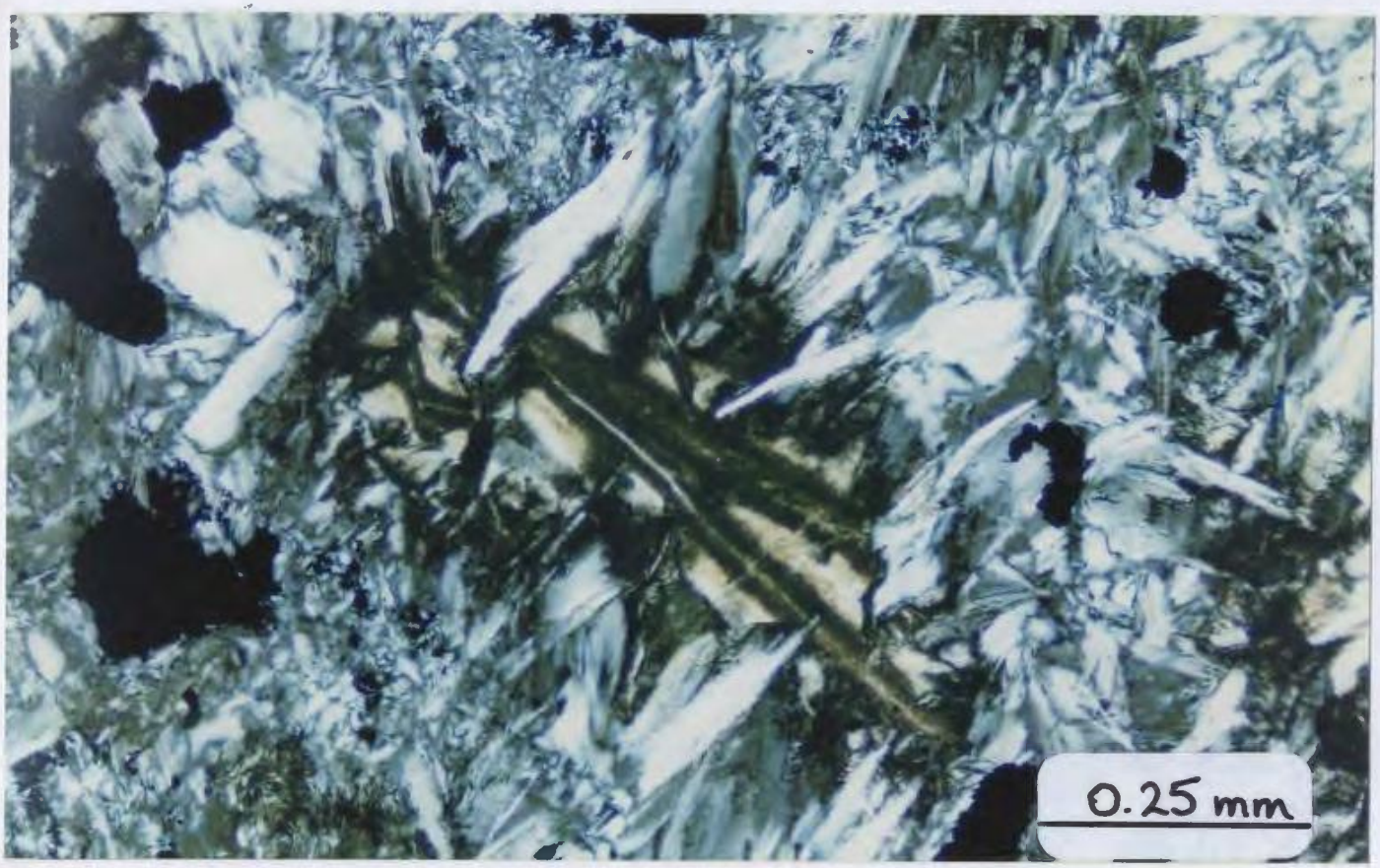

Fig. 6-14. Photomicrograph of nonpseudomorphic serpentine (antigorite) with radiating blade texture around lizardite serpentine. The dark color of the lizardite is probably tiny magnetite inclusions. (X-polarized light).

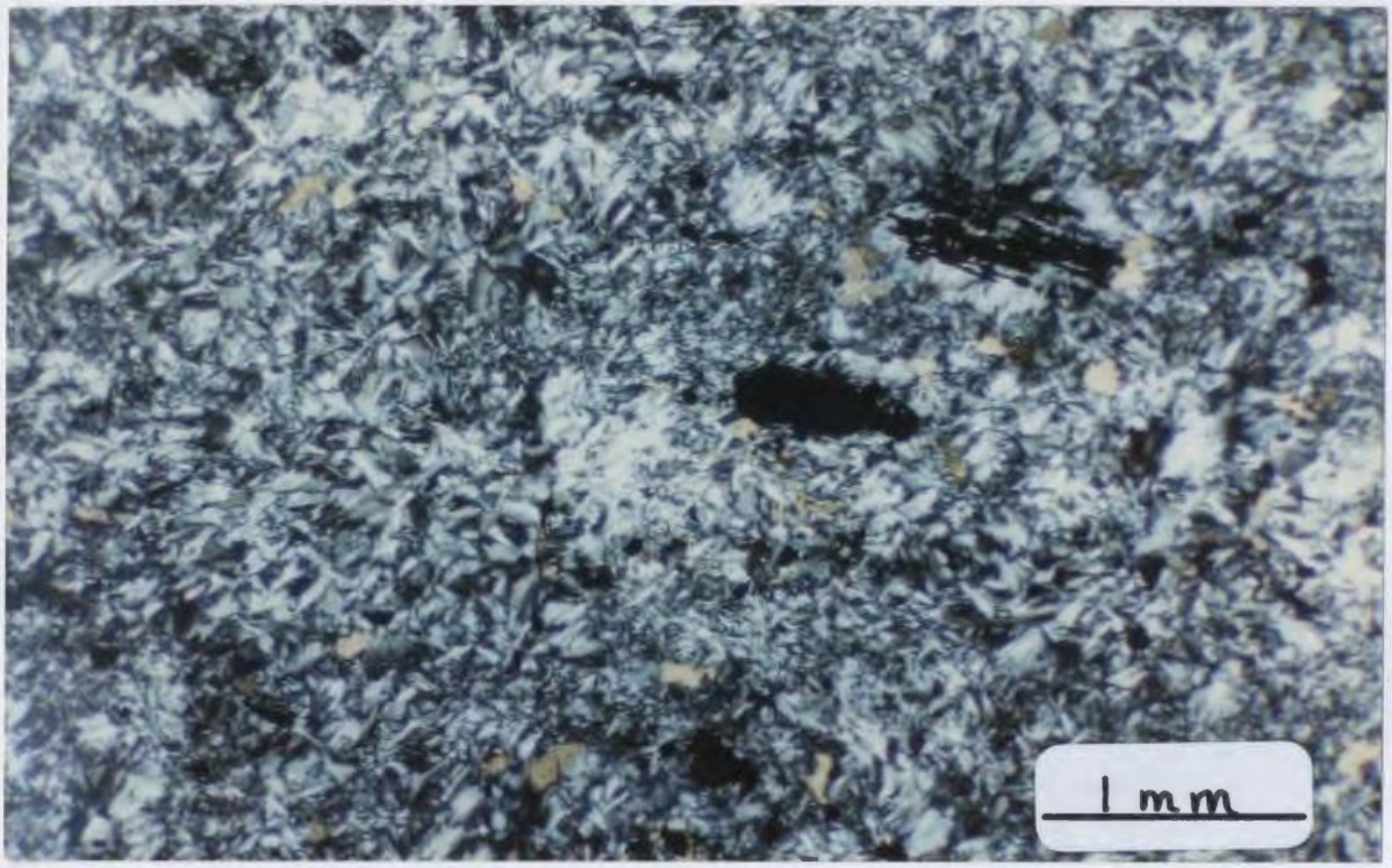

Fig. 6-15. Photomicrograph of interlocking texture of antigorite. (X-polarized light).

problem is to use polished thin sections under reflected light. The massive serpentine (antigorite) polishes much better than lizardite and the two are easily distinguished by this method (Fig. 6-16). In virtually every antigorite-bearing rock examined in this study at least some lizardite was found.

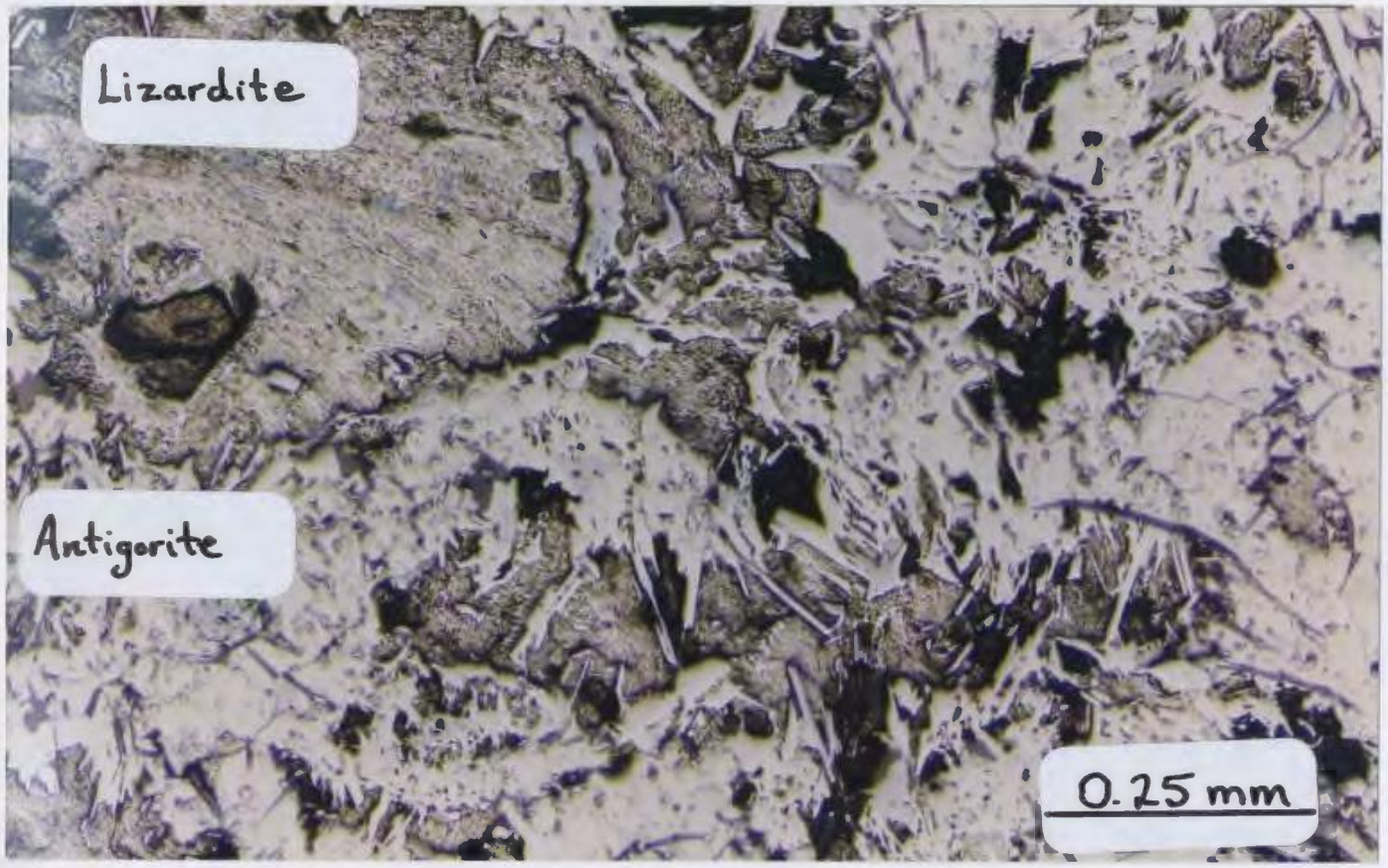

Fig. 6-16. Photomicrograph of antigorite and lizardite showing the difference between the two under reflected light.

6.4.3 XRD Analyses Of Serpentine Minerals

Since both the common serpentine pseudomorphic and nonpseudomorphic textures can be composed of lizardite, chrysotile or antigorite, it is necessary to determine the serpentine type by methods

other than petrography. The three serpentine group minerals have different crystal structures and are distinguishable by XRD methods. In this study, 9 whole rock powders were analyzed to determine the serpentine mineralogy (Appendix C). Sample D-4 contains serpentine that is closest to the lizardite standard and is the pseudomorphic type found in fractures in olivine (Fig. 6-9). Sample D-14 gave a positive identification of antigorite. This sample is composed of the nonpseudomorphic type of serpentine shown in Figure 6-15. In all other samples analyzed, the XRD peaks do not match the standards closely enough to make a positive identification of the serpentine type.

6.4.4 Serpentine Chemistry

Another approach to identifying serpentine end members is based on the chemistry of the minerals. Antigorite has a slightly different mineral formula than the ideal formula of $Mg_3Si_2O_5(OH)_4$ for lizardite and chrysotile. The ideal formula for antigorite is $Mg_{2.86}Si_2O_5(OH)_{3.68}$ (Wicks & O'Hanley, 1988). Based on this ideal formula, the mineral formula of antigorite can be calculated from microprobe analyses on an anhydrous basis by normalization to 6.8 oxygens. Whittaker & Wicks (1970) and Moody (1976) have shown that antigorite has a higher wt.% SiO_2 and lower wt.% MgO and H_2O^+ compared to lizardite and chrysotile.

In this study numerous examples of pseudomorphic and non-pseudomorphic serpentine were analyzed using the microprobe (Appendix A). Figure 6-17 shows a plot of wt.% SiO_2 against Mg cations, wt.% H_2O,

FeO, MgO, NiO and Al_2O_3 for all the serpentine analyses. The nonpseudomorphic type consistently has higher wt.% SiO_2, lower Mg cations and lower wt.% H_2O than the pseudomorphic serpentine. This confirms that the pseudomorphic serpentine is lizardite and the nonpseudomorphic type is antigorite. It is also apparent that the wt. % MgO values overlap and therefore cannot be used to distinguish the end-member serpentines.

Several other interesting trends are recognized from Figure 6-17. 1) Wt.% MgO increases from mesh textured lizardite samples still containing olivine to mesh textured lizardite with no olivine (total hydration). It then decreases in antigorite with minor talc-magnesite alteration and decreases more in antigorite samples containing a high degree of talc-magnesite alteration. 2) Wt.% FeO follows exactly the opposite trend, decreasing from lizardite-olivine samples to samples containing only lizardite and increasing again in antigorite coexisting with a low abundance talc-magnesite through to antigorite with abundant talc-magnesite alteration. 3) Wt.% NiO decreases from lizardite to antigorite. 4) The wt.% Al_2O_3 is similar in lizardite and antigorite (minor talc-magnesite alteration) but increases in antigorite with abundant talc-carbonate alteration. These observations probably reflect relative mobilities of these elements during serpentinization and talc-magnesite alteration. Variations in FeO and Ni will be strongly controlled by oxygen fugacities. If the oxygen fugacity is high, magnetite will be stabilized and FeO will be lower in the serpentines.

Fig. 6-17. Plot of Wt.% SiO_2 against Mg cations and Wt.% H_2O, FeO, MgO, NiO and Al_2O_3 for all serpentines analyzed in this study.

Open circles = lizardite mesh texture within olivine grains.

closed circles = lizardite with antigorite but no olivine indicating total hydration.

open triangles = antigorite with some lizardite remaining in the sample and low talc-carbonate alteration.

closed triangle = antigorite with little lizardite remaining and high talc-carbonate alteration.

These four variations are interpreted to represent different degrees of serpentinization and talc-carbonate alteration. Antigorite consistently contains lower H_2O, and lower Mg cations in the mineral formula. Variations between the other components and serpentine texture is discussed in the text.

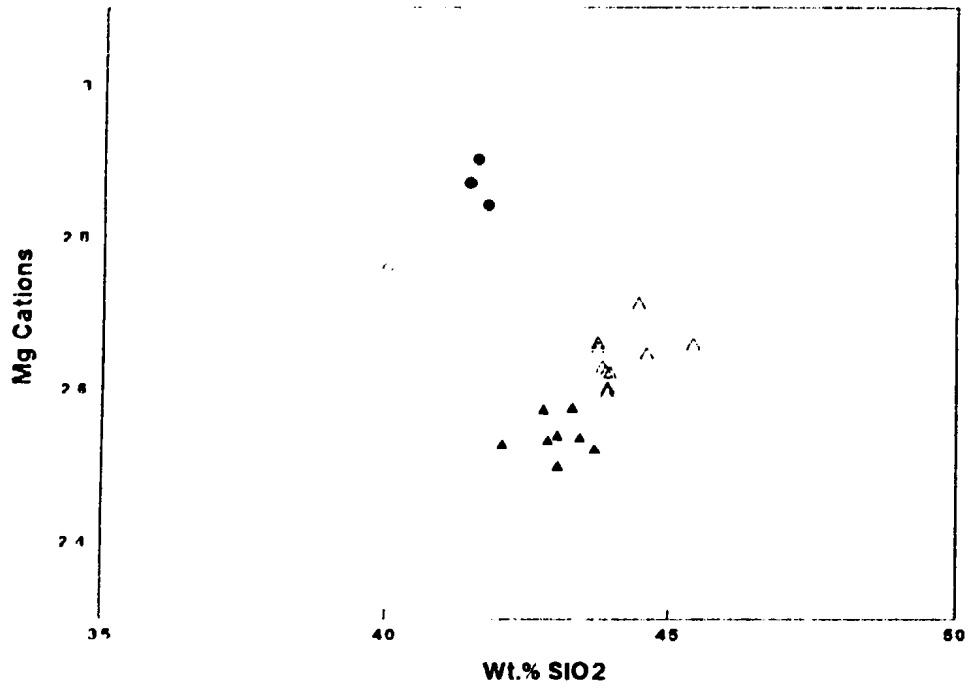
Mg Cations
35
40
45
50
Wt.% SIO2

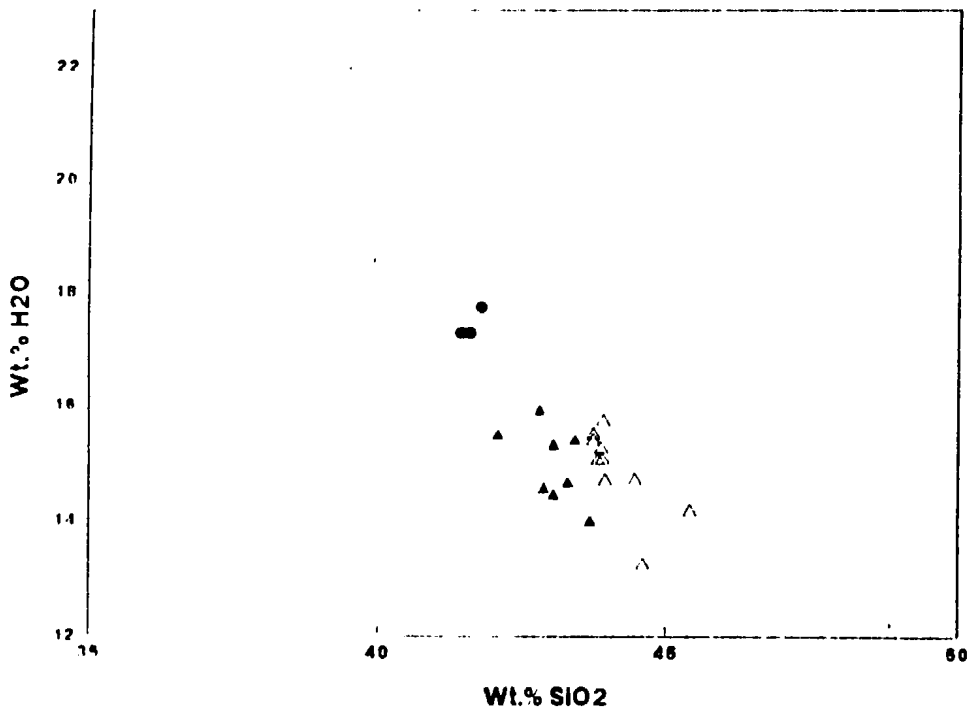
Wt.% H2O
22
20
18
16
14
12
40
45
50
Wt.% SIO2

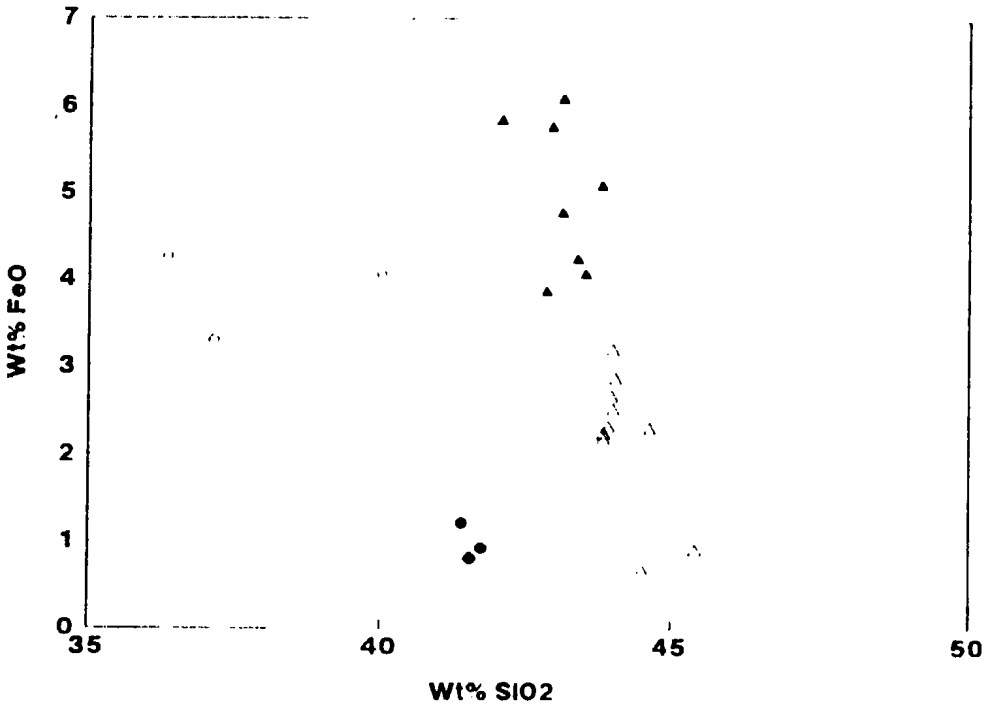
Wt% FeO
7
6
5
4
3
2
1
0
35
40
45
50
Wt% SIO2

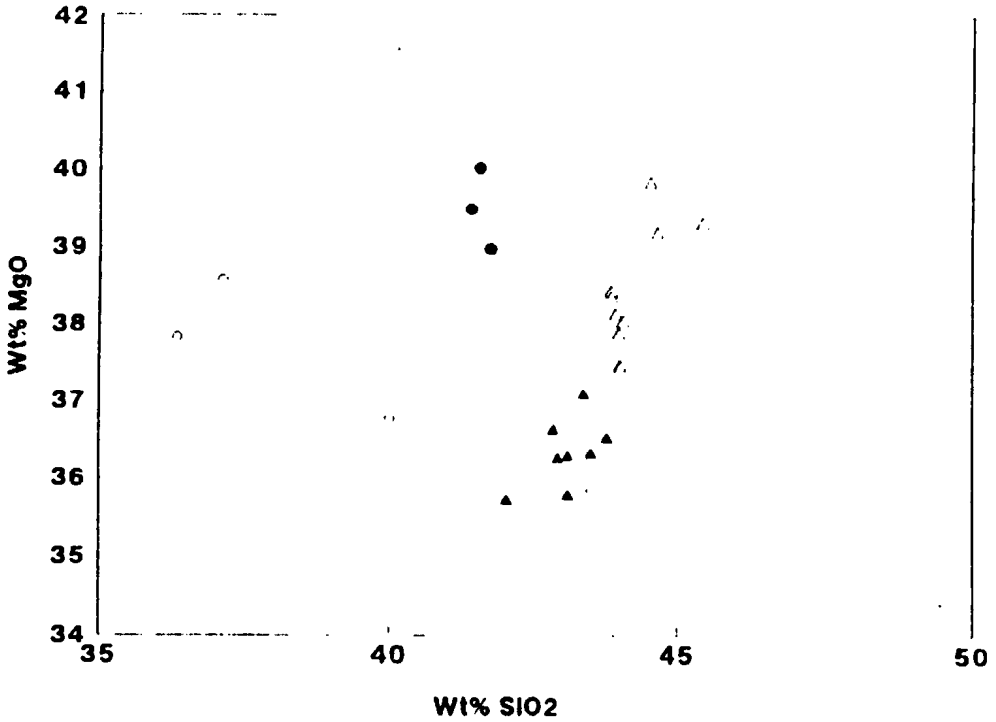
Wt% MgO
42
41
40
39
38
37
36
35
34
35
40
45
50
Wt% SIO2

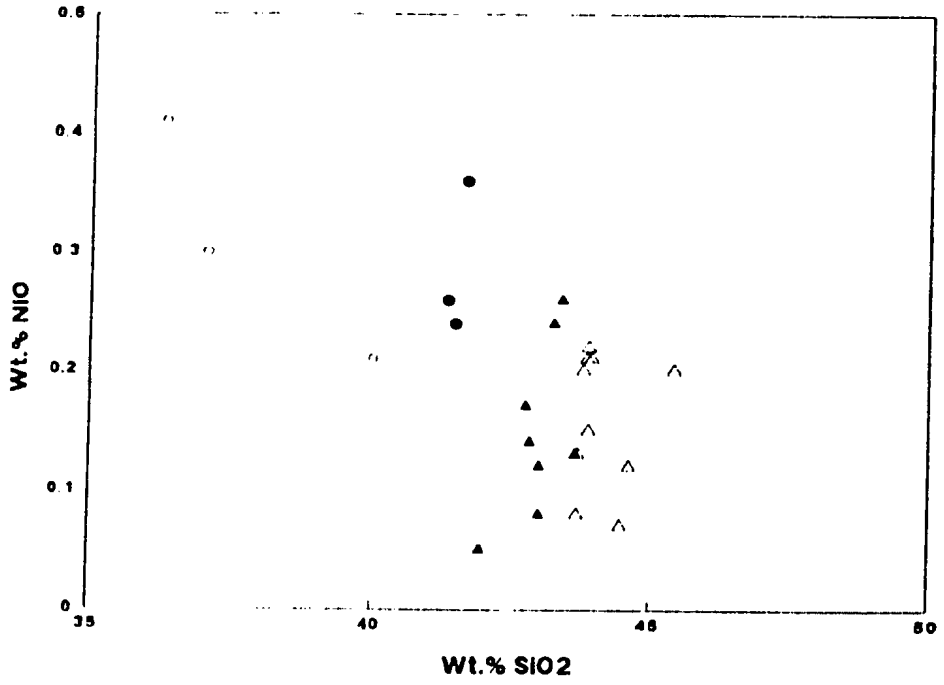
0.5
0.4
0.3
0.2
0.1
0
Wt.% NiO
35
40
45
50
Wt.% SiO2

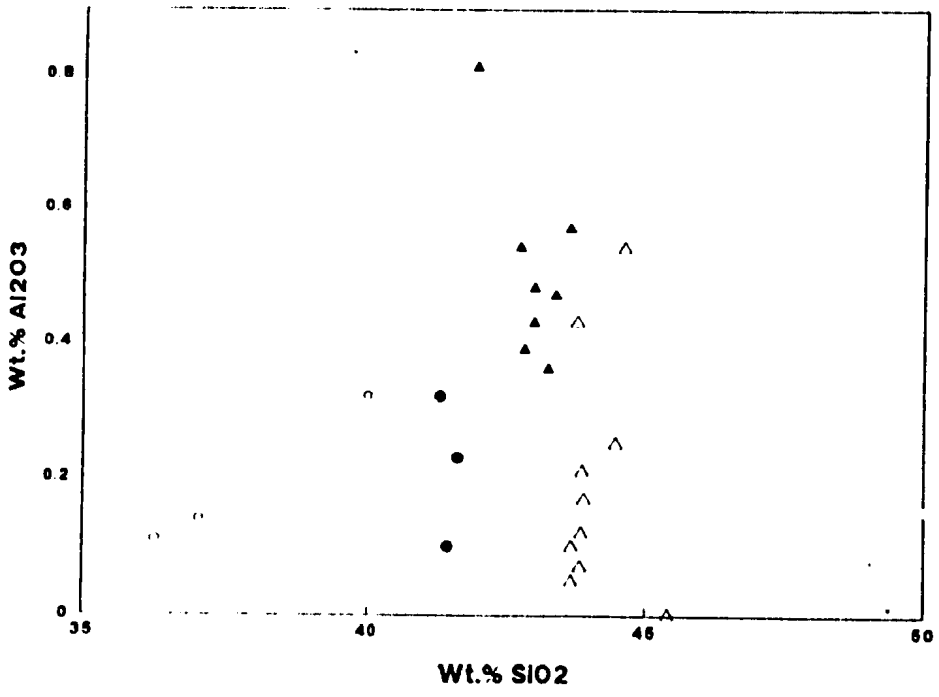
0.8
0.6
0.4
0.2
0
Wt.% Al2O3
35
40
45
50
Wt.% SiO2

6.4.5 Interpretation Of Serpentine Textures

Following O'Hanley (1991), serpentine textures can be generally interpreted in terms of three processes: (1) retrograde serpentinization (hydration); (2) serpentine recrystallization during mild prograde metamorphism; and (3) deserpentinization during higher temperature prograde metamorphism (see Appendix E). It is widely accepted that lizardite mesh textures are only produced by the first process (i.e. retrograde hydration). However, antigorite can be produced by any of the three processes during either retrograde or prograde metamorphism.

Antigorite in the rocks of this study is interpreted to have been produced from the breakdown of olivine in a retrograde (hydration) event and subsequent to this, any olivine remaining was further hydrated to lizardite mesh textures. Therefore all the serpentine types are interpreted to result from one retrograde metamorphic event. Evidence for the retrograde development of antigorite after olivine is found in a layered metadunite sample (Fig. 3-17). Figures 6-18 and 6-19 show the nature of the layering which is composed of nonpseudomorphic serpentine (antigorite-rich) layers (with minor olivine and lizardite) alternating with olivine-rich layers (with minor lizardite and antigorite). No pyroxene or plagioclase occurs in this sample and therefore the layering is not the result of initial igneous processes. Neither could the antigorite-rich layers be the result of serpentine recrystallization of lizardite to antigorite during prograde metamorphism because this would be expected to developed over a larger extent and not preferentially in layers as in this sample. The preferred

Fig. 6-18. Photomicrograph of layering in metadunite. A) antigorite with minor lizardite. B) Olivine-rich layers with lizardite mesh texture. This layering is interpreted to result from shearing and serpentine recrystallization and does not represent original igneous phase layering. This interpretation is supported by the fact that no pyroxenes or plagioclase occurs in the sample. (X-polarized light).

Fig. 6-19. Photomicrograph of same sample shown in Figure 6-18 showing more details of the nature of the layering. In this photograph the layering extends from the lower left to the upper right and shows the sharp contact between olivine-rich layer with mesh textured lizardite (A) and antigorite-rich layer with minor lizardite (B). Small grains of olivine are also still preserved in the antigorite layers. (X-polarized light).

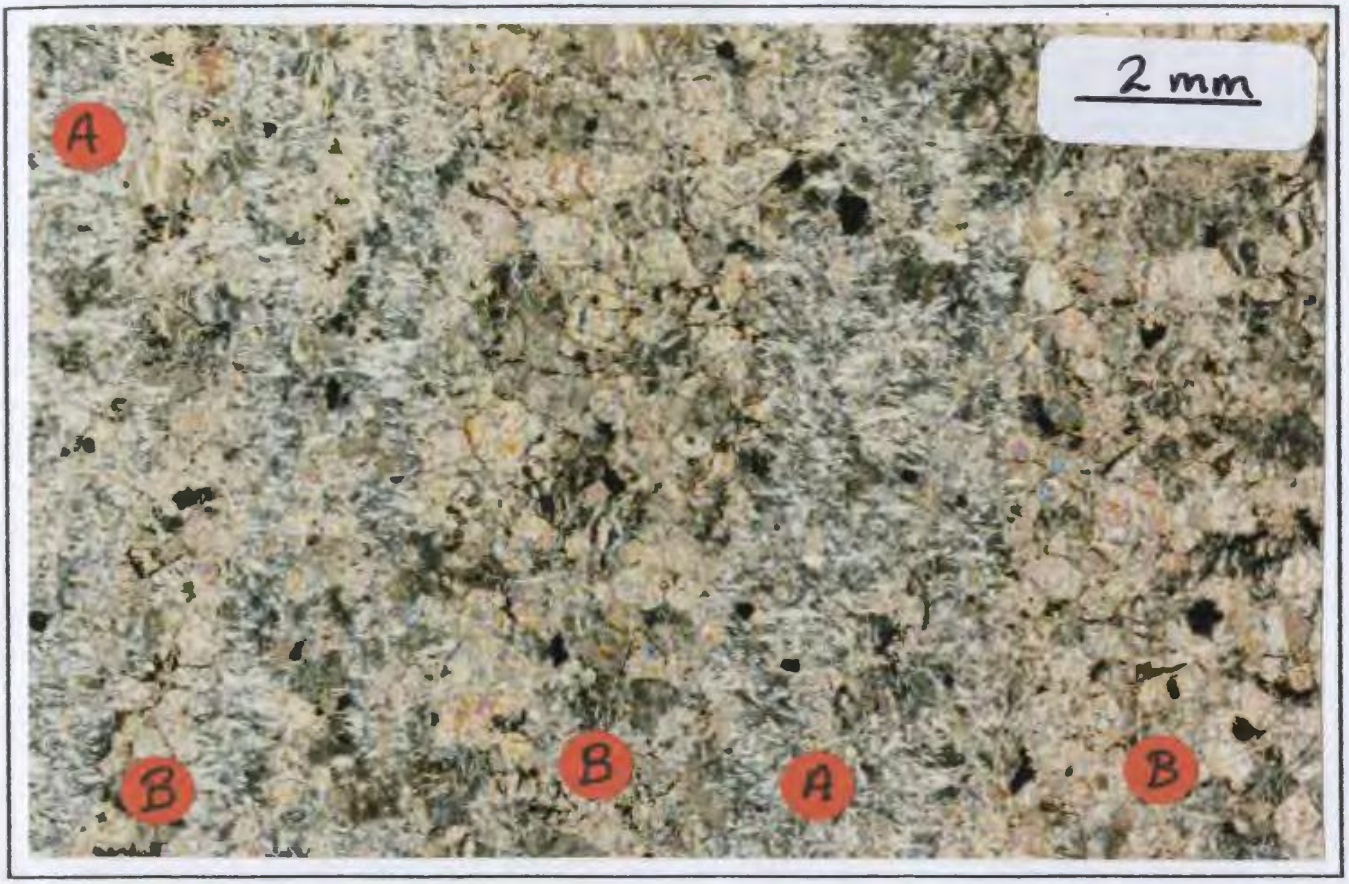
2 mm
A
B
B
A
B

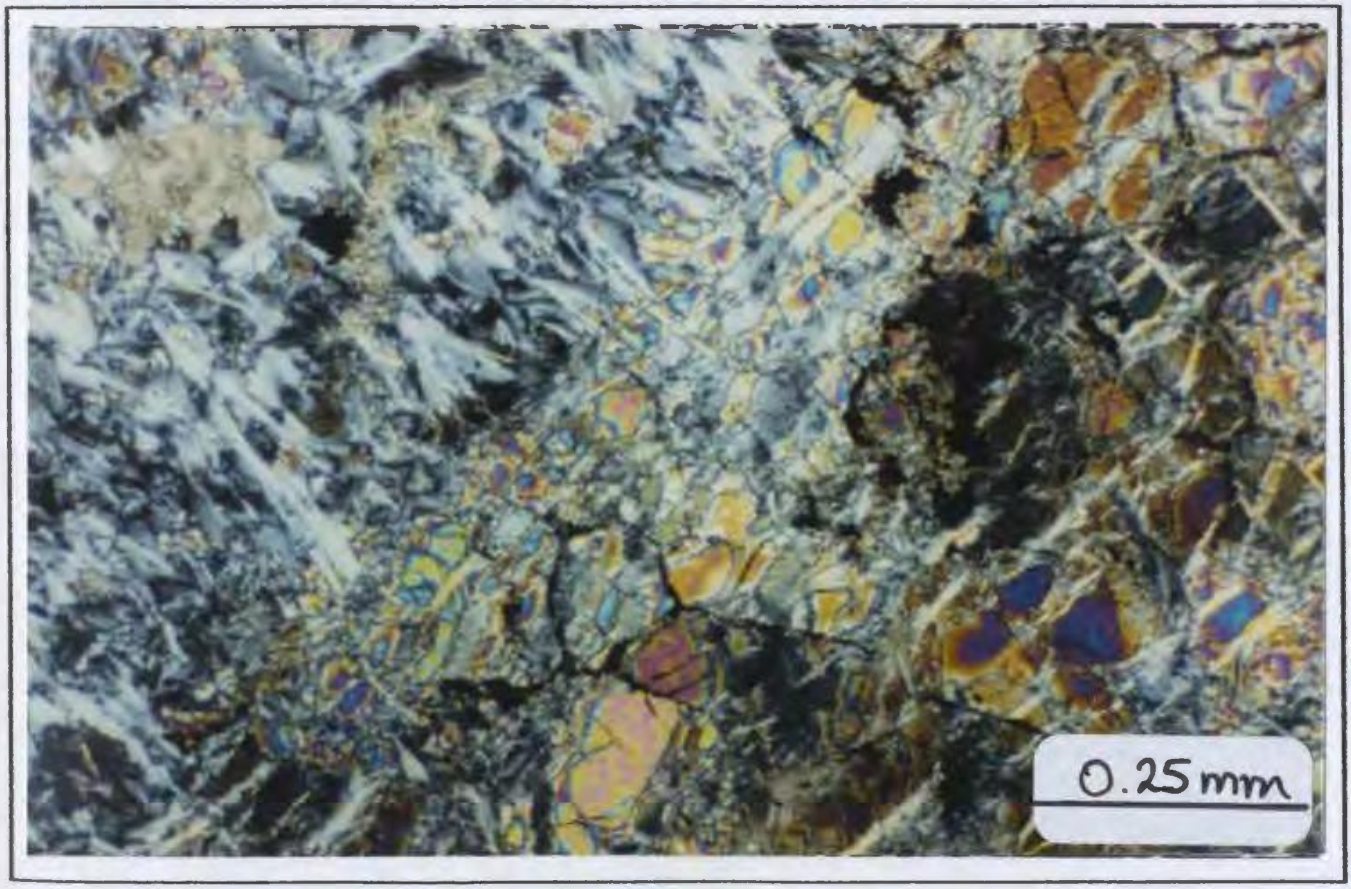
0.25 mm

interpretation is that fluids migrated along zones of weakness and reacted with olivine to form antigorite. Olivine remaining in any of the layers was subsequently hydrated to lizardite at lower temperatures.

Although evidence for the retrograde development of antigorite after olivine is not common in the geological literature, this interpretation has been suggested by Wicks (1984) and Peacock (1987) and is further substantiated in this study by comparison of the metadunites to the metamorphic history of the metasedimentary rocks presented previously. In Chapter 4 it was interpreted that the mafic-ultramafic rocks are pre-kinematic. Since the metasediments show a history of cooling from high temperatures in a retrograde environment, the mafic-ultramafic rocks should also show the same history. Therefore it is much more likely that antigorite was produced in a retrograde rather than a prograde metamorphic event.

It is important to note here that the olivine in this study is interpreted to be of metamorphic origin. However, regardless of the origin of the olivine, all serpentine minerals grew after olivine. This means that if the olivine is metamorphic, the evidence whereby that process was achieved has been subsequently obliterated. Even if the argument is made that the olivine is igneous, the subsequent retrograde development of antigorite and lizardite still holds.

6.4.6 Talc-Magnesite

The assemblage talc-magnesite is variably developed throughout the metadunites. In some areas the assemblage comprises less than 1% of the rock whereas other areas contain more than 50% talc-magnesite. Where talc-magnesite is present, it occurs either in veinlets that mark the path of fluid migration through the rocks (Fig. 6-20); as pseudomorphs after antigorite; or as discrete grains in antigorite-rich metadunites. It should be noted here that talc also occurs in zoned metadunite bodies (described below) where it is usually associated with tremolite rather than magnesite.

Magnesites from four samples were analyzed with the microprobe and the results are presented in Appendix A. They contain between 44.5 and 47.2 wt.% MgO with a minor siderite component (generally less than 8%). Wt.% CaO is negligible.

6.4.7 Chlorite

Chlorite occurs locally in the metadunites around chromite grains (Fig. 6-21) and in late talc veins in samples containing abundant talc-magnesite (Fig. 6-22). This indicates that Al was mobile late in the serpentinization history of these rocks.

6.4.8 Mineral Reactions in Metadunites

As discussed previously, there is evidence to suggest that antigorite

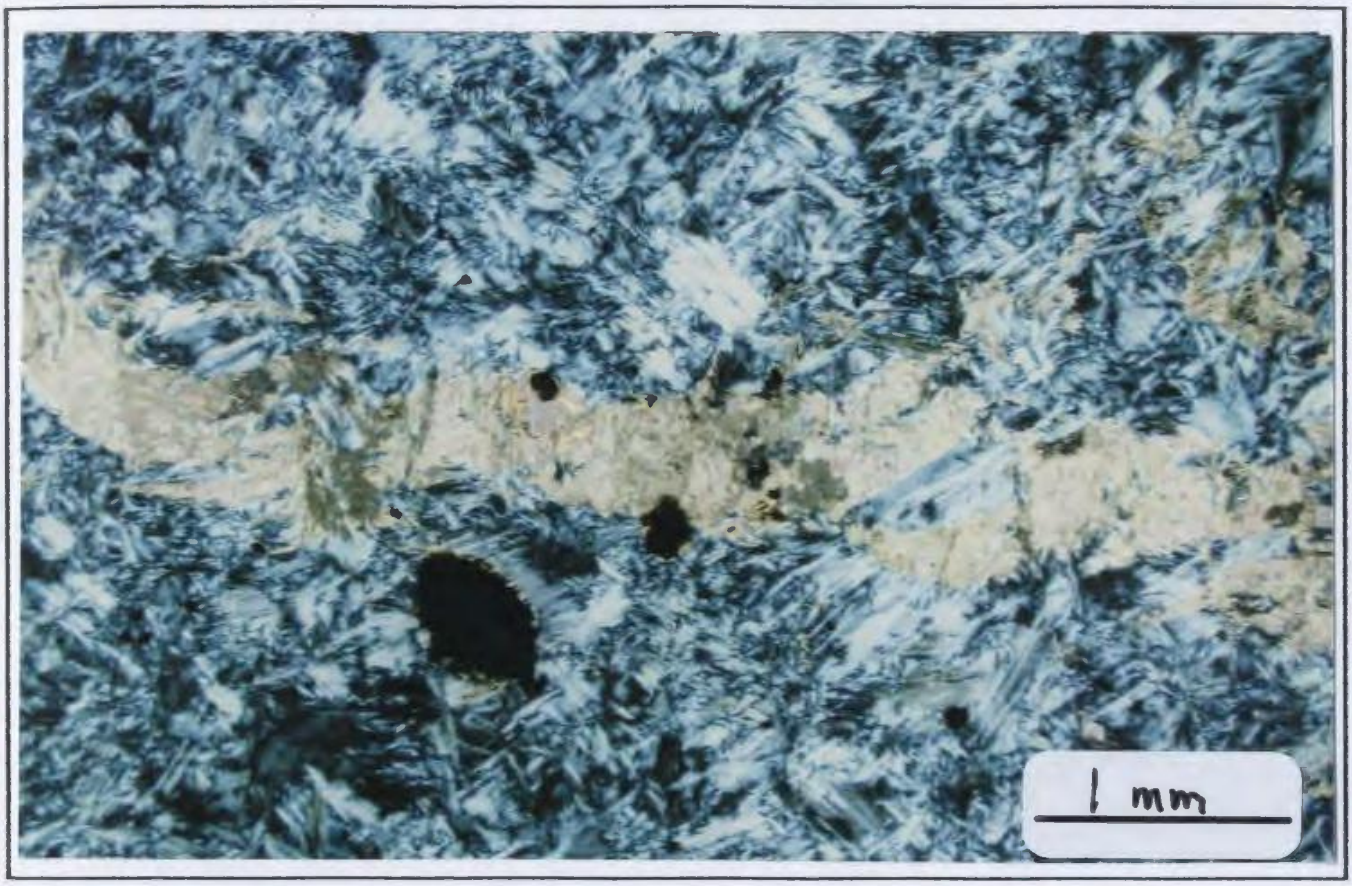

Fig. 6-20. Photomicrograph of talc-carbonate vein that cuts antigorite. (X-polarized light).

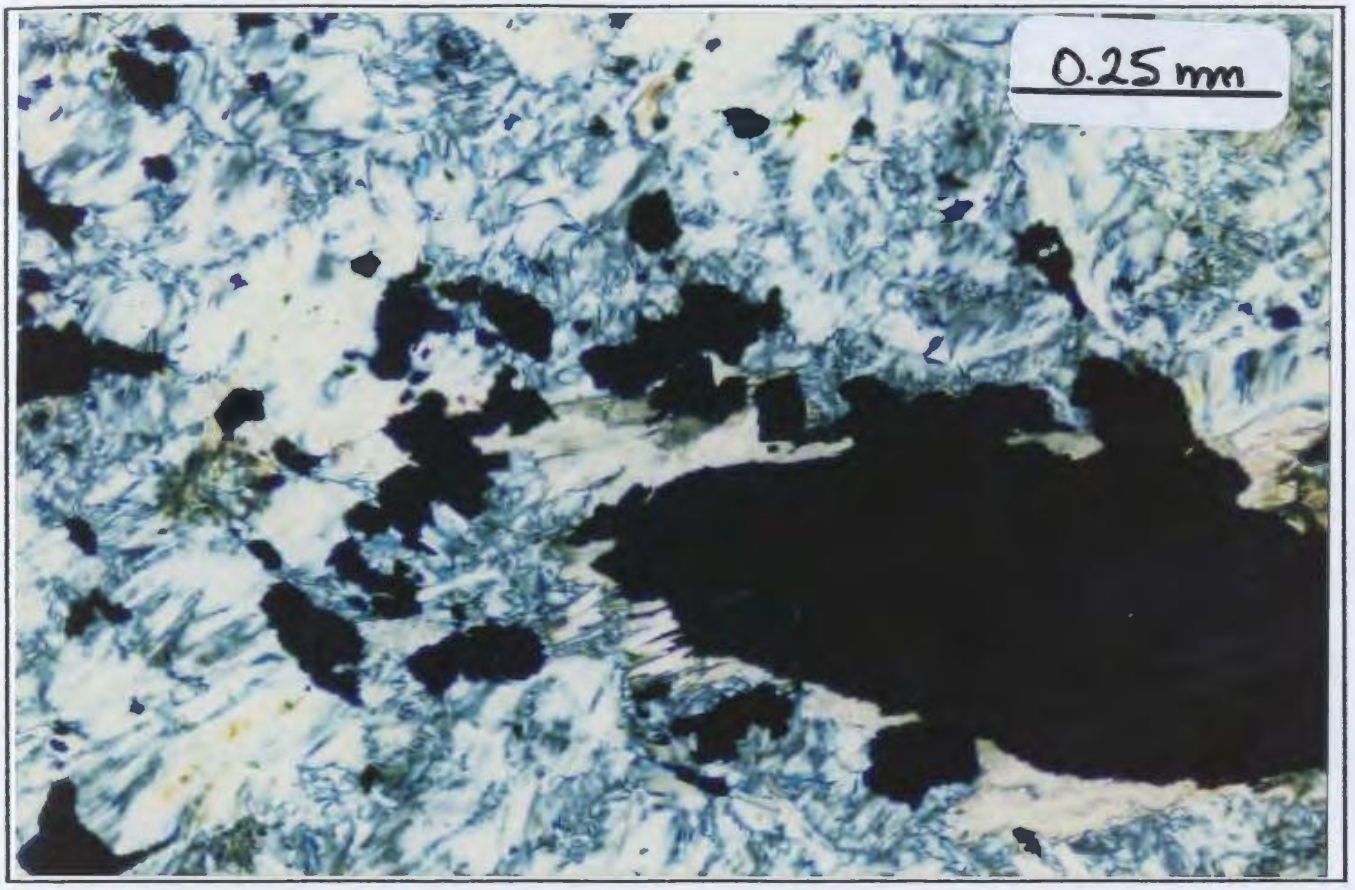

Fig. 6-21. Photomicrograph of chlorite around spinel grain in an antigorite-rich metadunite sample. (X-polarized light).

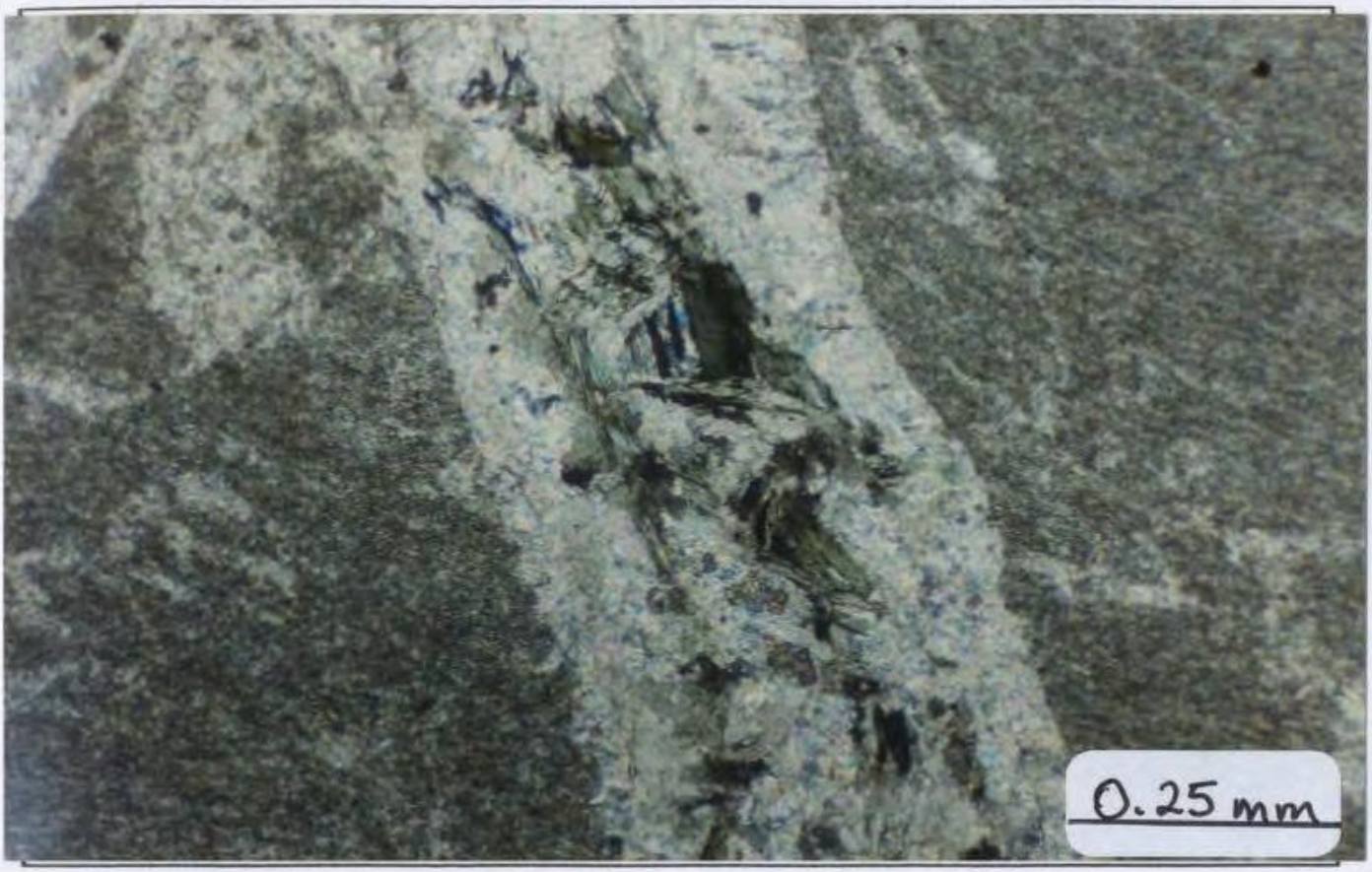

Fig. 6-22. Photomicrograph of talc vein that contains chlorite in a talc-magnesite rock. The chlorite development in the late vein may indicate that Al was mobile during serpentinization. (X-polarized light).

formed directly from olivine in a retrograde hydration reaction. This reaction may be represented by:

(I) forsterite + H_2O = Antigorite + Brucite

However, the presence of brucite with antigorite has not been confirmed in the rocks of this study. This may be due to one of several reasons. 1) Brucite is stable only in the presence of H_2O-rich fluids. In the presence of CO_2 it will breakdown to magnesite (Moody, 1976 after Johannes & Metz, 1968). Since many of the rocks of this study have a later talc-carbonate overprint indicating the presence of CO_2 bearing fluids, any brucite in those samples may have reacted to form magnesite. 2) Brucite may not form if the reaction is metasomatic, such that Mg is removed by the fluid phase:

(J) forsterite + H_2O = Antigorite + Mg (removed)

As previously discussed in Chapter 3, some of the metadunite bodies are zoned and contain near monomineralic rims of talc, tremolite-actinolite and chlorite from the center to the rim of the body. This is excellent evidence that metasomatism has affected at least some of the metadunites. An "idealized" zonation pattern (from Fowler et al., 1981) is presented in Figure 6-23 and shows Mg and H_2O are removed from the system and Si, Ca and Al are added. This zonation pattern is similar to most zoned serpentinites described in the literature, however partial metasomatism may give rise to various combinations of mineral zones. The zoning is due to metasomatic element transfer between the ultramafic and country rocks and

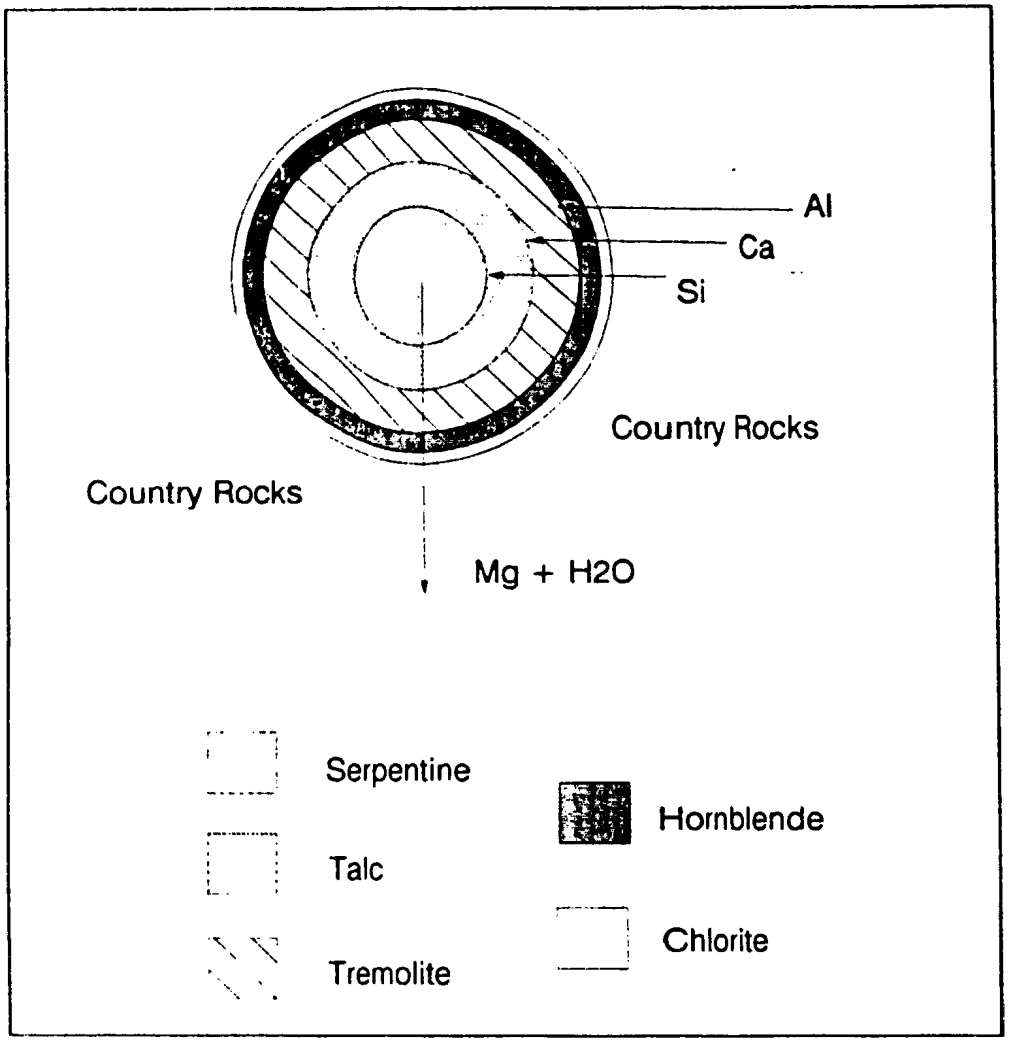

Fig. 6-23. Idealized zonation pattern and element exchange between a serpentinite body and its surrounding country rocks (after Fowler et al., 1981).

thus represents an arrested diffusion profile formed as elements diffused via a fluid phase between serpentinite bodies and the surrounding rocks. In the rocks of this study, zoned serpentinite bodies have been observed in sheared, greenschist facies metagabbro and in pelitic metasedimentary rocks.

Talc-magnesite assemblages may have formed via the following reaction:

(K) 4 serpentine + 5 CO_2 + H_2O = 1 talc + 5 magnesite

It is clear from the above petrographic descriptions of the metadunites from this study that olivine was in part also replaced by lizardite. This event is expressed by the reaction (magnetite is omitted):

(L) forsterite + H_2O = lizardite + brucite

O'Hanley et al., (1989) have calculated reaction curves in P-T space for the lizardite reactions and suggest that lizardite stability is affected by the presence of Al and that Al-lizardite has a larger stability field than Al free lizardite. However the lizardites in this study contain less than 0.5 wt.% Al_2O_3 and therefore the effects of Al are likely to be negligible.

The stability field for Al-free lizardite is not well constrained due to the lack of thermodynamic data. The reaction has been shown to be metastable (O'Hanley et al., 1989) and the conversion of olivine to Al free lizardite may be enhanced by $P(H_2O)$ (O'Hanley et al., 1989; Sanford, 1981) and the presence of Fe^{II} (O'Hanley, in press). However, using stable isotope data, Wenner & Taylor (1971) concluded that lizardite serpentinites formed at temperatures less than 200°C and O'Hanley et al. (1989) further suggest that the formation of lizardite at the expense of olivine occurs at low $P(H_2O)$ (i.e. less than 1 Kbar, with aH_2O approx. = 1).

6.4.9 Composition Of The Fluid Phase

Since olivine and serpentine are the major minerals in the metadunites of this study, their metamorphism can be analyzed using the model $MgO-SiO_2-CO_2-H_2O$ system. Figure 6-24 shows schematically a series of reaction curves in the system after Johannes (1969). The formation of serpentine (antigorite) and brucite from forsterite (reaction 6) occurs with a decrease of temperature from a fluid that is H_2O rich. Note that the reaction occurs at slightly higher temperatures with increased fluid pressures (Fig. 6-25).

The formation of talc-magnesite occurred with an increase in the amount of CO_2 present in the fluid phase (reaction 3). This may be accomplished by the buffering of the H_2O-rich fluid phase along reaction 6 with decreasing temperature or by infiltration of a separate CO_2-richer fluid phase subsequent to serpentine formation. It seems likely that both processes may have occurred. An example of a buffered assemblage is seen in Figure 6-15 where only minor talc-magnesite is formed as discrete grains with serpentine still preserved. Infiltration metasomatism occurred in the zoned metadunites where massive talc (associated with tremolite) is formed (Fig. 3-20) and where talc-magnesite veins occur.

6.5 METAPYROXENITES

These rocks consist predominantly of Ca-amphibole with minor talc, chlorite and Fe-Ti oxides. The Ca-amphibole is weakly pleochroic and forms

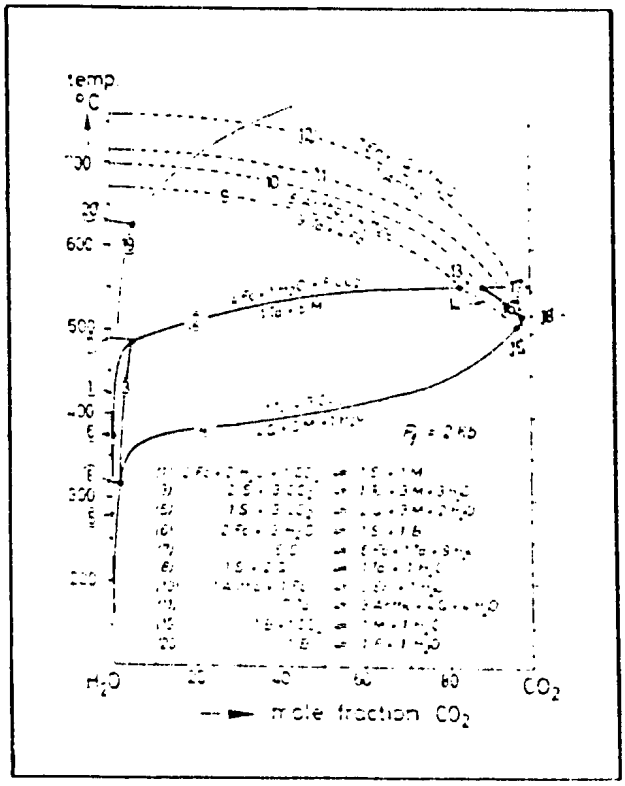

Fig. 6-24. T-X(H_2O) phase diagram at P = 2 kbars showing mineral reactions for ultramafic rocks (after Winkler, 1979). Reactions 6 and 3 are interpreted to be representative of the rocks in this study and are discussed in the text.

Fo=forsterite	S=serpentine
M=magnesite	Ta=talc
Q=quartz	B=brucite
En=enstatite	Antho=anthophyllite
P=periclase	

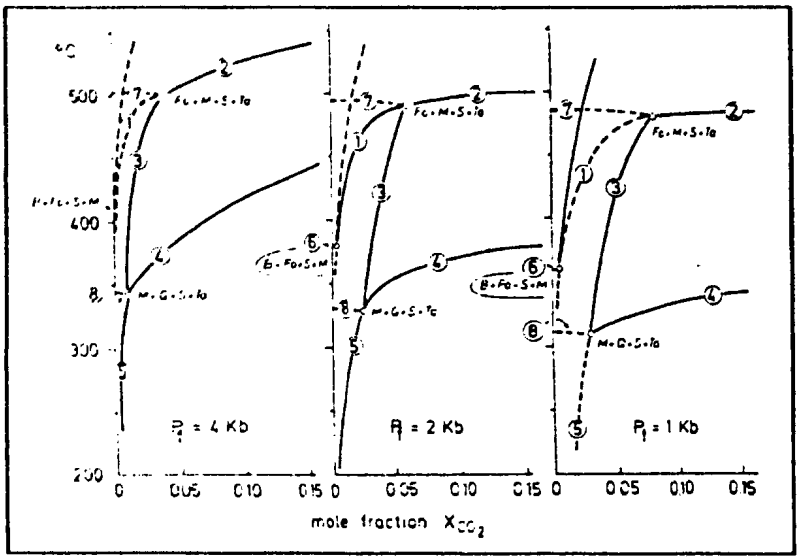

Fig. 6-25. T-X(H_2O) phase diagrams at P = 1, 2 and 4 kbars showing mineral reactions for ultramafic rocks in an H_2O-rich environment. (after Winkler, 1979). Mineral abbreviations same as in Fig. 6-24.

a mosaic of undeformed xenoblastic to subidioblastic grains (Fig. 6-26). Fe-Ti oxides are commonly formed along cleavage planes and in places cross-cut the boundaries of several amphibole grains (Figs. 6-26 and 6-27). This is evidence that the Ca-amphibole is replacing an earlier phase, probably clinopyroxene. Microprobe analyses of amphibole from three samples are presented in Appendix A. On the Ca-amphibole composition diagram of Leake (1978) the amphiboles consist of both tremolite and actinolite (Fig. 6-28).

The original protolith for these tremolite-actinolite rich rocks is difficult to determine in the study area due to the total recrystallization to greenschist facies assemblages. Scotford and Williams (1983), studied

Fig. 6-26. Photomicrograph of undeformed tremolite/actinolite grains from metapyroxenite showing Fe-Ti oxide exsolution. (X-polarized light).

Fig. 6-27. Same as Figure 6-26 but plane polarized light.

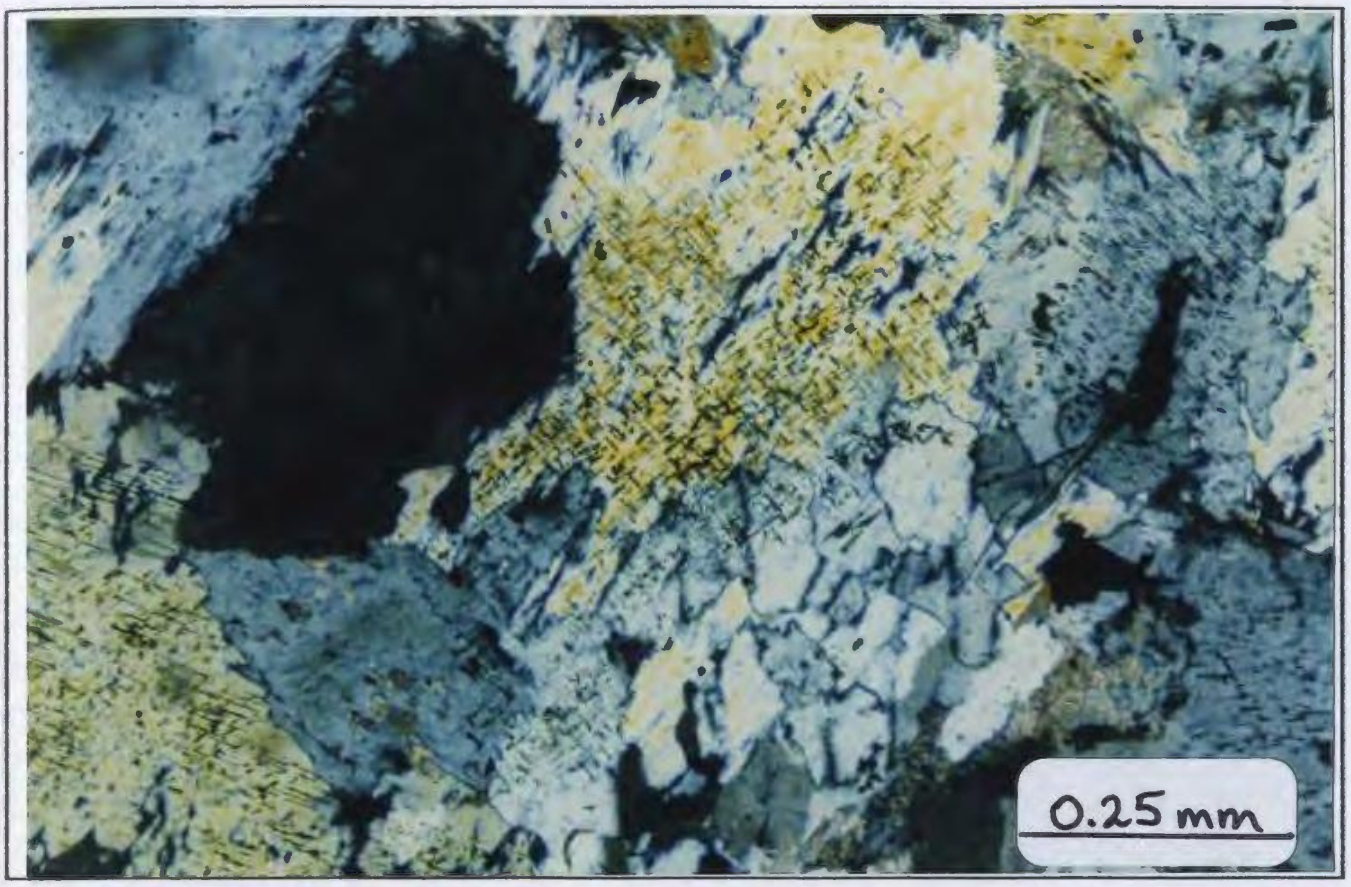
0.25 mm

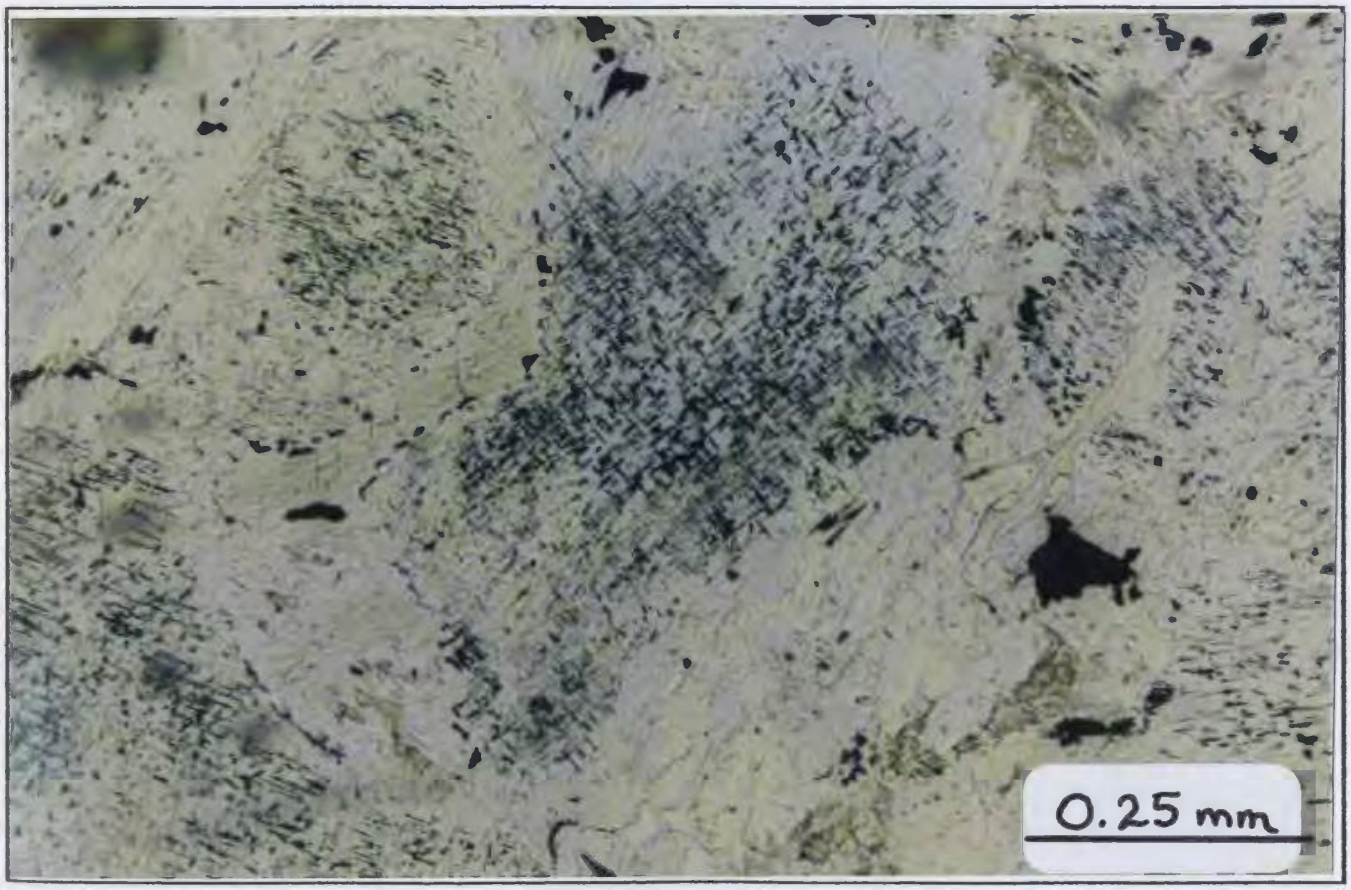
0.25 mm

metamorphosed ultramafic bodies in the Blue Ridge of North Carolina and Virginia and proposed that tremolite-rich ultramafic rocks formed by metasomatism of serpentinites by the following reaction:

(M) 3antigorite + 2Ca + 2Si = tremolite + 4Mg + $3H_2O$ + $4H^+$

This reaction is one possible interpretation, however no replacement textures of tremolite after antigorite have been found in the rocks of this study. The preferred alternative is that the amphiboles resulted from recrystallization of clinopyroxenite that was interlayered with dunites. This origin is preferred because, as noted above the Fe-Ti oxides are interpreted to result from a previous phase, and Fe-Ti exsolution is common in clinopyroxenes.

6.6 METAGABBRO

Two texturally distinct gabbroic rocks have been identified in the field, massive metagabbro and layered metagabbro. As described on Chapter 3, the layered metagabbro may be a deformed equivalent to the massive type. Mineral assemblages of both types indicate the rocks have been metamorphosed to at least amphibolite facies, then retrogressed to greenschist facies. The amphibolite facies assemblage is Ca-amphibole and plagioclase (± minor quartz, biotite and Fe-Ti oxides). The amphibole is often sieved by blebs of quartz or quartz is found at the triple point junctions of amphibole grains. This texture is typical of amphibole that has recrystallized from former clinopyroxene. Microprobe analyses of amphibole

and plagioclase from two samples are presented in Appendix A. Compositionally the amphiboles plot in the hornblende field (Fig. 6-28).

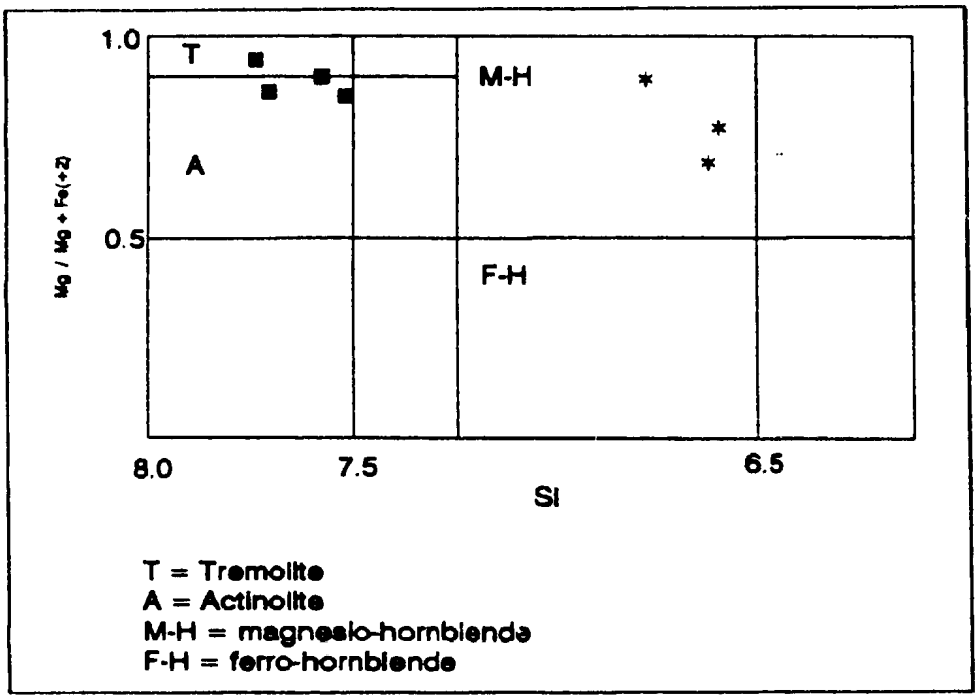

Fig. 6-28. Nomenclature for calcic amphiboles (after Leake, 1978). Amphiboles from the ultramafic rocks plotted as squares and amphiboles from the metagabbros are plotted as asterisks. Compositions of the amphiboles are from microprobe analyses.

The plagioclase is very anorthite-rich ranging between An_{82} and An_{92}. The high An content is not typical of gabbro metamorphosed to amphibolite facies conditions and may imply the protolith also had contained feldspars with elevated An contents.

Greenschist facies assemblages overprint the amphibolite facies assemblage to variable degrees. Hornblende is commonly rimmed or totally replaced by an amphibole that is weakly pleochroic (probably

tremolite/actinolite). The abundance of chlorite increases substantially with a decrease in the amount of hornblende. Plagioclase is commonly saussuritized to an assemblage of calcite, sericite and clinozoisite/epidote (Fig. 6-29). Some of the mafic rocks are completely retrogressed so that only an assemblage of chlorite, clinozoisite/epidote, quartz and Fe-Ti oxides remain.

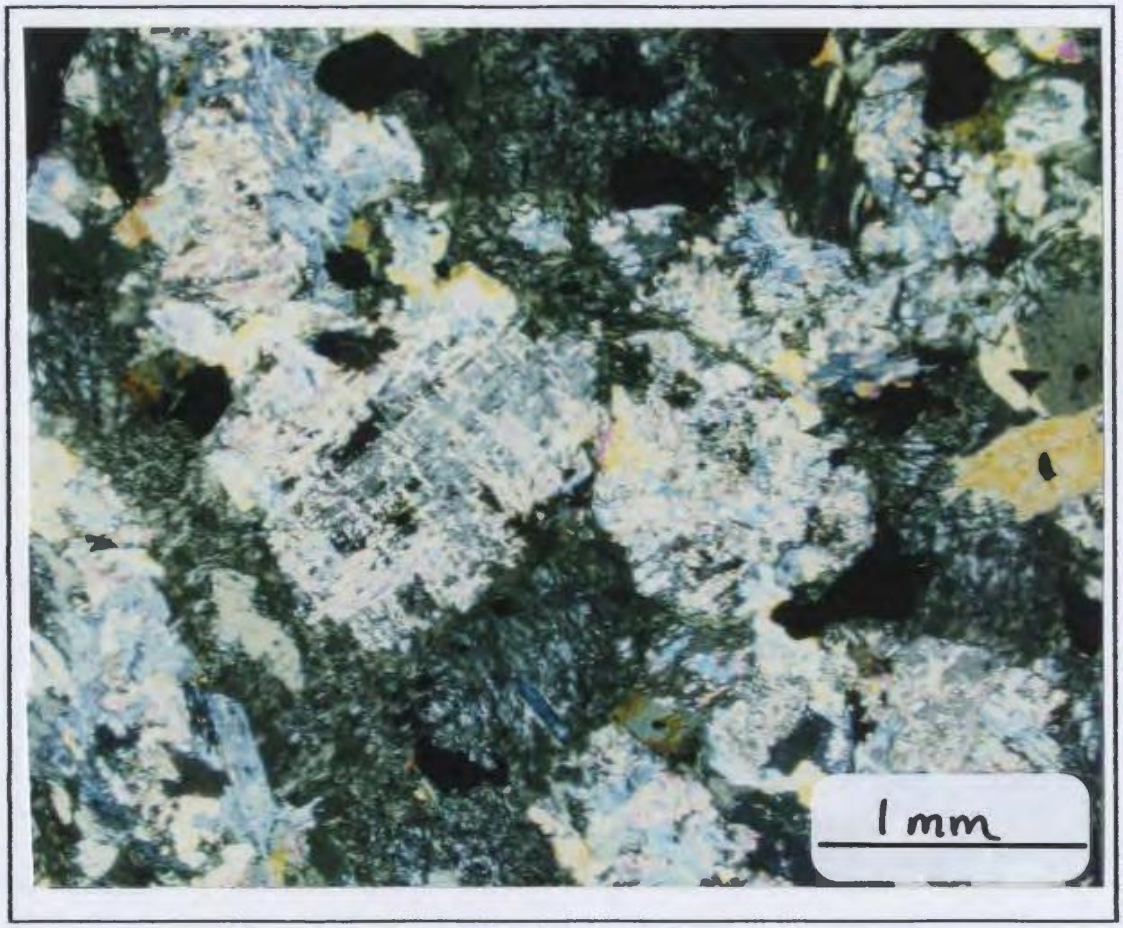

Fig. 6-29. Photomicrograph of plagioclase alteration in metagabbro. (X-polarized light).

6.7 SUMMARY

This chapter has outlined the regional metamorphism of the main lithologies within the map area (metasedimentary and mafic-ultramafic rocks). The psammitic metasedimentary rocks display a well-developed migmatitic layering typical of high grade amphibolite facies metamorphism. However, there is no evidence for partial melting in these rocks and their layering may be an injection feature. A pelitic schist layer within this unit contains the assemblage sillimanite + garnet + biotite which implies conditions above the stability of staurolite + muscovite + quartz.

The pelitic metasedimentary unit contains mainly sheared rocks that have been retrogressed in the greenschist facies. However, evidence of an earlier high grade metamorphic event has been recognized in several unsheared samples. The assemblage spinel (hercynite) + quartz implies high temperatures that may have reached 800°C or more. There is also evidence of the coexistence of garnet + cordierite and the rocks may have partially melted. Cooling has subsequently resulted in the development of kyanite, staurolite and chlorite. Andalusite was recognized in one sample but is not widespread. Therefore the cooling path may have been in the vicinity of (or slightly above) the Al_2SiO_5 triple point junction.

The mafic-ultramafic rocks examined in detail in this study are from the shear zones in the pelitic metasedimentary unit. Three main lithologies are recognized: metadunite, metagabbro and metpyroxenite. All rocks are highly retrogressed to greenschist facies assemblages. The metadunites

contain minor olivine (interpreted to be metamorphic) but mostly serpentine minerals. It is interpreted that antigorite formed from olivine in a retrograde environment and that lizardite formed subsequent to this with a further decrease in temperature. The metagabbro and metapyroxenite show evidence of preexisting amphibolite facies assemblages but are now almost entirely retrogressed to greenschist facies minerals.

The significance of the metamorphic history of the rocks in the study area lies in the interpretation that all lithologies were previously metamorphosed in the upper amphibolite facies and all have subsequently been retrogressed in the greenschist facies. This indicates that the mafic-ultramafic rocks were emplaced prior to (or during) the high grade regional metamorphic event and have undergone the full range of metamorphism that the metasedimentary rocks have undergone. This conclusion is supported by field relationships that suggest the mafic-ultramafic rocks have also undergone similar deformation as the metasedimentary rocks (see Chapter 3 and 5).

The most likely upper limit on the age of high grade metamorphism in the rocks of this study is middle Ordovician. This would coincide with the Taconic Orogeny and transport of ophiolitic allochthons westward. As noted by Currie & van Berkel (1989), the Silurian mafic intrusions in the Dashwoods subzone are little deformed or metamorphosed suggesting stabilization of the Dashwoods subzone at least by Silurian time.

CHAPTER 7

GEOTHERMOMETRY/GEOBAROMETRY

7.1 INTRODUCTION

In this chapter, metamorphic temperatures and pressures of the early high temperature metamorphism in the metapsammitic and metapelitic units are estimated using: 1) garnet-biotite thermometry and plagioclase-garnet-Al_2SiO_5-quartz barometry and 2) oxygen isotope thermometry. First the mineral chemistry is presented followed by the results of thermometry and barometry.

Two samples of metapsammite (T-35, T-73), one sample of pelitic schist within the metapsammite unit (T-13), and three samples of unsheared rocks from the metapelite unit (T-3, T-24, T-32) contain the assemblage garnet-biotite used for temperature estimates. Of these six samples, four (T-3, T-24, T-32, T-13) also contain the assemblage sillimanite + garnet + plagioclase + quartz used to estimate pressures.

Temperatures of the early high temperature metamorphism were also estimated from three samples of metapsammite and six of unsheared metapelite by oxygen isotope exchange thermometry. Finally, temperatures of two samples of shear zone rocks in the metapelite unit are estimated by oxygen isotope exchange thermometry in order to estimate the temperature of the retrograde shearing event. Sample locations are shown in Figure 7-1.

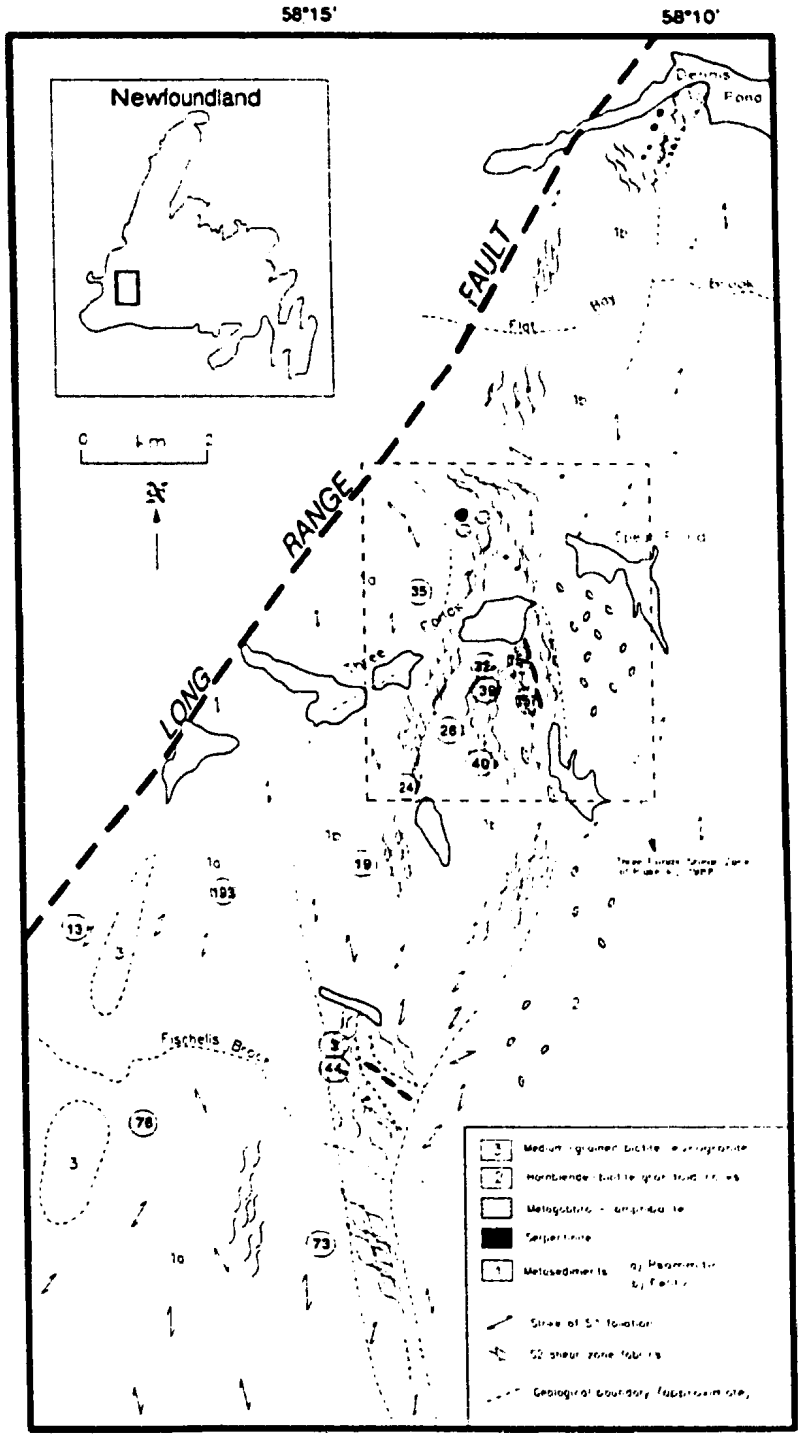

Fig. 7-1. Location map of metasedimentary samples used for geothermometer/geobarometry.

7.2 MINERAL CHEMISTRY

An overview of mineral chemistry from rocks in the psammitic and pelitic metasedimentary units is presented below. All microprobe analyses are presented in Appendix A. A discussion of garnet zoning from samples used for garnet-biotite thermometry is presented in the next section.

Garnet, biotite and plagioclase have been analyzed from one pelitic schist sample within the psammitic metasedimentary unit (sample T-13). Plagioclase is andesine ($An_{30.8}$-$An_{33.4}$) and two biotite analyses indicate X_{Fe} = 0.49. Garnet is almandine-rich (Fe/Fe+Mg+Ca+Mn x 100 = 75.9%-80.0%) with pyrope ranging from 11.7% to 15.7%. Grossular and spessartine are typically < 5%.

Microprobe analyses of garnet and biotite from two samples of the metapsammites (T-35, T-73) show that biotites have X_{Fe} ranging from 0.55 to 0.60 and garnets are almandine-rich (68.3%-77.6%) with a significant spessartine component (up to 20.6%) in sample T-35. Grossular and pyrope are typically < 15%.

Microprobe analyses of garnet, biotite and plagioclase from samples in the metapelite unit (T-3, T-24 and T-32) show the plagioclase is andesine ($An_{37.5}$ to $An_{49.2}$) and X_{Fe} of biotite ranges from 0.45 to 0.56. Garnets are almandine-rich (50.6%-69.0%) with appreciable pyrope (10.8%-18.3%) and spessartine (10.3%-26.5%) components. The grossular component is low (typically < 6%).

Additional microprobe analyses of spinel (T-3); staurolite (sample T 19); garnet, staurolite and chlorite (sample T-39); and staurolite and cordierite (sample T-44) are presented in Appendix A. Spinel is hercynite with X_{Fe} ranging from 0.78-0.85. Garnet from sample T-39 is almandine (65.1%-65.6%) with pyrope ranging from 21.9%-22.3% and grossular and spessartine are less than 10%. Cordierite has low Fe concentrations (X_{Fe} = 0.26) and staurolite is Fe-rich (X_{Fe} = 0.76-0.82).

7.3 GARNET ZONING

Garnet from a pelitic schist layer in the metapsammitic unit (sample T-13) is abundant (up to 25%) and occurs as relatively large subhedral grains (< 1mm) and contain inclusions of quartz, biotite and magnetite (Fig. 7-2). Garnets from two metapsammite samples (T-35 and T-73) are tiny (< 0.5mm) euhedral to subhedral grains and are relatively rare (< 5%). They are also relatively inclusion-free except for very small inclusions of quartz in places (Figs. 7-3 & 7-4).

A microprobe traverse across one garnet from sample T-13 shows appreciable Mg decrease and Fe increase from core to rim and Ca-Mn are essentially unzoned (Fig. 7-5). This may result from retrograde diffusion zoning and cation exchange (Tracy, 1982) with biotite which is abundant in the sample. Microprobe traverses across one garnet from each of samples T-35 and T-73 are also shown in Fig. 7-5. Garnet in sample T-35 shows a systematic Mg decrease from the core to the rim with a corresponding increase in the Mn content. Similar patterns noted by Tracy

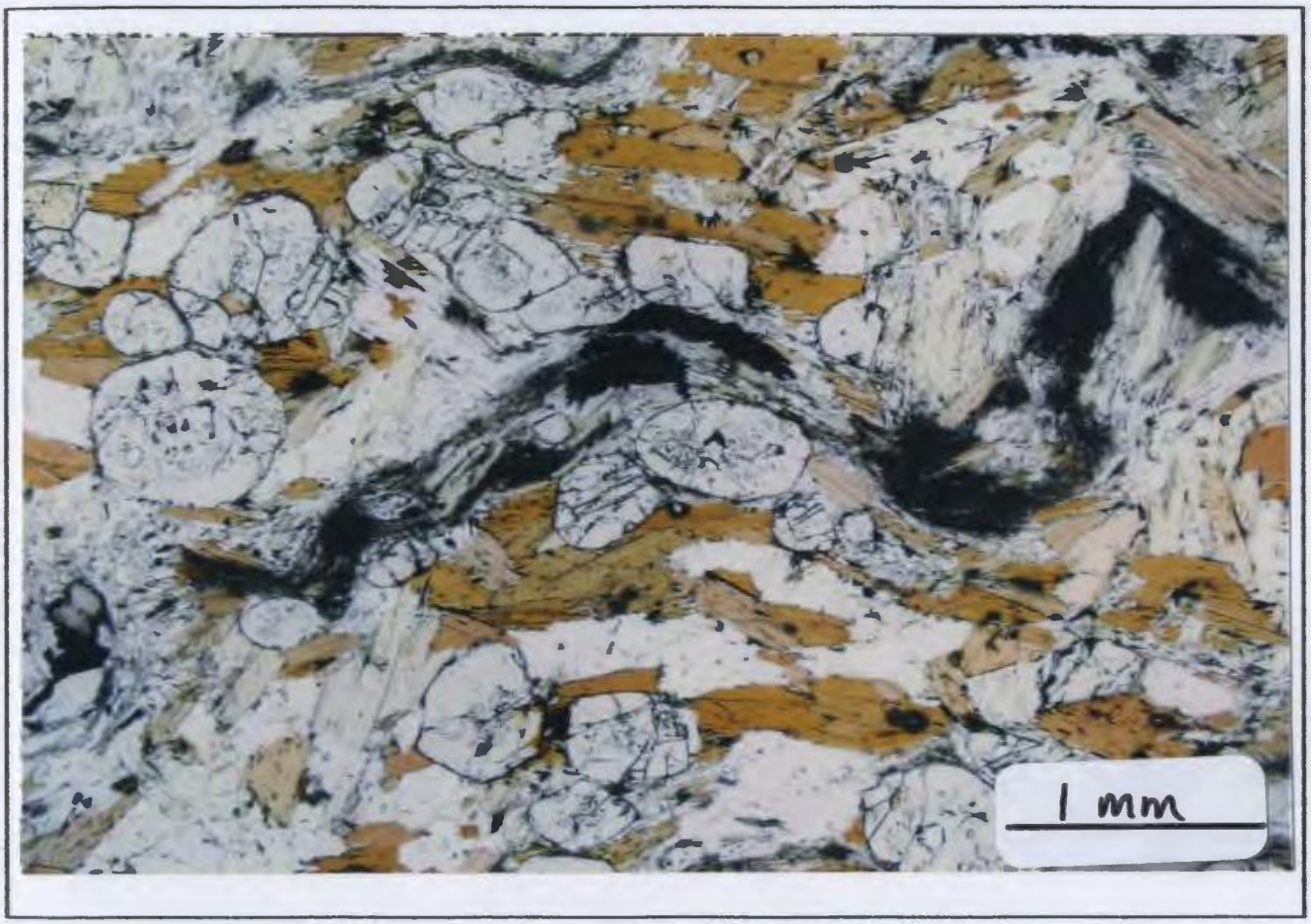

Fig. 7-2. Photomicrograph of garnets in sample T-13. Some garnets contain inclusions of quartz, biotite and opaques. (Plane polarized light).

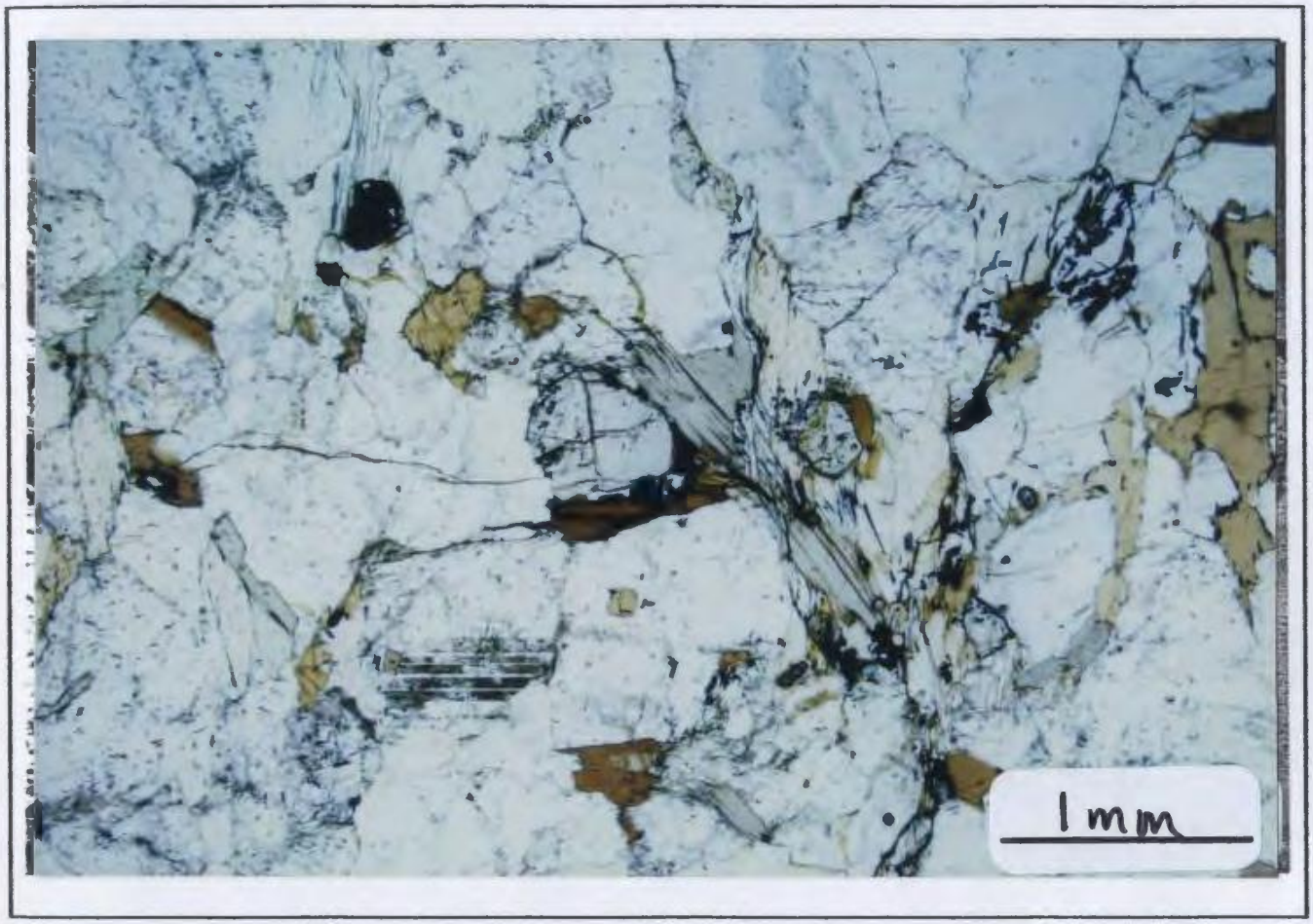

Fig. 7-3. Photomicrograph of tiny garnets (center of photograph) from sample T-35. Most are inclusion free. (Plane polarized light).

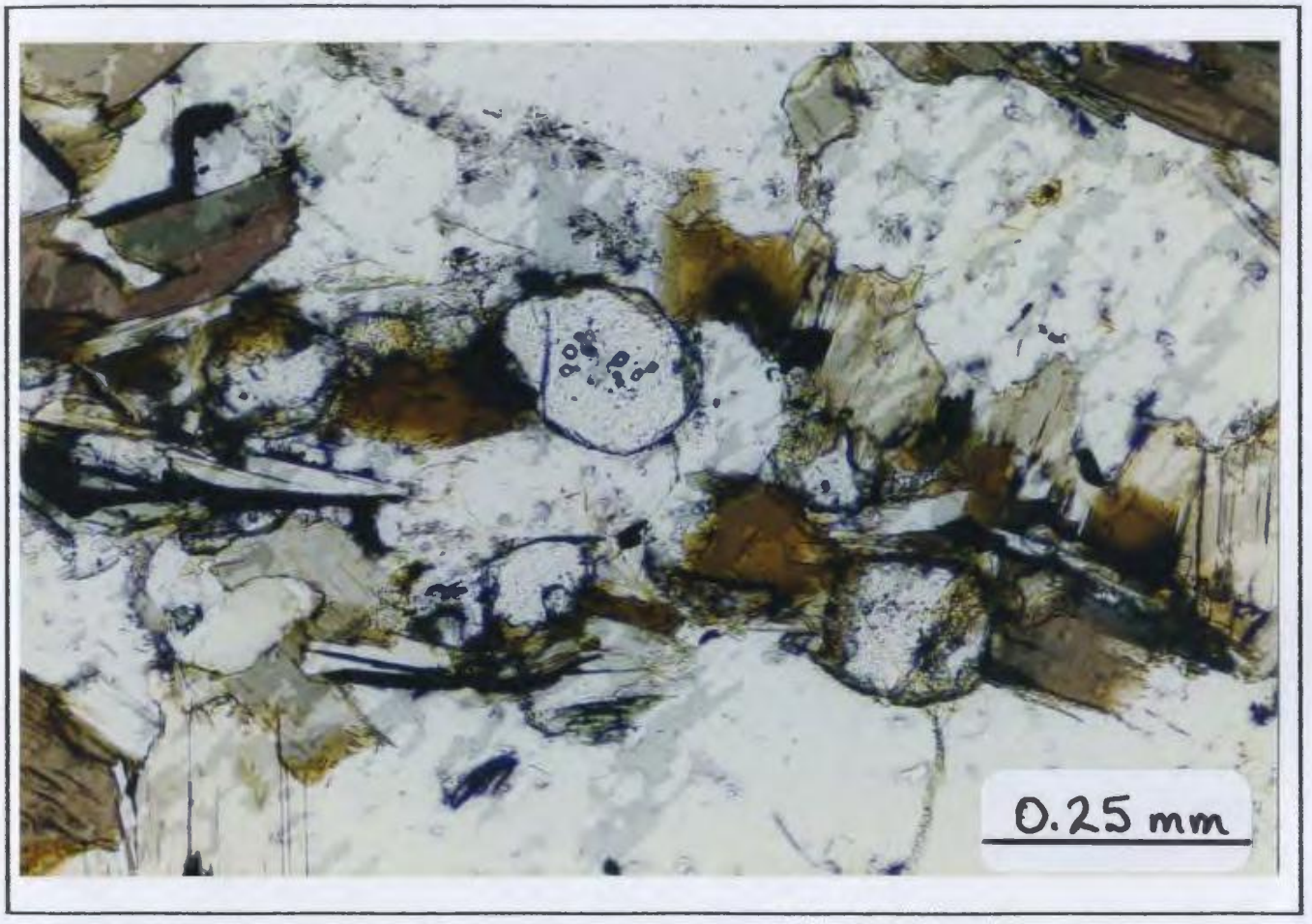

Fig. 7-4. Photomicrograph of tiny, inclusion free garnets from sample T-73. (Plane polarized light).

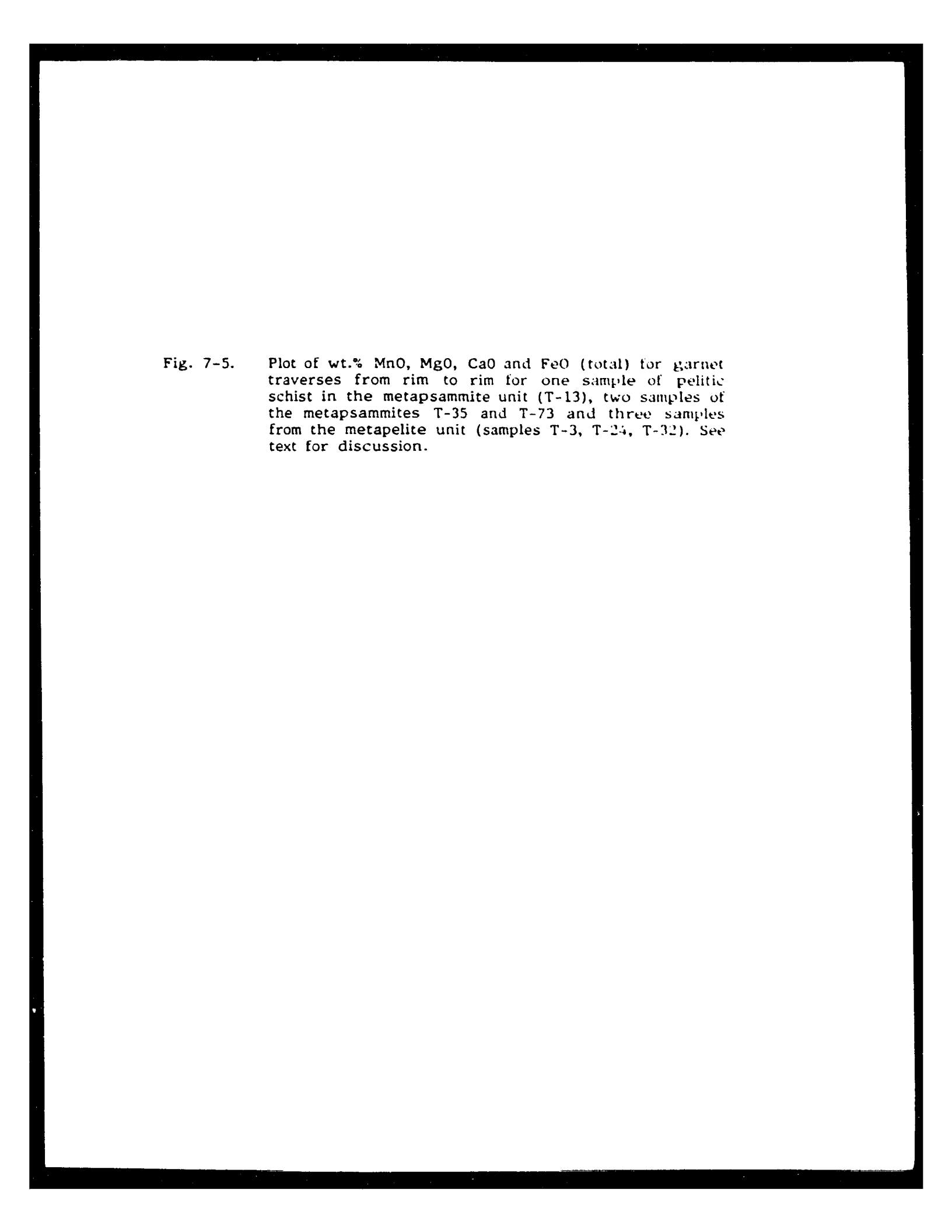

Fig. 7-5. Plot of wt.% MnO, MgO, CaO and FeO (total) for garnet traverses from rim to rim for one sample of pelitic schist in the metapsammite unit (T-13), two samples of the metapsammites T-35 and T-73 and three samples from the metapelite unit (samples T-3, T-24, T-32). See text for discussion.

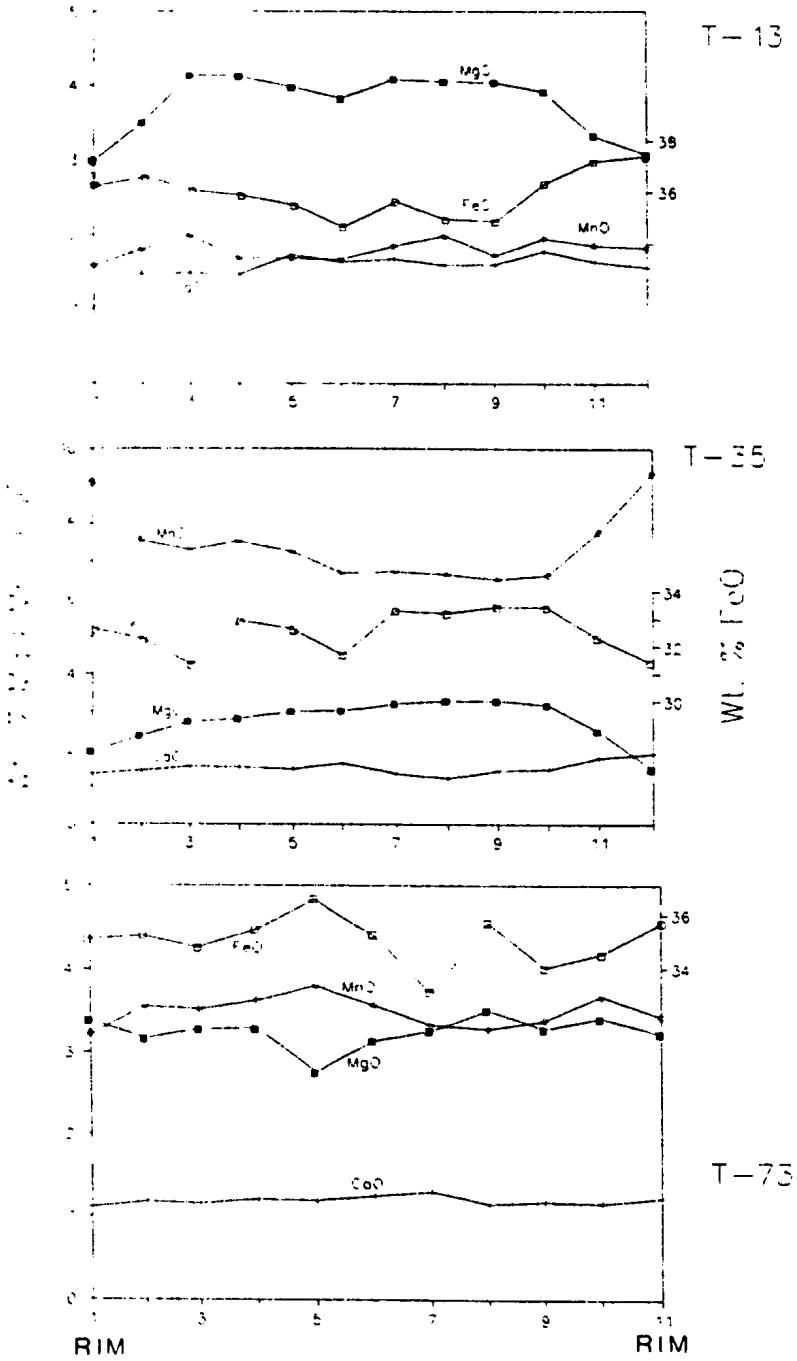
T-13
MgO
FeO
MnO
38
36
T-35
34
32
30
T-73
36
34
CaO
RIM
RIM
Wt. % FeO

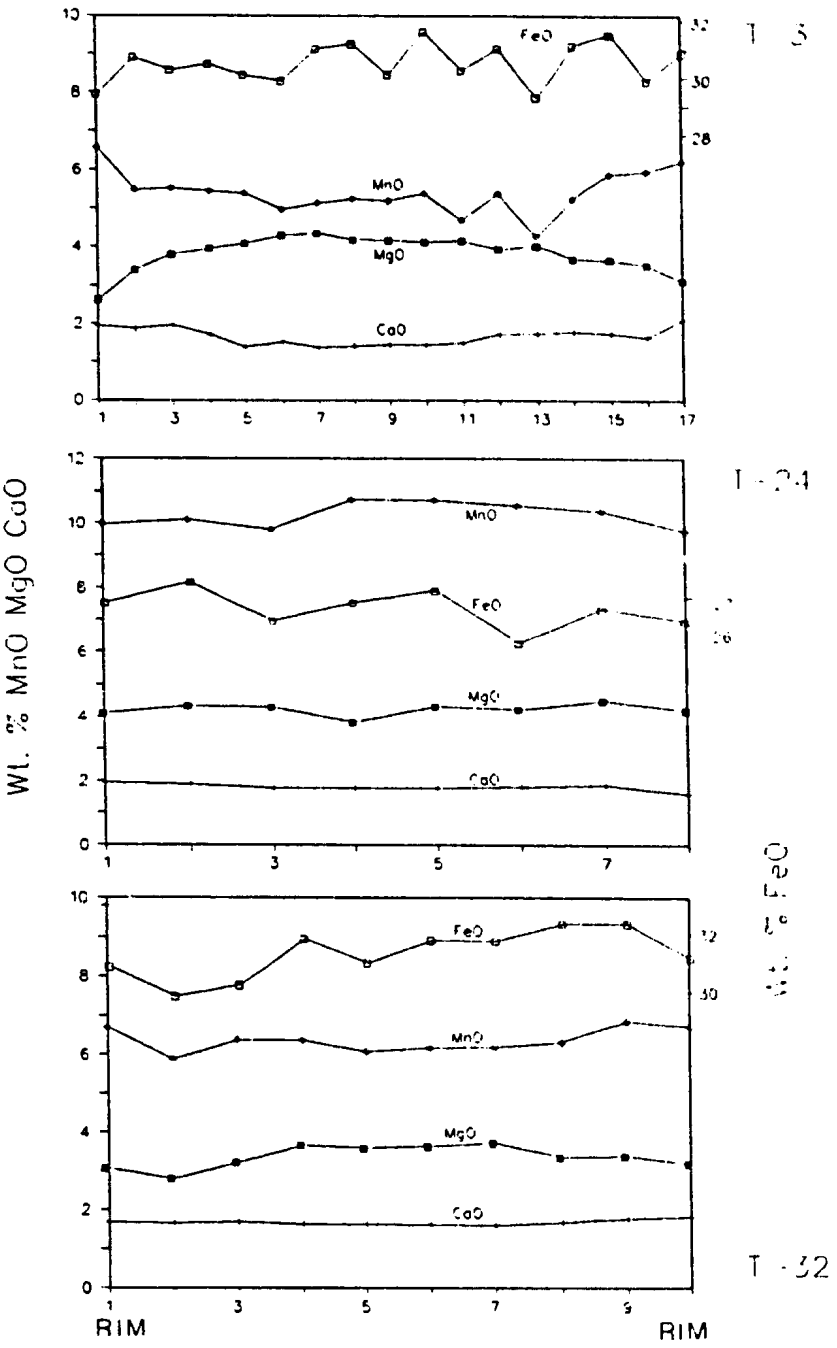
Wt. % MnO MgO CaO
FeO
MnO
MgO
CaO
RIM
RIM

(1982) have been observed in upper amphibolite facies garnets from various studies and has been attributed to resorption of Mn into the outer rim of the garnet during retrogression (Grant & Weiblen, 1971). Garnet in sample T-73 is essentially homogeneous.

Garnet textures from three samples of the metapelite unit vary between samples. T-3 contains garnets that are generally less than 1mm in diameter and contain inclusions of spinel (hercynite), magnetite, biotite, quartz and plagioclase (Fig. 7-6). Garnet in sample T-24 is up to 3mm in diameter with diffuse boundaries and contains abundant inclusions of sillimanite, biotite, magnetite and quartz (Fig. 7-7). In sample T-32 the garnet appears similar to the metapsammite samples T-35 and T-73 and are less than 0.5mm in diameter, euhedral and inclusion free (Fig. 7-8). Garnet is also very scarce in this sample (< 2%).

Microprobe traverses across one garnet from each sample are shown in Fig. 7-5. Sample T-3 shows a Mg decrease and corresponding Mn increase from the center to rim and Ca-Fe are essentially unzoned (similar to the garnet in sample T-35). This may also be a result of retrograde resorption as noted above for sample T-35. Garnets in samples T-24 and T-32 are essentially homogeneous which is typical of high grade garnets which have attained temperatures at which homogenization of growth zoning occurs.

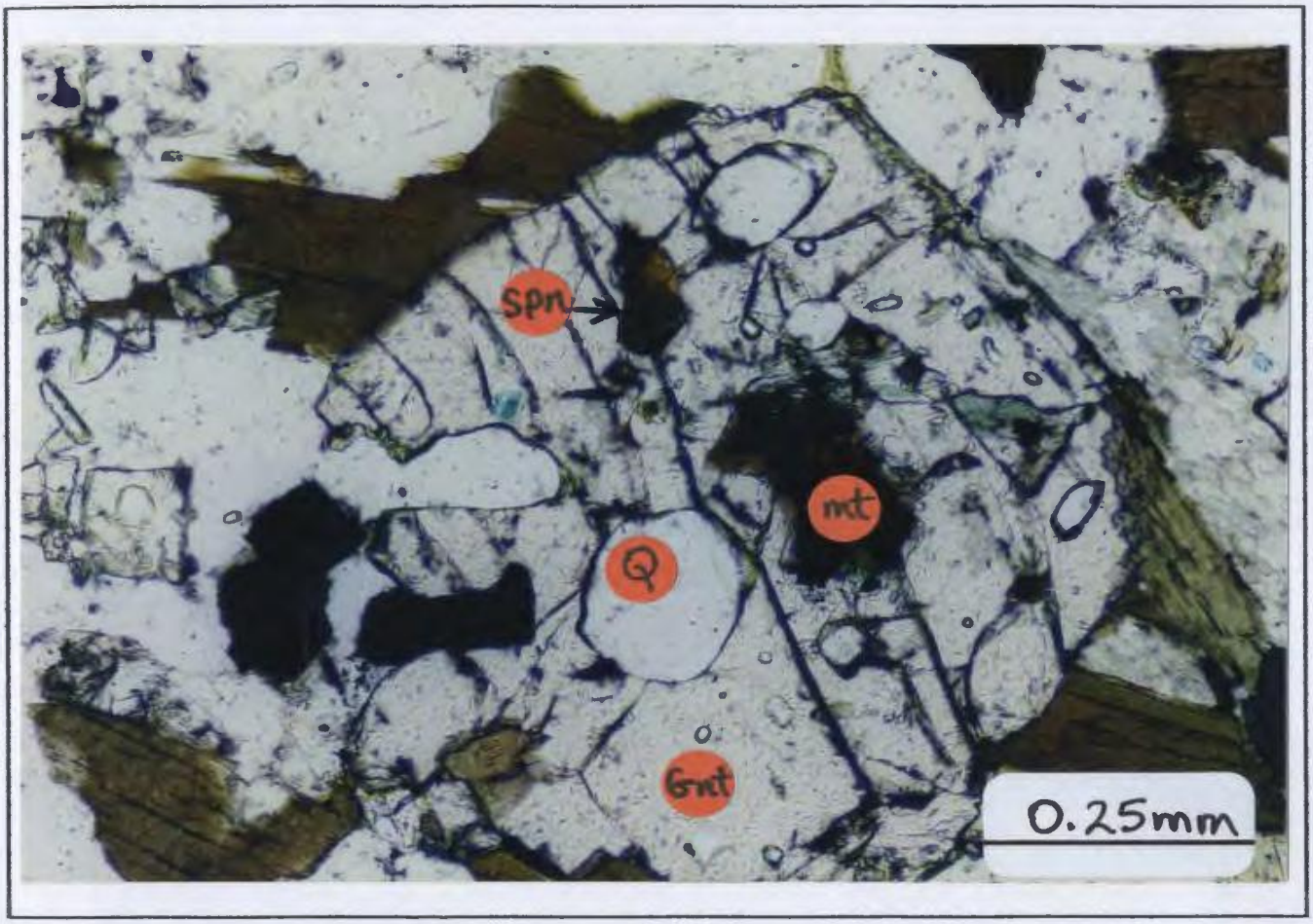

Fig. 7-6. Photomicrograph of garnet in sample T-3 showing spinel inclusions in addition to magnetite + quartz + biotite. (Plane polarized light).

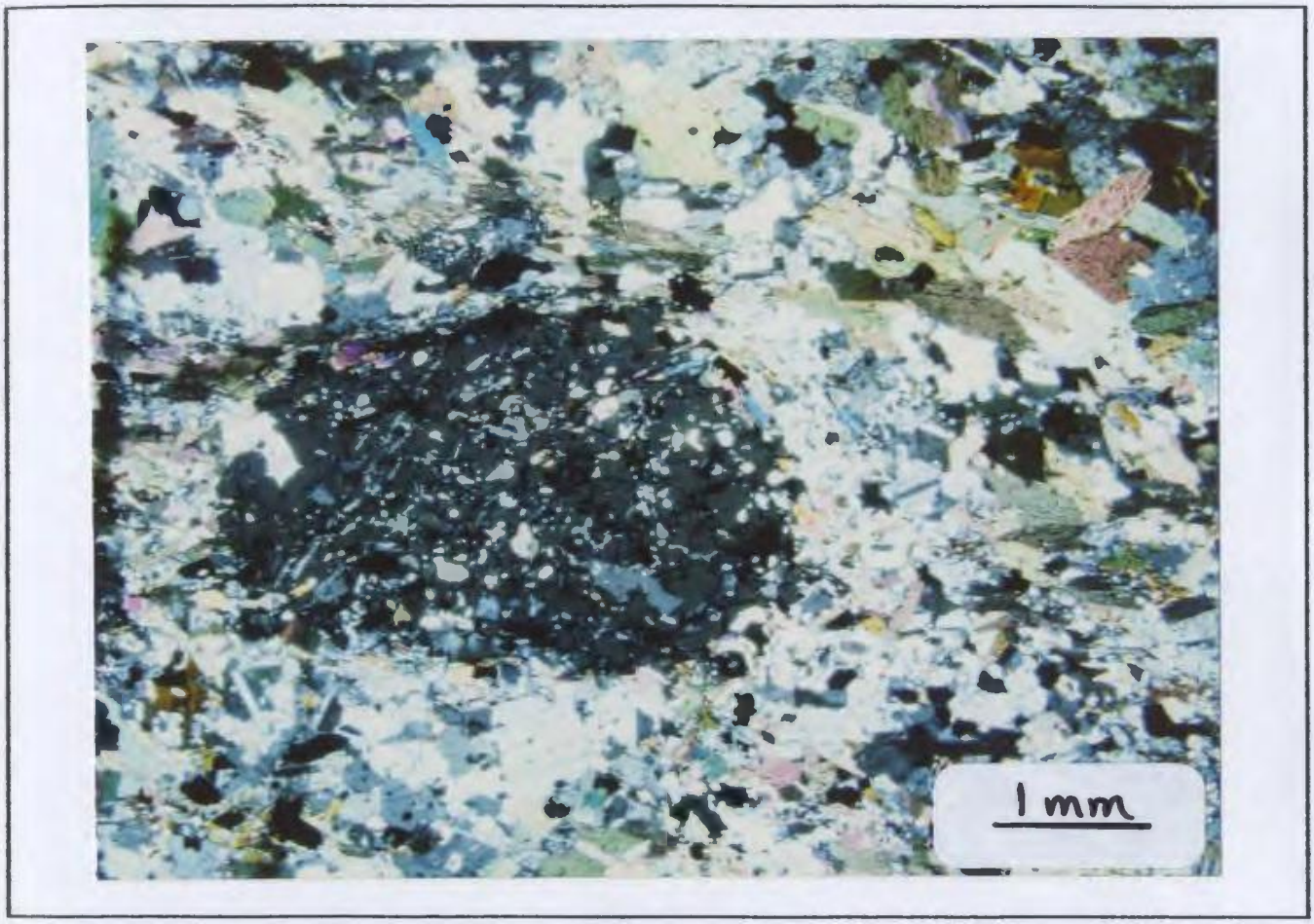

Fig. 7-7. Photomicrograph of sample T-24 showing large garnet (approx. 3mm across) with inclusions of sillimanite + quartz + Fe-Ti oxides. (X-polarized light).

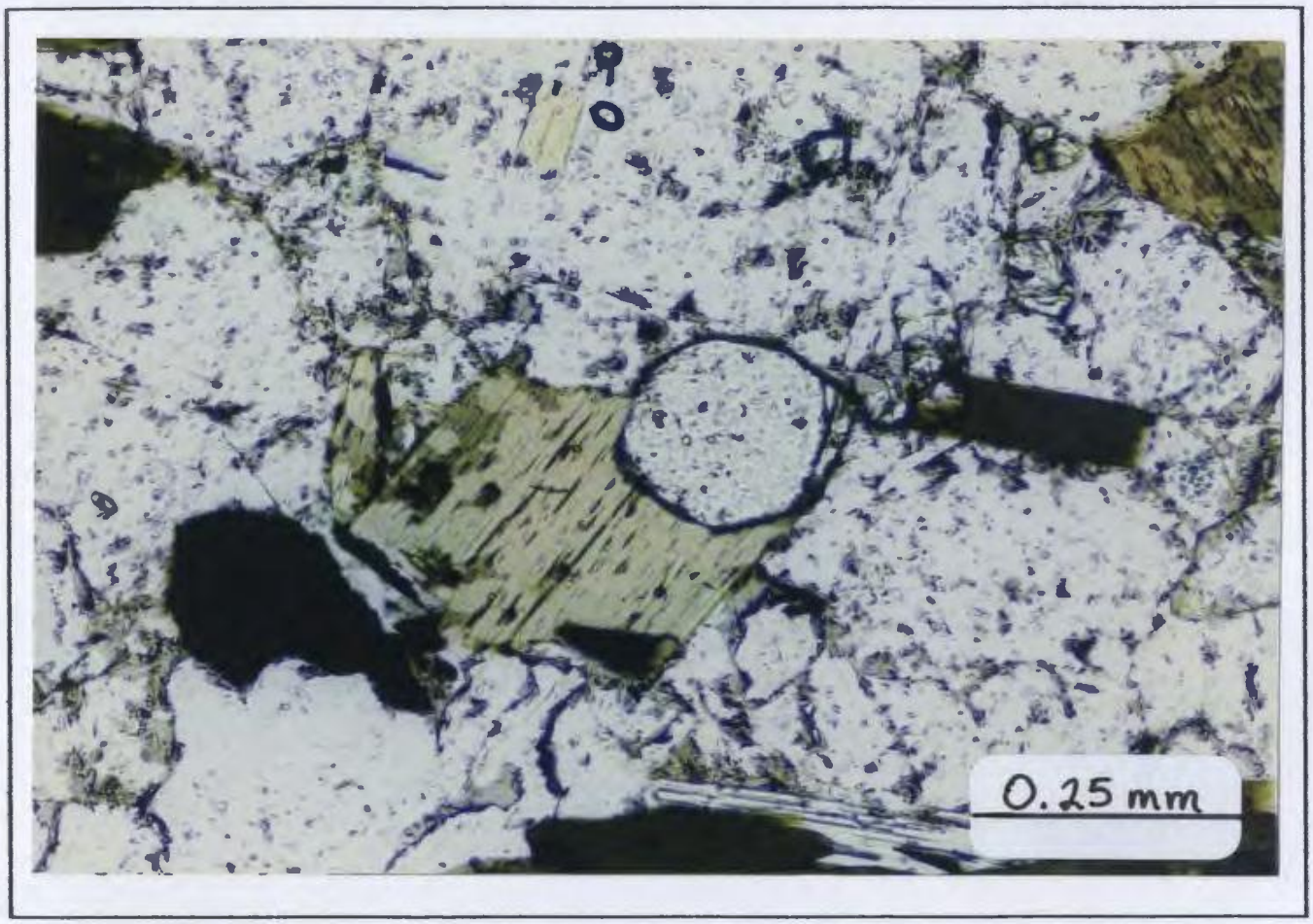

Fig. 7-8. Photomicrograph of tiny, inclusion-free garnet in sample T-32. (Plane-polarized light).

7.4 RESULTS FROM GARNET-BIOTITE THERMOMETRY

Biotite and garnet in six samples (T-13, T-35, T-73, T-3, T-24, T-32) are in contact with each other, however as discussed in the previous section, several of the garnets are chemically zoned. As a result of the chemical zoning, temperatures were estimated using one garnet core and one garnet rim with the same biotite (in contact with the garnet) to determine possible temperature differences that may have occurred during retrogression. In addition to this, several garnet cores were used with biotites in contact with the garnets and biotites away from the garnets in order to check for internal homogeneity of biotite and garnet chemistry.

The use of garnet cores and rims will only work effectively as an estimate of temperature if there is a large reservoir of biotite in the matrix so that biotite composition varies very little as a result of the exchange reaction. This is the case in all samples used in this study. Biotite is abundant in all samples and their composition varies little within and between samples (see microprobe analyses in Appendix A).

Temperature estimations for the various mineral pairs in all six samples are presented in Table 7-1. The temperatures have been calculated for a range of pressures (4, 6 and 8 kbars) using the calibration of Ferry & Spear (1978) and the calibration of Ferry & Spear with corrections from Hodges & Spear (1982); T1 and T2 respectively. A review of these calibrations is presented in Appendix E. K_D values within samples are relatively consistent using garnet cores with different

Table 7-1

Temperature estimates from garnet-biotite thermometry.

Sample T-3 Sillimanite-biotite-garnet metapelite
Sample T-24 Sillimanite-biotite-garnet metapelite
Sample T-32 Sillimanite-biotite-garnet metapelite
Sample T-13 Sillimanite-biotite-fibrolite pelitic schist from metapsammite unit
Sample T-35 Biotite-garnet metapsammite
Sample T-73 Biotite-garnet metapsammite

1) Numbers on gnt/bio pairs correspond to the number of analysis in Appendix A.
2) Garnet core-rim analyses are as shown.
3) "a" in biotite analysis is biotite in contact with garnet
4) "b" in biotite analysis is biotite away from garnet

T1 = Calibration of Ferry & Spear (1978)
T2 = Calibration of Ferry & Spear (1978) with corrections from Hodges & Spear (1982)

$$\textit{Distribution Coefficient } K_D = \frac{X_{Mg}^{GNT} + X_{Fe}^{GNT}}{X_{Mg}^{BIO} + X_{Fe}^{BIO}}$$

Sample T-3

GNT/BIO	P	T1	T2	KD
1core/1a	4	793	815	0.297
	6	803	824	
	8	812	833	
2core/2a	4	717	735	0.255
	6	726	744	
	8	735	753	
1core/3b	4	735	760	0.267
	6	744	769	
	8	754	778	
2core/3b	4	739	757	0.267
	6	748	765	
	8	757	774	
3rim/2a	4	560	582	0.170
	6	567	590	
	8	575	597	
3core/2a	4	738	753	0.265
	6	747	762	
	8	757	770	

Sample T-24

GNT/BIO	P	T1	T2	KD
1core/1a	4	778	799	0.289
	6	787	808	
	8	797	817	
2rim/2b	4	672	693	0.230
	6	681	702	
	8	689	710	
2core/2b	4	796	815	0.299
	8	806	825	
	8	815	834	

Sample T-32

GNT/BIO	P	T1	T2	KD
1core/1a	4	664	684	0.226
	6	672	692	
	8	681	700	
2core/2b	4	648	667	0.217
	6	656	675	
	8	664	683	
3rim/1a	4	592	611	0.187
	6	600	619	
	8	607	626	
3core/1a	4	644	663	0.215
	6	653	671	
	8	661	679	

Sample T-13

GNT/BIO	P	T1	T2	KD
1core/1a	4	557	575	0.168
	6	564	583	
	8	572	590	
2core/2b	4	606	623	0.194
	6	614	631	
	8	622	638	
3rim/1a	4	508	524	0.143
	6	515	531	
	8	522	538	
3core/1a	4	616	635	0.200
	6	624	643	
	8	632	650	

Sample T-35

GNT/BIO	P	T1	T2	KD
1core/1a	4	566	588	0.173
	6	574	596	
	8	581	603	
2core/2b	4	576	597	0.178
	6	583	604	
	8	591	612	
3rim/1a	4	422	441	0.102
	6	428	447	
	8	433	453	
3core/1a	4	638	656	0.211
	6	646	664	
	8	654	672	

Sample T-73

GNT/BIO	P	T1	T2	KD
1core/1a	4	681	695	0.235
	6	690	704	
	8	698	712	
2core/2b	4	719	733	0.256
	6	728	742	
	8	737	750	
3rim/1a	4	716	729	0.254
	6	724	737	
	8	733	746	
3core/1a	4	679	694	0.234
	6	688	702	
	8	696	711	

combinations of biotite grains. This is interpreted to indicate internal homogenization of matrix biotites and garnet cores. Also K_D values are much lower for garnet rims than garnet cores in all samples except T-73. In this sample the garnet is essentially homogeneous and K_D values are similar for all mineral pairs.

A summary of the results is given below.

1) Temperatures vary by approximately 20°C between the two calibrations with T2 (Ferry & Spear with Hodges and Spear corrections) giving the higher temperatures.

2) Within sample variation of temperature is generally low using combinations of garnet cores with different biotite grains.

3) In each case except sample T-73, estimated temperatures are lower using garnet rims than garnet cores.

At 4 kbars pressure (using T2 as an example), temperatures using garnet cores are highest for two metapelite samples (T-3, T-24) which range from 815°C to 735°C. The range in temperature of the other metapelite sample (T-32) is 663°C to 684°C. Temperatures of the two metapsammites range from 733°C to 588°C. The range for the one pelitic schist in the metapsammite unit is 635°C to 575°C. Although there is some overlap in temperatures, it appears the metapelites record the highest temperatures of the rocks within the map area. It is also noteworthy that these rocks lie closest to the granitoid suite to the east and that the lowest temperatures are from the pelitic schist that lies the farthest from the granitoid rocks (see Fig. 7-1).

Comparing garnet rim-core temperature variations to the microprobe

traverses presented in the previous section, the samples with the most pronounced zoning with respect to Mg and Mn (i.e. T-3 and T-35) have the widest range of temperatures between garnet rim and garnet core. This is consistent with previous interpretations of retrograde origin for the zoning in the garnet. Sample T-73 shows no appreciable chemical zoning and temperatures at 4 kbars pressure for all mineral pairs within this sample do not vary substantially (694°C to 733°C).

7.5 PLAGIOCLASE-GARNET-Al_2SiO_5-QUARTZ BAROMETRY

Of the six samples used for garnet-biotite thermometry, four (T-13, T-3, T-24, T-32) also contain the assemblage garnet-Al_2SiO_5-plagioclase-quartz. Table 7-2 shows the results of pressure estimations for these four samples at 600°C and 800°C. Pressures P1, P2, P3 and P4 are estimates using different calibrations and activity models for grossular and anorthite as shown in the table. Pressures were calculated using combinations of garnet rims and cores with several different plagioclase grains as indicated in Table 6-3. The ranges in -lnK values (using Newton & Haselton grossular and anorthite activity models) are from 8.191 to 6.785 at a temperature of 600°C. Using Hodges & Royden activity models, -lnK ranges from 6.167 to 7.850 at 600°C.

Estimated pressure differences are negligible between garnet cores and rims. The highest pressures were obtained using the calibration of Koziol & Newton (1988) with activities calculated using the method of Hodges & Royden (1984). It is noteworthy that pressures estimated from

Table 7-2

Pressure estimates using garnet-sillimanite-plagioclase-quartz barometry.

T-3 metapelite
T-24 metapelite
T-32 metapelite
T-13 pelitic schist in metapsammite unit

1) Numbers on gnt-plag correspond to the number of analysis in Appendix A
2) Garnet core-rim analyses are as shown

P1 = calibration of Ghent et al. (1979)
P2 = calibration of Goldsmith (1980) with a_{gr1} and a_{An2} from Newton & Haselton (1981)
P3 = calibration of Koziol & Newton (1988) with a_{gr1} and a_{An1} from Newton & Haselton (1981)
P4 = calibration of Koziol & Newton (1988) with a_{gr2} and a_{An2} from Hodges & Royden (1984)

-lnK1 calculated using a_{gr1} and a_{An1} from Newton & Haselton (1981)
-lnK2 calculated using a_{gr2} and a_{An2} from Hodges & Royden (1984)

sample #	GNT/PLAG	T	P1	P2	P3	P4	lnK1	lnK2
T-3	2core/2	600	21	23	31	36	8.013	7.686
		800	47	52	59	61	7.676	7.362
	1core/1	600	28	29	38	43	7.554	7.217
		800	54	60	67	69	7.140	6.988
	3rim/1	600	32	32	40	45	7.383	7.053
		800	60	64	71	73	6.918	6.770
	3core/1	600	19	21	30	34	8.191	7.850
		800	44	49	56	59	7.785	7.679
T-24	1core/1	600	33	31	40	48	7.399	6.780
		800	61	64	71	76	6.891	6.573
	2rim/1	600	39	36	45	51	7.030	6.349
		800	69	71	78	83	6.459	6.173
	2core/1	600	34	32	40	49	7.385	6.638
		800	63	65	72	78	6.817	6.483
T-32	1core/1	600	35	32	40	48	7.350	6.731
		800	63	65	72	77	6.786	6.487
	2core/2	600	34	31	39	47	7.443	6.817
		800	62	64	71	76	6.869	6.567
	3rim/1	600	35	31	39	47	7.432	6.813
		800	63	64	71	76	6.833	6.548
	3core/1	600	32	29	38	45	7.570	6.918
		800	60	61	69	73	7.001	6.699
T-13	1core/1	600	43	39	48	55	6.785	6.367
		800	73	75	82	86	6.153	5.912
	2core/2	600	35	33	41	49	7.386	6.661
		800	64	66	73	77	6.698	6.433
	3rim/1	600	39	35	43	51	7.103	6.486
		800	69	70	77	81	6.454	6.215
	3core/1	600	42	39	47	48	6.791	6.170
		800	72	74	82	82	6.179	5.937

Newton & Haselton (1981) are almost identical to the calibration of Ghent et al., (1979) even though Newton & Haselton specifically account for the non-ideal mixing in garnet and plagioclase (see Appendix E). However, Newton & Haselton specify that their method should be used only for low Mn garnets and that it does not account for the interaction affects that Mn may have on grossular activities. The Mn contents of the garnets in this study are quite high (see Appendix A). In addition to this, the new experimental calibration of the end-member reaction by Koziol & Newton (1988) is considered to be more accurate than the older experimental calibration of Goldsmith (1980) used by Newton & Haselton. Therefore P4 pressures (end-member calibration of Koziol & Newton with activities from Hodges and Royden) are interpreted to be the most reasonable for the rocks of this study.

7.6 SIMULTANEOUS APPLICATION OF GARNET-BIOTITE TEMPERATURES AND PLAGIOCLASE-GARNET-Al_2SiO_5-QUARTZ PRESSURES

The simultaneous application of independent thermometers and barometers assumes that both systems closed at the same time and that the rate of element diffusion for the two different systems was the same. However, it is difficult to prove that this was indeed the case and therefore, any estimate of temperatures and pressures may not be "peak" metamorphic conditions. In spite of this, simultaneous applications of thermometers and barometers can lead to part of the P/T path a suite of rocks has experienced even if this path does not include part of the peak conditions.

Figure 7-9 shows a P-T diagram with a plot of the intersection of temperatures (calibration of Ferry & Spear with corrections from Hodges & Spear) and pressures (Koziol & Newton with corrections from Hodges & Royden) calculated in the previous sections. Reactions noted in Chapter 6 are also shown. The resulting P-T vectors from garnet core to garnet rim suggest that the cooling was accompanied by decompression, a conclusion that is further supported by the following:

1) P-T vectors are in the same direction indicating internal consistency of data.

2) The highest pressure estimates occur with the highest temperature estimates which indicates that there was a systematic closure of the barometer and thermometer.

3) The resulting vectors, for the most part point from the sillimanite to the kyanite field. This is consistent with the occurrence of coarse kyanite in the retrograde rocks as noted in Chapter 6. One sample however does contain andalusite which indicates the retrograde path must be very close to the Al_2SiO_5 triple point junction.

7.7 ISOTOPE THERMOMETRY

Three samples of the metapsammite, six samples of metapelite and two samples of sheared rocks in the metapelite unit were used to calculate temperatures by O isotope fractionation between quartz biotite, quartz magnetite and quartz-chlorite mineral pairs. A review of the procedure used for temperature estimations is presented in Appendix E.

All analyses and corresponding temperature estimates are presented in Table 7-3. Temperatures for all samples range from 485°C to 628°C except for one anomalous estimate of 921°C (sample T-24). This is an

Fig. 7-9. Plot of P-T estimates for three samples of the metapelites (T-3, T-24, T-32) and one sample of pelitic schist in the metapsammite unit (T-13). The points represent the intersection of an average of temperatures for garnet cores using the Ferry & Spear (1978) garnet-biotite thermometer with corrections from Hodges & Spear (1982) and temperatures using garnet rim analyses with average pressures estimated using the garnet-plagioclase-sillimanite-quartz barometer with the calibration of Koziol & Newton (1988) and a_{gr} and a_{An} calculated from Hodges & Royden (1984). Arrows point from garnet core temperature estimates to garnet rim temperature estimates. Reactions are the same as in Fig. 6-8. Also shown are the range of temperatures estimated by oxygen isotope thermometry (see Table 7-3).

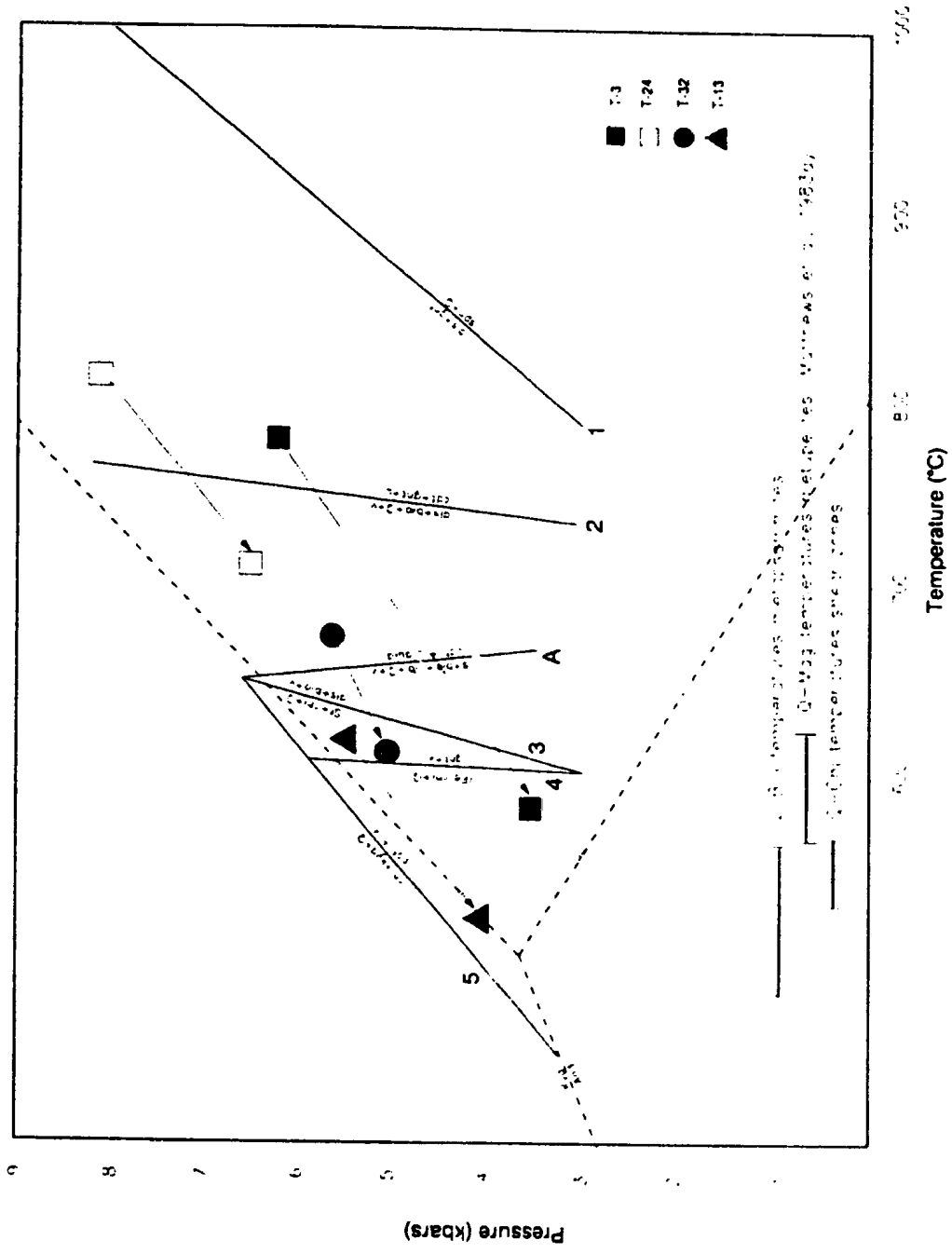
T-3
T-24
T-32
T-13
1
2
3
4
5
A
Temperature (°C)
Pressure (kbars)

Table 7-3

Equations for the determination of temperature using:

A) Bottinga & Javoy (1975) $\Delta^{18}O_{(quartz\text{-}biotite)} = 3.69(10^6T^{-2}) - 0.6$

B) Bottinga & Javoy (1975) $\Delta^{18}O_{(quartz\text{-}magnetite)} = 5.57(10^6\ T^{-2})$

C) Matthews et al. (1983a) $\Delta^{18}O_{(quartz\text{-}magnetite)} = 6.11\ (10^6\ T^{-2})$

D) Wenner & Taylor (1971) $\Delta^{18}O_{(quartz\text{-}chlorite)} = 2.01(10^6T^{-2}) + 1.99$

Sample #	Unit	Delta O(18) per mil SMOW				Temperature (°C)			
		Quartz	Biotite	Chlorite	Magnetite	A	B	C	D
11	Granodiorite								
31	Granodiorite								
193	metapsammite	11.00	6.29			561			
73	metapsammite	10.98	5.51			507			
76	metapsammite	10.15	4.32			485			
19	metapelite	10.06			1.54		536	574	
24	metapelite	9.36	7.37			921			
26	metapelite	10.88	6.03			550			
39	metapelite	9.47			1.36		556	595	
40	metapelite	8.93			1.15		573	613	
44	metapelite	8.59			1.06		587	628	
154	shear zone	11.13		6.34					574
157	shear zone	11.48		6.39					532
61	shear zo *	11.39							
77	shear zone	11.74							

unreasonable result and is possibly a result of sample contamination. The three samples of metapsammite give quartz-biotite temperatures in the range of 485°C- 561°C, whereas quartz-magnetite pairs from metapelites yielded temperatures in the range of 536°C- 587°C (Bottinga & Javoy, 1975 calibration) and 574°C-628°C (Matthews et al., 1983 calibration). The one reasonable metapelite quartz-biotite temperature is 550°C. Quartz-chlorite pairs from shear zone samples yielded temperatures of 574°C and 532°C.

7.8 DISCUSSION OF GEOTHERMOBAROMETRY RESULTS

Temperatures estimated by quartz-biotite and quartz-magnetite isotope thermometry are generally lower than those estimated by garnet core-biotite thermometry for both the psammitic and pelitic metasedimentary rocks. This result is to be expected since it is well known that "peak" metamorphic temperatures are difficult to estimate by isotope thermometry because minerals generally continue to equilibrate oxygen during subsequent cooling. This is especially the case for high-grade rocks that have been retrogressed in the presence of fluids, which enhance the diffusivity of oxygen (Ganguly & Saxena, 1987).

On the other hand, garnet rim-biotite temperatures are more closely comparable to the isotopic temperatures including those estimated by quartz-chlorite pairs from shear zone rocks. These observations indicate that all the rocks within the map area including the shear zones have re-equilibrated during subsequent cooling and that the exchange of oxygen and cations closed at similar temperatures and time. In Chapter 5, evidence was presented that indicated shearing overprinted the high grade fabric in the metasedimentary rocks but also the high grade fabric is sheared (as

seen by sheared relics of sillimanite and garnet). This combined with the results presented above indicate that shearing was synchronous with the overall metamorphic history of the surrounding metasedimentary rocks.

The regional metamorphic history of the psammitic and pelitic metasedimentary rocks appears to be one that includes decompression as well as cooling as indicated by the decrease in temperature and corresponding drop in pressure. Garnet-biotite thermometry and garnet-Al_2SiO_5-plagioclase-quartz barometry from three samples of the pelitic metasedimentary rocks has outlined a P-T path from high grade metamorphic conditions (800°C, 6-8 kbars) to lower grade conditions (P and T approaching the Al_2SiO_5 triple point junction). The estimated pressure and temperature conditions are in agreement with metamorphic conditions indicated by mineral assemblages in Chapter 6. In several examples, garnets also show evidence for retrograde diffusion zoning.

Garnet-biotite thermometry and garnet-Al_2SiO_5-plagioclase-quartz barometry from one sample of the psammitic metasedimentary rocks has outlined a P-T path from approximately 650°C and 5-6 kbars to approximately 525°C and 4 kbars (i.e. very near the Al_2SiO_5 triple point junction). Overall the peak metamorphic conditions in the psammitic metasedimentary rocks appear to be lower than in the pelitic metasedimentary rocks and therefore the grade of metamorphism increases from west to east within the study area. However, it is recognized that this conclusion is based on a small number of samples.

CHAPTER 8

SUMMARY AND CONCLUSIONS

This study is a contribution to an understanding of the regional geology of southwestern Newfoundland. The study area lies between the Long Range Fault and the Cape Ray Fault in the Dashwoods subzone of the Dunnage zone. The major lithologic units in the study area are an undifferentiated granitoid suite, metasedimentary rocks (psammitic and pelitic units) and mafic-ultramafic rocks. These lithologies are characteristic of the Dashwoods subzone elsewhere and have been previously studied in other localities throughout the subzone.

The granitoid rocks, first studied in the Port aux Basques region by Brown (1975, 1977), were described as tonalitic gneisses and were considered to be Precambrian in age. Subsequent mapping in the southwest and the northeast parts of the Dashwoods subzone (by Chorlton, 1984 & Dunning, 1984) have shown that the granitoid rocks intrude Ordovician ophiolite complexes (Long Range Mafic-Ultramafic and Annieopsquotch Complexes) and are now considered to be Ordovician in age.

Metasedimentary rocks are widespread throughout the Dashwoods subzone. Along the eastern side of the subzone, the Keepings Gneiss and the Cormacks Lake Complex consist of paragneiss considered to be Ordovician in age (Chorlton, 1984; van Berkel, 1987). In both cases, the metasediments are associated with mafic amphibolites and foliated granite

but the origin of these metasedimentary rocks is not well established. As discussed by van Berkel (1987) they may represent continental ritt facies metasediments associated with rift facies volcanic rocks. Along the southwestern side of the Dashwoods subzone near the Long Range Fault, Chorlton (1984) has described relatively small inclusions or layers of metasedimentary rocks within high strain zones and the granitoid suite. These rocks include semipelitic paragneiss and marble. Chorltons interpretation for these metasediments is that they formed on top of ophiolitic rocks of the Long Range Mafic-Ultramafic Complex and were subsequently thrust onto the continental margin of eastern North America.

Mafic-ultramafic rocks are also widespread throughout the Dashwoods subzone and two main types have been recognized (i.e. ophiolite complexes and Silurian gabbro-diorite intrusions). The main ophiolite complexes are the Long Range Mafic-Ultramafic Complex and the Annieopsquotch Complex. Silurian mafic intrusions are scattered throughout the northern part of the subzone and include the Main Gut Intrusion and the Boogie Lake Intrusion.

Field mapping as part of this study has added additional information to the regional geology outlined above. Two relatively extensive belts of metasedimentary rocks have been outlined immediately east of the Long Range Fault in the western part of the Dashwoods subzone. The metasedimentary rocks are correlated with the Fleur de Lys metasedimentary rocks of northern Newfoundland on the basis of similar stratigraphic position along the eastern edge of the miogeocline of eastern North America. As a result of this correlation, the Fleur de Lys Supergroup

probably extends along the entire length of western Newfoundland (including the metasedimentary inclusions in the Port aux Basques region).

Rocks of the granitoid suite have been observed along the contact with the pelitic metasedimentary unit in the present study area. Hornblende-biotite granodiorite clearly intrudes the metasediments and matic-ultramafic rocks. This is in agreement with observations elsewhere in the Dashwoods subzone. The granodiorite has been dated at 456 ±3 Ma (Dunning et at. 1989) and gives an upper age limit on deposition of the metasedimentary rocks (i.e. probably early to middle Ordovician).

The metasedimentary rocks contain either a gneissic layering or foliation referred to as an S_1 fabric. This fabric is sub-parallel to original layering (S_0) and is inferred to be a result of regional isoclinal folding. A second generation of isoclinal folding has affected these rocks but the timing of development of this folding event is not well constrained. This folding event is apparently non-penetrative and an associated fabric is not well-developed. Generally the S_1 fabric strikes NE-SW and is steeply dipping to vertical.

Overprinting shear zone fabrics are widespread in the pelitic metasediments and are referred to as S_2 fabrics. The shear zone fabric is recognized in the field mainly by the presence of quartz plates and ribbons. Further evidence of the mylonitic fabric can be seen in thin section where boudinaged garnets and elongated aggregates of sillimanite, feldspar and Fe-Ti oxides have been observed. It is not clear whether the

shearing occurred before, during or after the second generation of isoclinal folding. Shear zone fabrics are sub-parallel to the S_1 fabric.

One of the goals of this study was to determine the origin of the mafic-ultramafic rocks. However due to polymetamorphism and deformation in the study area, this is not a straightforward process. Figure 8-1 schematically shows different types of mafic-ultramafic complexes (ophiolites and arc complexes) after several stages of metamorphism and deformation. It is evident the end-member types may be very similar after undergoing normal orogenic processes. Silurian gabbro/diorite bodies also occur in the Dashwoods subzone. Lithologically the rocks of this study are not distinct from these bodies except that serpentinites are not a common feature of the Silurian bodies. The presence (or absence) of deformation has been used by several authors to distinguish between ophiolites and Silurian gabbro/diorite bodies in the Dashwoods subzone, but this is not a useful characteristic for the mafic-ultramafic rocks of this study because some bodies are highly deformed while others show little sign of deformation. However, the mafic-ultramafic rocks of this study apparently form a part of a disrupted belt conformable with the Long Range Mafic-Ultramafic Complex in the southwest part of the Dashwoods subzone. This Complex has traditionally been called an ophiolite complex and therefore the mafic-ultramafic rocks of this study are tentatively interpreted to be part of a disrupted ophiolite complex.

Regardless of the interpretation of the origin of the mafic-ultramafic rocks, it is evident they have been structurally emplaced. The mafic-ultramafic rocks studied in detail as part of this study lie within shear zones in the pelitic metasedimentary rocks and evidence suggests they are pre- to syn-kinematic. The block-in-matrix relationships described in

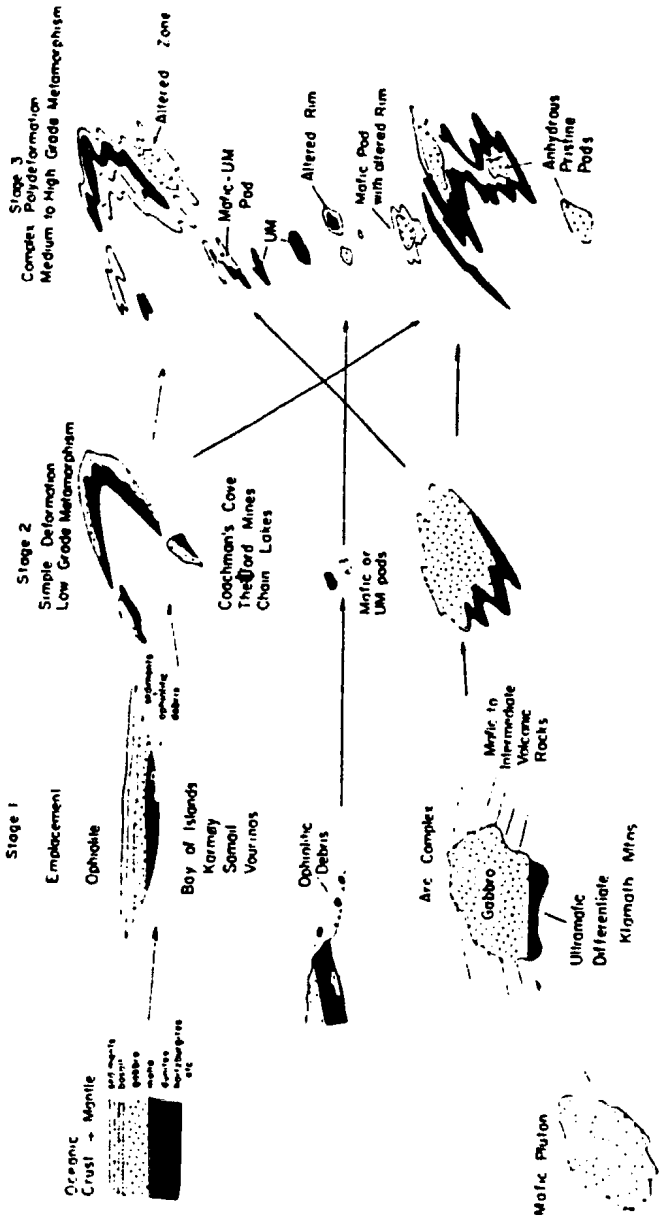

Fig. 8-1. Schematic diagram showing histories for several types of mafic-ultramafic bodies after deformation and metamorphism. After stage three the bodies are very similar and it is difficult to distinguish ophiolites from other types of intrusions (after Hatcher et al., 1984).

Chapters 3 and 5 can be referred to in terms of a mélange zone provided it is understood that evidence for sedimentary processes has not been found. Because of the high degree of deformation within the study area, any such features that may have developed are now obliterated and the present evidence suggests that deformation was the main mechanism for disruption.

The regional metamorphism of the metasedimentary rocks includes initial high grade amphibolite facies conditions followed by greenschist facies overprinting. The psammitic metasediments contain a well-developed migmatitic layering but there is no evidence for partial melting in these rocks and their layering may be an injection feature. A pelitic schist layer within this unit contains the assemblage sillimanite + garnet + biotite which implies conditions above the stability of staurolite + muscovite + quartz.

One sample of the pelitic metasedimentary rocks contains the assemblage spinel (hercynite) + quartz that implies high temperatures possibly in the order of 800°C or more. There is also evidence of coexisting garnet + cordierite in the pelitic metasedimentary unit and these rocks probably have been partially melted. Cooling has subsequently resulted in the development of kyanite, minor andalusite, staurolite and chlorite. Therefore the cooling path may have been in the vicinity of (or slightly above) the Al_2SiO_5 triple point junction.

Garnet-biotite thermometry and garnet-Al_2SiO_5-plagioclase-quartz barometry from several samples of the psammitic and pelitic metasediments has outlined a cooling P-T path from high grade metamorphic conditions (800°C, 6-8 kbars) to greenschist facies conditions approaching the Al_2SiO_5 triple point junction. The estimated pressure and temperature conditions

are in close agreement with metamorphic conditions indicated by observed mineral assemblages. Garnets show evidence for retrograde diffusion zoning or are completely homogenized presumably as a result of high metamorphic temperatures.

The matic-ultramatic rocks also show evidence of an initial high grade metamorphism but are now highly retrogressed to greenschist facies assemblages. Metadunites contain minor olivine (interpreted to be metamorphic) but mostly serpentine minerals. It is interpreted that antigorite formed from olivine in a retrograde environment and that lizardite formed subsequent to this with a further decrease in temperature. Metagabbro contains an early assemblage of hornblende + plagioclase but most samples are now almost entirely retrogressed to an assemblage of tremolite/actinolite + chlorite + calcite + sericite + clinozoisite/epidote + quartz + Fe-Ti oxides. Metapyroxenites show evidence of preexisting amphibolite facies assemblages but are now entirely retrogressed to greenschist facies minerals of tremolite/actinolite + chlorite. It is interpreted the matic-ultramatic rocks have undergone the full range of deformation and metamorphism that affected the metasedimentary rocks.

The high grade metamorphism and high degree of deformation outline for the rocks of this study are interpreted to be the result of the Taconic Orogeny and emplacement of ophiolitic allochthons during that time. As noted above, the upper age of deposition of the metasedimentary rocks is probably early to middle Ordovician. The Silurian matic bodies in the Dashwoods subzone were not subjected to the high grade metamorphism or high degree of deformation and as noted by Currie & van Berkel (1989), the Dashwoods subzone had probably stabilized by late Ordovician to Silurian time.

REFERENCES

Aggarwal, P.K. & Longstaffe, F.J., 1987. Oxygen-isotope geochemistry of metamorphosed, massive sulfide deposits of the Flin Flon-Snow Lake Belt, Manitoba. Contributions to Mineralogy and Petrology, 96, 314-325.

Ashworth, J.R., 1985. Introduction. In Migmatites. J.R. Ashworth (ed). Blackie, Glasgow, 1-35.

Berkland, J.O., Raymond, L.A., Kramer, J.C., Moores, E.M. & O'Day, M., 1972. What is Franciscan?. American Association of Petroleum Geology Bulletin, 56, 2295-2302.

Berthé, D., Choukroune, P. & Jegouzo, P., 1979. Orthogneiss, mylonite and noncoaxial deformation of granites: the example of the South Armorican shear zone. Journal of Structural Geology, 1, 31-42.

Bliss, N.W. & MacLean, W.H., 1975. The paragenesis of zoned chromite from central Manitoba. Geochimica et Cosmochimica Acta, 39, 973-990.

Bohlen, S.R., Wayne, A.D. & Wall, V.J., 1986. Calibration and applications of spinel equilibria in the system $FeO-Al_2O_3-SiO_2$. Journal of Petrology, 27, 1143-1156.

Bottinga, Y. & Javoy, M., 1975. Oxygen isotope partitioning among the minerals in igneous and metamorphic rocks. Reviews of Geophysics and Space Physics, 13, 401-418.

Brown, M., 1983. The petrogenesis of some migmatites from the Presqu'te de Rhuys, southern Brittany, France. In Migmatites, Melting and Metamorphism. M.P. Atherton & C.D. Gribble eds., Shiva, Cheshire, 174-200.

Brown, P.A., 1975. Basement-cover relationships in southwest Newfoundland. Ph.D. thesis, Memorial University of Newfoundland, St. John's, Newfoundland, 221 p.

Brown, P.A., 1976. Ophiolites in southwest Newfoundland. Nature, 264, 712-715.

Brown, P.A., 1977. Geology of the Port aux Basques map area (110/11), Newfoundland. Nfld. Dept. of Mines, Report 76-5, 16p.

Bursnall, J.T., 1975. Stratigraphy, structure and metamorphism west of Baie Verte, Burlington Peninsula, Newfoundland. Ph.D. thesis, Cambridge University, England, 337 p.

Carew, W., 1979. A layered appinitic intrusion in southwest Newfoundland: A field, petrographical and geochemical investigation. B.Sc. thesis, Memorial University of Newfoundland, St. John's, Newfoundland, 53 p.

Carpenter, J.R. & Phyfer, D.W., 1976. Olivine compositions from southern Appalachian ultramafics. Southeastern Geology, 20, 21-25.

Chorlton, L.B., 1980. Geology of the La Poile River area (110/16), Newfoundland. Nfld. Dept. of Mines and Energy, Report 80-3, 86 p.

Chorlton, L.B., 1984. Geological development of the southern Long Range Mountains, southwest Newfoundland: A regional synthesis. Ph.D. thesis, Memorial University of Newfoundland, St. John's, Newfoundland, 581 p.

Chorlton, L.B. & Knight, I., 1983. Geology of the Grandys Lake area (110/15), Newfoundland. Nfld. Dept. of Mines and Energy, Mineral Development Division, Report 83-7, 116p.

Coleman, R.G., 1977. Ophiolites: ancient oceanic lithosphere?. Springer-Verlag, Berlin-Heidelberg, 229p.

Cowan, D.S., 1985. Structural styles in Mesozoic and Cenozoic mélanges in the western Cordillera of North America. Geological Society of America Bulletin, 96, 451-462.

Currie, K.L. & van Berkel, J.T., 1989. Geochemistry of post-tectonic mafic intrusions in the Central Gneiss Terrane of southwestern Newfoundland. Atlantic Geology, 25, 181-190.

Curtis, C.D. & Brown, P.E., 1969. The metasomatic development of zoned ultrabasic bodies in Unst, Shetland. Contributions to Mineralogy and Petrology, 24, 275-292.

Dungan, M.A., 1979. A microprobe study of antigorite and some serpentine pseudomorphs. Canadian Mineralogist, 17, 771-784.

Dunning, G.R., 1981. The Annieopsquotch ophiolite belt, southwest Newfoundland. In Current Research, Part B, Geological Survey of Canada Paper 81-1B, 11-15.

Dunning, G.R., 1984. The geology, geochemistry, geochronology and regional setting of the Annieopsquotch Complex and related rocks of southwest Newfoundland. Ph.D. thesis, Memorial University of Newfoundland, St. John's, Newfoundland, 403p.

Dunning, G.R. & Herd, R.K., 1980. The Annieopsquotch ophiolite complex, southwest Newfoundland, and its regional relationships. In Current Research, Part A, Geological Survey of Canada Paper 80-1A, 227-243.

Dunning, G.R., Carter, P. & Best, M.A., 1982. Geology of the Star Lake (west half), southwest Newfoundland. In Current Research, Part B, Geological Survey of Canada Paper 82-1B, 21-26.

Dunning, G.R. & Chorlton, L.B., 1985. The Annieopsquotch ophiolite belt of southwest Newfoundland: Geology and tectonic significance. Geological Society of America Bulletin, 96, 1466-1476.

Dunning, G.R. & Krogh, T.E., 1985. Geochronology of ophiolites of the Newfoundland Appalachians. Canadian Journal of Earth Science, 22, 1659-1670.

Dunning, G.R., Wilton, D.H.C. & Herd, R.K., 1989. Geology, geochemistry and geochronology of a taconic batholith, southwestern Newfoundland. Transactions of the Royal Society of Edinburgh: Earth Sciences, 80, 159-168.

Dunning, G.R., O'Brien, S.J., Colman-Sadd, S.P., Blackwood, R.F., Dickson, W.L., O'Neill, P.P. & Krough, T.E., 1990. Silurian Orogeny in the Newfoundland Appalachians. Journal of Geology, 98, 895-913.

Evans, B.W., 1977. Metamorphism of alpine peridotite and serpentinite. Annual Review of Earth and Planetary Science, 5, 397-447.

Faure, G., 1977. Principles of Isotope Geology. John Wiley and Sons, New York, Copyright, 464p.

Ferry J.M. & Spear, F.S., 1978. Experimental calibration of the partitioning of Fe and Mg between biotite and garnet. Contributions to Mineralogy and Petrology, 66, 113-117.

Fowler, M.B., Williams, H.R. & Windley, B.F., 1981. The metasomatic development of zoned ultramafic balls from Fiskenaesset, west Greenland. Mineralogical Magazine, 44, 171-177.

Ganguly, J. & Saxena, S.K., 1987. Mixtures and Mineral Reactions, Springer Verlag, New York.

Gansser, A., 1974. The ophiolitic mélange, a world-wide problem on Tethyan examples. Eclogae Geologicae Helvetiae, 67, 479-507.

Geological Survey of Canada, 1968. Dept. of Energy, Mines & Resources, Aeromagnetic Series, Geophysics Paper 7050.

Ghent, E.D., Robbins, D.B. & Stout, M.Z., 1979. Geothermometry, geobarometry and fluid compositions of metamorphosed calc-silicates and pelites, Mica Creek, British Columbia. American Mineralogist, 64, 874-885.

Girardeau, J. & Mevel, C., 1982. Amphibolitized sheared gabbros from ophiolites as indicators of the evolution of the oceanic crust: Bay of Islands, Newfoundland. Earth and Planetary Science Letters, 61, 151-165.

Goldsmith, J.R., 1980. Melting and breakdown reactions of anorthite at high pressure and temperatures. American Mineralogist, 65, 272-284.

Grant, J.A. & Weiblen, P.W., 1971. Retrograde zoning in garnet near the second sillimanite isograd. American Journal of Science, 270, 281-296.

Greenly, E., 1919. The geology of Anglesey. Geological Survey of Great Britain, Memoir, 980 p.

Herd, R.K., 1978. Geology of the Puddle Pond area, Red Indian Lake map sheet, Newfoundland. In Current Research, Part A, Geological Survey of Canada, Paper 78-1A, 195-197.

Herd, R.K. & Dunning, G.R., 1979. Geology of the Puddle Pond map area. In Current Research, Part A, Geological Survey of Canada, Paper 79-1A, 305-310.

Hess, P.C., 1969. The metamorphic paragenesis of cordierite in pelitic rocks. Contributions to Mineralogy and Petrology, 24, 191-207.

Hibbard, J., 1983. Geology of the Baie Verte Peninsula, Newfoundland. Nfld. Dept. of Mines and Energy, Mineral Development Division, Memoir 2, 279p.

Hoffman, M.A. & Walker, D., 1978. Textural and chemical variations of olivine and chrome spinel in the East Dover ultramafic bodies, south-central Vermont. Geol. Soc. America Bull., 89, 699-710.

Hodges, K.V. & Spear, F.S., 1982. Geothermometry, geobarometry and the Al_2SiO_5 triple point at Mt. Moosilauke, New Hampshire. American Mineralogist, 67, 1118-1134.

Hodges, K.V. & Royden, L., 1984. Geologic thermobarometry of retrograded metamorphic rocks: An indication of the uplift trajectory of a portion of the northern Scandinavian Caledonides. Journal of Geophysical Research, 89, 7077-7090.

Hoffer, E., 1978. Melting reactions in aluminous metapelites: Stability limits of biotite + sillimanite + quartz in the presence of albite. N. Jb. Miner. Mh., 9, 396-407.

Holdaway, M.J., 1971. Stability of andalusite and the aluminium silicate phase diagram. American Journal of Science, 271, 97-131.

Horton, J.W., Blake, D.E., Wylie, A.S. & Stoddard, E.F., 1986. Metamorphosed mélange terrane in the eastern Piedmont of North Carolina. Geology, 14, 551-553.

Hoschek, G., 1969. The stability of staurolite and chloritoid and their significance in metamorphism of pelitic rocks. Contributions to Mineralogy and Petrology, 22, 208-232.

Hsu, K.J., 1968. Principles of mélange and their bearing on the Franciscan-Knoxville paradox. Geological Society of America Bulletin, 79, 1063-1074.

Hsu, L.C., 1968. Selected phase relationships in the system Al-Mn-Fe-Si-O-H: A model for garnet equilibria. Journal of Petrology, 9, 40-83.

Irvine, T.N., 1965. Chromian spinel as a petrogenetic indicator, Part 1. Theory. Canadian Journal of Earth Science, 2, 648-672.

Irvine, T.N., 1967. Chromian spinel as a petrogenetic indicator, Part 2. Petrologic applications. Canadian Journal of Earth Science, 4, 71-103.

Johannes, W., 1969. An experimental investigation of the system $MgO-SiO_2-H_2O-CO_2$. American Journal of Science, 267, 1083-1104.

Knapp, D., 1980. The stratigraphy, structure, and metamorphism of central Glover Island, western Newfoundland. In Current Research, Part B, Geological Survey of Canada, Paper 80-1B, 89-96.

Knight, I. & Brown, P.A., 1977. Geology, Codroy area (110/14), Newfoundland. Nfld Dept. of Mines and Energy, Mineral Development Division, Map 775. Scale 1:50,000, Open File 110/14.

Koziol, A.M. & Newton, R.C., 1988. Redetermination of the anorthite breakdown reaction and improvement of the plagioclase-garnet-Al_2SiO_5-quartz geobarometer. American Mineralogist, 73, 216-223.

Lipin, B.R., 1984. Chromite from the Blue Ridge Province of North Carolina. American Journal of Science, 284, 507-529.

Lister, G.S. & Snoke, A.W., 1984. S-C Mylonites. Journal of Structural Geology, 6, 617-638.

Leake, B.E., 1978. Nomenclature of amphiboles. American Mineralogist, 63, 1023-1053.

Malpas, J. & Stevens, R.K., 1977. The origin and emplacement of the ophiolite suite with examples from western Newfoundland. Geotectonics, 11, 453-466.

Malpas, J. & Strong, D.F., 1975. A comparison of chrome-spinels in ophiolites and mantle diapirs of Newfoundland. Geochimica et Cosmochimica Acta, 39, 1045-1060.

Maltman, A.J., 1978. Serpentine textures in Anglesey, North Wales, United Kingdom. Geological Society of America Bulletin, 89, 972-980.

Matthews, A, Goldsmith J.R. & Clayton, R.N., 1983. Oxygen isotope fractionations involving pyroxenes: the calibration of mineral pair geothermometers. Geochim. Cosmochim. Acta, 47, 631-644.

Misra, K.C. & Keller, F.B., 1978. Ultramafic bodies in the southern Appalachians: a review. American Journal of Science, 278, 389-418.

Moody, J.B., 1976. Serpentinization: a review. Lithos, 9, 125-138.

Newton, R.C. & Haselton, H.T., 1981. Thermodynamics of the garnet-plagioclase-Al_2SiO_5-quartz-geobarometer. In Thermodynamics of Minerals and Melts, R.C. Newton et al. (eds), Springer-Verlag. New York, 131-147.

O'Hanley, D.S., 1991. Fault-related phenomena associated with hydration and serpentine recrystallization during serpentinization. Canadian Mineralogist, 29, 21-37.

O'Hanley, D.S., Chernosky, J.V. & Wicks, F.J., 1989. The stability of lizardite and chrysotile. Canadian Mineralogist, 27, 483-493.

O'Laughlin, J.P.S., 1981. Geology of the Deer Lake ophiolite complex. Unpublished M.Sc. Thesis, Acadia University, Wolfville Nova Scotia, 151p.

Onyeagocha, A.C., 1974. Alteration of chromite from the Twin Sisters Dunite, Washington. American Mineralogist, 59, 608-612.

Peacock, S., 1987. Serpentinization and infiltration metasomatism in the Trinity peridotite, Klamath province, northern California: implications for subduction zones. Contribution to Mineralogy and Petrology, 95, 55-70.

Piasecki, M.A.J., 1988. Strain-induced mineral growth in ductile shear zones and a preliminary study of ductile shearing in western Newfoundland. Canadian Journal of Earth Science, 25, 2118-2129.

Piasecki, M.A.J., Williams, H. & Colman-Sadd, S.P., 1990. Tectonic relationships along the Meelpaeg, Burgeo, and Burlington lithoprobe transects in Newfoundland. In Current Research, Nfld. Dept. of Mines and Energy, Geological Survey Branch, Report 90-1, 327-339.

Riley, G.C., 1962. Stevenville map area, Newfoundland, Geological Survey of Canada, Memoir 323, 72p.

Robinson, P., Spear, F. S., Schumacher, J.C., Laird, J., Klein, C., Evans, B.W. & Doolan, B.L., 1982. Phase relations of metamorphic amphiboles:natural occurrence and theory. In: Amphiboles: Petrology and Experimental Phase Relations. Veblen, D.R. & Ribbe, P.H., Eds. Reviews in Mineralogy, Mineralogical Society of America, 9B, 1-211.

Sanford, R.F., 1982. Mineralogical and chemical effects of hydration reactions and applications to serpentinization. American Mineralogist, 66, 290-297.

Sanford, R.F., 1982. Growth of ultramafic reaction zones in greenschist to amphibolite facies metamorphism. American Journal of Science, 282, 543-616.

Scotford, D.M. & Williams, J.R., 1983. Petrology and geochemistry of metamorphosed ultramafic bodies in a portion of the Blue Ridge of North Carolina and Virginia. American Mineralogist, 68, 778-94.

Serri, G., 1981. The petrochemistry of ophiolite gabbroic complexes: A key for the classification of ophiolites into low-Ti and High-Ti types. Earth and Planetary Science Letters, 52, 203-212.

Sibson, R.H., 1977. Fault rocks and fault mechanisms, Journal of the Geological Society of London, 133, 191-213.

Silver, E.A. & Beutner, E.C., 1980. Mélanges, Geology, 8, 32-34.

Simpson, C. & Schmid, S.M., 1983. Microstructural indicators of sense of shear in shear-zones, Bulletin of the Geological Society of America, 94, 1281-1288.

Spangenberg, K., 1943. Die chromitlagerstatte von Tampadel am Zobten, Zeitschr. prakt. Geologie, 5, 13-35.

Spear, F.S., Selverstone, J., Hickmott, D., Crowley, P. & Hodges, K.V., 1984. P-T paths from garnet zoning: a new technique for deciphering tectonic processes in crystalline terranes. Geology, 12, 87-90.

Stevens, R.D., Delabio, R.N. & Lachance, G.R., 1982. Age determinations and geological studies. K/Ar isotopic ages, Report 16, Geological Survey of Canada Paper 82-2.

Thompson, A.B., 1976. Mineral reactions in pelitic rocks. II. Calculation of some P-T-X-(Fe-Mg) relations. American Journal of Science, 276, 401-454.

Tracy, R.J., 1982. Compositional zoning and inclusions in metamorphic minerals. In Characterization of Metamorphism Through Mineral Equilibria. J.M. Ferry ed., Reviews in Mineralogy 10, Mineralogical Society of America, 355-397.

Ulmer, G.C., 1974. Alteration of chromite during serpentinization in the Pennsylvania-Maryland District. American Mineralogist, 59, 1236-1241.

Van Berkel, J.T., 1987a. Geology of the Dashwoods Pond, St. Fintan's and Main Gut map areas, southwest Newfoundland. Current Research, Part A, Geological Survey of Canada, Paper 87-1A, 399-408.

Van Berkel, J.T., 1987b. Geology of the Main Gut map area (12B/8), southwest Newfoundland. Geological map (scale 1:50,000) with descriptive notes. Geological Survey of Canada, Open File Report 1467.

Van Berkel, J.T., 1987c. Geology of the Dashwoods Pond (12B/1) and St. Fintans (12B/2) map areas, southwest Newfoundland. Geological map (scale 1:50,000) with descriptive notes. Geological Survey of Canada, Open File Report 1466.

Van Berkel, J.T., Johnston, H.P. & Currie, K.L., 1986. A preliminary report on the geology of the southern Long Range, southwest Newfoundland. Current Research, Part B, Geological Survey of Canada, Paper 86-1b, 157-170.

Van Berkel, J.T. & Currie, K.L., 1986. Geology of the southern Long Range, southwest Newfoundland (12B/1, 12B/8, 12B/9, 12A/4, 12A/5, 12A/2). Geological Survey of Canada, Open File 1328.

Van Berkel, J.T. & Currie, K.L., 1988. Geology of the Puddle Pond (12A/5) and Little Grand Lake (12A/12) map areas, southwestern Newfoundland. Current Research, Nfld. Dept. of Mines, Mineral Development Division, Report 88-1, 99-107.

Wakita, H., Rey, P. & Schmitt, R.A., 1971. Abundances of the 14 rare-earth elements and 12 other trace elements in Apollo 12 samples: five igneous and one breccia rocks and four soils. Proc. 2nd Lunar Science Conf., 1319-1329.

Wenner, D.B. & Taylor, H.P. Jr., 1971. Temperatures of serpentinization of ultramafic rocks based on $^{18}O/^{16}O$ fractionation between coexisting serpentine and magnetite. Contributions to Mineralogy and Petrology, 32, 165-185.

White, S.H., Burrows, S.E., Carreras, J., Shaw, N.D. & Humphreys, F.J. 1980. On mylonites in ductile shear zones. Journal of Structural Geology, 2, 175-187.

Whittaker, E.J.W. & Wicks, F.J., 1970. Chemical differences among the serpentine "polymorphs": a discussion. American Mineralogist, 55, 1025-1047.

Wicks, F.J., 1984. Deformation histories as recorded by serpentinites. I. Deformation prior to serpentinization. Canadian Mineralogist, 22, 185-195.

Wicks, F.J. & Plant, A.G., 1979. Electron microprobe and X-ray microbeam studies of serpentine textures. Canadian Mineralogist, 17, 785-830.

Wicks, F.J., Whittaker, E.J.W. & Zussman, J., 1977. An idealized model for serpentine textures after olivine. Canadian Mineralogist, 15, 446-458.

Wicks, F.J. & Whittaker, E.J.W., 1975. A reappraisal of the structures of the serpentine minerals. Canadian Mineralogist, 13, 227-243.

Wicks, F.J. & Whittaker, E.J.W., 1977. Serpentine textures and serpentinization. Canadian Mineralogist, 15, 459-488.

Wicks, F.J. & Zussman, J., 1975. Microbeam X-ray diffraction patterns of the serpentine minerals. Canadian Mineralogist, 13, 244-258.

Wicks, F.J. & O'Hanley, D.S., 1988. Serpentine minerals: structures and petrology. In Hydrous Phyllosilicates other than Micas. S.W. Bailey (ed.), Mineralogical Society of America, Rev. Mineral., 19, 91-168.

Williams, H., 1977. Ophiolitic melange and its significance in the Fleur de Lys Supergroup, northern Appalachians. Canadian Journal of Earth Science, 14, 987-1003.

Williams, H., 1979. Appalachian Orogen in Canada. Canadian Journal of Earth Science, 16, 792-807.

Williams, H., Kennedy, M.J. & Neale, E.R.W., 1972. The Appalachian structural province. In: Variations in tectonic styles in Canada. Geological Association of Canada, Special Paper 11, 181-262.

Williams, H. & St-Julien, P. 1982. The Baie Verte-Brompton Line: early paleozoic continent-ocean interface in the Canadian Appalachians. In: Major structural zones and faults of the northern Appalachians, P. St-Julien and J.Beland eds., Geological Association of Canada, Special Paper 24, 177-207.

Williams, H. & Hatcher, R.D., 1983. Appalachian suspect terranes. Geological Society of America, Memoir 158, 33-53.

Williams, H. & Piasecki, M.A.J., 1990. The Cold Spring Mélange and a possible model for Dunnage-Gander zone interaction in central Newfoundland. Canadian Journal of Earth Science, 27, 1126-1134.

Wilton, D.H.C., 1983. The geology and structural history of the Cape Ray Fault Zone in southwestern Newfoundland. Canadian Journal of Earth Science, 20, 1119-1133.

Wilton, D.H.C., 1984. Metallogenic, tectonic, and geochemical evolution of the Cape Ray fault zone with emphasis on electrum mineralization. Ph.D. thesis, Memorial University of Newfoundland, St. John's, Newfoundland, 618 p.

Wilton, D.H.C., 1985. Tectonic evolution of southwester Newfoundland as indicated by granitoid petrogenesis. Canadian Journal of Earth Science, 22, 1080-1092.

Winkler, H.G.F., 1979. Petrogenesis of metamorphic rocks. Springer-Verlag, 320p.

Woodsworth, G.J., 1977. Homogenization of zoned garnets from pelitic schists. Canadian Mineralogist, 15, 230-242.

APPENDIX A

MICROPROBE ANALYSES

Mineral analyses were performed on a Jeol JXA50A electron microprobe at Memorial University of Newfoundland. The composition of material used for calibrating the instrument is presented in Table A1.

Table A-1

	ACPX	SWOL	K-GNT	HEDEN	53IN8	SPINB	DNY
Na2O	1.27			0.44			21.53
MgO	16.65	43.50	18.50	1.47	6.12	20.84	
Al2O3	7.86	0.01	23.73	1.58	12.82	59.40	
SiO2	50.73	38.95	41.46	47.12			0.11
K2O				0.05			
CaO	15.82		5.16	21.97			30.90
TiO2	0.74	0.04	0.47	0.01	1.60	0.09	
Cr2O3		0.02			49.31	8.05	
MnO	0.13	0.30	0.28	2.62	0.32	0.09	
FeO	6.76	16.62	10.67	24.41	28.15	10.69	0.01
NiO					0.06		

The standards used for each mineral and the number of oxygens used to calculate the structural formula is presented in Table A2.

TABLE A-2

Mineral	Standard	# O for formula
olivine	DNY/K-GNT	4
chrome spinel	SPINB/531N8	4
serpentine	ACPX/SWOL	7 (lizardite) 6.8 (antigorite)
carbonate	DNY/K-GNT	6
amphibole	ACPX	see appendix A
plagioclase	ACPX	8
garnet	HEDEN	12
biotite	ACPX	22
staurolite	ACPX	22
cordierite	ACPX	18
spinel (hercynite)	ACPX	4
chlorite	ACPX	28

For the amphibole analyses, the code denotes the formula calculation scheme. 13ex is for Ca-amphiboles normalized to 13 cations excluding Ca, Na, and K (Robinson et al., 1982) and Fe^{+2} denotes normalizing to 16 cations using all Fe as Fe^{+2}.

For chrome spinel analyses spot 1, spot 2, etc. represent microprobe traverses starting at the center of the grain (spot 1) to the rim (spot 3, 4, or 5).

For the analyses of the minerals in the pelitic and psammitic metasedimentary rocks the following codes apply:

A) 1, 2, and 3 are numbers of the minerals used for thermobarometry.

B) codes r = garnet rim; c = garnet core; a = biotite in contact with garnet; b = biotite away from garnet. The ratio of Ca + Mn / Ca + Mn + Fe + Mg in garnets should be < 0.2 and Al^{VI} + Ti / Al^{VI} + Ti + Fe + Mg in biotites should be < 0.15 when using the Ferry & Spear thermometer.

C) The abbreviations ALM, PYR, GRO, and SPE are the garnet end-members almandine, pyrope, grossular and spessartine respectively.

D) The abbreviations Ab, An, and Or are the plagioclase end-members albite, anorthite and orthoclase respectively.

All mineral analyses presented are an average of at least 2 probe analyses of the same grain and most are an average of three analyses. In many cases, several grains from the same sample are presented to test for within sample consistency. Analyses with the same sample number are usually different grains within the same sample unless they are part of a traverse across one grain in which case they are designated as spot 1, spot 2, etc.

Pelitic schist in metapsammite unit

Sample #	I 13	I 13	I 13	I 13	I 13	I 13	I 13	I 13
Mineral	GNT	GNT	GNT	GNT	BIO	BIO	PLAG	PLAG
Code	1	2	3r	3c	1a	2b	1	2
Na2O	0.00	0.00	0.00	0.00	0.34	0.37	8.15	7.00
MgO	3.37	3.08	3.08	4.09	10.86	11.66	0.03	0.03
Al2O3	22.08	22.31	22.61	21.47	19.08	19.50	21.18	23.40
SiO2	38.13	37.87	37.42	37.09	36.80	35.25	60.93	59.31
K2O	0.00	0.00	0.00	0.00	9.37	8.62	0.07	0.13
CaO	1.63	1.47	1.56	1.67	0.00	0.00	6.61	6.78
TiO2	0.00	0.00	0.10	0.05	1.76	1.41	0.00	0.00
Cr2O3	0.00	0.00	0.00	0.00	0.04	0.05	0.00	0.00
MnO	1.75	1.61	1.83	1.81	0.03	0.03	0.00	0.02
FeO	34.85	34.50	37.41	35.64	18.90	19.73	0.04	0.08
NiO	0.00	0.00	0.00	0.00	0.07	0.03	0.01	0.00
Sum	102.70	101.73	104.01	101.84	97.20	96.32	100.02	98.19
Na	0.000	0.000	0.000	0.000	0.095	0.075	0.703	0.650
Mg	0.390	0.365	0.358	0.481	2.396	2.610	0.001	0.001
Al	2.104	2.063	2.075	2.003	3.332	3.412	1.969	1.986
Si	2.962	2.971	2.919	2.938	5.454	5.295	2.712	2.689
K	0.000	0.000	0.000	0.000	1.761	1.618	0.004	0.007
Ca	0.134	0.122	0.130	0.139	0.000	0.000	0.315	0.329
Ti	0.000	0.000	0.001	0.002	0.195	0.159	0.000	0.000
Cr	0.000	0.000	0.000	0.000	0.004	0.004	0.000	0.000
Mn	0.114	0.105	0.119	0.121	0.000	0.000	0.000	0.001
Fe	2.264	2.264	2.437	2.359	2.340	2.478	0.001	0.003
Ni	0.000	0.000	0.000	0.000	0.004	0.000	0.000	0.000
Sum	7.968	7.991	8.035	8.045	15.582	15.681	5.007	4.986
ALM	0.779	0.765	0.800	0.759				
PYR	0.134	0.157	0.117	0.155				
GRO	0.047	0.012	0.013	0.046				
SPE	0.040	0.036	0.040	0.040				
Ca + Mn / Ca + Mn + Fe2 + Mg	0.09	0.08	0.00	0.08				
Fe/Fe + Mg					0.49	0.49		
Al(IV) + Ti / Al(IV) + Ti + Fe2 + Mg					0.17	0.15		
Ab							0.688	0.659
An							0.308	0.334
Or							0.004	0.007

Mineral Analyses in Metapsammites

Sample #	T-35	T-35	T-35	T-35	T-35	T-35
Mineral	GNT	GNT	GNT	GNT	BIO	BIO
Code	1	2	3r	3c	1a	2b
Na2O	0.00	0.00	0.00	0.00	0.14	0.16
MgO	2.38	2.45	1.46	3.04	9.19	9.47
Al2O3	21.72	21.81	21.04	22.46	17.95	18.00
SiO2	37.09	37.55	36.79	37.33	36.30	36.06
K2O	0.00	0.00	0.00	0.00	9.63	9.79
CaO	1.92	1.83	1.88	1.62	0.00	0.00
TiO2	0.00	0.00	0.02	0.02	1.75	1.78
Cr2O3	0.00	0.00	0.00	0.00	0.02	0.01
MnO	7.25	6.91	9.36	6.70	0.14	0.14
FeO	30.28	31.04	31.44	31.70	20.25	21.38
NiO	0.00	0.00	0.00	0.00	0.00	0.01
Sum	100.64	101.59	101.98	102.88	95.38	96.79
Na	0.000	0.000	0.000	0.000	0.040	0.044
Mg	0.282	0.289	0.174	0.354	2.088	2.138
Al	2.052	2.042	1.994	2.078	3.231	3.209
Si	2.974	2.981	2.957	2.930	5.543	5.463
K	0.000	0.000	0.000	0.000	1.873	1.889
Ca	0.165	0.154	0.160	0.136	0.000	0.000
Ti	0.000	0.000	0.000	0.000	0.197	0.200
Cr	0.000	0.000	0.000	0.000	0.000	0.000
Mn	0.492	0.464	0.637	0.444	0.013	0.018
Fe	2.030	2.061	2.114	2.080	2.585	2.707
Ni	0.000	0.000	0.000	0.000	0.000	0.000
Sum	7.994	7.989	8.036	8.022	15.571	15.668
Al M	0.683	0.694	0.685	0.689		
PYR	0.096	0.098	0.057	0.118		
GRO	0.055	0.052	0.052	0.045		
SPE	0.166	0.156	0.206	0.148		
Ca + Mn	0.22	0.21	0.26	0.19		
Ca + Mn + Fe2 + Mg						
Fe/Fe + Mg					0.55	0.56
Al(IV) + Ti					0.17	0.15
Al(IV) + Ti + Fe2 + Mg						

Mineral Analyses in Metapsammites

Sample #	T-73	T-73	T-73	T-73
Mineral	GNT	GNT	BIO	BIO
Code	1	2	1a	2b
Na2O	0.00	0.00	0.08	0.11
MgO	3.17	3.41	8.69	8.56
Al2O3	21.92	21.29	17.96	17.50
SiO2	37.38	37.02	34.89	35.27
K2O	0.00	0.00	9.74	9.84
CaO	1.19	1.17	0.00	0.00
TiO2	0.00	0.00	1.85	1.95
Cr2O3	0.00	0.00	0.03	0.02
MnO	3.02	2.96	0.14	0.17
FeO	35.46	35.93	22.86	23.10
NiO	0.00	0.00	0.02	0.03
Sum	102.14	101.79	96.25	96.52
Na	0.000	0.000	0.022	0.031
Mg	0.374	0.404	1.991	1.960
Al	2.042	1.998	3.255	3.175
Si	2.956	2.947	5.369	5.421
K	0.000	0.000	1.910	1.929
Ca	0.100	0.098	0.000	0.000
Ti	0.000	0.000	0.212	0.221
Cr	0.000	0.000	0.000	0.000
Mn	0.202	0.198	0.013	0.018
Fe	2.343	2.393	2.939	2.972
Ni	0.000	0.000	0.000	0.000
Sum	8.015	8.039	15.712	15.728
ALM	0.776	0.773		
PYR	0.124	0.131		
GRO	0.033	0.032		
SPE	0.067	0.064		
Ca+Mn	0.10	0.10		
Ca+Mn+Fe2+Mg				
Fe/Fe+Mg			0.60	0.60
Al(IV)+Ti			0.14	0.14
Al(IV)+Ti+Fe2+Mg				

Mineral Analyses in Metapelites

Sample #	T-3	T-3	T-3	T-3	T-3	T-3	T-3	T-3	T-3	T-3	T-3	T-3
Mineral	GNT	GNT	GNT	GNT	BIO	BIO	BIO	PLAG	PLAG	SPINEL	SPINEL	SPINEL
Code	1	2	3r	3c	1a	2a	3b	1	2	1	2a	2b
Na2O	0.00	0.00	0.00	0.00	0.19	0.24	0.16	5.82	5.89	0.00	0.00	0.00
MgO	4.14	4.26	2.01	4.17	9.59	10.04	9.67	0.00	0.00	3.93	5.0x	2.57
Al2O3	20.72	20.79	21.21	21.78	18.43	18.57	18.44	27.0x	27.4x	58.74	55.24	63.40
SiO2	38.01	37.14	36.38	37.55	35.45	35.80	35.66	56.15	56.41	0.00	0.05	0.05
K2O	0.00	0.00	0.00	0.00	9.25	9.79	9.69	0.07	0.07	0.00	0.00	0.02
CaO	1.84	1.55	1.93	1.43	0.02	0.00	0.00	10.27	10.10	0.05	0.03	0.02
TiO2	0.01	0.02	0.05	0.03	2.25	2.35	2.52	0.00	0.04	0.92	0.04	0.19
Cr2O3	0.03	0.04	0.00	0.00	0.02	0.02	0.03	0.01	0.02	0.78	0.39	0.06
MnO	5.22	4.73	6.57	5.19	0.05	0.12	0.08	0.00	0.00	0.62	0.17	0.21
FeO	31.12	32.01	29.47	30.1x	21.42	19.25	19.39	0.07	0.07	35.07	31.57	25.3x
NiO	0.01	0.03	0.00	0.00	0.05	0.04	0.03	0.03	0.01	0.07	0.00	0.06
Sum	101.12	100.57	98.21	100.30	96.70	96.22	95.66	99.48	100.08	99.88	92.55	92.48
Na	0.006	0.000	0.000	0.000	0.053	0.06x	0.044	0.509	0.512	0.000	0.000	0.000
Mg	0.489	0.500	0.317	0.492	2.164	2.26x	2.190	0.000	0.000	0.170	0.228	0.110
Al	1.936	1.962	2.047	2.038	3.288	3.30x	3.301	1.441	1.453	1.837	1.9x7	2.173
Si	3.013	2.975	2.979	2.983	5.36x	5.407	5.419	2.539	2.532	0.024	0.001	0.001
K	0.000	0.000	0.000	0.000	1.78x	1.883	1.878	0.002	0.004	0.000	0.000	0.000
Ca	0.156	0.132	0.168	0.121	0.000	0.000	0.000	0.498	0.485	0.001	0.001	0.000
Ti	0.000	0.000	0.002	0.000	0.253	0.26x	0.285	0.000	0.001	0.021	0.000	0.003
Cr	0.000	0.000	0.000	0.000	0.000	0.000	0.000	0.000	0.000	0.018	0.009	0.002
Mn	0.349	0.320	0.454	0.347	0.004	0.013	0.009	0.000	0.000	0.015	0.004	0.005
Fe	2.864	2.144	2.016	2.003	2.710	2.428	2.462	0.002	0.002	0.924	0.797	0.x12
Ni	0.000	0.000	0.000	0.000	0.004	0.004	0.000	0.000	0.000	0.002	0.000	0.002
Sum	8.005	8.040	7.983	7.984	15.x31	15.63x	15.588	4.991	4.990	3.019	3.005	2.90x
ALM	0.674	0.690	0.681	0.675								
PYR	0.160	0.164	0.108	0.166								
GRO	0.051	0.043	0.057	0.041								
SPE	0.115	0.103	0.154	0.118								
Ab								0.504	0.511			
An								0.492	0.485			
Or								0.004	0.004			
$\frac{Ca+Mn}{Ca+Mn+Fe2+Mg}$	0.17	0.15	0.21	0.1x								
$\frac{Al(IV)+Ti}{Al(IV)+Ti+Fe2+Mg}$					0.16	0.17	0.18					
Fe/Fe+Mg					0.5x	0.52	0.53					

Mineral Analyses in Metapelites

Sample #	T-24	T-24	T-24	T-24	T-24	T-24	T-24	T-24
Mineral	GNT	GNT	GNT	GNT	BIO	BIO	PLAG	PLAG
Code	1	2r	2c	3	1a	2b	1	2
Na2O	0.00	0.00	0.00	0.00	0.21	0.24	6.65	7.27
MgO	4.61	4.17	4.70	4.32	11.76	11.94	0.00	0.00
Al2O3	20.89	20.86	20.69	20.87	19.74	19.16	26.98	25.88
SiO2	37.63	37.39	37.36	37.94	37.69	37.54	59.29	59.79
K2O	0.00	0.00	0.00	0.00	9.53	9.73	0.09	0.05
CaO	1.78	1.84	1.64	1.88	0.00	0.00	9.04	7.94
TiO2	0.02	0.00	0.04	0.02	1.43	1.71	0.00	0.00
Cr2O3	0.02	0.00	0.02	0.01	0.02	0.04	0.00	0.02
MnO	10.75	8.89	11.99	9.69	0.11	0.09	0.00	0.01
FeO	24.10	26.65	23.14	25.64	17.74	17.56	0.07	0.02
NiO	0.00	0.00	0.01	0.01	0.05	0.07	0.03	0.02
Sum	99.80	99.80	99.58	100.31	98.29	98.06	102.15	101.01
Na	0.000	0.000	0.000	0.000	0.055	0.064	0.564	0.623
Mg	0.548	0.496	0.560	0.511	2.547	2.598	0.000	0.000
Al	1.966	1.969	1.955	1.956	3.384	3.296	1.393	1.348
Si	3.004	2.997	2.995	3.018	5.470	5.462	2.598	2.642
K	0.000	0.000	0.000	0.000	1.767	1.809	0.003	0.002
Ca	0.152	0.157	0.139	0.151	0.000	0.000	0.424	0.376
Ti	0.000	0.000	0.000	0.000	0.153	0.184	0.000	0.000
Cr	0.000	0.000	0.000	0.000	0.000	0.000	0.000	0.000
Mn	0.726	0.602	0.814	0.651	0.013	0.008	0.000	0.000
Fe	1.607	1.785	1.550	1.704	2.155	2.163	0.001	0.000
Ni	0.000	0.000	0.000	0.000	0.004	0.004	0.000	0.000
Sum	8.004	8.006	8.013	7.990	15.556	15.568	4.983	4.991
ALM	0.530	0.566	0.506	0.564				
PYR	0.181	0.164	0.183	0.169				
GRO	0.050	0.052	0.046	0.051				
SPE	0.239	0.198	0.265	0.216				
Ab							0.568	0.622
An							0.427	0.375
Or							0.005	0.003
$\frac{Ca+Mn}{Ca+Mn+Fe2+Mg}$	0.29	0.25	0.31	0.27				
$\frac{Al(VI)+Ti}{Al(VI)+Ti+Fe2+Mg}$					0.18	0.17		
Fe Fe+Mg					0.46	0.45		

Mineral Analyses in Metapelites

Sample #	T-32	T-32	T-32	T-32	T-32	T-32	T-32	T-32
Mineral	GNT	GNT	GNT	GNT	BIO	BIO	PLAG	PLAG
Code	1	2	3r	3c	1a	2b	1	2
Na2O	0.00	0.00	0.00	0.00	0.18	0.27	7.00	7.09
MgO	3.63	3.48	3.06	3.63	10.04	10.04	0.00	0.00
Al2O3	20.95	20.71	21.57	21.81	18.50	18.63	25.60	25.78
SiO2	37.39	37.72	37.47	37.82	36.03	35.78	58.78	58.55
K2O	0.00	0.00	0.00	0.00	9.45	9.49	0.05	0.05
CaO	1.65	1.60	1.68	1.62	0.00	0.00	7.03	7.04
TiO2	0.00	0.00	0.02	0.03	2.18	2.18	0.00	0.03
Cr2O3	0.02	0.01	0.00	0.00	0.01	0.00	0.00	0.04
MnO	5.45	5.89	6.67	6.14	0.12	0.07	0.02	0.01
FeO	30.30	30.13	30.85	31.79	18.91	18.85	0.04	0.04
NiO	0.00	0.02	0.00	0.00	0.05	0.04	0.04	0.01
Sum	99.40	99.56	101.32	102.84	95.46	95.34	99.45	99.54
Na	0.000	0.000	0.000	0.000	0.053	0.076	0.608	0.616
Mg	0.435	0.416	0.361	0.422	2.266	2.271	0.000	0.000
Al	1.987	1.962	2.020	2.013	3.301	3.332	1.354	1.363
Si	3.011	3.034	2.978	2.962	5.457	5.430	2.638	2.628
K	0.000	0.000	0.000	0.000	1.822	1.835	0.002	0.002
Ca	0.142	0.137	0.142	0.135	0.000	0.000	0.380	0.382
Ti	0.000	0.000	0.000	0.000	0.244	0.245	0.000	0.000
Cr	0.000	0.000	0.000	0.000	0.000	0.000	0.000	0.000
Mn	0.371	0.401	0.448	0.407	0.013	0.004	0.000	0.000
Fe	2.040	2.026	2.050	2.082	2.395	2.392	0.001	0.001
Ni	0.000	0.000	0.000	0.000	0.004	0.000	0.000	0.000
Sum	7.984	7.976	7.999	8.021	15.556	15.584	4.983	4.993
ALM	0.682	0.679	0.682	0.683				
PYR	0.146	0.140	0.121	0.139				
GRO	0.048	0.046	0.048	0.045				
SPE	0.124	0.135	0.149	0.134				
Ab							0.613	0.616
An							0.384	0.381
Or							0.003	0.003
$\frac{Ca+Mn}{Ca+Mn+Fe2+Mg}$	0.17	0.18	0.20	0.18				
$\frac{Al(1V)+Ti}{Al(1V)+Ti+Fe2+Mg}$					0.18	0.18		
Fe/Fe+Mg					0.51	0.51		

Mineral Analyses in Metapelites

Sample #	T-19	T-39	T-39	T-39	T-39	T-39	T-44	T-44	T-44
Mineral	STA	GNT	GNT	STA	CHL	CHL	STA	CRD	CRD
Code									
Na2O	0.00	0.00	0.00	0.00	0.01	0.05	0.00	0.28	0.25
MgO	1.50	5.57	5.71	1.74	19.44	17.78	2.05	9.53	9.68
Al2O3	51.96	21.21	21.14	51.20	22.46	22.63	51.29	31.39	31.83
SiO2	27.86	37.97	37.95	27.38	26.45	25.35	27.23	48.64	49.27
K2O	0.01	0.00	0.00	0.02	0.02	0.01	0.01	0.01	0.01
CaO	0.00	1.95	1.97	0.02	0.00	0.02	0.00	0.02	0.01
TiO2	0.36	0.01	0.02	0.48	0.05	0.09	0.41	0.00	0.00
Cr2O3	0.02	0.02	0.02	0.03	0.00	0.02	0.03	0.02	0.02
MnO	0.27	3.14	3.20	0.27	0.17	0.13	0.48	0.30	0.25
FeO	12.49	29.74	29.68	12.97	17.90	18.29	11.80	6.05	6.21
NiO	0.05	0.00	0.00	0.02	0.03	0.05	0.03	0.01	0.03
Sum	94.53	99.61	99.67	94.11	86.53	84.42	93.33	96.24	97.55
Na	0.000	0.000	0.000	0.000	0.000	0.018	0.000	0.055	0.048
Mg	0.318	0.656	0.674	0.372	5.926	5.583	0.441	1.481	1.482
Al	8.737	1.982	1.973	8.688	5.415	5.614	8.741	3.857	3.857
Si	3.973	3.010	3.005	3.942	5.408	5.341	3.938	5.073	5.068
K	0.000	0.000	0.000	0.004	0.000	0.000	0.000	0.000	0.000
Ca	0.000	0.165	0.165	0.000	0.000	0.000	0.000	0.000	0.000
Ti	0.038	0.000	0.000	0.050	0.004	0.011	0.043	0.000	0.000
Cr	0.000	0.000	0.000	0.000	0.000	0.000	0.000	0.000	0.000
Mn	0.029	0.209	0.213	0.029	0.025	0.018	0.055	0.024	0.021
Fe	1.486	1.970	1.964	1.559	3.063	3.220	1.426	0.526	0.534
Ni	0.004	0.000	0.000	0.000	0.000	0.004	0.000	0.000	0.000
Sum	14.585	7.992	7.994	14.644	19.838	19.814	14.645	11.018	11.010
ALM		0.656	0.651						
PYR		0.219	0.223						
GRO		0.055	0.055						
SPE		0.070	0.071						
XFE	0.82			0.81	0.34	0.37	0.76	0.26	0.26

Olivine Analyses in Metadunites

Sample #	D 4	D 4	D -56	D-56	D- 67	D-67	D-67
MgO	50.06	50.14	50.36	50.36	49.45	50.00	49.09
Al2O3	0.00	0.00	0.00	0.00	0.00	0.04	0.00
SiO2	41.72	40.52	40.35	40.55	40.16	40.27	40.23
CaO	0.00	0.00	0.00	0.00	0.00	0.00	0.00
TiO2	0.00	0.00	0.00	0.00	0.01	0.00	0.00
Cr2O3	0.00	0.00	0.00	0.00	0.02	0.00	0.02
MnO	0.13	0.14	0.13	0.14	0.12	0.12	0.15
FeO	7.82	7.34	7.96	7.45	8.25	8.34	8.31
NiO	0.26	0.30	0.23	0.19	0.38	0.36	0.31
Sum	100.09	98.47	99.04	98.77	98.37	99.14	98.11
Mg	1.809	1.841	1.845	1.843	1.827	1.834	1.817
Al	0.000	0.000	0.000	0.002	0.000	0.000	0.000
Si	1.011	0.998	0.992	0.996	0.995	0.991	1.000
Ca	0.000	0.000	0.000	0.000	0.000	0.000	0.000
Ti	0.000	0.000	0.000	0.000	0.000	0.000	0.000
Cr	0.000	0.000	0.000	0.000	0.000	0.000	0.000
Mn	0.002	0.002	0.002	0.002	0.002	0.002	0.002
Fe	0.158	0.151	0.163	0.152	0.171	0.171	0.172
Ni	0.006	0.005	0.004	0.003	0.007	0.006	0.005
Sum	2.986	2.998	3.005	2.999	3.002	3.004	2.997
%Fo	91.97	92.42	91.88	92.38	91.44	91.47	91.35

Lizardite Analyses

Sample #	D-4	D-32	D-37	D-37	D-56	D-67
MgO	37.83	38.98	39.49	40.02	36.77	38.58
Al2O3	0.11	0.23	0.32	0.10	0.32	0.14
SiO2	36.28	41.73	41.41	41.55	40.00	37.07
CaO	0.00	0.00	0.00	0.00	0.00	0.00
TiO2	0.00	0.00	0.00	0.00	0.00	0.00
Cr2O3	0.00	0.00	0.00	0.00	0.00	0.00
MnO	0.06	0.04	0.03	0.01	0.08	0.04
FeO	4.26	0.93	1.22	0.81	4.06	3.30
NiO	0.41	0.36	0.26	0.24	0.21	0.30
Sum	78.95	82.28	82.73	82.73	81.44	79.42
H2O	21.05	17.72	17.27	17.27	18.56	20.58
Mg	2.964	2.842	2.872	2.903	2.759	2.981
Al	0.006	0.013	0.017	0.005	0.019	0.008
Si	1.907	2.041	2.020	2.022	2.014	1.921
Ca	0.000	0.000	0.000	0.000	0.000	0.000
Ti	0.000	0.000	0.000	0.000	0.000	0.000
Cr	0.000	0.000	0.000	0.000	0.000	0.000
Mn	0.002	0.001	0.000	0.000	0.002	0.002
Fe	0.187	0.037	0.049	0.033	0.170	0.142
Ni	0.016	0.013	0.010	0.009	0.007	0.012
Sum	5.082	4.947	4.967	4.972	4.971	5.064

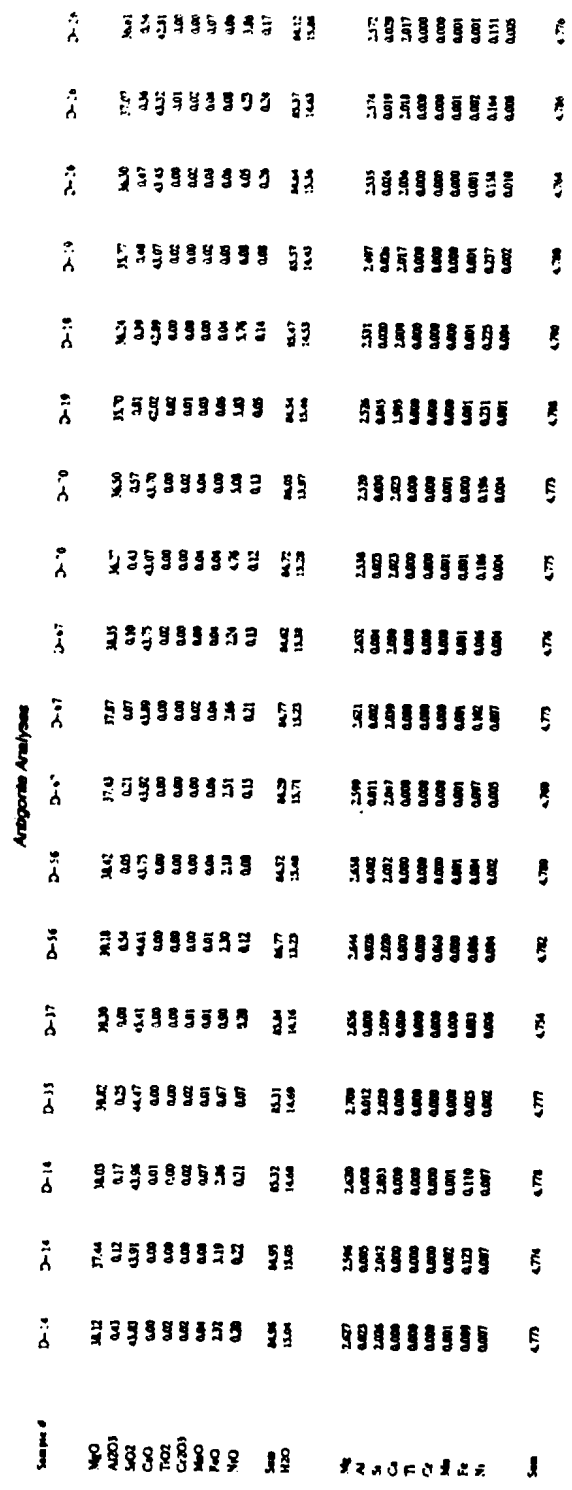

Antigenic Analyses

Sample #	6VMD-36	6VMD-36	6VMD-36	6VMD-69	7VMD-19	7VMD 19	7VMD 19	7VMD 21
MgO	45.41	45.32	44.57	47.12	45.11	45.13	45.07	45.47
CaO	0.09	0.12	0.07	0.14	0.49	0.35	0.25	0.09
MnO	0.20	0.21	0.11	0.30	0.38	0.31	0.41	0.10
FeO	6.43	6.58	7.06	1.63	6.70	6.60	6.11	4.79
SrO	0.03	0.07	0.01	0.00	0.00	0.00	0.00	0.06
Sum	52.16	52.3	51.83	49.2	52.69	52.39	51.85	50.71
Mg	1.844	1.840	1.831	1.950	1.822	1.832	1.841	1.878
Ca	0.002	0.003	0.001	0.004	0.014	0.009	0.007	0.002
Mn	0.004	0.004	0.002	0.007	0.009	0.007	0.009	0.006
Fe	0.146	0.149	0.163	0.037	0.152	0.150	0.140	0.111
Sr	0.000	0.001	0.000	0.000	0.000	0.000	0.000	0.001
Sum	1.996	1.997	1.998	1.998	1.996	1.998	1.997	1.998
Mg/Mg+Fe	92.66	92.49	91.84	98.12	92.30	92.42	92.93	94.44
Fe/Fe+Mg	7.34	7.51	8.16	1.88	7.70	7.58	7.07	5.56

Chrome Spinel

Sample #	D-57 center	D-57 center	D-57 spot 1	D-57 spot 2	D-57 spot 3	D-57 spot 4	D-57 spot 5
MgO	3.01	3.22	2.86	3.40	2.77	3.11	0.85
Al2O3	10.46	10.10	11.20	11.04	10.32	11.64	3.24
TiO2	0.14	0.20	0.19	0.09	0.16	0.18	0.65
Cr2O3	49.54	50.63	48.69	48.62	48.03	48.35	45.30
MnO	0.90	0.90	0.91	0.96	0.92	0.89	1.13
FeO	35.41	35.31	35.82	35.48	37.34	36.13	48.06
Sum	99.46	100.35	99.67	99.59	99.54	100.30	99.23
Mg	0.155	0.165	0.146	0.174	0.142	0.158	0.046
Al	0.429	0.409	0.456	0.448	0.422	0.469	0.138
Ti	0.003	0.005	0.004	0.002	0.004	0.004	0.017
Cr	1.362	1.380	1.332	1.325	1.320	1.309	1.302
Mn	0.026	0.025	0.026	0.027	0.026	0.024	0.034
Fe3+	0.198	0.202	0.206	0.228	0.254	0.220	0.545
Fe2+	0.831	0.816	0.831	0.795	0.831	0.815	0.916
Sum	3.004	3.002	3.001	2.999	3.000	2.999	2.999
Cr / Cr+Al	0.76	0.77	0.75	0.75	0.76	0.74	0.90
Mg / Mg+Fe(+2)	0.16	0.17	0.15	0.18	0.15	0.16	0.05
Fe(+3) / Fe(+3)+Al+Cr	0.10	0.10	0.10	0.11	0.13	0.11	0.27
Fe(+2) / Fe(+2)+Mg	0.84	0.83	0.85	0.82	0.85	0.84	0.95

Chrome Spinel

Sample #	D-69 center	D 69 rim	D-69 center	D 69 rim	D 69 center
MgO	3.57	0.94	3.54	0.73	3.13
Al2O3	11.46	0.74	13.77	0.20	12.60
TiO2	0.22	0.29	0.09	0.27	0.11
Cr2O3	43.68	38.48	41.96	33.80	42.10
MnO	0.79	1.08	0.92	0.93	1.01
FeO	38.96	57.14	38.74	62.69	40.07
Sum	98.69	98.67	99.01	98.62	99.01
Mg	0.184	0.050	0.179	0.039	0.160
Al	0.467	0.031	0.554	0.009	0.511
Ti	0.005	0.007	0.002	0.006	0.002
Cr	1.195	1.120	1.132	0.986	1.145
Mn	0.022	0.033	0.026	0.028	0.029
Fe3+	0.332	0.841	0.313	0.999	0.344
Fe2+	0.795	0.917	0.794	0.933	0.810
Sum	3.000	3.000	3.000	3.000	2.999
$\frac{Cr}{Cr+Al}$	0.72	0.97	0.67	0.99	0.69
$\frac{Mg}{Mg+Fe(+2)}$	0.19	0.05	0.18	0.04	0.16
$\frac{Fe(+3)}{Fe(+3)+Al+Cr}$	0.17	0.42	0.16	0.50	0.17
$\frac{Fe(+2)}{Fe(+2)+Mg}$	0.81	0.95	0.82	0.96	0.84

Chrome Spinel

Sample #	D-4 center	D-4 rim	D-4 center	D-4 center	D-67 center	D-67 rim	D-67 center
MgO	5.49	5.41	5.37	5.51	7.19	2.58	7.25
Al2O3	7.57	6.61	7.95	8.39	18.30	4.78	19.08
TiO2	0.30	0.26	0.24	0.25	0.21	0.29	0.15
Cr2O3	54.53	50.86	53.29	53.09	42.99	39.07	42.71
MnO	0.81	1.18	0.99	0.99	0.50	1.17	0.70
FeO	31.66	36.84	33.96	32.74	31.43	52.36	31.25
Sum	100.37	101.18	101.80	100.97	100.63	100.26	101.14
Mg	0.280	0.275	0.270	0.279	0.346	0.134	0.346
Al	0.306	0.265	0.316	0.334	0.696	0.198	0.719
Ti	0.007	0.006	0.006	0.006	0.004	0.007	0.002
Cr	1.478	1.370	1.422	1.424	1.096	1.086	1.079
Mn	0.022	0.033	0.027	0.027	0.013	0.034	0.019
Fe3+	0.203	0.353	0.250	0.230	0.199	0.703	0.200
Fe2+	0.704	0.698	0.709	0.700	0.648	0.836	0.635
Sum	3.000	3.000	3.000	3.000	3.001	2.999	2.999
Cr / Cr+Al	0.83	0.84	0.82	0.81	0.61	0.85	0.60
Mg / Mg+Fe(+2)	0.28	0.28	0.28	0.29	0.35	0.14	0.35
Fe(+3) / Fe(+3)+Al+Cr	0.10	0.18	0.13	0.12	0.10	0.35	0.10
Fe(+2) / Fe(+2)+Mg	0.72	0.72	0.72	0.71	0.65	0.86	0.65

Chrome Spinel

Sample #	D-32 center	D 32 center	D 20 center	D 20 center
MgO	3.81	11.62	2.54	0.54
Al2O3	1.66	29.97	13.58	0.15
TiO2	0.18	0.20	0.27	0.26
Cr2O3	29.12	32.68	39.74	35.64
MnO	2.45	0.34	0.90	0.74
FeO	61.51	24.21	43.66	65.31
Sum	98.73	99.02	100.68	102.64
Mg	0.201	0.524	0.127	0.028
Al	0.069	1.069	0.541	0.005
Ti	0.003	0.004	0.006	0.006
Cr	0.820	0.782	1.064	1.000
Mn	0.072	0.008	0.025	0.022
Fe3+	1.106	0.141	0.383	0.981
Fe2+	0.727	0.472	0.854	0.959
Sum	2.999	3.000	3.000	3.001
$\frac{Cr}{Cr+Al}$	0.92	0.42	0.66	0.99
$\frac{Mg}{Mg+Fe(+2)}$	0.22	0.53	0.13	0.03
$\frac{Fe(+3)}{Fe(+3)+Al+Cr}$	0.55	0.07	0.19	0.49
$\frac{Fe(+2)}{Fe(+2)+Mg}$	0.78	0.47	0.87	0.97

Amphiboles in Metapyroxenites

Sample #	D- 191	D-191	D-197	D-244	D-256	D-256
Mineral	AMP	AMP	AMP	AMP	AMP	AMP
code	Fe+2	13ex	13ex	Fe+2	13ex	13ex
Na2O	0.17	0.21	0.21	0.41	0.58	0.60
MgO	17.69	19.88	17.12	22.46	18.46	18.21
Al2O3	1.79	1.43	1.77	2.73	3.61	4.29
SiO2	55.25	55.84	54.61	56.57	54.80	54.08
K2O	0.04	0.04	0.07	0.01	0.04	0.04
CaO	13.02	12.22	12.22	12.69	11.87	12.41
TiO2	0.60	0.05	0.25	0.06	0.16	0.07
Cr2O3	0.10	0.09	0.20	0.09	0.18	0.24
MnO	0.18	0.25	0.59	0.11	0.28	0.23
FeO	8.82	7.34	10.31	3.03	8.48	8.11
NiO	0.01	0.04	0.03	0.05	0.03	0.04
Sum	97.66	97.39	97.38	98.22	98.48	98.32
T-site						
Si	7.809	7.755	7.741	7.732	7.566	7.519
Al4	0.191	0.234	0.256	0.268	0.434	0.481
Fe3	0.000	0.011	0.000	0.000	0.000	0.000
M1,2,3 site						
Al6	0.108	0.000	0.039	0.172	0.153	0.223
Fe3	0.000	0.525	0.357	0.000	0.553	0.350
Ti	0.064	0.005	0.027	0.006	0.017	0.007
Cr	0.011	0.010	0.022	0.010	0.020	0.026
Mg	3.726	4.114	3.618	4.575	3.798	3.773
Fe2	1.043	0.316	0.865	0.236	0.426	0.593
Mn	0.022	0.029	0.071	0.000	0.033	0.027
Ca	0.027	0.000	0.000	0.000	0.000	0.000
M4-site						
Mg	0.000	0.000	0.000	0.000	0.000	0.000
Fe2	0.000	0.000	0.000	0.110	0.000	0.000
Mn	0.000	0.000	0.000	0.013	0.000	0.000
Ca	1.945	1.818	1.857	1.859	1.756	1.849
Na	0.047	0.057	0.058	0.019	0.155	0.151
A-site						
Ca	0.000	0.000	0.000	0.000	0.000	0.000
Na	0.000	0.000	0.000	0.090	0.000	0.011
K	0.007	0.007	0.013	0.002	0.007	0.007

Hornblende/Plagioclase in Metagabbro/Amphibolite

Sample #	D-247	Sample #	D-247	D-247
Mineral	HBLD	Mineral	PLAG	PLAG
code	13ex			
Na2O	0.80	Na2O	0.99	0.95
MgO	15.65	MgO	0.00	0.00
Al2O3	8.13	Al2O3	34.23	34.11
SiO2	49.28	SiO2	46.00	46.27
K2O	0.21	K2O	0.00	0.01
CaO	11.57	CaO	18.34	18.52
TiO2	0.18	TiO2	0.00	0.03
Cr2O3	0.00	Cr2O3	0.00	0.00
MnO	0.24	MnO	0.00	0.03
FeO	11.50	FeO	0.10	0.13
NiO	0.00	NiO	0.03	0.03
Sum	97.57	Sum	99.70	100.09
T-site		Na	0.088	0.083
		Mg	0.000	0.000
Si	6.953	Al	1.863	1.851
Al4	1.047	Si	2.123	2.130
Fe3	0.000	K	0.000	0.000
		Ca	0.906	0.913
M1,2,3-site		Ti	0.000	0.000
		Cr	0.000	0.000
Al6	0.305	Mn	0.000	0.000
Fe3	0.950	Fe	0.002	0.004
Ti	0.019	Ni	0.000	0.000
Cr	0.000			
Mg	3.291	Sum	4.982	4.981
Fe2	0.407			
Mn	0.029	Ab	0.089	0.085
Ca	0.000	An	0.911	0.915
		Or	0.000	0.001
M4-site				
Mg	0.000			
Fe2	0.000			
Mn	0.000			
Ca	1.749			
Na	0.220			
A-site				
Ca	0.000			
Na	0.000			
K	0.038			

Hornblende/Plagioclase in Metagabbro/Amphibolite

Sample #	D-258	D-258
Mineral	HBLD	HBLD
code	13ex	13ex
Na2O	1.14	1.17
MgO	12.65	12.61
Al2O3	10.96	10.64
SiO2	46.60	45.60
K2O	0.55	0.54
CaO	11.36	11.22
TiO2	1.10	1.03
Cr2O3	0.02	0.02
MnO	0.26	0.21
FeO	14.09	14.46
NiO	0.03	0.04
Sum	98.76	97.53
T-site		
Si	6.641	6.587
Al4	1.359	1.413
Fe3	0.000	0.000
M1,2,3-site		
Al6	0.482	0.399
Fe3	0.754	0.888
Ti	0.118	0.112
Cr	0.002	0.002
Mg	2.687	2.715
Fe2	0.925	0.859
Mn	0.031	0.026
Ca	0.000	0.000
M4 site		
Mg	0.000	0.000
Fe2	0.000	0.000
Mn	0.000	0.000
Ca	1.735	1.737
Na	0.265	0.263
A site		
Ca	0.000	0.000
Na	0.050	0.064
K	0.100	0.100

Sample #	D-258	D-258
Mineral	PLAG	PLAG
Na2O	1.92	1.93
MgO	0.00	0.00
Al2O3	32.21	32.20
SiO2	48.02	47.82
K2O	0.02	0.02
CaO	16.62	16.69
TiO2	0.01	0.00
Cr2O3	0.00	0.00
MnO	0.00	0.00
FeO	0.16	0.11
NiO	0.04	0.00
Sum	98.99	98.79
Na	0.171	0.172
Mg	0.000	0.000
Al	1.756	1.759
Si	2.222	2.216
K	0.001	0.001
Ca	0.823	0.828
Ti	0.000	0.000
Cr	0.000	0.000
Mn	0.000	0.000
Fe	0.005	0.004
Ni	0.001	0.000
Sum	4.979	4.980
Ab	0.173	0.173
An	0.826	0.826
Or	0.001	0.001

APPENDIX B

SAMPLE CALCULATION FOR THE ESTIMATION OF Fe^{3+} IN CHROMITE

Fe^{3+} was calculated on the basis of charge balance, as outlined below. This sample calculation uses the first chromite analysis presented in Appendix A (D-57-page 222).

	FM	FM(nc)	Associated charges
Mg	0.159	0.155	0.31
Al	0.439	0.429	1.29
Ti	0.003	0.003	0.01
Cr	1.394	1.361	4.08
Mn	0.027	0.026	0.05
Fe(T)	1.053	1.028	2.06
total	3.072	3.000	7.80

-normalization constant (nc) = 3.000 / 3.072 = 0.9766

-charges necessary to bring total to 8 = 8.00 - 7.80 = 0.20

-FeO = 1.028 - 0.20 = 0.828

-Fe_2O_3 = 0.20

A) Column 1 is the mineral formula (FM) calculated on the basis of 4 oxygens.

This gives a normalization constant (nc) of 0.9766 and multiplying this constant by the mineral formula.

C) column 3 is the number of charges associated with each of the cations. The total should be less than the ideal number.

D) For each positive charge, convert the amount of Fe^{+2} to Fe^{+3}.

It should be noted that accuracy of this procedure is based on the accuracy of the initial probe data and is only an estimate. The most accurate recalculations will be for the minerals that are closest to the ideal end-member composition.

APPENDIX C

XRD ANALYSES OF SERPENTINE MINERALS

Whole rock powders of 9 samples of the serpentine-rich ultramafic rocks were analyzed by x-ray diffraction to determine the serpentine end-members. Samples were hand crushed to a fine powder and placed in a standard Phillips XRD unit with CuKα radiation. A scan rate of 1°2θ/minute was used for all analyses.

The following lists are the d-spacings (A°) and the intensity of all peaks from each sample. The numbers in parentheses are those values that are closest to the values of known serpentine minerals. The serpentine mineral in samples D-4 and D 14 is identified as lizardite and antigorite respectively. The corresponding standards are also shown.

The other 7 samples could not be positively identified as to the serpentine end-member, although their are certainly serpentine minerals present in these samples as indicated by the similarity of d(A°) and I values.

GVMD 4 d(A)	I
(7.24)	70
5.079	13
(4.575)	6
3.875	19
(3.64)	41
3.47	6
2.76	13
(2.508)	20
2.456	21
2.345	8
2.266	10
2.246	8
2.158	7
2.025	11
(1.74)	16

standard d(A)	11-386 I
7.25	60
2.503	100
1.744	5

lizardite

GVMD-14 d(A)	I
(7.296)	>100
(4.637)	7
(3.626)	80
(2.536)	22
2.429	9
2.336	6
2.025	17
1.82	5
1.569	8
(1.543)	8

standard d(A)	21-963 I
7.29	100
3.61	80
2.596	20
2.429	20

Antigorite

6VMD-32

d(A)	I
(7.166)	>100
(4.561)	9
3.759	10
(3.594)	>100
2.906	6
(2.517)	20
(2.488)	17
2.414	11
2.143	9
2.026	7
1.814	6
1.613	4
1.567	8
(1.543)	10
1.513	7

6VMD-35

d(A)	I
(7.17)	>100
(4.56)	7
(3.60)	77
2.95	7
2.73	10
(2.51)	26
(2.49)	7
(2.45)	7
(2.41)	8
2.14	8
2.09	5
2.02	5

6VMD-37

d(A)	I
(7.225)	83
(4.573)	17
(3.639)	63
(2.49)	42
2.144	17
2.024	5
1.791	9
(1.533)	17
1.502	12

6VMD-57

d(A)	I
(7.178)	>100
3.763	18
(3.59)	>100
3.444	9
2.879	5
(2.525)	21
2.413	16
2.338	9
2.118	6
2.025	52
1.812	12
(1.567)	6
(1.541)	6
1.448	6
1.433	4

6VMD-67

d(A)	I
(7.196)	>100
(4.573)	6
3.867	11
3.762	11
(3.593)	>100
2.763	10
2.734	7
(2.508)	24
2.453	14
2.414	10
2.338	10
2.627	10
2.244	11
2.159	7
2.025	26
1.812	7
1.749	11
1.637	4
1.572	10

6VMD-69

d(A)	I
(7.144)	>100
3.754	10
(3.583)	>100
3.10	6
2.952	5
2.734	10
2.522	12
2.405	11
2.335	10
2.117	7
2.095	8
2.024	67
1.809	6
1.613	4
(1.564)	5

6VMD-70

d(A)	I
9.203	50
(7.178)	>100
(4.647)	11
3.765	12
(3.596)	>100
3.449	7
3.249	5
3.104	45
2.523	16
2.417	13
2.335	9
2.025	27
1.867	5
1.812	10
1.566	6

APPENDIX D

GEOCHEMISTRY OF THE MAFIC-ULTRAMAFIC ROCKS

One of the major goals of geochemical analyses of mafic igneous rocks is to determine their primary tectonic setting. This is typically done using the mafic volcanic rocks that are commonly associated with many mafic igneous environments. Numerous discrimination diagrams that utilize relatively immobile elements such as Ti, Zr, Nb and Y have been proposed for such rocks.

In the absence of fine-grained volcanic rocks, the tectonic setting is difficult to assess. In this study it is also recognized that some elements may have been mobilized during metamorphism such that their original igneous features may be obliterated. In light of this, a detailed geochemical analysis of the rocks in this study would probably produce equivocal results. However, a brief discussion is presented here for comparisons to similar rocks and for descriptive purposes.

A total of 22 rock samples were analyzed by X-Ray Assay Laboratories Limited, Don Mills Ontario for major, trace and REE's. The samples analyzed included 8 tremolite/actinolite-rich ultramafic rocks (metapyroxenites?), 11 metagabbros and 2 serpentinites. The method of analysis and detection limits for each element are presented in Table D-1. Analyses are presented in Table D-2.

TABLE D-1

ELEMENT	METHOD	DETECTION LIMIT
Majors	XRF	0.01
Cr,Rb,Sr,Y,Zr,Nb,Ba	XRF	10.00
Au	NA	5.00
Sc	NA	0.10
Co	NA	1.00
As	NA	2.00
Se	NA	3.00
Br	NA	1.00
Mo	NA	5.00
Sb	NA	0.20
Cs	NA	0.50
La	NA	0.50
Ce	NA	3.00
Nd	NA	5.00
Sm	NA	0.10
Eu	NA	0.20
Tb	NA	0.50
Yb	NA	0.20
Lu	NA	0.05
Hf	NA	1.00
Ta	NA	1.00
W	NA	3.00
Ir	NA	20.00
Th	NA	0.50
U	NA	0.50
Cr	NA	2.00
Mn	DCP	2.00
Be	DCP	1.00
B	DCP	10.00
V	DCP	2.00
Ni	DCP	1.00
Cu	DCP	0.50
Zn	DCP	0.50
Ge	DCP	10.00
Ag	DCP	0.50
Cd	DCP	1.00
Pb	DCP	2.00
FeO %	Wet Chemical	0.10

XRF = X-Ray Fluorescence Spectrometry
NA = Neutron Activation
DCP = Direct-Current Plasma Emission Spectrometry

TABLE D-2 Major, trace and REE geochemistry of tremolite/actinolite rich ultramafic rocks, metagabbros and serpentinites.

1) Major Elements in wt. %, Au and Ir in ppb, all other elements are in ppm.

2) Cr values not detectable by XRF were determined by NA.

3) Mn values not detectable by XRF were determined by DCP.

4) Fe_2O_3 was determined by difference between FeO and total Fe.

5) nd = not detectable

Metagabbro

sample #	D-21	D-201	D-210	D-259	D-222
SiO2	41.35	42.30	45.25	43.90	38.40
Al2O3	18.35	17.55	15.45	16.45	20.10
CaO	11.10	11.50	9.40	11.70	12.20
MgO	7.52	7.57	10.90	8.46	5.26
Na2O	0.73	1.10	1.31	1.47	0.46
K2O	0.32	0.38	1.11	1.02	0.28
Fe2O3	9.00	5.90	4.10	5.30	8.70
FeO	7.10	7.30	7.30	7.80	6.50
MnO	0.26	0.21	0.23	0.22	0.09
TiO2	0.94	0.60	0.94	0.75	2.55
P2O5	0.11	0.02	0.02	0.14	0.02
LOI	1.70	2.54	2.47	1.23	3.93
SUM	99.80	98.98	98.78	98.39	98.79
Be	5	3	4	5	4
B	nd	nd	19	nd	nd
Sc	54	55	64	70	39
V	470	530	330	410	500
Cr	11	63	389	180	160
Co	46	50	50	75	72
Ni	27	17	170	56	60
Cu	87	290	9	90	66
Zn	150	86	98	110	110
Ge	nd	10	nd	nd	10
As	nd	nd	nd	4	nd
Se	nd	nd	5	nd	nd
Br	1	nd	nd	1	nd
Rb	nd	10	10	30	20
Sr	380	160	130	330	430
Y	20	nd	50	10	10
Zr	70	nd	100	30	20
Nb	20	20	10	10	20
Mo	nd	8	nd	7	nd
Ag	nd	nd	nd	nd	nd
Cd	nd	nd	nd	nd	nd
Sb	nd	nd	nd	nd	nd
Cs	2	nd	3	nd	1
Ba	160	140	350	420	130
La	12	1	6	24	6
Ce	34	nd	27	53	18
Nd	nd	nd	21	20	6
Sm	4	0	7	4	1
Eu	1	1	2	1	1
Tb	nd	nd	1	nd	nd
Yb	1	0	3	1	1
Lu	0	nd	1	0	0
Hf	3	nd	3	2	2
Ta	nd	nd	2	nd	1
W	26	87	43	110	180
Ir	nd	nd	nd	nd	nd
Au	nd	nd	nd	nd	5
Pb	nd	nd	2	8	4
Th	nd	nd	nd	2	nd
U	nd	nd	nd	1	nd

Metagabbro

sample #	D-204	D-216	D-240	D-245	D-247	D-270
SiO2	44.90	47.30	46.20	47.10	46.00	46.20
Al2O3	17.10	15.40	17.20	14.20	17.10	16.30
CaO	14.40	12.60	14.40	15.40	12.50	13.40
MgO	10.50	11.20	10.80	12.20	9.97	9.59
Na2O	0.70	1.00	1.03	0.78	1.29	1.25
K2O	0.66	1.33	0.53	0.21	0.77	0.42
Fe2O3	3.55	3.22	3.51	3.57	3.77	4.48
FeO	4.30	4.70	3.40	3.40	5.30	4.60
MnO	0.06	0.08	0.06	0.07	0.08	0.10
TiO2	0.12	0.13	0.19	0.11	0.18	0.20
P2O5	0.01	0.01	0.04	0.01	0.01	0.02
LOI	2.62	1.93	2.62	2.39	1.77	2.31
SUM	98.92	98.90	99.98	99.44	98.74	98.87
Be	4	3	3	3	3	3
B	10	10	10	20	nd	20
Sc	47	57	49	56	59	77
V	240	220	150	190	200	220
Cr	130	350	260	470	22	410
Co	56	49	70	61	66	81
Ni	36	51	42	71	35	45
Cu	52	46	54	68	7	2
Zn	31	55	44	41	90	92
Ge	nd	nd	nd	nd	nd	nd
As	nd	nd	nd	nd	nd	nd
Se	nd	nd	8	nd	nd	nd
Br	nd	2	1	nd	3	nd
Rb	30	40	20	20	20	20
Sr	130	170	190	140	160	220
Y	nd	10	10	20	nd	nd
Zr	nd	nd	nd	nd	nd	nd
Nb	20	10	10	nd	20	10
Mo	nd	nd	nd	nd	nd	nd
Ag	nd	nd	nd	nd	nd	nd
Cd	nd	nd	nd	nd	nd	nd
Sb	nd	nd	nd	nd	nd	nd
Cs	nd	nd	nd	3	nd	nd
Ba	220	370	130	90	290	110
La	1	1	3	2	2	4
Ce	nd	nd	3	nd	nd	7
Nd	nd	nd	nd	nd	nd	nd
Sm	0	0	1	0	0	2
Eu	nd	0	nd	nd	0	1
Tb	nd	nd	nd	nd	nd	nd
Yb	0	0	0	0	0	1
Lu	nd	nd	nd	nd	0	0
Hf	nd	nd	nd	nd	nd	nd
Ta	nd	nd	nd	1	1	1
W	86	39	130	100	87	250
Ir	nd	nd	nd	nd	nd	nd
Au	nd	nd	6	nd	5	5
Pb	2	nd	nd	nd	nd	6
Th	nd	nd	nd	nd	nd	nd
U	1	nd	1	1	nd	1

Tremolite/Actinolite-rich metapyroxenites

sample #	D 17	D-52	D-191	D 197	D-244	D-256	D-258	D-273
SiO2	51.60	50.00	49.30	49.10	49.40	53.30	45.90	47.90
Al2O3	2.45	3.34	4.20	4.51	3.11	3.63	4.49	5.92
CaO	12.90	12.20	10.70	10.60	12.40	12.10	10.00	8.73
MgO	21.00	20.40	18.80	21.20	21.20	17.90	22.00	17.10
Na2O	0.43	0.50	0.44	0.35	0.45	0.66	0.42	0.58
K2O	0.08	0.03	0.05	0.05	0.07	0.07	0.06	0.08
Fe2O3	3.23	3.78	2.90	2.22	5.04	2.78	5.60	5.40
FeO	4.00	5.10	8.50	6.60	3.80	6.30	4.70	9.60
MnO	0.08	0.07	0.25	0.07	0.06	0.10	0.06	0.32
TiO2	0.12	0.19	0.25	0.18	0.17	0.12	0.12	0.19
P2O5	0.01	0.05	0.01	0.01	0.01	0.01	0.01	0.03
LOI	2.77	2.70	3.00	3.70	2.62	1.23	4.70	3.00
SUM	98.73	98.36	98.40	98.59	98.33	98.40	98.06	98.85
Be	1	3	3	1	3	4	3	4
B	10	nd	nd	nd	10	nd	nd	10
Sc	63	72	83	87	76	79	63	75
V	170	220	240	320	190	190	100	200
Cr	2660	2520	600	2100	1400	1690	1610	780
Co	58	57	65	60	74	86	100	97
Ni	170	190	70	110	170	140	230	200
Cu	19	2	2	2	78	nd	4	12
Zn	50	61	50	28	40	130	57	94
Ge	10	10	nd	10	10	nd	nd	10
As	nd	nd	nd	nd	nd	nd	nd	nd
Se	nd	5	nd	nd	4	6	4	nd
Br	1	1	3	3	1	nd	1	nd
Rb	10	10	nd	10	10	nd	10	20
Sr	nd	nd	nd	nd	nd	nd	nd	nd
Y	30	nd	10	nd	nd	nd	nd	nd
Zr	nd	nd	nd	nd	nd	nd	nd	nd
Nb	nd	20	10	10	20	20	10	20
Mo	nd	nd	5	nd	5	nd	nd	nd
Ag	nd	nd	nd	nd	nd	nd	nd	nd
Cd	nd	nd	nd	nd	nd	nd	nd	nd
Sb	nd	nd	nd	nd	nd	nd	nd	nd
Cs	2	nd	nd	3	nd	nd	nd	nd
Ba	30	nd	40	40	30	60	20	70
La	2	2	1	nd	2	nd	2	1
Ce	11	3	nd	nd	8	6	8	nd
Nd	nd	nd	nd	nd	nd	nd	nd	nd
Sm	1	1	0	0	1	0	0	1
Eu	nd	nd	nd	nd	0	nd	nd	0
Tb	nd	nd	nd	nd	nd	nd	nd	nd
Yb	0	0	0	0	0	0	0	1
Lu	0	0	nd	nd	nd	nd	0	0
Hf	nd	nd	nd	nd	nd	nd	nd	nd
Ta	nd	nd	nd	nd	1	1	nd	nd
W	22	29	13	50	52	130	30	66
Ir	nd	nd	nd	nd	nd	nd	nd	nd
Au	nd	nd	nd	nd	13	5	nd	nd
Pb	nd	nd	nd	nd	nd	nd	nd	nd
Th	nd	nd	1	nd	nd	nd	nd	nd
U	nd	nd	nd	nd	nd	1	nd	1

Metadunites

sample #	D-191	D-260
SiO2	39.00	40.60
Al2O3	0.62	0.49
CaO	0.29	0.29
MgO	37.70	39.50
Na2O	0.23	0.29
K2O	0.01	0.01
Fe2O3	5.69	1.93
FeO	3.70	3.10
MnO	0.04	0.03
TiO2	0.05	0.01
P2O5	0.01	0.01
LOI	12.00	13.20
SUM	99.34	99.49
Re	3	2
B	20	20
Sc	6	7
V	40	26
Cr	3360	3680
Co	94	100
Ni	2100	2400
Cu	nd	nd
Zn	45	37
Ge	10	10
As	3	5
Se	nd	nd
Br	4	nd
Rb	nd	nd
Sr	nd	nd
Y	nd	nd
Zr	nd	nd
Nb	10	nd
Mo	nd	nd
Ag	nd	nd
Cd	nd	nd
Sb	nd	nd
Cs	nd	nd
Ba	nd	20
La	1	1
Ce	nd	5
Nd	nd	nd
Sm	0	0
Eu	nd	nd
Tb	nd	nd
Yb	0	nd
Lu	nd	nd
Hf	nd	nd
Ta	nd	nd
W	28	45
Ir	nd	nd
Au	nd	10
Pb	2	nd
Th	nd	1
U	1	nd

All plots in the following discussions use analyses that are recalculated on an anhydrous basis.

Figure D-1 shows major element variation plots of Wt. % SiO_2, TiO_2, Al_2O_3, Na_2O, Fe_2O_3, FeO, K_2O, MnO, CaO and P_2O_5 against Wt. % MgO for all rocks analyzed. Although the elements may have been mobilized to some degree due to metamorphism, a possible igneous crystal fractionation trend is evident. The rocks are characterized by low Na_2O and K_2O and high MgO, FeO (total), CaO and Al_2O_3. SiO_2 shows a positive correlation and TiO_2, Al_2O_3, Na_2O and K_2O show a negative correlation with increasing MgO. Of interest in these plots is that the tremolite/actinolite-rich ultramafic rocks typically plot between the metagabbros and serpentinites along the differentiation trends and are located where pyroxenites would be expected to plot.

Figure D-2 shows standard AFM diagrams of Irvine & Baragar (1971). D-2A is a plot of the rocks in this study, and D-2B is a plot of rocks from the Bay of Islands Complex as well as fields from various other well-known ophiolite complexes. The rocks of this study follow a typical tholeiitic fractionation trend towards Fe-enrichment from the serpentinites, through tremolite/actinolite-rich ultramafic rocks to metagabbros. This is similar to the pattern of typical ophiolite complexes as shown in Figure D-2B.

Figure D-3 compares the Cr and Ni contents of the rocks of this study to those in the Bay of Islands Complex. All rocks except the two serpentinite samples plot within the shaded box on the diagram. The Ni content of the tremolite/actinolite-rich ultramafic rocks and the metagabbros is typical of layered intrusions.

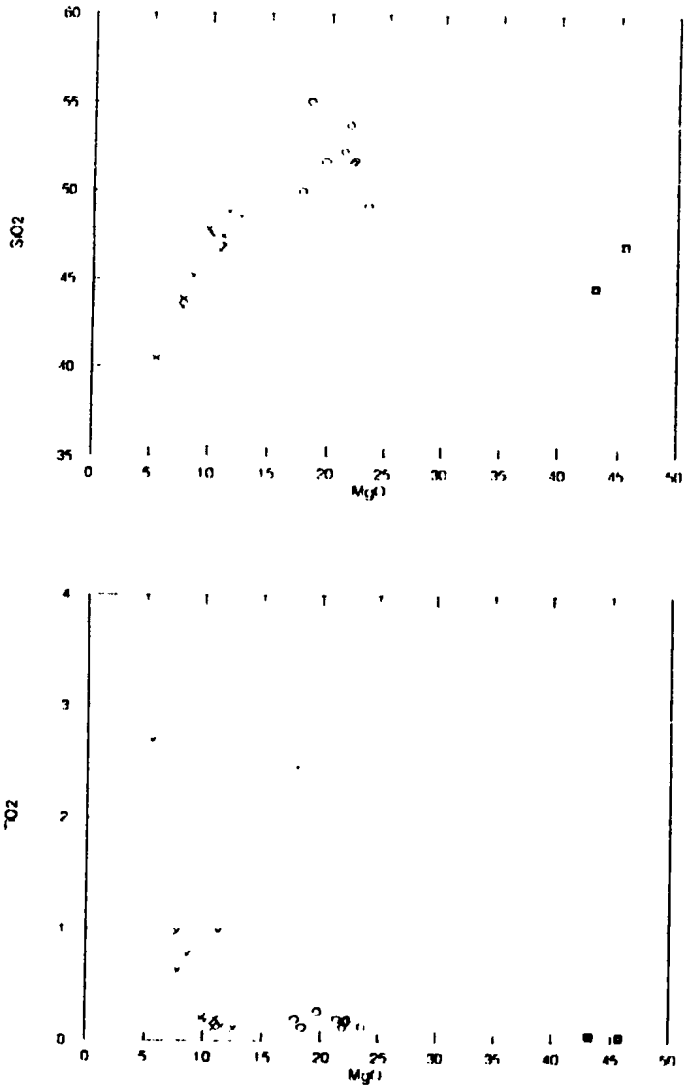

Figure D-1. Major element variation diagrams for all major elements plotted against wt. % MgO. X's represent metagabbros, open circles represent tremolite/actinolite-rich ultramafic rocks (metapyroxenites) and squares are serpentinites.

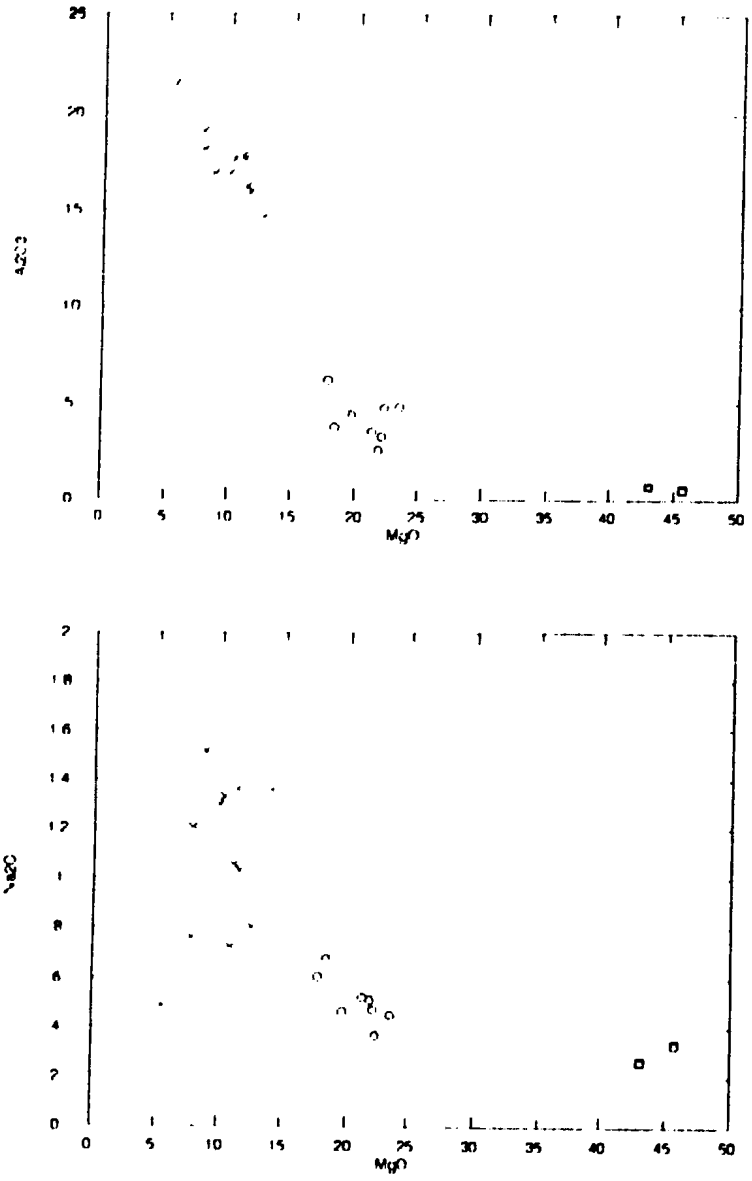

Figure D-1 (Continued)

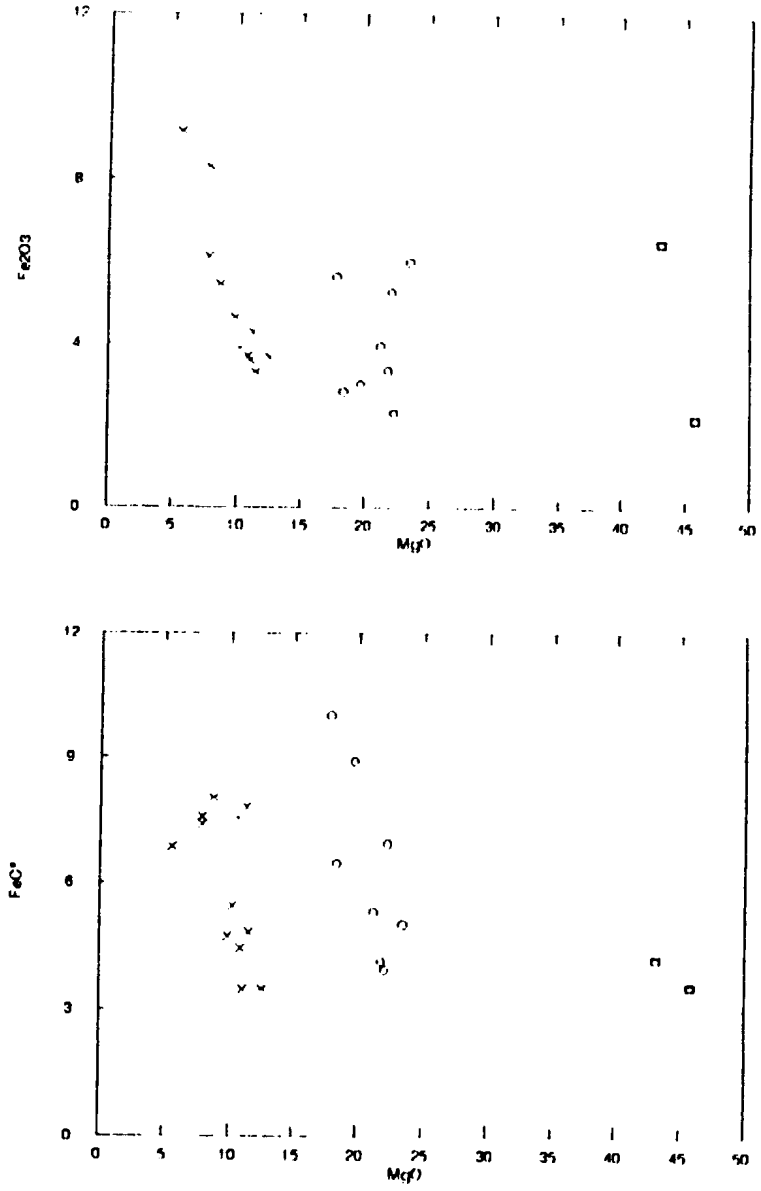

Figure D-1 (Continued)

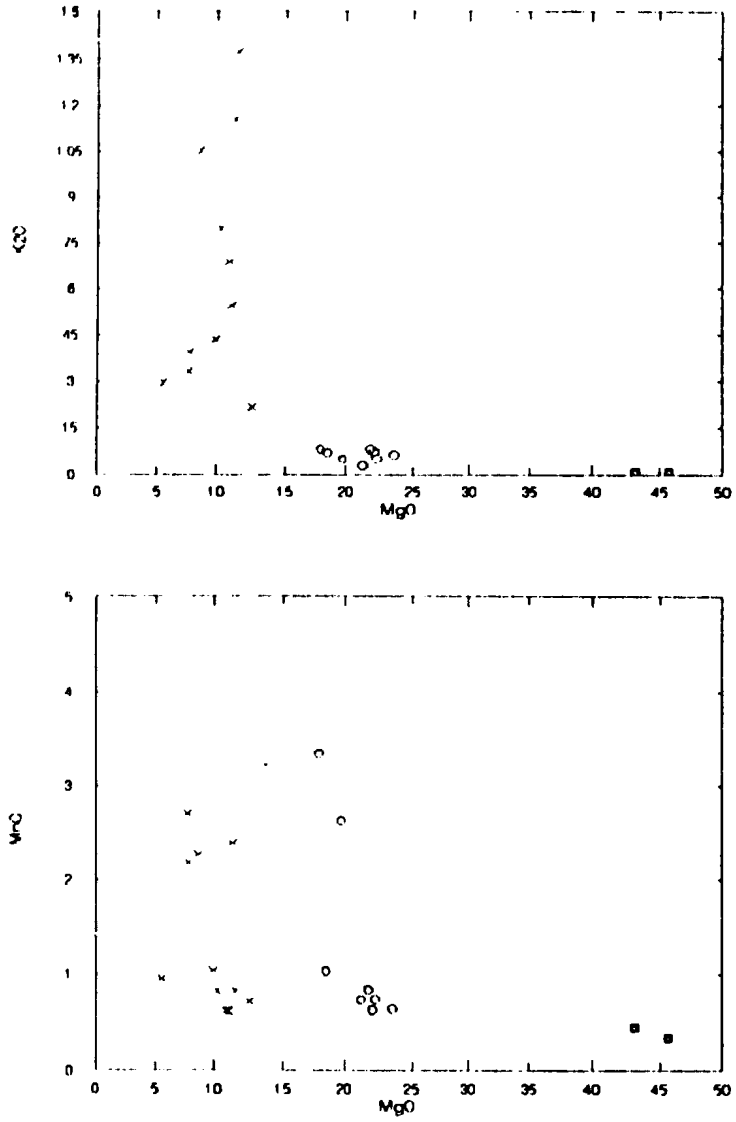

Figure D-1. (Continued)

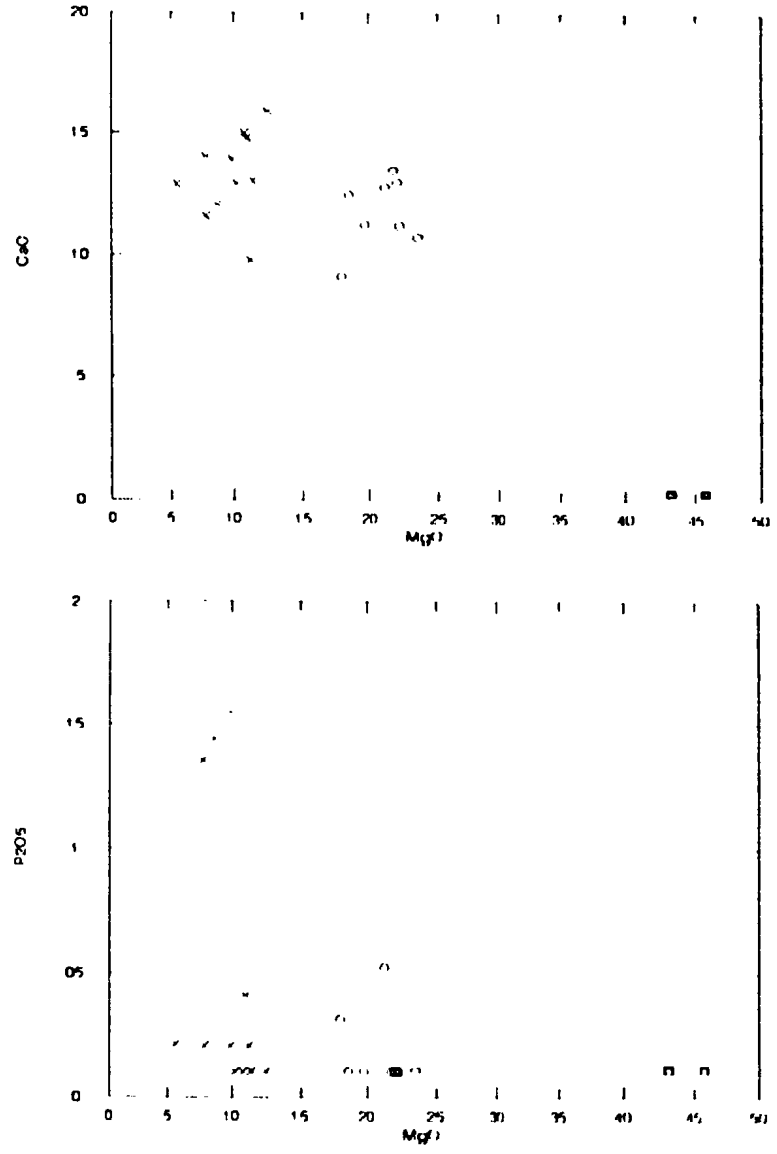

Figure D-1. (Continued)

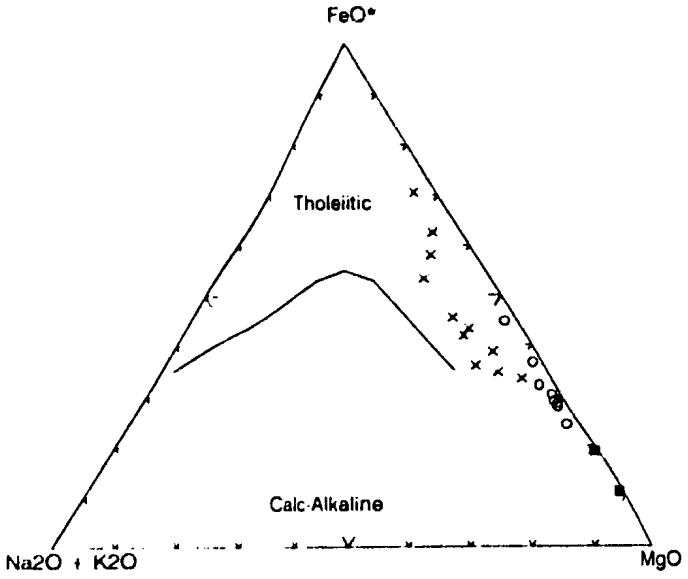

Figure D-2A. AFM diagram for all rocks analyzed in this study. Symbols as in Figure D-1.

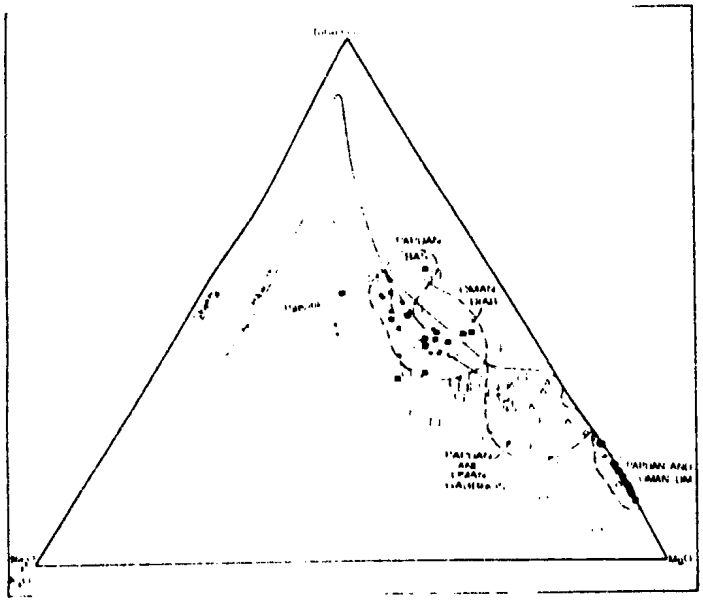

Figure D-2B. AFM diagram showing rocks from the Bay of Islands complex. Closed circles = dunites. Open triangles = pyroxenites. Open squares = gabbros. Closed squares = dikes. Closed small dots = pillow lavas. Open cirles = quartz-diorite. Also plotted are fields for Papuan and Oman ultramafics and gabbros, Oman diabases and Papuan basalts (Malpas & Stevens, 1977).

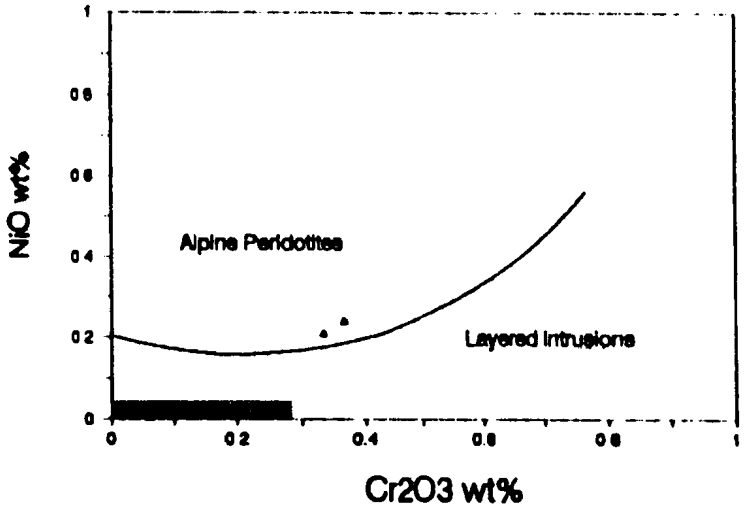

Figure D-3A. wt.% NiO vs. wt.% Cr_2O_3 for all rocks analyzed in this study. Tremolite/actinolite-rich ultramafic rocks and metagabbros plot in the shaded area. Open triangles are serpentinites.

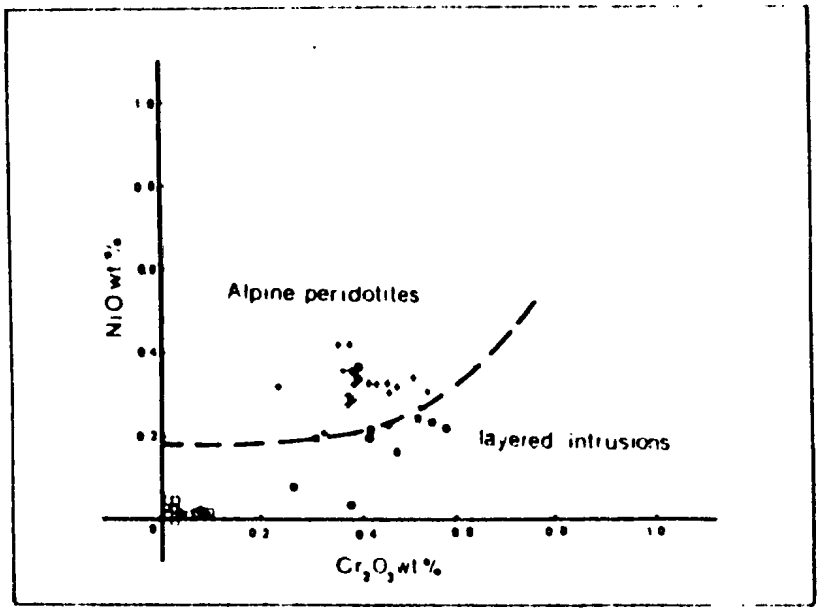

Figure D-3B. wt.% NiO vs. wt.% Cr_2O_3 for rocks from the Bay of Islands complex. Open square = gabbros. Shaded circles = dunites and crosses = tectonite ultramafics (Malpas & Stevens, 1977).

The serpentinite samples plot near the location of dunites from the Bay of Islands Complex.

Relatively little work has been done using discrimination diagrams for gabbro complexes of ophiolites. However, Serri (1981) used the Ti content of gabbroic complexes to distinguish between high-Ti and low-Ti ophiolites. He concluded that these two distinct ophiolite types originate in different environments. Low-Ti ophiolites form in the early stages of back-arc basins as opposed to high-Ti ophiolites that form in either: 1) intermediate to late stages of back-arc opening, 2) ensialic back-arc basins or 3) all stages associated with major oceanic basins.

The gabbroic rocks from the Bay of Islands Complex plot well within the high-Ti ophiolite field. However, Betts Cove and Mings Bight rocks on the Baie-Verte Peninsula in northern Newfoundland, as well as ophiolitic bodies in southern Quebec are low Ti-ophiolites. Figure D-4 shows a plot for the rocks of this study. They are of the low-Ti type and compare to Mings Bight, Betts Cove and ophiolitic rocks in southern Quebec.

Most of the rocks of this study contain below detectable quantities of the REE's except for several of the metagabbro samples. Figure D-5 shows a chondrite normalized plot of these samples, as well as averages of typical upper level gabbros and mafic cumulate gabbros from ophiolites (Coleman, 1977). The rare-earth elements were normalized to the chondritic values of Wakita et al. (1979).

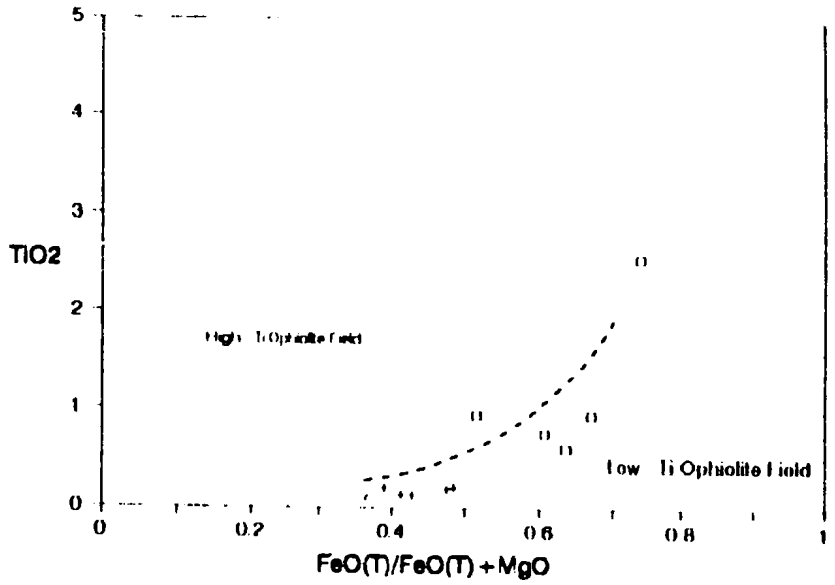

Figure D-4. High vs low-Ti ophiolite discrimination diagram showing plot of metagabbros from this study. Open boxes are more differentiated metagabbros than the ones represented by crosses. The metagabbros generally plot in the low-Ti field. Diagram from Serri, (1980).

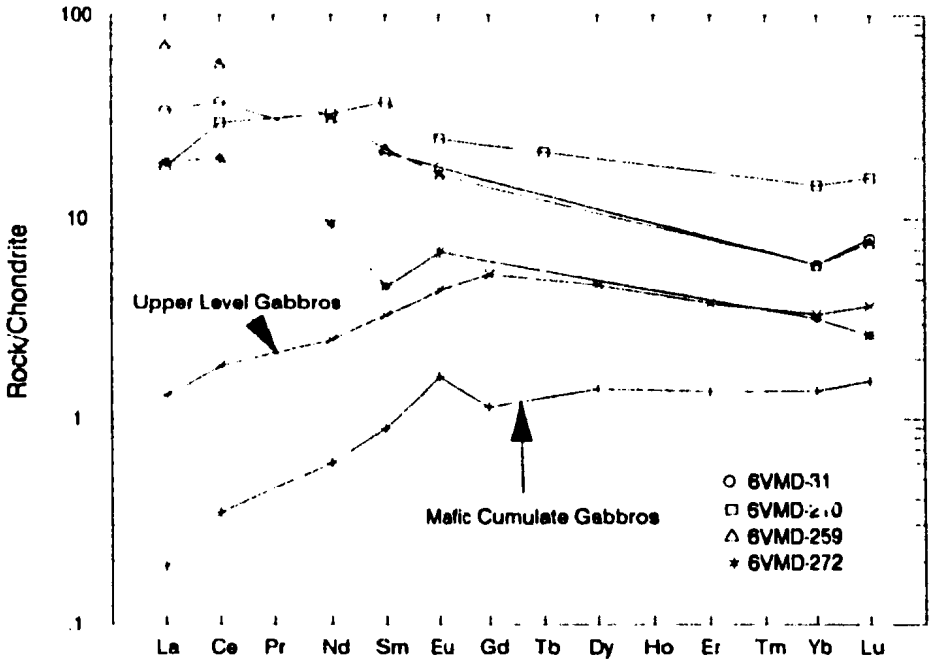

Figure D-5. Ree plot of four metagabbros from this study. Also shown are averages for upper level gabbros and mafic cumulate gabbros (after Coleman, 1977). The metagabbros of this study are light Ree enriched compared to typical ophiolitic gabbros. Chondrite normalization values from Wakita et. al (1979).

The rocks of this study are light rare-earth element enriched compared to typical ophiolitic gabbros. This pattern may indicate a light rare-earth element enriched source for these rocks, although it is recognized the rocks are altered to greenschist facies assemblages and the effect of alteration on the rare-earth element patterns is not known. Since unaltered samples of the metagabbros of this study are not preserved, these data cannot reliably be used to indicate igneous petrogenesis. However, if the rare earth element pattern is a reflection of the original igneous rocks, they compare well to the undeformed Silurian mafic-ultramafic complexes in the Dashwoods subzone described by Currie & van Berkel (1989). These complexes were shown to have "within-plate" and "island-arc" affinities.

APPENDIX E

Review of Serpentine Mineralogy and Textures

Serpentine minerals are classified on the basis of their crystal structure and three major types are recognized; lizardite, chrysotile and antigorite. Of these three only lizardite and chrysotile are true polymorphs and can be further classified into polytypes on the basis of their structural stacking schemes (Wicks & Whittaker, 1975). Antigorite has a different crystal structure which accounts for its slight difference in chemical composition from that of lizardite-chrysotile (see below).

A further classification of serpentine mineralogy is based on their optical properties of the apparent fiber axis. The term apparent fiber axis is used because only chrysotile has a truly fibrous habit whereas the other serpentine minerals may look fibrous in thin section. α serpentine is length fast (negative elongation) and γ serpentine is length slow (positive elongation). α serpentine is most commonly lizardite whereas γ serpentine is commonly antigorite but can also be lizardite or chrysotile (Wicks & Zussman, 1975; Wicks et al., 1977; Wicks & Whittaker, 1977).

Serpentine textures are complex and variable even on the scale of a single thin section. Wicks & Whittaker (1977) and Wicks et al. (1977) provide a summary of textures and corresponding serpentine types and the following discussion stems from their work. Generally serpentine textures can be classified into one of the following: 1) pseudomorphic, 2) non-pseudomorphic or 3) vein type.

Pseudomorphic textures

Pseudomorphic serpentine replaces preexisting rock forming minerals such as olivine, opx, cpx, amphibole, phlogopite, talc, or chlorite. These textures are particularly useful because they preserve the original igneous textures of the rock. The pseudomorphism of all minerals except olivine is called bastites and the convention is to use the mineral as a modifier (hence opx bastite, talc bastite etc.). The two most common textures of pseudomorphic serpentinization after olivine are mesh textures and hourglass textures.

Figure E-1 is a schematic diagram showing the terminology used for mesh textures. Central partings occupy sites of initial fractures in olivine grains. They may be empty or are filled with tiny grains of magnetite or serpentine (any type) or are the site of slip due to shearing. A single central parting divides the mesh rim into two equal sides and is called bipartite veining. Two central partings produce tripartite veining and three partings produce compound mesh rims.

Mesh rims contain serpentine with either of two habits: apparent fibers or serpentine plates. Serpentine with apparent fiber habit generally has its axis aligned at right angles to the central partings and is most often σ serpentine. Mesh centers may still preserve olivine or hydration may be complete and serpentine is developed. The centers may be symmetrical or asymmetrical and are commonly intergrown with submicroscopic brucite. Serpentine types in mesh centers are more variable than mesh rims and may be α or γ serpentine. Most commonly α serpentine mesh textures are composed of lizardite whereas γ serpentine mesh textures may be either lizardite, chrysotile or antigorite.

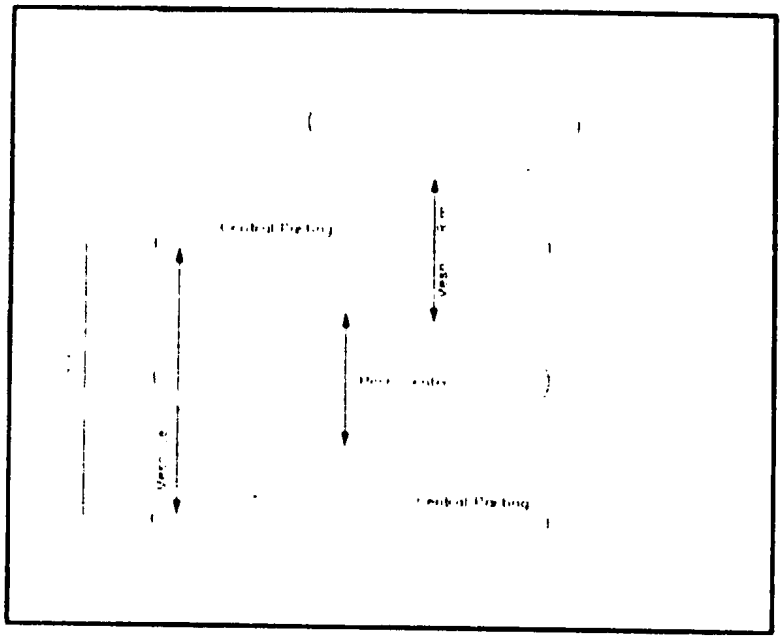

Figure E 1. Schematic diagram showing the terminology for idealized mesh texture of serpentine after olivine. Mesh centres may still preserve olivine or, where serpentinization is complete the mesh centers are completely hydrated to serpentine. Mesh rims are most commonly composed of lizardite with its apparent fiber exis at right angles to the central parting. The central partings form along initial fractures in olivine grains and are composed of tiny magnetite grains or serpentine. The scale in the diagram represents the average distance between central partings in the study of Wicks & Whittaker (1977).

Hourglass textures do not contain mesh rims. In general, they can be considered as regular mesh textures in which the mesh rims have grown inward until all the mesh center is gone. These textures are composed of either α or γ serpentine. As in the mesh textures α serpentine hourglass textures are most commonly lizardite whereas γ serpentine hourglass textures may be composed of lizardite, chrysotile or antigorite.

Non-pseudomorphic textures

Non-pseudomorphic textures form from the recrystallization of pseudomorphic textures but may also form directly by serpentinization of primary minerals. Two types of textures are recognized: 1) interpenetrating and 2) interlocking.

Interpenetrating textures begin to develop as isolated flakes distributed throughout lizardite pseudomorphic textures. They are composed of elongate blades typically with a flame structure that forms tight interpenetrating fabrics. γ serpentine is the main type in this texture and is usually antigorite although chrysotile has also been identified.

Interlocking textures are somewhat similar to the interpenetrating textures except that blades in interlocking textures tend to be more equant than elongate. The equant blades form a tight interlocking fabric that starts to form in isolated patches that grow together as recrystallization continues. Both α and γ serpentine has been recognized in this texture and can be either of antigorite, chrysotile or lizardite.

The most common type of serpentine in veins is chrysotile that occurs either as cross or slip fibers. Cross fibers tend to grow with their long axis perpendicular to vein

boundaries whereas slip fibers grow parallel or subparallel to vein boundaries. These forms are commonly known as chrysotile asbestos veins. Non-asbestiform veins are also known and may contain either lizardite, chrysotile or antigorite.

Discussion

Although the above review is simplified, the textures that are important to this study are presented. It should be noted here that a complete range of intermediate textures between those discussed above are also known to occur. Also note that these textures are developed in the absence of shearing. Where shearing is an important factor, additional textures such as ribbon (or schistose) serpentinites (Maltman, 1978) may develop.

Interpretation of serpentine textures

The most common interpretation of serpentine textures is a general scheme whereby they are classified as retrograde (pseudomorphic) and prograde (non-pseudomorphic). These variations in serpentine textures (and mineralogy) are typically explained by three subprocesses of serpentinization (O'Hanley, 1991): 1) hydration (retrograde); 2) recrystallization (mild prograde); and 3) deserpentinization (prograde).

Hydration produces the well-known lizardite mesh textures. Lizardite hourglass and lizardite (± chrysotile, ± antigorite) interlocking textures are believed to be transitional between pseudomorphic and non-pseudomorphic textures, possibly developed in a mild prograde event (Wicks & Whittaker, 1977; Wicks & Plant, 1979). Deserpentinization produces antigorite interpenetrating textures from preexisting

lizardite and with additional prograde metamorphism, serpentine minerals are replaced by anhydrous silicates such as olivine and pyroxene.

APPENDIX F

THERMOMETRY/BAROMETRY CALCULATIONS

GARNET-BIOTITE THERMOMETRY

Element partitioning between mineral phases is temperature dependent and metamorphic crystallization temperatures of garnet-biotite equilibria can be estimated using the intercrystalline exchange of Fe^{2+} and Mg in the following equilibrium reaction:

Phlogopite + Almandine $\rightleftharpoons$ Annite + Pyrope

The general equation used as a basis for temperature calculations is:

$$\Delta H - T\Delta S + P\Delta V + RT\ln K_D - RT\ln K_\gamma = 0$$

where K_D is the distribution coefficient and K_τ is the activity coefficient.

One of the most commonly applied, experimental calibrations for this reaction is that of Ferry and Spear (1978) who assumed that Fe and Mg mix ideally in garnet-biotite solid solutions. The following equation was proposed from their experimental data:

$$12454 - 4.662\ T(^\circ K) + 0.057\ P(bars) + 3RT\ln K_D = 0$$

where $K_D = \dfrac{X_{Mg}^{GNT} + X_{Fe}^{GNT}}{X_{Mg}^{BIO} + X_{Fe}^{BIO}}$

They recognized that K_D is also a function of Ca-Mn in garnet and Ti-Al^{VI} in biotite and cautioned that the thermometer should not be used where the garnet composition has (Ca + Mn) / (Ca + Mn + Fe + Mg) greater than 0.2 and or when the biotites have (Al^{VI} + Ti) / (Al^{VI} + Ti + Fe + Mg) greater than 0.15. The accuracy of this thermometer is estimated to be approximately ± 50°C by the authors.

Since the introduction of the Ferry and Spear calibration, it has been recognized that non-ideal mixing between components in garnets could be an important factor in temperature calculations. Hodges & Spear (1982) assume non ideal solution behavior for garnet and ideal Fe-Mg mixing for biotite. They caution that application of their thermometer should not be used on samples in which Ti is a major component in biotite because of their assumption of ideal behaviour. They further assumed that all components in garnets mix ideally except for the Ca-Mg end members. For these end members, they used a Margules parameter of W_{CaMg} 3300 - 1.5 T(°K).

The temperature expression proposed by Hodges & Spear (1982) is:

$$T = \frac{(2089 + 9.56\,P + 1661\,X^{Ca})}{(\ln K + 0.782 + 0.755\,X^{Ca})}$$

where X^{Ca} = (Ca+Mg+Fe+Mn) in garnet, T °K and P bars.

GARNET-Al_2SiO_5-QTZ-PLAGIOCLASE BAROMETRY

The net transfer reaction:

3anorthite = grossular + 2 Al_2SiO_5 + quartz

has been used extensively in the past as a geobarometer. Ghent (1976) assumed ideal

solid solution behaviour for garnet and plagioclase for the reaction and based on experimental data proposed the following equation for sillimanite-bearing rocks:

$$0 = \frac{-2551.4}{T(^\circ K)} + 7.1711 \quad \frac{0.2842(P-1)}{T(^\circ K)} + \log a_{Ca}^{gnt} - 3\log a_{Ca}^{plag}$$

This equation was subsequently modified by Ghent et al. (1979) by adding a log K_T value of 0.4 to the equation as an empirical correction for the activities of grossular (garnet) and anorthite (plagioclase) values. This is the procedure used in the present study.

Newton & Haselton (1981) modified the barometer by changing the mixing parameters for garnet and plagioclase solid solution. Their version of the barometer for sillimanite bearing rocks is expressed as:

$$0 = 10055 \quad 31.101T(^\circ K) + \Delta V(P-1) + 1.9872T(^\circ K) \ln\left(\frac{a_{gr}^{gnt}}{a_{an}^{plag}}\right)$$

where V is expressed in cal/bar and P in Kbars.

Hodges & Royden (1984) use essentially the same activity expression for the activity of grossular as Newton & Haselton except that the expression $X_{py}X_{sp}$ is added. The Hodges & Royden expression is:

$$a_{gr} = X_{gr} \exp \frac{(3300-1.5T)(X_{py}^2 + X_{alm}X_{py} + X_{py}X_{sp})}{RT}$$

ISOTOPE THERMOMETRY

The samples were hand crushed and mafic minerals were separated using a magnetic separator. Magnetite was hand picked from the mafic portion. The felsic portions were then leached with HCL to identify quartz from feldspar and quartz was sebsequently hand picked. Oxygen isotope analyses were performed by Dr Fred Longstaffe of the University of Western Ontario. A review of the technique used to obtain the isotope values is presented by Aggarwal & Longstaffe (1987)

THERMOMETRY EQUATIONS

Oxygen isotope fractionation between co-existing metamorphic minerals can be used to estimate metamorphic temperatures provided the minerals are in equilibrium. However, it is well known that "peak" metamorphic temperatures are difficult to estimate by isotope thermometry because minerals generally continue to equilibrate oxygen during subsequent cooling.

The relationship between temperature and fractionation of $\delta^{18}O$ between mineral pairs is expressed by the equation:

$$\Delta x\text{-}y = A \times 10^6 T^{-2} + B$$

where $X = \delta^{18}O$ of mineral 1

$Y = \delta^{18}O$ of mineral 2

A and B are constants

T is the absolute temperature in °K (Faure, 1986).

The constants A and B have been determined experimentally for many minerals with water of known isotopic compositions. By combining two mineral-water equations (eg quartz-water and biotite-water), it is then possible to estimate the equilibrium temperature for the two minerals (quartz-biotite).

The temperatures of quartz-biotite pairs can be estimated using the following relationship:

$$\Delta\ quartz\ biotite = 0.59\ \Delta\ (quartz\text{-}magnetite)$$

(Laure, 1986)

where

$$\Delta\ quartz\text{-}magnetite = 5.57 \times 10^{6}\ T^{-2}$$

(Bottinga & Javoy, 1975)

Temperatures for quartz-chlorite pairs can be estimated using the following equation:

$$\Delta\ quartz\ chlorite = 2.01 \times 10^{6}\ T^{-2} + 1.99$$

(Wenner & Taylor, 1971).